A novel Hydromechatronics System Towards: Micro-Independent Metering

Karem Abuowda

Department of Engineering
Bournemouth University

This dissertation is submitted for the degree of
Doctor of Philosophy

Science and Technology College
January 2020

I would like to dedicate this thesis to my loving parents, brothers, and sisters. Also, my dedication would be to my friends in UK, USA and Germany.

Declaration

I hereby declare that except where specific reference is made to the work of others, the contents of this dissertation are original and have not been submitted in whole or in part for consideration for any other degree or qualification in this, or any other university. This dissertation is my own work and contains nothing which is the outcome of work done in collaboration with others, except as specified in the text and Acknowledgements. This dissertation contains fewer than 65,000 words including appendices, bibliography, footnotes, tables and equations and has fewer than 200 figures.

Karem Abuowda
January 2020

Acknowledgements

I would like to acknowledge firstly my kind main supervisor Prof. Siamak Noroozi for his support, motivation, and guidance during this work. Besides, I would like to express my sincere gratitude to Mr. Phil Godfrey for his experience, patience, and supports. I would like to thank Dr. Mihai Dupac for his special efforts towards this work successfully. I also would like to thank my previous colleague Dr. Ivan Okhotnikov for his collaboration works in this project, especially the modelling of the rotary orifice. Finally, I wont forget to thank Prof. Tony Hope for his appreciated assistance in editing this thesis.

Publications

- Journals
  - Abuowda, K. et al. (2019) ‘A dynamic model and performance analysis of a stepped rotary flow control valve’, Proceedings of the Institution of Mechanical Engineers, Part I: Journal of Systems and Control Engineering. **DOI: 10.1177/0959651818820978**.
  - Abuowda, K., Noroozi, S., Dupac, M., and Godfrey, P. (2019) ’A review of the Hydraulic Independent Metering Technology’, ISA transactions, Elsevier. **https://doi.org/10.1016/j.isatra.2019.08.057**.
  - Abuowda, K., Noroozi, S., Dupac, M., and Godfrey, P. (n.d.) ’Model Based Design for the Novel Hydro-Mechatronics Control System: Micro-Independent Metering’,Proceedings of the Institution of Mechanical Engineers, Part I: Journal of Systems and Control Engineering, (), pp... **Under Review**.
  - Okhotnikov, I., Abuowda, K., Noroozi, S., Godfrey, P., (n.d.) ’ Numerical and experimental investigation of the metering characteristic and pressure losses of the rotary tubular spool valve’, Measurement , Elsevier, (), pp. . **Under Review**.
  - Abuowda, K., Noroozi, S., Dupac, M., and Godfrey, P. (n.d.) ’Mathematical based control method and performance analysis of a novel hydromechatronics driving system Micro-Independent Metering’, Mathematical Methods in the Applied Science, Wiley library, (), pp... **Under Review**.
- Conferences
  - Abuowda, K., Noroozi, S., Dupac, M. and Godfrey, P. (2018). Sensor-less Control of a novel stepped hydraulic flow control valve. In: Proceedings of The Fifteenth International Conference on Condition Monitoring and Machinery Failure Prevention Technologies – CM/MFPT 2018, held 10-12 September 2018 at the East Midlands Conference Centre and Orchard Hotel, Nottingham, UK. **ISBN: 9780903132702**.
  - Abuowda, K., Noroozi, S., Dupac, M. and Godfrey, P. (2018). Friction Analysis and Modelling of a novel stepped rotary flow control valve. In: proceedings of

The Fifteenth International Conference on Condition Monitoring and Machinery Failure Prevention Technologies – CM/MFPT 2018, held 10-12 September 2018 at the East Midlands Conference Centre and Orchard Hotel, Nottingham, UK. **ISBN: 9780903132702**

- Abuowda, K., Dyke, D., Noroozi, S. and Okhotnikov, I. (2018). Dynamic Performance Analysis of PID and Fuzzy Logic Controllers Applicable in Electro-hydraulic Servo Actuator. In: "Proceedings of the 2018 13th APCA International Conference on Automatic Control and Soft Computing (CONTROLO), held 4-6 June, Ponta Delgada, Azores, Portugal. **ISBN: 9781538653456**
- Abuowda, K., Noroozi, S., Dupac, M. and Godfrey, P. (2019). Algorithm Design for the Novel Mechatronics Electro-hydraulic Driving System: Micro-Independent Metering. In: 2019 IEEE International Conference on Mechatronics (ICM), held 18-20 March,ILMENAU, Germany.
  DOI: 10.1109/ICMECH.2019.8722851
- Abuowda, K., Noroozi, S., Dupac, M. and Godfrey, P. (2019).Application of IMUs in monitoring the positional accuracy during micro stepping processes. In: Proceedings of The sixteenth international conference on condition monitoring and asset management Technologies – CM/MFPT 2019, held 25-27 June 2019 at the Principle Grand Hotel, Glasgow, UK, UK. **ISBN: 9780903132702**.
- Abuowda, K., Noroozi, S., Dupac, M. and Godfrey, P. (2019). Model based driving analysis for a stepped rotary flow control valve. In: 21st IFAC Symposium on Automatic Control in Aerospace - ACA, Cranfield, UK: International Federation of Automatic Control (IFAC). **https://doi.org/10.1016/j.ifacol.2019.11.301**.

Abstract

This thesis presents the outcome of an investigation into the development of an existing hydraulic control system known as Independent Metering towards Micro-Independent Metering (MIM).

The Independent Metering system uses a different configuration of the connection between the main elements of the hydraulic systems when compared to a traditional hydraulic circuit arrangement. These elements are pump, tank, and actuator. In a conventional control valve, meter-in connects pump flow to one side of the actuator, while meter-out connects the other side of the actuator back to the tank, these metering features are physically linked. With Independent Metering, these metering features are separated such that they can be independently controlled with a potential resultant reduction of energy losses, improved controllability, but with the increased complexity of the control system.

In a conventional Independent Metering system, a spool, poppet or cartridge valve is generally utilised. However, in this research, a new stepped rotary flow control valve is used for the development of a novel configuration that also meets the rules of Independent Metering. The use of this valve alongside the electronic driving technique micro-stepping, commonly used in electronically controlled electrical drives, improved the system controllability by introducing a smoothing operation in the hydraulic system. This resulted in the new Micro-Independent Metering algorithm which is one of the main contributions to knowledge in this research. To develop the MIM system, the Model-Based Design technique including the system analysis, modelling and simulation, software-in-the-Loop (SIL) simulation, and the hardware-in-the-Loop (HIL) test, are used.

Mathematical model and performance analysis of the valve were conducted in this research. The multi-step response analysis was used to evaluate the dynamical performance of the valve. This indicated that the micro-step driving technique is more suitable for driving the valve as it reduces the effect of the transient response due to friction, while increasing the resolution.

Root Locus Analysis (RLA) was used to study valve stability and the performance limitations. The RLA demonstrated the effect of key parameters on the valve operation. For example, the study show that the valve starts losing stability when the applied pressure drop exceeds 35 MPa.

A new algorithm was developed to formulate and apply the rules of the MIM system. The algorithm includes an operational modes selection procedure, valve conductance calculation procedure, anti-cavitation procedure, and close value detection (CVD) procedure. The proposed CVD determines the stepper motor position based on a predetermined vector selection.

A Software in Loop (SIL) simulation was used to study the model of a telehandler machine boom cylinder. This indicated that the system is able to control the piston speed under variable loading conditions by automatically implementing the suitable operation mode. Moreover, a comparative analysis between the MIM model and the traditional IM model indicated that the system is able to reject fluid disturbances that affect the speed and thus improve system stability.

Finally, Hardware-in-the-Loop testing was performed on the system. This included implementing the control algorithm on two linked processors to control four stepper motor driving circuits. Using serial communications between the hardware and model of the system, the control algorithm obtained the user input and performed an Independent Metering technique. The performance was analysed by qualitatively observing the stepper motors rotation. This showed the hardware platform had the ability to activate the control algorithm under variable operating conditions.

Table of contents

List of figures

List of tables

Nomenclature

$\Delta\theta$	The change of the angle	$degree$
θ	Flow jet angle	$degree$
θ_i	The initial stepper motor rotor position	$degree$
B	Stepper motor viscous friction constant	$N.m.s/rad$
i_a	Stepper motor coil A current	A
i_b	Stepper motor coil B current	A
J	Stepper motor moment of inertia	Kgm^2
K_m	Stepper motor detent torque constant	Nm/A
L	The length of the spool located inside the sleeve	m
n	The number of the balancing grooves	
N_r	The number of stepper motor's teeth	
R	Stepper motor coil resistance	Ω
T_L	Stepper motor total load torque	Nm
V_a	Stepper motor coil A supplied voltage	V
V_b	Stepper motor coil B supplied voltage	V
w	The width of the balancing grooves	m
Z	The deflection average of the asperities on two contacting surfaces	
α	The ration between the two activated valves in the operation mode	

Δp	Pressure difference	Pa
ω	Angular velocity	rad/s
ω_s	Stribeck characteristics velocity	m/s
σ_0	Stiffness coefficient	N/m
σ_1	Damping coefficient	Ns/m
σ_2	Friction coefficient	Ns/m
A_o	Opening area	m^2
a_{ml}	Area of main poppet exposed to control pressure	mm^2
a_{ms}	The inserted Area of main poppet exposed to supply pressure	mm^2
$A_{sp.op}$	Spool opening area	m^2
Aa	The head chamber area	m^2
Ab	The rod chamber area	m^2
am,s	The small area of the main poppet	m^2
ap	The cross sectional area of the pilot poppet	m^2
Be	Fluid bulk modulus	P_a
C_c	Contraction coefficient	
C_v	Velocity Coefficient	
d_f	The fluid flow disturbances	N
k_m	Main poppet spring coefficient	N/m
K_p	The pilot poppet spring coefficient	N/m
K_{eq}	The equivalent flow conductance	$(m^3/s)/\sqrt{MPa}$
m_m	The big area of the main poppet	m^2
m_p	Mass of the main poppet	Kg
P_{eq}	The equivalent pressure	Pa

P_P	The pressure between the main poppet and the pilot poppet	P_a
Pa	The head chamber pressure	Pa
Pa	The inlet pressure	P_a
Pb	The outlet pressure	Pa
Pb	The rod chamber pressure	Pa
Pr	Tank pressure	Pa
q	The fluid flow	m^3/s
Q_1	The main valve produced flow	m^3/s
Q_a	The inlet flow	m^3/s
Q_{at}	The flow form the valve on the connection between the tank and the rod chamber	m^3/s
Q_{bt}	The flow form the valve on the connection between the tank and the rod chamber	m^3/s
Q_{sa}	The flow form the valve on the connection between the pump and the head chamber m^3/s	
Q_{sb}	The flow form the valve on the connection between the pump and the rod chamber	m^3/s
Qp	The pilot valve produced flow	m^3/s
R	The ratio between the two chambers head areas.	
$R_{e.sp}$	External spool radius	m
$R_{e.sp}$	Internal spool radius	m
T_c	Columb friction	N
T_s	Static friction	N
$T_{st.fl}$	Steady state flow torque	Nm
$T_{tr.fl}$	Transient flow torque	Nm
U_v	The inserted electrical signal	A
V	The hydraulic actuator, motor or cylinder, velocity.	m/s

V_c	Fluid volume between main poppet and pilot poppet	m^3
x_m	The feedback slot length	m
x_p	The distance by the pilot poppet	m

Abbreviations

PE Power Extension
PR Power Retraction
IM Independent Metering
AI Artificial Intelligence
CNC Computerised Numerically Controller
MIM Micro-Independent Metering
CAN Controller Area Network
ECP Electronic Controlled Pump
SIL Software-in-the-Loop
HIL Hardware-in-the-Loop
HSRE High Side Regeneration Extension
LSRE Low Side Regeneration Extension
LSRR Low Side Regeneration Retraction
PWM Pulse Width Modulation

Chapter 1

Introduction

1.1 Backgrounnd

Hydraulic systems are extensively used in a variety of applications ranging from construction and earth moving to industrial, military, and aerospace, due to their unique and valuable characteristics. Compared to electrical actuators, hydraulic drives are characterized by high load capabilities, high power to weight ratio and robustness (Parr, 2011) and (Mattila et al., 2017). They are effective in applications with abrupt loading, frequent stops and variations. However, hydraulic drives still suffer from some shortcomings, such as energy losses and nonlinearities, which makes the control system more challenging (Mattila et al., 2017) and (Edge, 1997). For example, 52% of the consumed energy in mobile load sensing system is losses as shown in Figure 1.1

To overcome the hydraulic drives drawbacks, Hydraulic individualization methodology is used. It improves the power density, robustness and flexibility. Individualization can be split into displacement and valve control (Weber et al., 2016). Typical displacement individualization is shown in Figure 1.2. The most common technique, also the lowest level, is one pump feeding several actuators. This approach is common in injection moulding machines (Yan, 2011). The second technique is mainly used in hydraulically driven machines. A Green Wheel Loader was investigated by the Institute of Fluid Power at Dresden University of technology (Schneider et al., 2016), and a Displacement Control Series-Parallel (DC S-P) hybrid mini excavator was improved at Maha Fluid power research centre at Purdue University (Hippalgaonkar and Ivantysynova, 2013), both implementing this second method. The third or the last method/technology, shown in Figure 1.2, is used in high power applications where every actuator has its own pump. These systems' main characteristics are lower energy consumption rates, hence better fuel economy and fewer greenhouse gases. Their main drawbacks are slower dynamics compared to servo actuators (Yan, 2011). Iterations were used to improve the response of this method using electronics (Habibi and Goldenberg, 1999) and (Ahn et al., 2014).

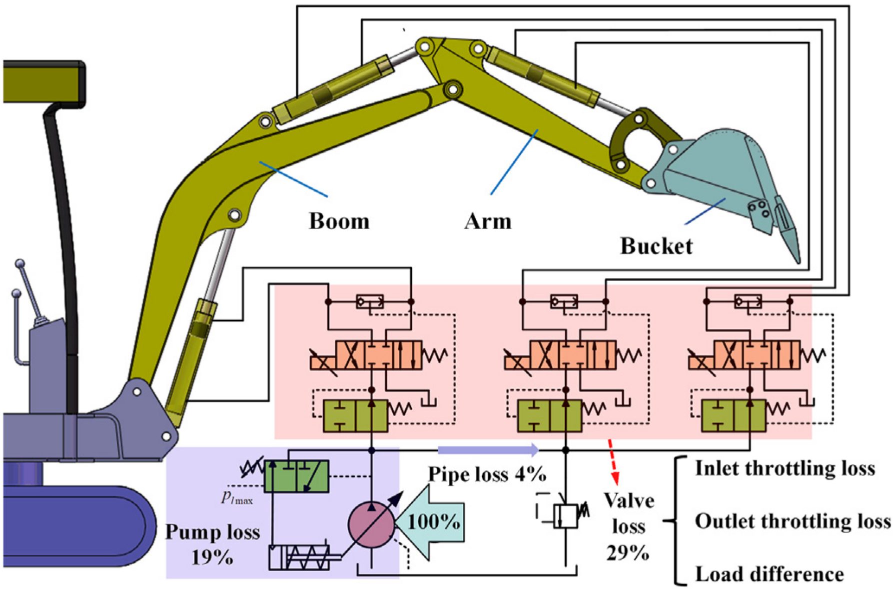

Fig. 1.1 Losses in a hydraulic mobile machine controlled by traditional spool valve and variable displacement valve (Ding et al., 2018b).

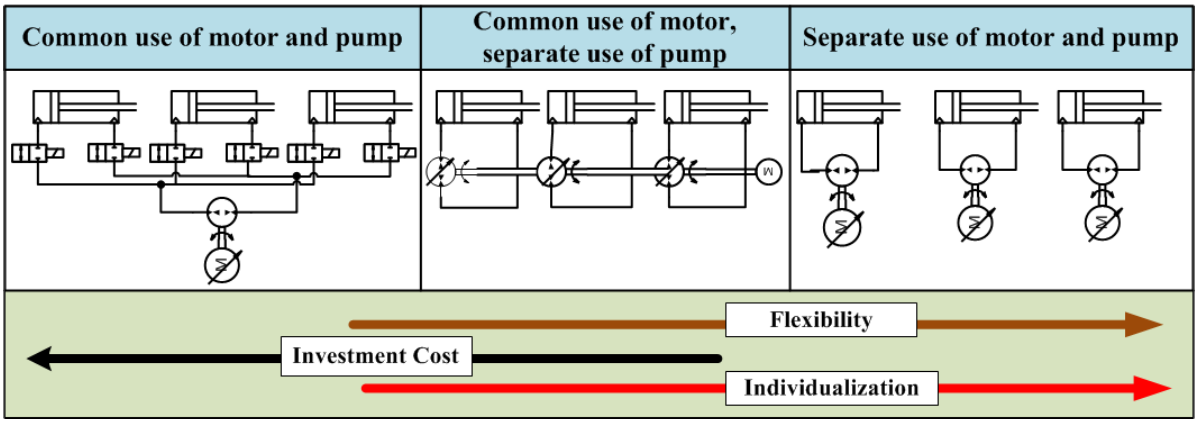

Fig. 1.2 Illustrates different types of hydraulic drives individualization based on the use of pump and motor (Weber et al., 2016).

Regarding individualization using hydraulic control valves, which is the main point of this research, three main types of individualization are summarized in Figure 1.3. The first approach is the common metering edge, which is the traditional control approach. Each actuator is controlled by one valve. Due to the mechanical connection between the metering edges of the actuator using traditional valves, the system has one degree of freedom which means that one chamber pressure is controlled (Lübbert et al., 2016). This configuration limits the system flexibility, but it increases the robustness (Eriksson and Palmberg, 2011). Iterations were performed to adjust the traditional spool and by that control the meter-in and the meter-out, but this was developed for a specific machine type with one optimized flow rate. To improve the efficiency and the energy saving, the trend was to break the mechanical connection between the meter-in and the meter-out edges, which is why it is called Independent Metering (IM). Different terms are used for the IM such as a separate metering, programmable valves, multi-functional valves and separate meter-in separate meter-out control (Liu and Yao, 2002; Kong et al., 2004; Eriksson, 2007). It is called programmable because it changes the control system from the hydro-mechanical concept into an intelligent control system that relies on software. Breaking the mechanical connection leads to many advantages and disadvantages as concluded from several publications. (Sitte and Weber, 2013; Jansson et al., 1991; Opdenbosch et al., 2011).

The main advantages are:

1. Independent control of the inlet and the outlet orifices.
2. Increase energy efficiency by allowing individual control paths or modes. This was proved in the excavator manipulator by (Choi et al., 2015).
3. Application of simple valves.
4. Avoiding cavitation during a pulling load.
5. Flexible system configuration.
6. Functionality Transfer from hardware to software. This is performed by integrating sensors and intelligent software into the system.
7. An ability to apply advanced control methods.

The main disadvantages are as follows:

1. Increased component costs when compared to a simple system.
2. More complex controllers are required.
3. Switching between operation modes causes a sudden change in the velocity, because selecting the modes is based on a rule based method.
4. Difficulty in pressure compensator integration because of its slow dynamic performance. (Vukovic and Murrenhoff, 2014).

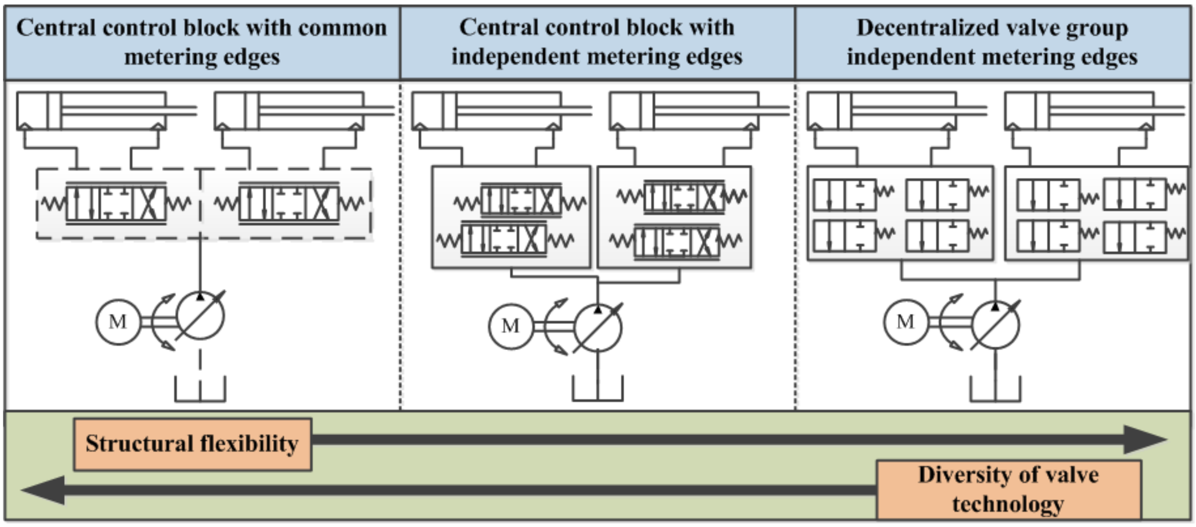

Fig. 1.3 Hydraulic drive individualization based on valve structure, it shows the flexibility could be obtained using independent metering and comparing to common metering edge (Weber et al., 2016).

Research on IM systems has been conducted using various approaches. Figure (1.4) is a general statistical chart indicating the up to date developments in IM. The main scientific institutes developing intelligent hydraulic systems and particularly IM technology are summarized in Table (1.1). The research outputs and patents developed by these institutes and companies are illustrated in Figure (1.5). The first improvement was parameters quantities decoupling (Jansson and Palmberg, 1990). Many techniques have been applied to improve decoupling such as the Linear Quadratic (LQ) technique and pressure feedback (Hippalgaonkar and Ivantysynova, 2013) and (Nielsen, 2005). The effects of feedback linearization and open loop control were investigated by Mattila and Virvalo (2000) and Hu and Zhang (2003). In another approach, adaptive control was used in these systems by Liu and Yao (2002), Yao and DeBoer (2002) and Lu and Yao (2014). Tabor developed a quasi-static mathematical technique for the IM (Tabor, 2005b). Improving this model was achieved by inserting a continuous mode switching (Shenouda, 2006). A significant technology improvement for IM was by inserting digital hydraulics (Laamanen and Vilenius, 2003). Every consumer, actuator, was actuated by four digital fluid control units (DFCU) which contained an array of on/off valves (Ketonen and Linjama, 2017a). There was also a new system based on a hybrid concept such as STEAM (**St**eigerung der **E**nergieeffizienz in der **A**rbeitshydraulik **m**obiler Arbeitsmaschinen). (Hippalgaonkar and Ivantysynova, 2013) and (Vukovic and Murrenhoff, 2015). More reviews about these studies are included in Chapter 2 of this thesis.

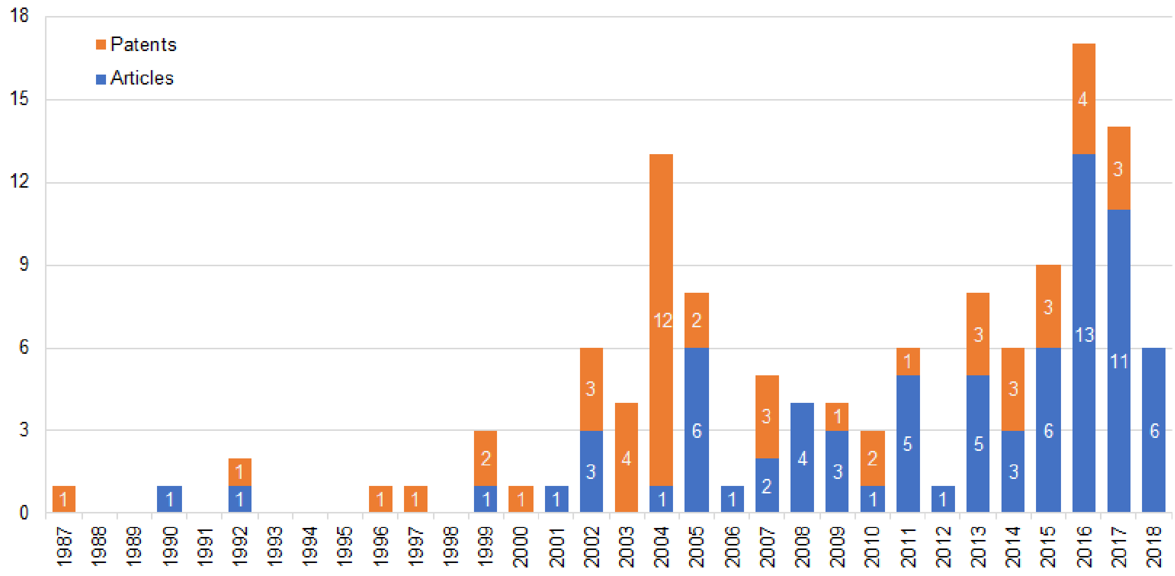

Fig. 1.4 Number of studies related to IM in the last three decades.

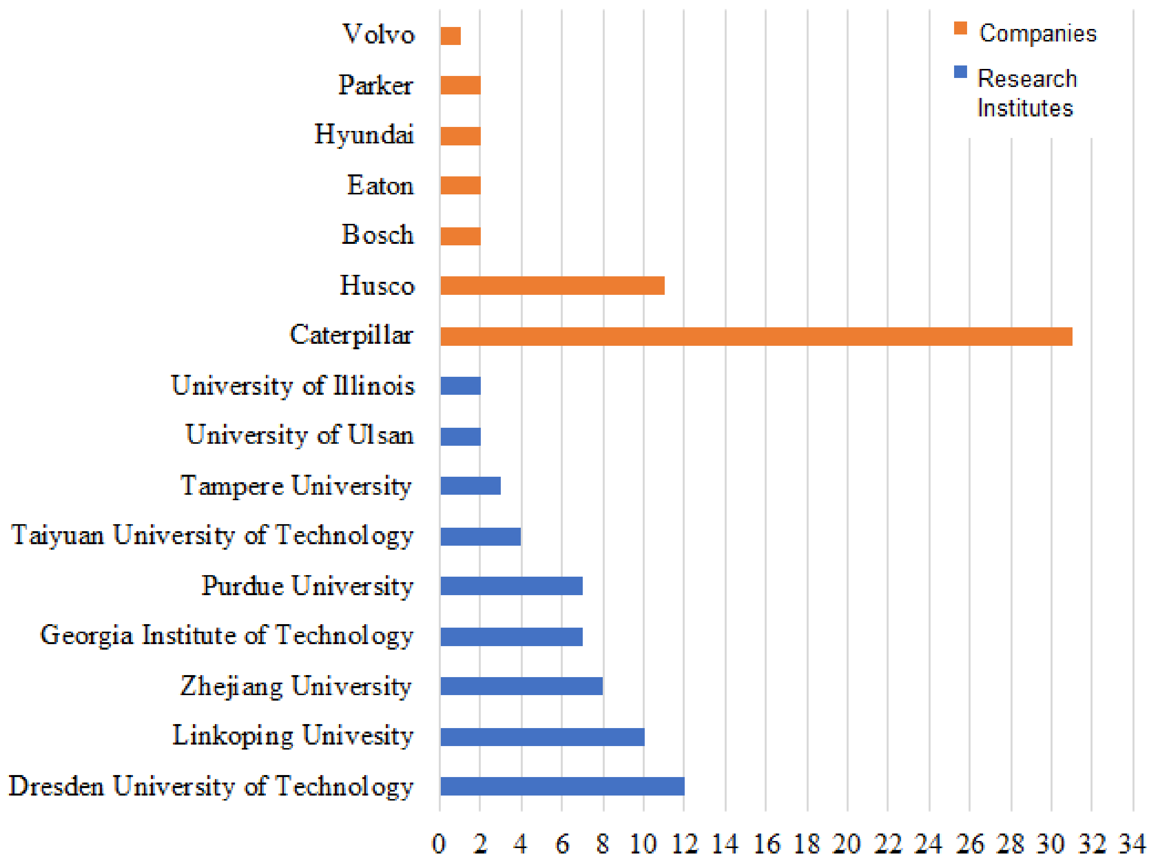

Fig. 1.5 Contribution of the leading research institutes and companies to the IM development.

Table 1.1 Main academic institutes developing IM.

University	Research Trends	Sample of Studies
Institute of Hydraulic and Automation at Tampere University of Technology, Finland.	1. Digital Hydraulic. 2. Hydraulic Manipulation Development.	1. IM Hydraulic System (Linjama et al., 2015, 2016). 2. Hydraulic Manipulations (Koivumäki et al., 2019).
Institute of Fluid and Mechatronics Systems at Linkoping University, Sweden.	1. IM and Load Sensing System. 2. Hybrid Hydraulic. 3. Real-Time-Simulation.	1. Load Sensing with IM (Axin, 2013; Dell'Amico et al., 2013; de Brun Mangs and Tillquist, 2018).
Institute of Fluid power at Dresden University of Technology, Germany.	1. Hybrid Hydraulic STEAM. 2. Developing Fluid-Mechatronics system.	1. Independent Metering and Decentralization for Energy Saving (Lodewyks and Zurbrügg, 2016). 2. Hybrid Hydraulic System (Vukovic et al., 2016).
The George W. Woodruff School of Mechanical Engineering at Georgia Institute of Technology, USA.	1. Hydraulics Component Development. 2. Intelligent Control of Hydraulic Manipulators	1. Poppet Valve Developments (Opdenbosch et al., 2009b; Opdenbosch et al., 2008). 2. Independent Metering System (Shenouda and Book, 2005a, 2008).
State Key Laboratory of Fluid Power and Mechatronics System, Zhejiang University, China .	1. Development of Independent Metering Switching Methods. 2. Hydraulic Drive Motion Improvement.	1. Independent Metering Mode Switching (Ding et al., 2016). 2. Energy saving (Xu et al., 2015; Ding et al., 2019).
Maha Fluid Power Center, Purude University, USA.	1. Hydraulic Components Modelling. 2. Mobile Hydraulic Systems	1. Load Sensing with IM (Campanini et al., 2017; DeBoer and Yao, 2001). 2. Modelling of Components (Liu and Yao, 2006).
Key Lab of Advanced Transducers and Intelligent System , Taiyuan University, China.	1. Hydraulic Manipulation System. 2. Modelling of Hydraulic System	1. Independent Metering Performance Analysis Ge et al. (2015)
School of Mechanical and Automotive Engineering, University of Ulsan, South Korea.	1. Independent Metering Implementation. 2. Hydraulic Manipulation Energy	1. IM Systems (Nahian et al., 2015). 2. IM Energy Saving (Park et al., 2016).
Institute of Mechanical Engineering, Illinois, USA.	1. Dynamic and Control	1. Valve Performance (Zhang et al., 2002b).

The research reported in this thesis is based on an in-depth review of these systems and the introduction of a novel hydromechatronics independent metering system. The term hydromechatronics represents an integration between the hydraulic elements and the mechatronics systems (Weber, 2018). This integration is a new industrial trend and that relies on software implementations. Therefore, the proposed system meets the rules of the hydraulic independent metering approach using a modern rotary flow control valve, part of which was proposed by Okhotnikov et al. (2017). The rules of the IM are controlling the hydraulic actuator velocity and allow fluid regeneration and recuperation. Combined with advanced control, driving, and communication techniques, (Figure 3.5), the new system represents the main theory of the research milestone in this technology. The proposed system was termed as " Micro-Independent Metering" (MIM), and the main reason for selecting this name will be explained in more detail later in this thesis. However, it was primarily selected due to the stepper motor driving technique used which was micro-stepping. Each step can be electronically divided into many steps resulting in a more controllable operating system. More details about the MIM system configuration are introduced in Chapter 3. During this investigation, specific questions were answered. They are included in the following section.

1.2 Research Questions

The aim of this research is to investigate the implementation of independent metering in a hydraulic application using a new stepped rotary flow control valve. The research questions are as follows:

- Has micro-independent metering been applied for control of hydraulic applications? (Chapter 2).
- What is the dynamical performance of the modern stepped rotary flow control valve? (Chapter 4).
- What will be the effect of replacing the traditional control valves conventionally used for independent metering with a new stepped rotary flow control valve? (Chapters 3 and 5).
- What will be the effect of the new configuration on the actuator's velocity performance comparing with the traditional configuration? (Chapter 5).

1.3 Aims and Objectives

The main aim of this research is to propose a novel control system using a new generation of rotary valve that is independently operated compared to the spool valve which is conventionally used in hydraulic applications. The system is characterized by using mechatronics techniques to create an independent metering method for hydraulic applications. This integration replaces the hydro-mechanical system by programmable control techniques that rely on electronics components. The system can control the velocity of the hydraulic actuator, cylinder or motor, according to the user requirements and adjustments. Also, it saves more energy compared to the traditional systems by incorporating energy regeneration. To achieve this aim, there is a need to :-

- Investigate the new valve dynamical performance and controllability.
- Investigate different independent metering architectures and select the most suitable configuration to replace the traditional valve with the new one.
- Research and investigate an advanced control algorithm that fits this new configuration. Since stepped rotary valves are inserted in the system instead of the traditional valves, the actuation technique must also be changed from the solenoid to stepper motors. This change, although producing new advantages, increases the complexity of the system. To do that a new control system needed to be designed. As illustrated in Figure 1.6, the presented control system is an open loop and the driver closes the loop by observing the output which is the actuator position. The system measures different pressure parameters and uses them to produce calculated flow rates according to the control algorithm that is implemented in the system's processor.

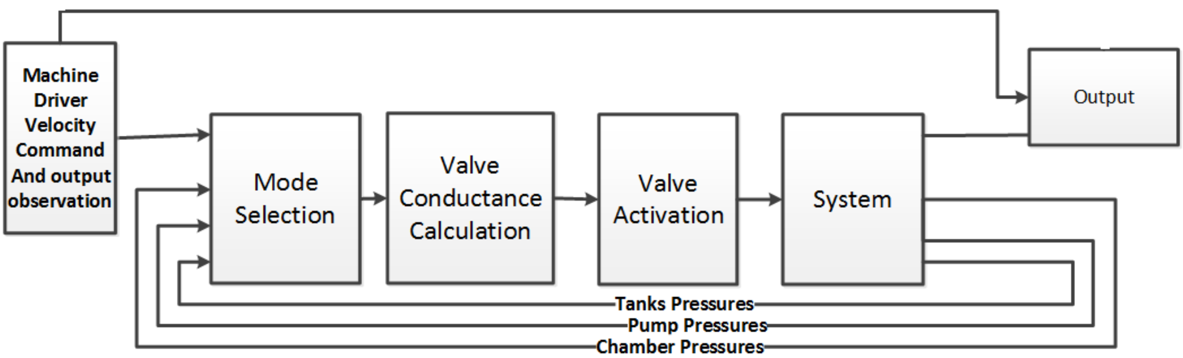

Fig. 1.6 The MIM programable control system

- Investigate and develop an electronic system that performs the main control algorithm. This new programmable control system relies on a combination of electronics, sensors and software.

- Investigate the effect of the control system on the cylinder velocity performance.

The main objectives are as follows:

1. Develop a flow control valve using the rotary orifice which was evolved by Okhotnikov et al. (2017).

2. Design the valve model and study the dynamical response. Conduct root locus analysis to study valve stability.

3. Design a control algorithm for the new IM configuration. The traditional control algorithm which was developed for the poppet valve is based on an infinite number of combinations between the used valves, but the valve in the new configuration acts according to finite positioning, therefore the new control algorithm has to consider finite combination.

4. Design a simulation model for the system and implement different conditions to test the system performance using the Software-in-Loop Simulation (SIL).

5. Design a Hardware-in-the-Loop (HIL) test platform which contains the electronics controllers, motor drivers, communication, joystick, screens, and the system model.

6. Test the practical reaction of the system under different simulated operation conditions.

1.4 Constraints

The main constraints in the research are financial and lack of facilities such as some advanced equipment. These limitations have been overcome using alternatives as follows:

- To evaluate the friction model of the rotary orifice, one rotary orifice was manufactured using 3D printing. Therefore, the maximum pressure drop which was applied to the valve during tests was 1 MPa.

- Lack of a fast response and high resolution flow meter where the orifice flow rate and it's model can be validated. To evaluate the flow performance, the pressure drop was fixed at 0.25 MPa, 0.5 MPa ,and 1 MPa pressure drops. At each pressure drop, the rotary orifice rotated 10 degrees and the flow was measured by a traditional flow meter.

- Lack of real time processor (Target Hardware) where the model can be uploaded and interfaced with the electronic system. A qualitative study was performed using the HIL test. The HIL used in the test contained a normal PC connected with Arduino processors and many stepper motors with their drivers. The test was performed on determined situations to reduce the effect of data communication problems between the PC and the processors.

1.5 Contributions and Key New Knowledge

This investigation is about the design and analysis of a new hydromechatronics control system using model-based design. The contributions to knowledge resulting from these investigations are as follows:

1. This study investigated the frictions that exist in the rotary orifice and their effect on the control of the new rotary valve. The multi-step response analysis of the rotary valve model indicated that the friction torque of the new rotary orifice is affected by the initial conditions at the rest points when using the full step driving technique. To reduce this effect, the micro-stepping technique was introduced, usually common in electrical drives, in order to drive the hydraulic valve. This has resulted in much smoother operation and better controllability of the new hydraulic drives.

2. In this investigation, the root locus technique was used to investigate and analyse the rotary valve stability. The study indicated that the new rotary valve can remain stable throughout its entire range of operation with the pressure drop of up to 35 MPa. In addition, this analysis demonstrated that there is a direct relation between the distribution of the system's poles due to the effect of the pressure drop and the friction coefficient.

3. A Close Value Detection (CVD) technique was developed, as part of this investigation, to create a link between the infinite position method used in poppet valves and the finite number of possible positions using a stepper motor.

4. The MIM (micro-independent-metering) system is able to handle and manage fluid disturbances that can affect the fluid flow into and out of the hydraulic cylinder. This in turn has improved the control of the velocity of the hydraulic cylinder.

1.6 Model Based Design Methodology

Due to the complexity of mechatronics systems, the Model Based Design was selected to be the main approach for the project. This method is used in many applications such as Aerospace, Mechtronics and Robotics (Toman et al., 2011) and (Lennon and Mass, 2008). For hydraulic mobile machines, the model based design including HIL was developed in (Lim et al., 2005) and (Prabhu, 2007). It has been used for independent metering development by (Shi et al., 2018). The INCOVA company used this technique to develop an intelligent control valve (Corey, 2019). It was also used for flight control developments (Karpenko and Sepehri, 2009). Figure 1.7 shows the main steps of this methodology. It starts by determining the main requirements, such as the controlled parameters performance and limitations. Next, forming the system model or the plant model and the controller model to perform analysis using the Model-in-the-Loop and the Software-in-the-Loop. After that, the integration of the models, at the simulation platform, and the system hardware to start performing the Hardware-in-Loop test. If some of the hardware components are not installed and substituted by their models, the test is called a Model-in-the-Loop test as indicated by Plummer (2006).

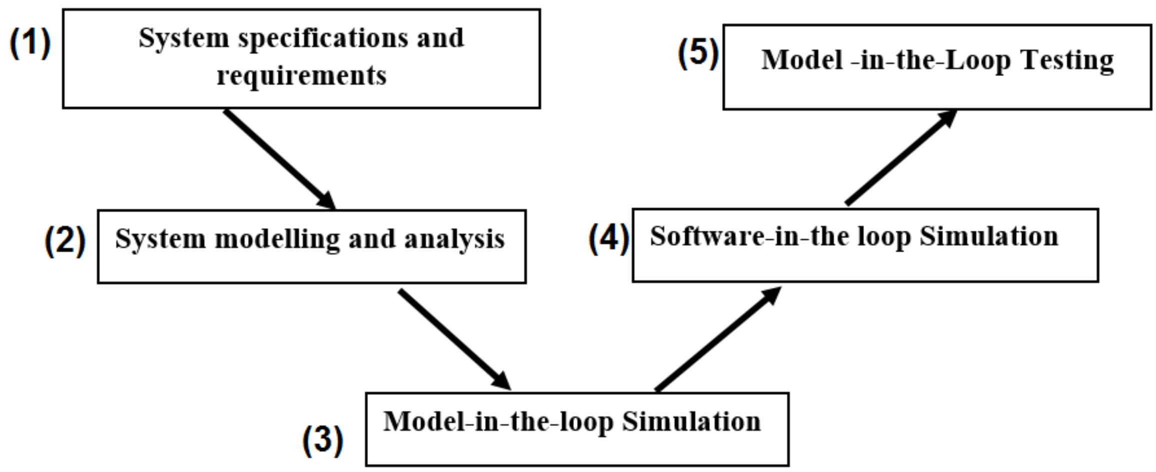

Fig. 1.7 The flowchart of the Model-Based design methodology

In this research, to regulate the system's specifications and requirements, the IM methodology was mathematically analysed. The response analysis of the valve nonlinear model was performed and evaluated. The valve model containing the stepper motor model combined with the rotary orifice model was used to analyze the driving techniques of the valve which could be a full step driving technique or a micro-step driving technique.

For the system modelling and analysis, a linear model for the stepped rotary flow control valve was developed to highlight the valve performance limitations that help to determine the testing technique. At this stage, a root locus analysis was used to determine these limitations.

In the third and the fourth stages, the control algorithm was modelled using State-Flow. This model helps to test the algorithm performance and improves it before moving into the code development. This State-Flow design is used to control the valve in the Software-in-the-Loop simulation. In the SIL simulation, joystick commands are implemented into the controller and measurements for the four-valves were detected. The measurements include the opening angles, the flow rate, the cylinder position, the cylinder acceleration and the pressure changes inside the cylinder chambers.

Regarding the model or hardware-in-the-loop stage, the hardware was designed to consist of four stepper motors and their drivers controlled by two ARM processors which are connected via serial communication to the model to analyse the system hardware performance.

1.7 Structure of the Thesis

This section shows the structure of the thesis. Figure 1.8 shows the main structure of the thesis.

- Chapter 1 Background of this research. It contains the main research points, the aim and the objectives, the limitations, the methodology, and the key contributions to knowledge.

- Chapter 2 State of the Art of Independent Metering Technology. In this chapter, different technologies and their interactions with the Independent Metering are reported. Moreover, the IM techniques, operation modes, valves, control systems, and layouts are reviewed.

- Chapter 3 Proposed Novel IM system. This chapter describes the proposed system, architecture, applications, advantages,and future potentials.

- Chapter 4 Independent Metering Mathematical Analysis. This describes the operation of IM modes, the valve control, and the anti-cavitation procedure. These mathematical models are used to build the control algorithm which is uploaded on the main control unit such as the DSP processor. In this research, an Arduino board was selected for this task because of its good performance and low price.

- Chapter 5 The Stepped Rotary Flow Control Valve Modelling and Performance Analysis is about the new control valve. In the chapter, analysis of the design, performance, and limitations are included. The performance was analysed using two methods which are multi-step response and Root Locus.

- Chapter 6 Software-in-the-Loop Simulation of the MIM System discusses the building of a Software-in-the-Loop simulation of the system. This includes building a State-flow for the novel algorithm, testing the operation modes, and comparing the performance with other systems to determine the main characteristics of the new design.
- Chapter 7 Hardware-in-the-Loop Testing of the MIM system covers the testing of the system performance using the Hardware-in-the-Loop technique. This chapter includes a hardware platform design and interfacing with the hydraulic model. The performance of the IM operation modes is evaluated in this chapter.
- Chapter 8 is the conclusion and recommendations for the future work.

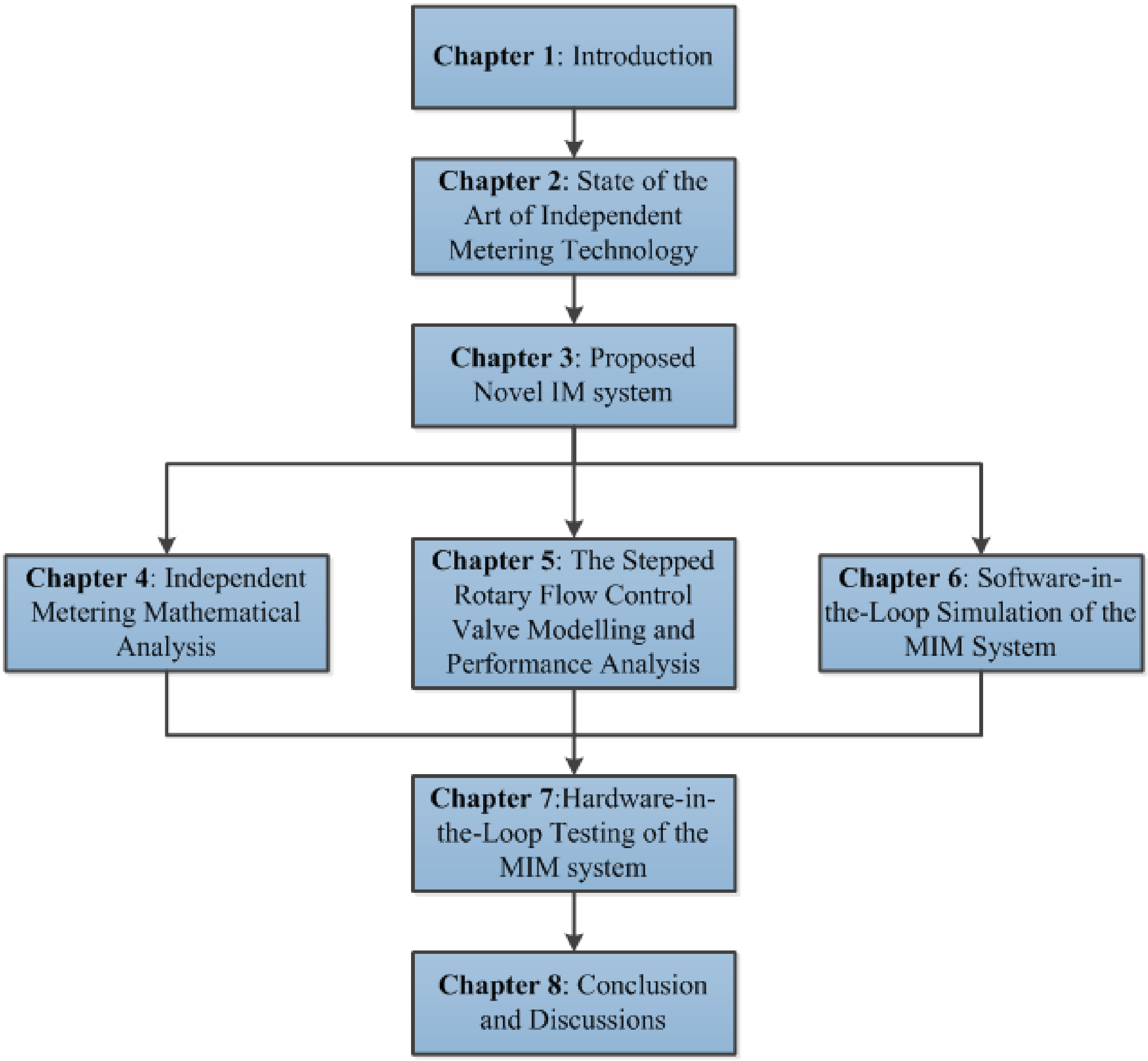

Fig. 1.8 The structure of the thesis.

Chapter 2

State of the Art of Independent Metering Technology

2.1 Introduction

This chapter provides an overview of the previous research on Independent Metering (IM) technology. Firstly, it explores the electrohydraulic systems that have been developed to improve the energy saving and controllability, and illustrates how they interact with the Independent Metering. Secondly, it investigates in depth the IM system from different aspects including, the IM valves, the IM operating modes, and the IM control systems. Thirdly, it represents the IM operating modes and their switching techniques. Finally, it analyses the IM control systems and their layouts.

For more than three decades, researchers from academia and industry have been developing systems to improve both hydraulic equipment and machine performance. These improvements range from pumps, valves, actuator and circuit configurations. The hydraulic circuits arrangements include the traditional Open center valve, Load sensing, Digital Hydraulics, Hybrid Systems, and the Independent Metering. These configurations have many interaction points between each other as explained in Section 2.2. IM valves could be either a poppet or spool, or a combination of the two types, and their implementations are summarized in Section 2.3. Different control parameters can be used to develop an IM system. These parameters, which are pressure, flow, and speed, with their different control techniques are studied in Section 2.4. In Section 2.5, the IM operation modes and their work principles are included. As there are power and velocity limitations for every mode, selecting a suitable operation mode based on these limitations is necessary, to meet the main aims of the IM technique which are saving more energy and increasing controllability. The operation modes switching techniques are discussed in Section 2.6. The layouts of IM among different hydraulic machines and equipment are investigated in Section 2.7.

This literature review relates to many sources which include industrial patents, especially from the registered Caterpillar patents, original published articles from Web of Science and the British Library, and different PhD studies from Georgia institute of technology, University of Illinois, Purdue University, Tampere University of technology. Many keywords were used during the research and some of them are Independent Metering, Separate Metering, Fluid Decoupling, Individual Metering, and Programmable Hydraulics.

2.2 Hydraulic Driving Systems

As indicated in Murrenhoff et al. (2014), the three main requirements to improve hydraulic machines' efficiency are as follows:

1. Reducing throttle losses,
2. Avoiding inefficient operating points,
3. Recovering potential energy.

Different methods were used to satisfy these requirements. They are Load sensing (LS), digital drive, holistic systems and independent metering. LS is one of the most common systems in hydraulic applications (Dengler et al., 2011). It was mainly designed to save energy by producing the required amount of flow rate or pressure for the consumer (Krus, 1988). This pressure is produced by a Variable Displacement Pump (VDP) based on the highest actuator pressure feedback (Sakurai et al., 2002). The conventional LS systems were hydro-mechanical. The shortcomings of this traditional system are poor damping and inconvenient performance (Hansen, 2009; Lovrec et al., 2009). The insertion of electronics was performed by Casappa and Walvoil about 30 years ago (Lettini et al., 2010). An example of practical implementation of electronic load sensing control was performed by HUSCO International, Inc (Jackson et al., 2006). LS systems can be split into two main categories, Open-Centre (OC) and Closed Centre (CC) Hydraulic systems. The OC uses a fixed displacement pump, and the CC uses a variable displacement pump (Dell, 2017). The former has more losses than the latter, especially when the load pressure is high and the required flow rate is small (Scherer et al., 2013). Adding a pressure compensator to the CC leads to the Load Sensing Pressure Compensated LSPC technique which is shown in Figure 2.1. The pressure compensator reduces the influence of the pressure to the controlled flow. The LSPC's drawbacks are oscillations and a pressure margin which are produced in the mechanical system by the compensator due to the produced poor damping and increased dynamic complexity. The pressure margin or control pressure is an extra pressure needed to be produced by the pump. The pump pressure should be more than the demand from the most loaded actuator. This margin keeps the pressure level at the pump higher than the pressure drop by the pressure compensator (Eriksson and Palmberg, 2011).

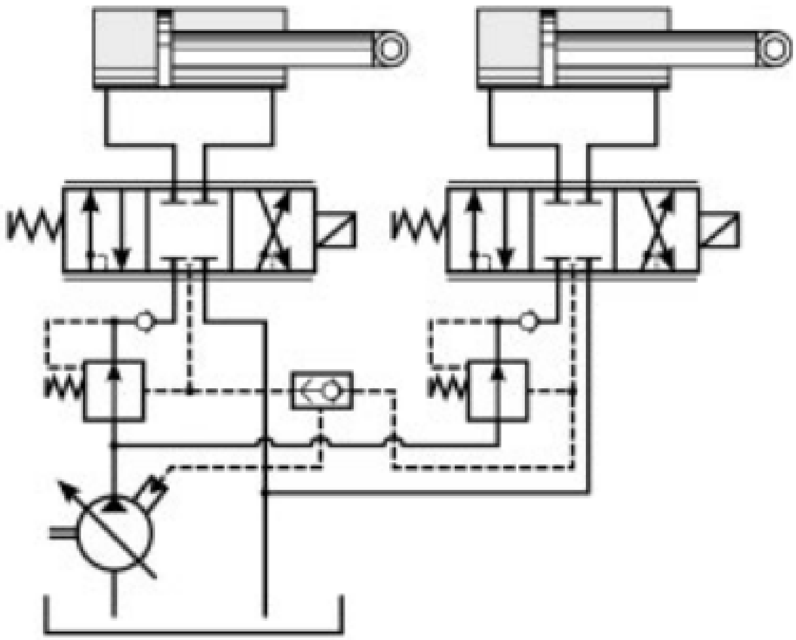

Fig. 2.1 Load sensing pressure compensated (LSPC) circuit where a variable displacement pump uses the pressure feedback to produce the required flow and pressure (Eriksson and Palmberg, 2011).

A conventional spool valves controlled load sensing system still suffers from throttle losses due to the mechanical connection between the inlet and the outlet (Murrenhoff et al., 2014). This connection is illustrated in Figure 2.2. To reduce these losses the mechanical connection should be broken and this leads to the IM technology (Smith and Mather, 2008). Combining both systems IM and LS is a suitable approach to save more energy and produce better controllability. It also transfers functionality from hardware to software, reduces the work cycle time, and implements electronically tunable operation modes (Liu et al., 2016; Ding et al., 2018b).

An advanced practical implementation using both systems was developed by Caterpiller Inc (Kleitsch, 2017). Also, an algorithm was developed for the combined systems when check valves are not used between the valve arrangement and the pump (Huang and Lunzman, 2003), and an algorithm when the required velocity flow is more than the pump flow (Aardema and Koehler, 1999).

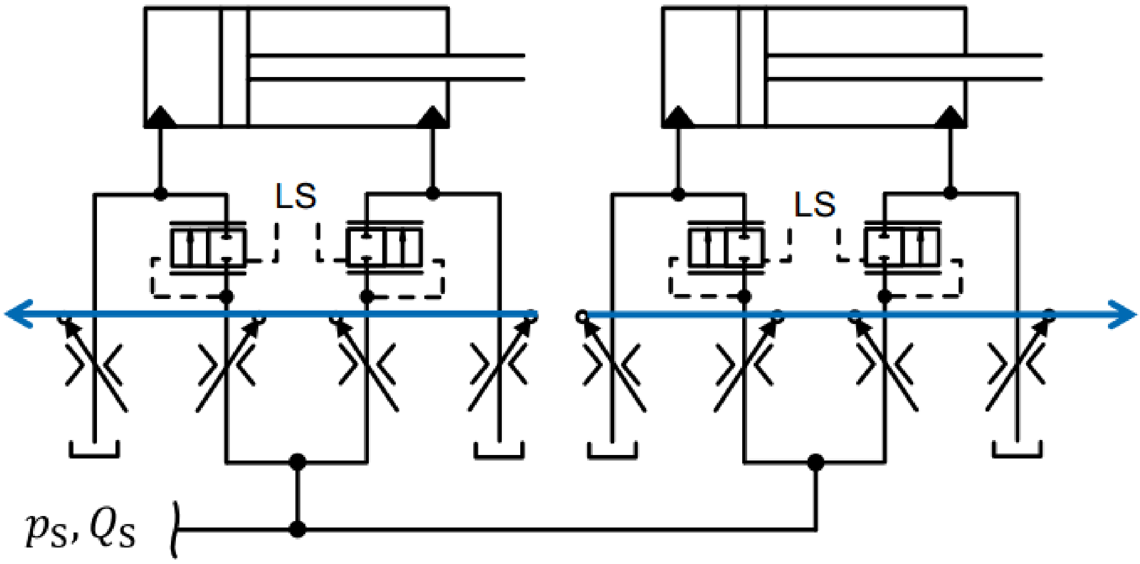

Fig. 2.2 The mechanical connections between the actuator meter-in and meter-out due to the traditional spool valves. LS represents the load sensing signal, Ps and Qs represent the main pressure and flow sources from the pump (Murrenhoff et al., 2014).

Digital hydraulics is a term describing the digitalization of hydraulics. The main idea is to replace the continuous variable with a discrete one. This covers different hydraulic equipment such as valves, motors, accumulators and pumps (Huova, 2015). For example, a digital pump-motor was used to implement a digital hydraulic power management system (DHPMS) (Heikkilä and Linjama, 2013). A Digital Flow Control Unit (DFCU) is a unit that connects a group of on/off valves in a parallel layout and their response is presented proportionally. These valves are not prone to leakage are reliable and are insensitive to oil contamination. Using the digital valves to form an IM system adds extra advantages to the traditional IM that uses poppet or spool valves (Ketonen and Linjama, 2017b). Digital hydraulics can be controlled by three main techniques as follows (Laamanen and Vilenius, 2003) and (Karvonen et al., 2014):

1. Pulse number modulation (PNM).
2. Pulse code modulation (PCM).
3. Fibonacci number.

The main drawbacks of digital fluid systems are as follows:

1. Larger overall size comparing with traditional valves.
2. The cost which depends on the application.
3. Noise and pressure peaks.

4. The flow control is based on a number of discrete steps rather than infinite control due to the number of valves in the digital array.

The Institute of fluid power drive and controls in Aachen, Germany, produced a new configuration for a hydraulic excavator called STEAM. It aims to reduce the valve control losses as well as the engine losses by hybrid architecture (Vukovic et al., 2016) and (Vukovic et al., 2013). The main fundamental principles concluded for the STEAM systems are as follows:

1. Using a constant pressure system saves more energy.

2. Using an intermediate pressure line reduces throttle losses.

3. Availability of regeneration and recuperation increases the energy efficiency.

The architecture of the STEAM system offers the following advantages:

1. Constant pressure system enables a fixed-point operation for the internal combustion engine (ICE) in the machine.

2. Using three pressure lines increases the number of operating states for each cylinder.

The main drawback of STEAM systems is poor controllability as the system is based on different pressure lines (Vukovic et al., 2014), which produces high oscillation during switching between the pressure levels (Dengler et al., 2011).

The mentioned technologies aim to save more energy and they intersect with IM. For example, IM was implemented using the digital hydraulic concept. STEAM systems can be applied by using IM. Also, a variable displacement pump can be used with IM. To conclude, independent metering, as mentioned before, is based on breaking the mechanical connections between metering ports. This requires different valves rather than the traditional spool type.

2.3 Independent Metering Valves

Generally, hydraulic valves used to implement IM can be classified into 3/3 and 2/2 valves (Eriksson and Palmberg, 2011). These are used to make different forms of decoupling between the input and the output. Decoupling can be mechanical or functional, as summarized in Figure 2.3 (Weber et al., 2016). The mechanical decoupling is based on changing the valve kind from 3/3 or 4/3 into 2/2 proportional valves which lead to different configurations of IM. The functional decoupling relies on the switching and proportional valves, where the functionality depends on the switching valve direction combined with flow controlled by proportional valves. The common configurations of the IM are the mechanical decoupling 3 and 3+SC. Additional valve enables a precise control of direct cross port flow.

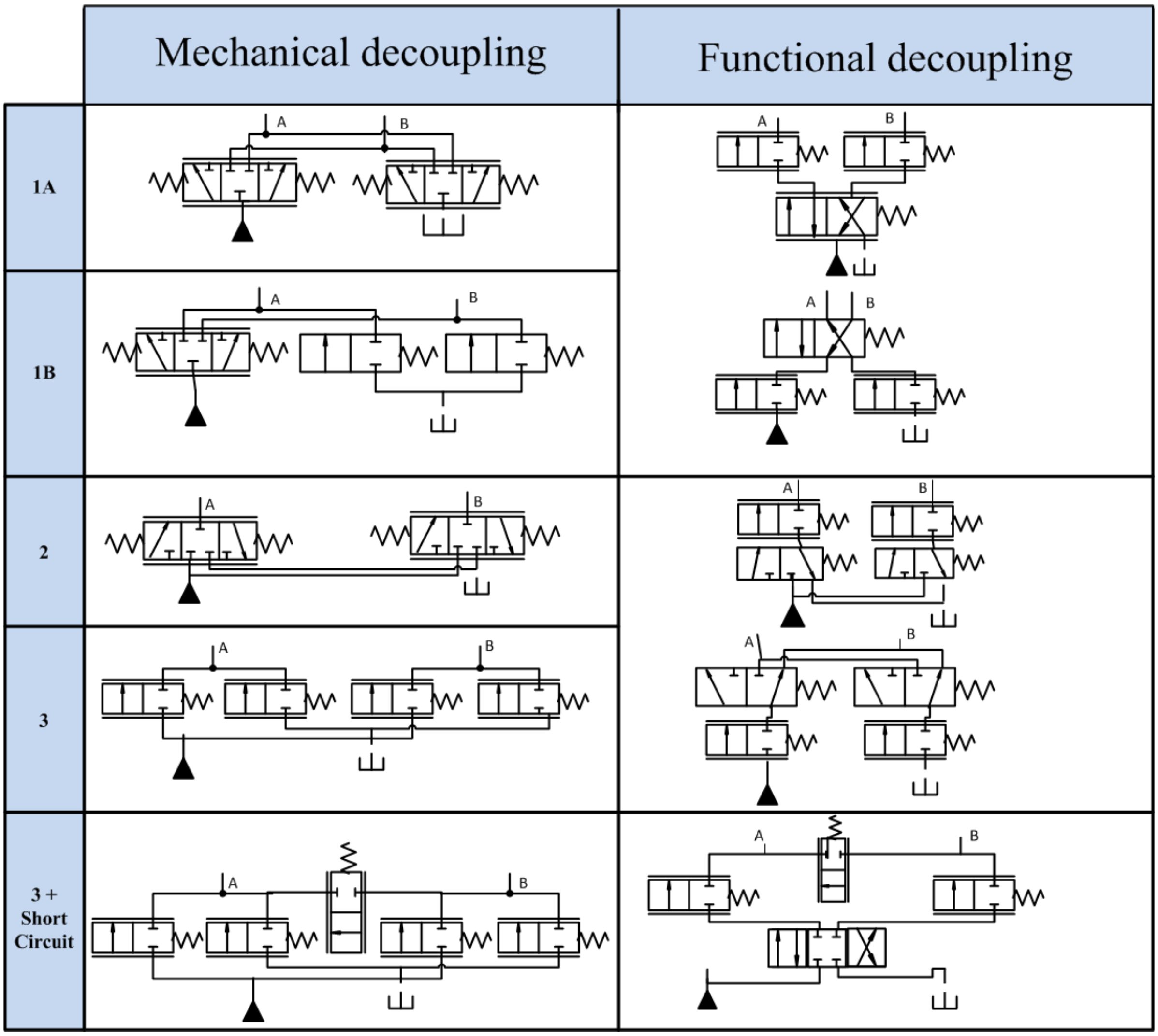

Fig. 2.3 Two types of decoupling which are mechanical and functional. These techniques are used for Independent Metering configuration (Weber et al., 2016).

The first iteration to implement IM using 4/3 valves was by Monsun-Tison (Eriksson, 2010), and the system was called MONTI. An example of IM configuration using two 4/3 valves is Caterpiller patent (Crosser, 1992). Then, the application of 3/3 valves were introduced by EATON company. 2/2 valves were developed by many companies such as Deere, Moog and Caterpillar (Smith and Mather, 2007). These valves are cartridge poppets and are widely used for IM control. The schematic design of the Valvistor valve is shown in Figure 2.4. It's work principle is similar to the electronic transistor where a pilot circuit drives a larger main flow. The main difference between P_b and P_a generted by Q_p moves m_m which is the main poppet for a distance x_m. The pilot stage which contains Pulse Width Modulation (PWM) solenoid controls the Q_p flow. A block arrangement containing four valves for every actuator was developed by Caterpillar (Smith, 1999) and (Hajek Jr and Tolappa, 2004). A programmable valve is a term that represents a configuration of a five electronically controlled poppet valves developed by Liu and Yao (2004). This valve performance was evaluated by Zhang et al. (2002a) and Eriksson (2010) and, their model was developed by Liu et al. (2002). After the manufacturing process of the independent metering arrangement which contained four of these valves, a deviation in their performance was noticed which affects the IM system overall and to overcome this a calibration algorithm was used (Yoo et al., 2009). A novel auto-calibration state-trajectory control method for IM uses a four poppet valve configuration or a Wheatstone Bridge developed by Opdenbosch et al. (2011) to adjust the deviation in valves performance. Inserting electronics and sensors to IM valves improves the controllability and overall system performance. HUSCO's INCOVA developed a brand of this configuration (EATON, 2010). Figure 2.5 shows the configuration of a twin spool valve architecture. Using electronics and sensors in these hydraulic systems increase the failures due to the harsh environment, and to overcome this drawback, EATON improved a failure operational control algorithm (Rannow, 2016). The digital hydraulic approach used a Digital Flow Control Unit (DFCU). Different kinds of valves are used for digital hydraulics. These are bi-stable on/off valves improved by Uusitalo, a monostable needle improved by Karvonen and a wide array of digital hydraulic systems improved by Bucher Hydraulics (Karvonen, 2016). These valve arrangements can be used for IM as simulated by Ketonen and Linjama (2017b). Table (2.1) includes the IM valves that have been produced to implement in the independent metering system in the mobile machines.

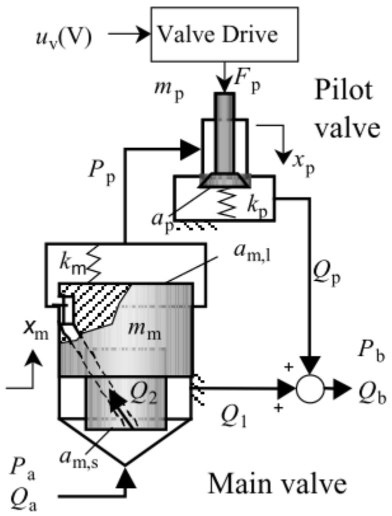

Fig. 2.4 The main schematic of electrohydraulic poppet valve where Q_p is the pilot flow, m_m is the main poppet, P_P is the pilot pressure, P_a is the main pressure source, Q_2 is the feedback control pressure, Q_b is the total flow Zhang et al. (2002a)

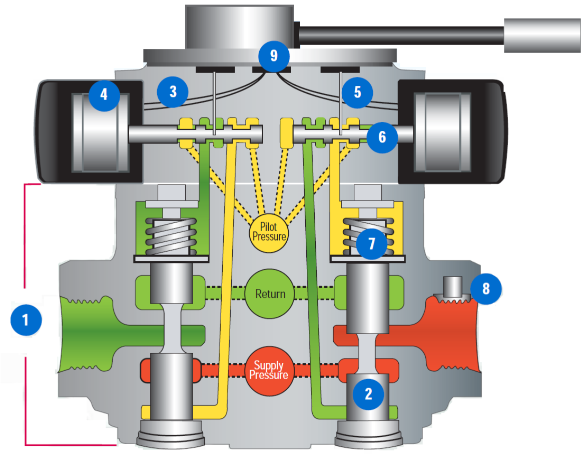

Fig. 2.5 The Eaton's Ultronics™ twin independent spool valve (EATON 2010). 1 - main stage valve block, 2 - independent spool for metering, 3 - pilot valve, 4 - low power voice coil actuator, 5 - centring spring, 6 - pilot spool, 7 - position sensor, 8 - thin film pressure sensor, 9 - embedded micro electronics

Table 2.1 Manufactured flow control valves for the independent metering applications

Manufacturer	***Product***	***Flow Rate***	***Hysteresis***	***Response Time***	***Pressure Drop***
EATON	EPV10(EATON, 2019).	30 L/min	$< 4\%$	35 ms	200 bar
BUCHER	WS22GD(BUCHER, 2016).	30 L/min	$< 5\%$	20 ms	350 bar
EATON	CMA90(EATON, 2016b).	90 L/min	sub-micron	24 ms	25 bar
EATON	CMA200(EATON, 2016a).	200 L/min	sub-micron	24 ms	35 bar
HUSCO	EHPV(International, 2019).	$75, 150, 800$ L/min	very Low	100 ms	15 bar

To summarize, different valves have been used to implement IM. Table (2.2) (Ding et al., 2018b), represents the main characteristics of these valves. The next section is a review of the control methods for comprehensive IM configurations.

Table 2.2 Different types of flow control valves and their characteristics

Characteristic	*Spool*	*Poppet*	*Digital*
Flexibility	Low	Medium	High
Flow accuracy	High	Medium	Low
Redundancy	Low	Medium	High
Manufacturing cost	High	Medium	Low
Anti-leakage	Low	Medium	High
Sensitive to contamination	High	Medium	Low

2.4 Independent Metering Control Systems

Inserting software control as a main part of the hydraulic system introduces intelligent control techniques. A hydraulic programmable control system contains three main levels which are illustrated in Figure (2.6) (Xu et al., 2015). The upper level is the mode switching level which allows energy regeneration and recuperation. It performs the mode switching to select the most efficient mode which allows energy regeneration and recuperation. The selecting technique relies on the system's status such as pressure and velocity. In the lower level, the selected valves in each mode are activated to produce a flow rate which controls the cylinder speed. The primary level is to control the pump pressure and flow (Ding et al., 2018b). This review focuses on the upper and lower levels.

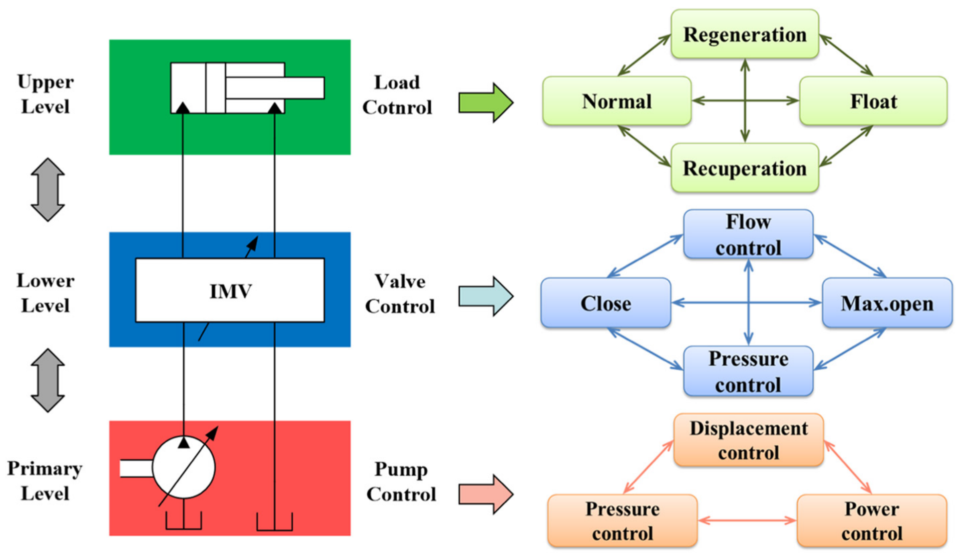

Fig. 2.6 The main three control levels of programmable hydraulic control system (Ding et al., 2018b).

For the lower level, different control parameters can be used for independent metering as shown in Figure 2.7. These parameters can be separated into flow, pressure difference and displacement control. As the flow and displacement controls rely on electronic sensors, they do not exist in hydro-mechanical types that use pure mechanical components.

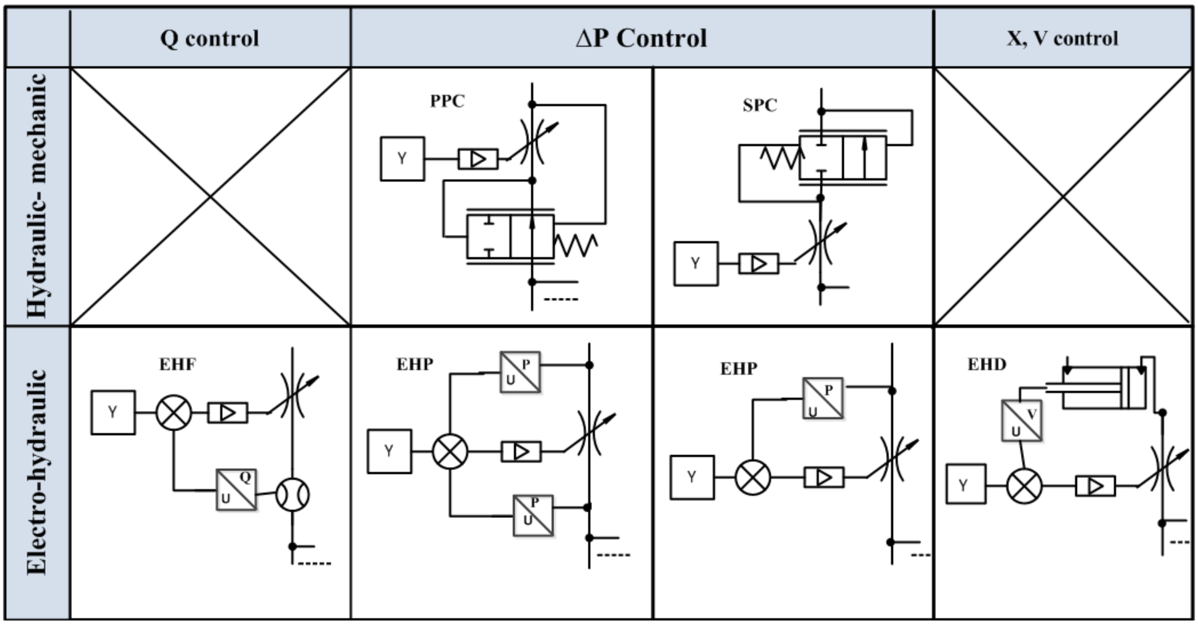

Fig. 2.7 Different control parameters implemented for the IM, where PPC-Primary pressure compensator, SPC-secondary pressure compensator, EH-Electrohydraulic, P-Pressure, F-Flow, and D-displacement (Weber et al., 2016).

As the separation of actuator metering increases the degrees of freedom, different control strategies can be applied and investigated on the system. Three main control systems can be implemented for IM as shown in Figure 2.8 (Weber et al., 2016).

The first approach which is Feed-forward control, is mainly used in mobile machinery, and the operator closes the loop (Weber et al., 2016) and (Eriksson, 2010). The second type is closed loop feedback control, Single Input Single Output (SISO), to ensure that the output follows the trajectory command. The last one which is Multiple Input Multiple Output (MIMO), is a closed loop control system. It is used to control more than one target variable where different states are controlled at the same time. These states are coupled together. The decoupling between them can be performed using MIMO control. A study of MIMO control approaches and the pressure compensator effect was conducted by Sitte and Weber (2013). Different iterations were performed to decouple these factors. Decoupling between the actuator velocity and pressure was achieved using a combined pump and valve control (Pedersen et al., 2013). The aim of the study by Jansson et al. (1991) was to decouple the response and the pressure level in the hydraulic actuator using four orifices. Some researchers designed decoupling between the velocity and pressure in the hydraulic actuator and this requires velocity feedback (Jansson et al., 1991). This control approach achieved a good decoupling, but it depends on the quality of

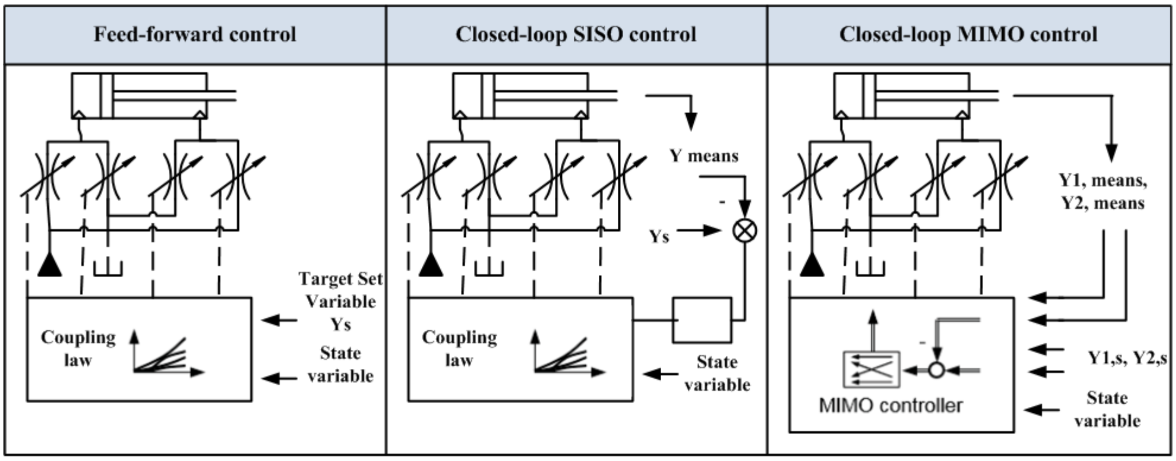

Fig. 2.8 Different control approaches for the Independent Metering (Weber et al., 2016).

the velocity feedback signal. A H_∞ loop-shaping approach without taking measures to dampen the system was investigated (Pedersen et al., 2013). Conversely, the pressure compensator is an important component reducing cross-talking or the coupling between two valves (Sitte and Weber, 2013) and (Eriksson, 2010). Moreover, a flatness-based control algorithm was used to allow manipulation of the cylinder speed and the pressure level separately. It was used in the inner layer for the continuous mode switching technique within the Modicieny approach (Kolks and Weber, 2016b) and (Kolks and Weber, 2016a). On the other hand, load oscillation appears during movement using the separate meter-in separate-meter out (SMISMO) system, precisely when the load was stopping after moving. An optimal approach based on the Hamiltonian method was developed by Rath and Zaev (2017).

Regarding single loop controllers, PID controllers are widely used to activate valves with their flow maps. The Fuzzy PID controller was improved and enhanced the dynamic performance of two stage servo valves to form an independent metering system (Zhong et al., 2017). Also PID controllers are used to activate variable displacement pumps (Xu et al., 2015). It was used for velocity and pressure control for actuators in multifunction systems (Hansen et al., 2011) and(Borghi et al., 2014). It was also used to improve performance for a hydraulic excavator (Zhang et al., 2009).

Adaptive control is an approach that changes the controller in real time. This maintains the desired level of a control system especially when the parameters of the model are uncertain or nonlinear as in hydraulic systems (Watton, 2009). Adaptive control was used for the five valves scheme (Liu and Yao, 2008) and (Yao and DeBoer, 2002). Usually, IM is configured using four valves which is called a Wheatstone Bridge. The additional valve enables precise control of direct cross port flow. This control technique was included in an improved hybrid system using a three-level control system and an accumulator (Lu and Yao, 2014). Moreover, the indirect adaptive robust dynamic surface control (IARDSC) method was developed to enhance the performance of the IM system by reducing the internal uncertainties and external disturbances using indirect adaptive robust controller (IARC), while the dynamic surface control (DSC) was used to deal with the inherited explosion of terms (Chen et al., 2018). As the IARC is good for constant parameters estimation, it's performance is poor when parameters are changing quickly. The effect of fast parameters change produces an explosion of the term and that is used to overcome it (Chen et al., 2017). Vibration is one of the drawbacks of the IM method due to the lack of damping on meter-out. A hybrid control method combining dynamic pressure feedback and an active damping controller was designed, and a pole-zero assignment approach was implemented to capture the optimal damping under a large range of operating conditions (Ding et al., 2017). Shi et al. (2018) developed a method to improve the positioning of a cylinder attached to independent metering valves. The approach is to split the IM operation modes into extension, retraction, and positioning. The positioning mode aims to improve the cylinder position despite the energy consumption. In this mode, the two valves are the inlet and the outlet. They are linked and controlled simultaneously, similar to the traditional spool valve. Finally, to save more energy, IM implements different modes of operations which are the topic of the next section.

2.5 Independent Metering Operation Modes

For the high level of programmable hydraulics, the independent metering structure allows different operating modes which reduce power consumption. These operation modes represent certain fluid paths in and out of the actuator. Also, they are variable due to load changes and supplied pressure. Some of these modes, such as regeneration, were not achievable using 4/3 valves (Shenouda and Book, 2005b). The main scheme used by Shenouda and Book (2005b) and Alkam (2014) was the Wheatstone Bridge as shown in Figure 2.9.

This configuration allows five modes which are as follows:

1. Power extension mode (PE).
2. Power retraction mode (PR).
3. High side regeneration extension mode (HSRE).
4. Low side regeneration extension mode (LSRE).
5. Low side regeneration retraction Mode (LSRR).

The power extension mode is performed by supplying the fluid from the pump to the actuator head chamber using the inlet port, while the fluid is drained from the actuator to the tank

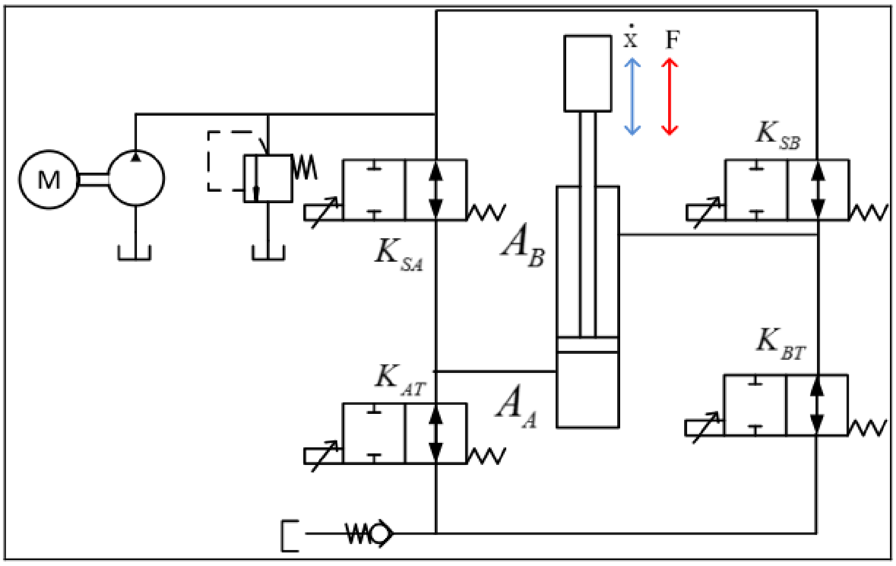

Fig. 2.9 The main IM diagram used by Shenouda (Shenouda, 2006) where K_{sa} is the valve between the pump line and the cylinder head chamber, K_{at} is the valve between the tank line and the cylinder head chamber, K_{sb} is the valve between the pump line and the cylinder rod chamber, and K_{bt} is the valve between the pump line and the cylinder head chamber.

using the outlet branch. The next operation mode is power retraction. Its the opposite of the power extension mode. These two modes are illustrated in Figure 2.10 and they are the most energy-consumable modes.

Regeneration modes are separated into high side and low side. The High Side Regeneration Extension Mode (HSRE) is shown in Figure 2.10. The high side regeneration is achieved when the fluid is passed from the rod chamber to the head chamber using the high connection point of the bridge. The recirculated flow is not enough, so the difference is supplied by the pump itself. The power extension mode provides more force than the high side regeneration extension while HSRE can achieve more speed than power extension (Shenouda, 2006).

The low side regeneration appears when fluid regeneration is performed at the low point connection. Low side regeneration has two types which are low side regeneration retraction mode and low side regeneration extension mode. These modes are shown in Figure 2.10. The latter occurs when the load is lowered and in helped by the gravity. The first mode occurs when the load is lowered using its gravity and the outlet fluid is fed into the head chamber.

As shown in Figure 2.11, different terms for the operation modes were defined based on the meter-in, meter-out, and the pump activation (Eriksson, 2010). These terms are as follows:

1. Recuperative mode: The energy is gathered only from the load to actuate actuators such as pumps and motors.

2. Neutral: No energy is needed to perform the operation.

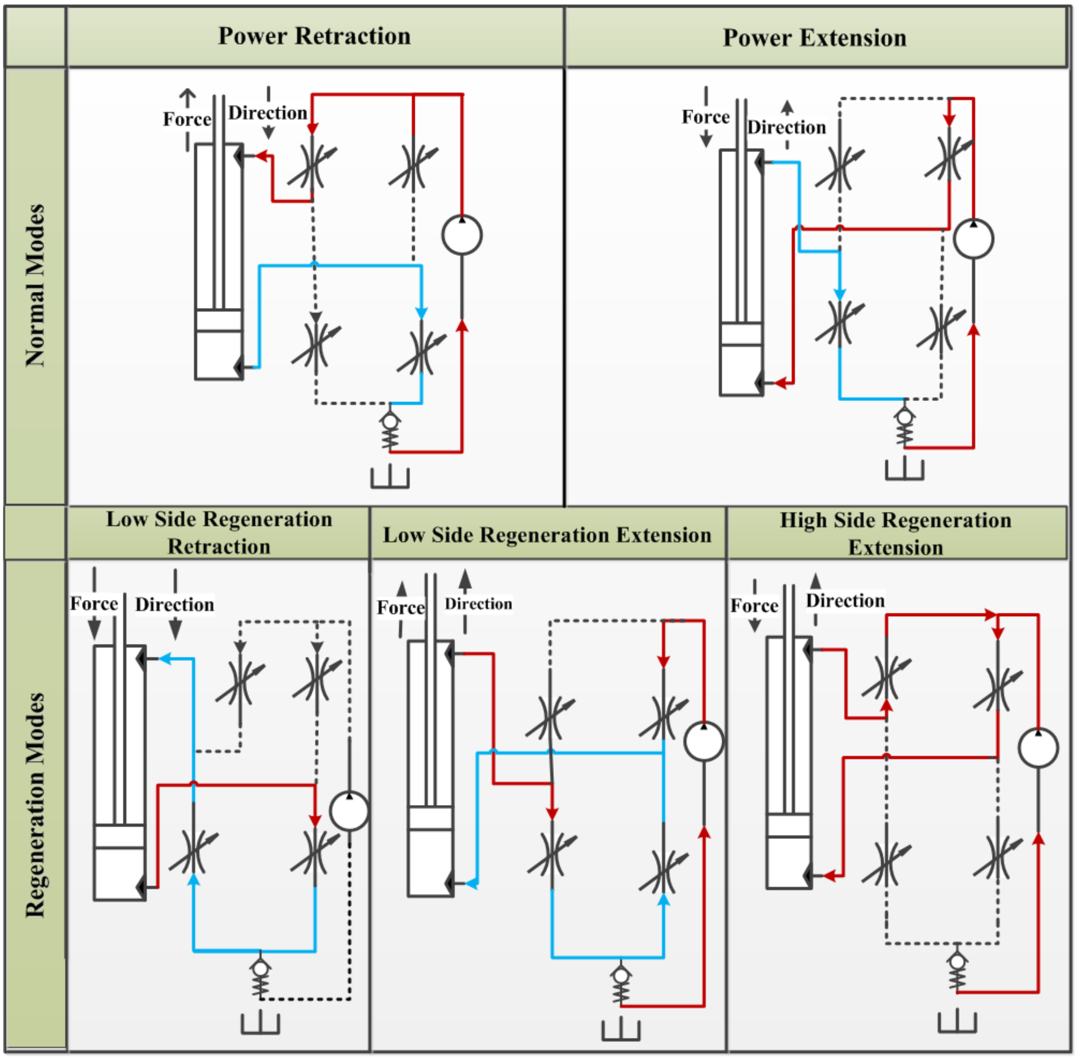

Fig. 2.10 The five operation modes of the independent metering

3. Regenerative: When the lower flow is required from the pump, flow is mainly obtained from the actuator with a high load.

4. Normal mode: This mode occurs when all the flow is obtained from the pump.

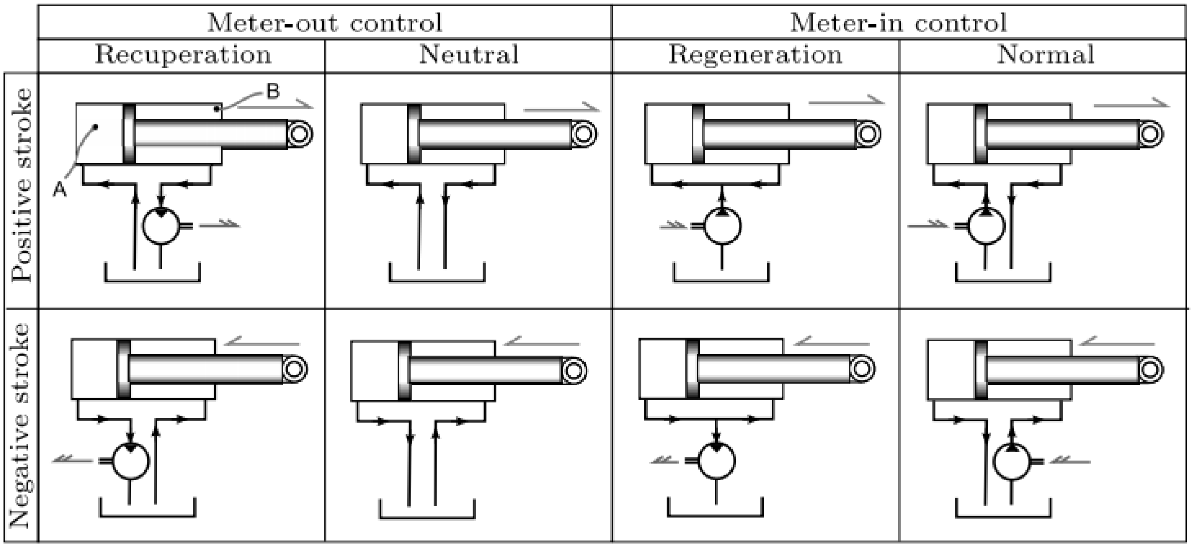

Fig. 2.11 Main operation modes as indicated by Eriksson (2010)

There are other terms for the modes in Figure (2.11) as indicated in Kolks and Weber (2016b). The terms of the Normal mode, Neutral mode, Regeneration mode, and Recuperation mode, respectively, are the Normal mode, the Low-Pressure Regeneration mode, the High-Pressure Regeneration mode, and the Reverse mode. Figure 2.12 shows valve activation in every control mode based on a five valve architecture. These modes, with their valves, are used to implement the Modiciency technique which is discussed in Kolks and Weber (2016b).

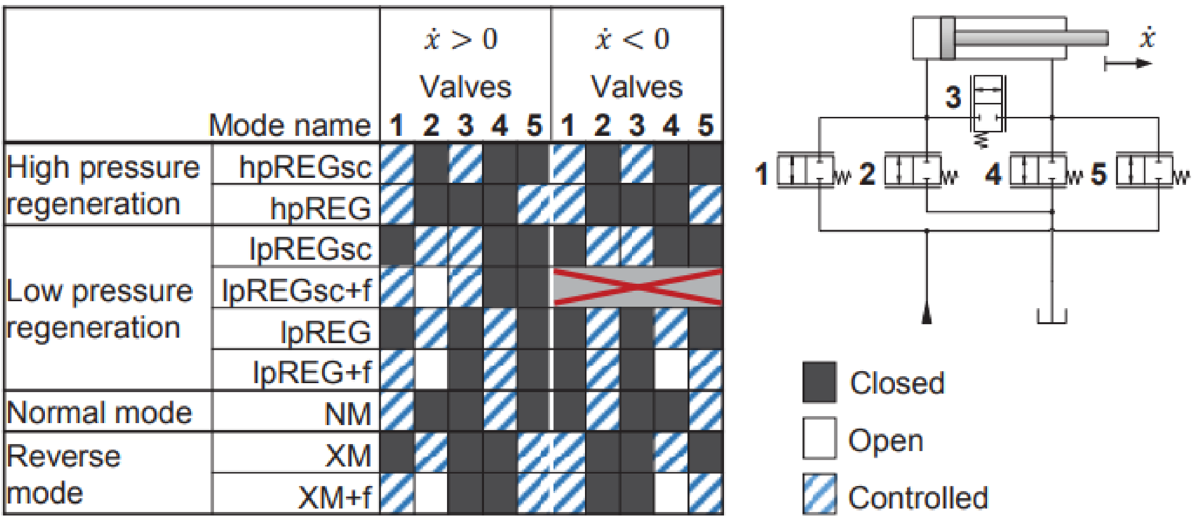

Fig. 2.12 Valve architecture for Modiciency technique. The hpREG is for the high pressure regeneration mode, lpREG is for the low pressure regeneration mode, Nm is the normal mode, the Xm is the reverse mode, the suffix (sc) is for the short circuit, and the suffix (f) is for additional pressure obtained from the supply pressure line. (Kolks and Weber, 2016b)

The STEAM system introduced a different division based on operating states. The operation state refers to each discrete valve setting while the operating mode is a composition of the state and the load (Vukovic et al., 2013). Figure 2.13 shows the discrete operating states for STEAM systems using low, medium and high-pressure lines.

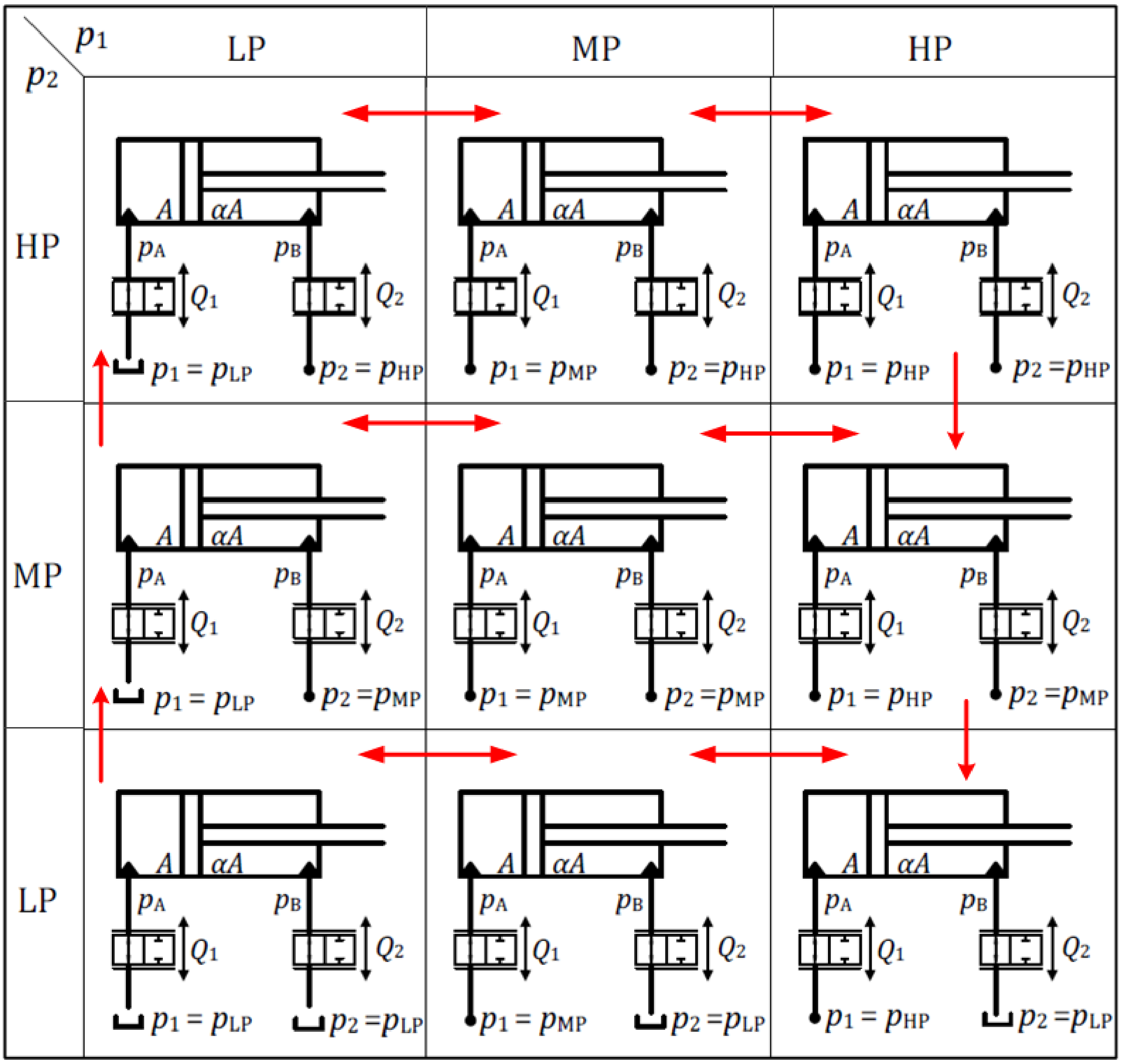

Fig. 2.13 STEAM system operation modes where P: pressure, L: low, H:high, M: medium and α: ratio. (Vukovic et al., 2013)

In IM, operation modes are separated into four quadrants as shown in Figure 2.14 (a) and their power division in red2.14 (b), (Ding et al., 2016).

These quadrants are separated as follows:

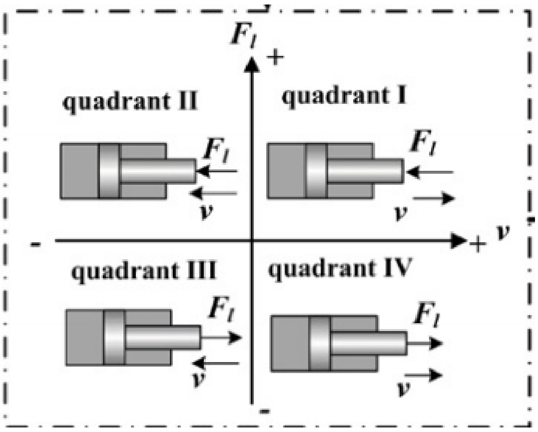

(a) Operation mode based on quadrants divisions

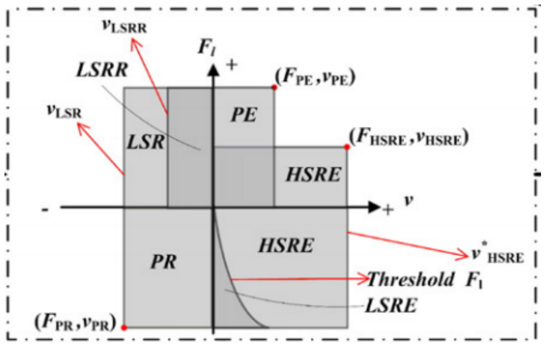

(b) Limits for the modes division

Fig. 2.14 Limitation for the operation modes in IM (Ding et al., 2016)

1. This quadrant has two operation modes which are power extension and high side regeneration retraction mode. The limits for PE are implemented by Equation 2.1, and for HSRE by Equation 2.2 (Xu et al., 2015).

$$[F_{PE}, V_{PE}] = \left[P_{s,max}.A_a, \frac{q_{s,max}}{A_a}\right] \tag{2.1}$$

where F_{PE} is the power extension force, $P_{s,max}$ is the pump's pressure, $q_{s,max}$ is the pump's flow, and A_a is the head chamber pressure (Xu et al., 2015).

$$[F_{HSRE}, V_{HSRE}] = \left[P_{s,max}.(A_a - A_b), \frac{q_{s,max}}{(A_a - A_b)}\right] \tag{2.2}$$

where F_{HSRE} is the high side regeneration force, V_{HSRE} is the high side regeneration velocity, and A_b is the rod chamber area.

2. The low side regeneration retraction limits are in Equation 2.3. This mode relies on the returned fluid from the cylinder. If extra velocity is required, in limited applications, then the pump can be used to supply extra fluid as indicated in Equation 2.4. (Xu et al., 2015).

$$[F_{LSRR}, V_{LSRR}] = \left[F_l, \frac{q_{LSRR}}{A_b}\right] \tag{2.3}$$

$$[F_{LSR}, V_{LSR}] = \left[F_l, \frac{q_{s,max}}{A_b}\right] \tag{2.4}$$

where F_L is the load force, q_{LSRR} is the recirculated flow in this mode.

3. The limits of the power retraction mode PR according to Xu et al. (2015) are,

$$[F_{PR}, V_{PR}] = \left[P_{s,max}.A_b, \frac{q_{s,max}}{A_b}\right] \tag{2.5}$$

4. Low side regeneration extension (LSRE) limits according to Xu et al. (2015) are,

$$[F_{LSRE}, V_{LSRE}] = \left[F_l.A_b, min(\frac{q_{LSRE1}}{A_a}, \frac{q_{LSRE2}}{A_b})\right] \tag{2.6}$$

The LSRE mode velocity depends on the returned fluid and the overruning load value (Xu et al., 2015).

$$q_{LSRE1} = C_q A_v (U_{max}) \sqrt{\frac{2.(P_r - P_b)}{\rho}} \tag{2.7}$$

$$q_{LSRE1} = C_q A_v (U_{max}) \sqrt{\frac{2.(\frac{Fl}{Ab} - P_r)}{\rho}} \tag{2.8}$$

where C_q is the valve conductance coefficeint, A_v is the orifice opening area, P_r is the tank pressure, P_b is the rod chamber pressure, and ρ is the fluid density.

Shenouda designed three valve modulation modes. These modes are continuous and they include the five discrete modes discussed previously by Shenouda (2006). They are the powered high side regeneration extension mode (PHSRE), the powered low side regeneration retraction mode (PLSRR) and the powered low side regeneration extension mode (PLSRE). As indicated in the same source, this method can achieve smoother velocity control and higher force capability compared to discrete modes.

Regarding STEAM systems, division is based on states as illustrated previously in Figure 2.13. These divisions could be regeneration, recuperation, resistive float or assistive float. It is normally difficult to apply all these divisions and this is based on the actuator type and dimensions (Vukovic et al., 2014).

2.6 Mode Switching Methods

Mode switching should occur when the mode capability, including velocity and power, is no longer sufficient. A suitable mode switching is used to minimise losses and decrease switching problems such as switching instability and unsmooth switching (Ding et al., 2016). Many algorithms were developed for mode switching. As these modes directly affect the performance of the actuator, smooth and fast switching is crucial. A selection method based on cylinder force, velocity and required force using an adaptive robust controller (ARC) was improved (Liu and Yao, 2002) and (Yao and DeBoer, 2002). A mode switching using a fitness function was implemented (Shenouda and Book, 2005b). This function receives problem parameters as inputs and the suggested solutions to select the optimum solution. It should be able to utilise fast computing speed and quantitatively measure the suggested solutions. Also, continuous mode switching using three valves simultaneously was discussed (Ding et al., 2016). A Mode transition, based on meter-in or meter-out control, was developed as shown in Figure 2.15 (Eriksson, 2010). Meter-out control uses a meter-out valve to control the speed and has two operation modes which are recuperation mode and a neutral mode. Changing between these two modes depends on if the load is higher or lower than the pump pressure. When neither of these operation modes can be used, the system will start using oil from the pump. This is called meter-in control which represents the right part of Figure 2.15. Please refer to Figure 2.11.

Moreover, the mode switching technique for the STEAM system relies on two pressure lines (YUAN et al., 2014) and (Dengler et al., 2012). This technique is based on a finite state machine. The main idea is to split the modes into three groups, namely Q_H, Q_M, and Q_l. The Q_H is the high pressure group, Q_M is the medium pressure group, and Q_l is the low pressure group. Each group contains three states, for instance Q_M includes $Q_{MP,HP}$, $Q_{MP,MP}$, and $Q_{MP,LP}$.The MP is the medium pressure, HP is the high pressure, and LP is the low pressure. The principle of the mode switching is to keep the pressure in one chamber and change it in the other to prevent interference between set of states in the same group as shown in Figure 2.13. For example, in the group Q_M, the head chamber valve was fixed on pressure line MP during changes and the transition was for the rod chamber pressure between HP,LP and MP according to the state power capability. The change between Q_H, Q_M, and Q_L was performed by fixing the rod chamber valve and adjust the head chamber valve.

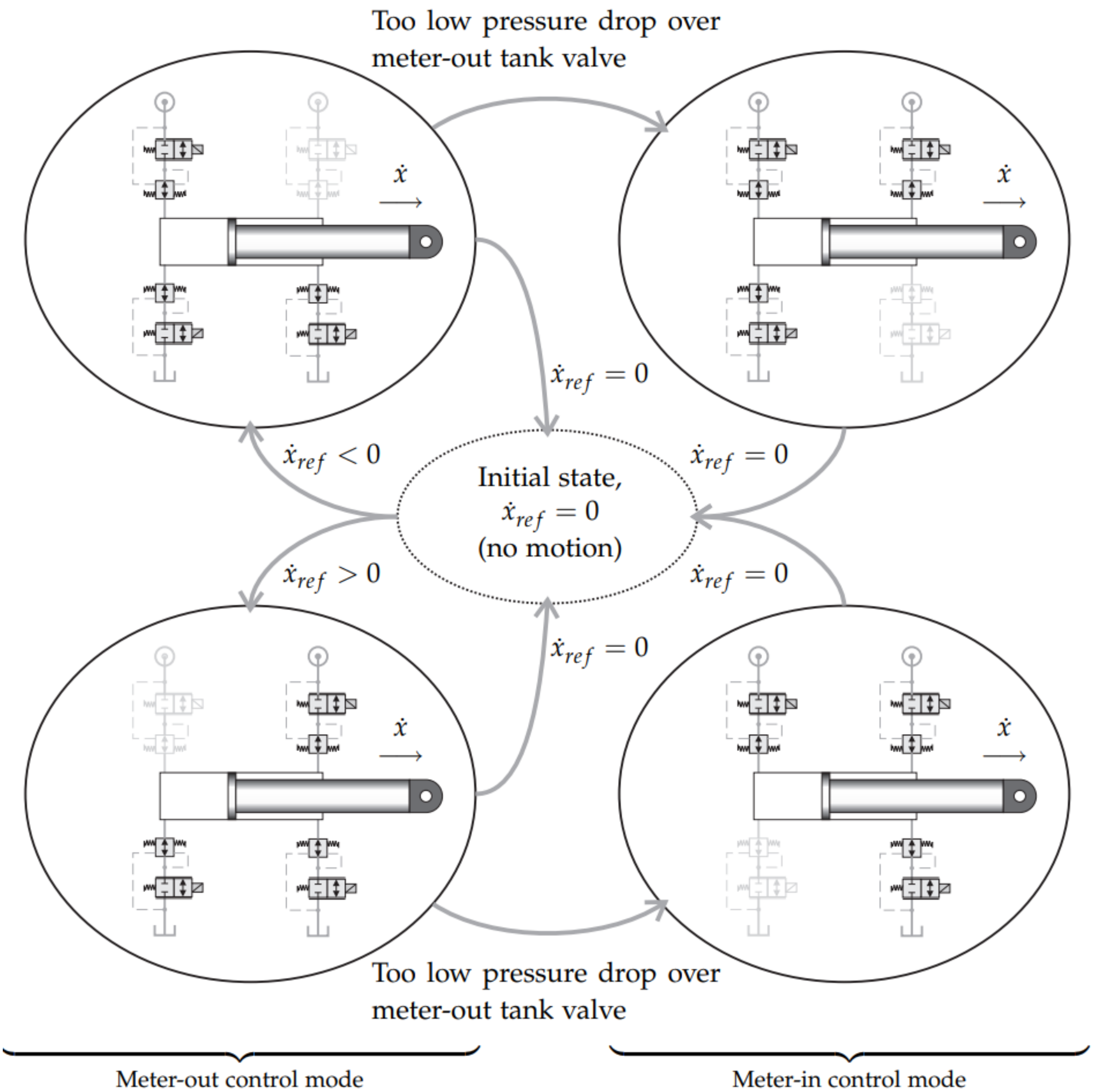

Fig. 2.15 Mode switching or transition between meter-in and meter-out control. Eriksson (2010).

On the other hand, the technique used for switching in the Modiciency approach is based on controlling the velocity and pressure level using MIMO control. This technique allows for continuous mode switching based on modes illustrated in Figure 2.12. The continuous mode switching is shown in Figure 2.16.

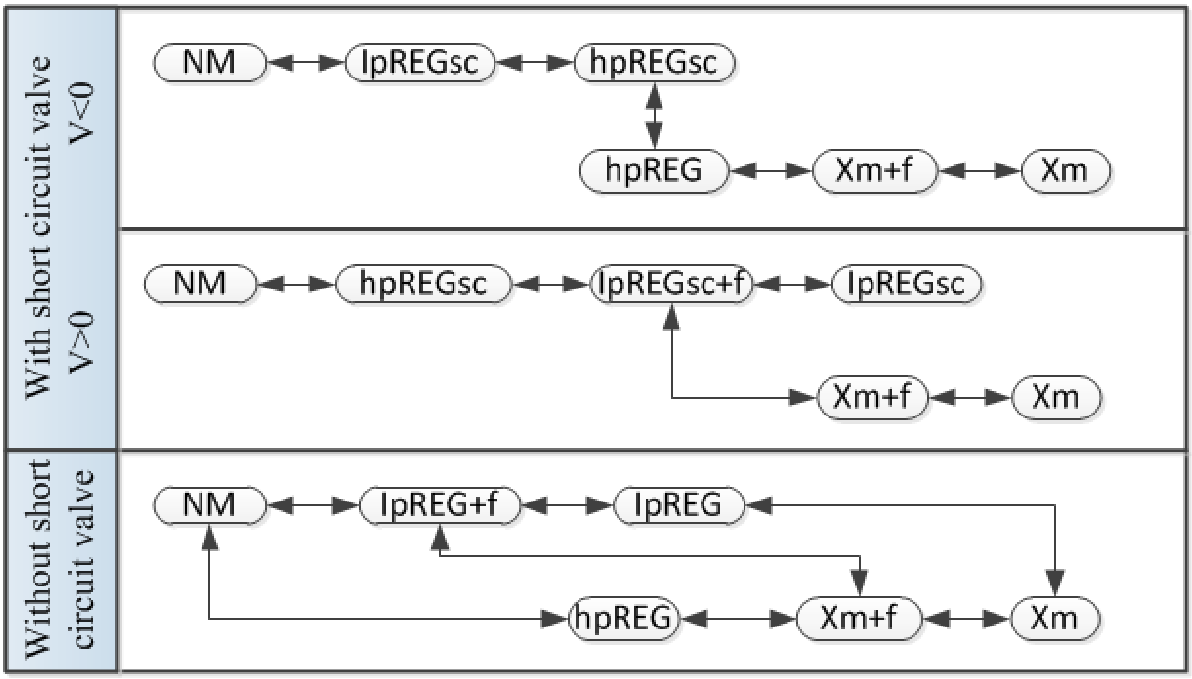

Fig. 2.16 Mode switching division for the Modiciency system configuration (Eriksson, 2010).

A bumpless mode switching algorithm is used to overcome discrete switching problems (Ding et al., 2016). This algorithm contains two parts which are dynamic dwell-time and bi-directional latent tracking loop. The dynamic dwell-time is used to reduce transient instability by slowing the transformation into sufficient time. The time value is obtained based on the Multi-Lyapunov function. The bidirectional latent tracking loop aims to solve unsmooth switching by eliminating the discontinuity of control signals. With regard to digital valve systems that can be used to implement independent metering, Linjama has improved a stepwise change in valve states (Linjama et al., 2008).The next section is about different IM layouts.

2.7 Independent Metering Layouts

In general, the combination between hydraulic circuits and IM has different forms (Figure 2.17) as follows:

a) Combination between traditional hydro-mechanical load sensing and IM. In this configuration, the pump is driven hydro-mechanically and poor damping is one of the main system shortcomings.

b) Combination between the electronic load sensing system and IM valve configuration. The electronic load sensing relies on an Electronic Controlled Pump (ECP) to control the circuit pressure and flow.

c) Combination of the closed circuit with IM to eliminate the throttle losses (Gong et al., 2019). The drawback of this configuration is a functional failure under overload condition (Ivantysyn and Weber, 2014). Hence, an electronic controlled pump open circuit combined with IM was introduced by Heybroek (2008).

d) The last configuration which includes using an accumulator as an energy storage unit that allows reuse of the fluid during operation (Lu and Yao, 2014).

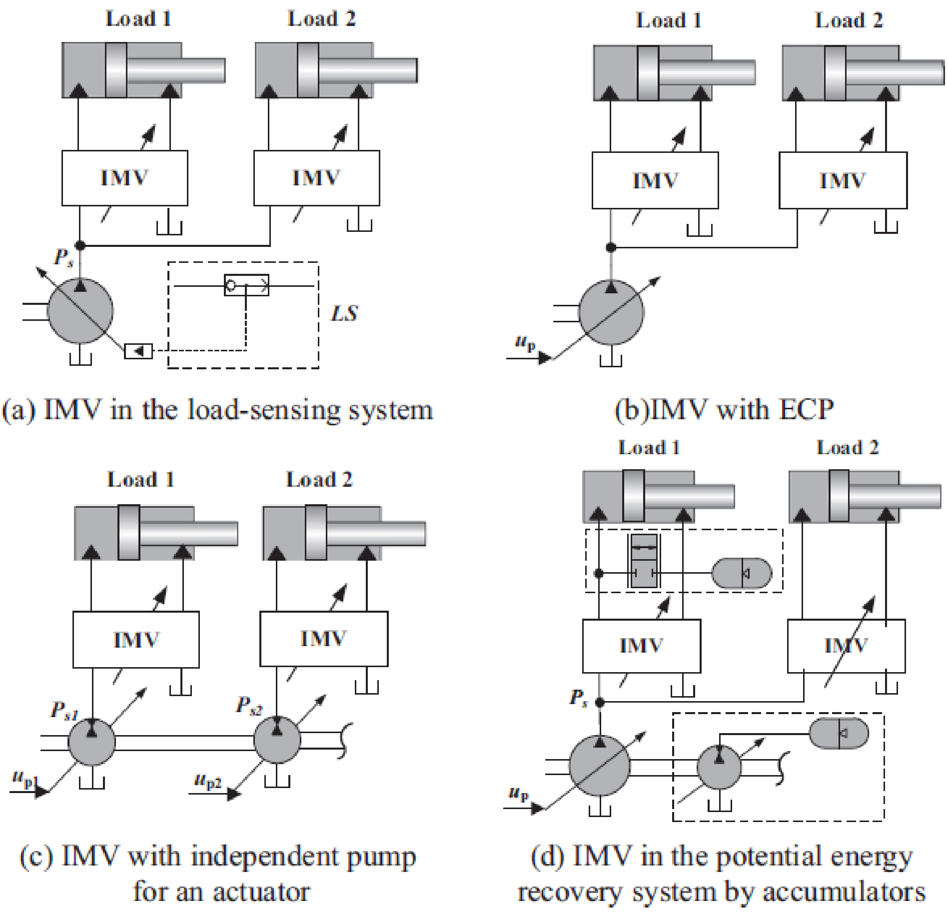

Fig. 2.17 The possible different combinations between IM and hydraulic circuits (Ding et al., 2018b).

Tabor designed a control system configuration for four valve independent metering as shown in Figure 2.18. The control system is based on a microprocessor that coordinates the work between different control portions which are a pressure controller, a function controller and a system controller (Tabor, 2005a). The function controller reads the pressure from the meter-in, meter-out, source pressure, and the tank pressure. The system controller is responsible for reading the pressure and speed commands, then it selects the operation modes and identifies the required flow rates for each valve (21-24) in Figure 2.18. Also, cavitation is observed during operation, if it appears the controller loses its functionality.

Finally, the pressure controller is used to control the pressure from the pump and the tank in order to save energy and prevent cavitation. The practical implementation of a similar IM valve control system combined with a pump control algorithm was performed on a 20-ton excavator by Hyundai Heavy Industries Co., Ltd (Lee et al., 2016) and indicated a saving of energy of up to 10 % compared to conventional excavator which relis on normal spool valves.

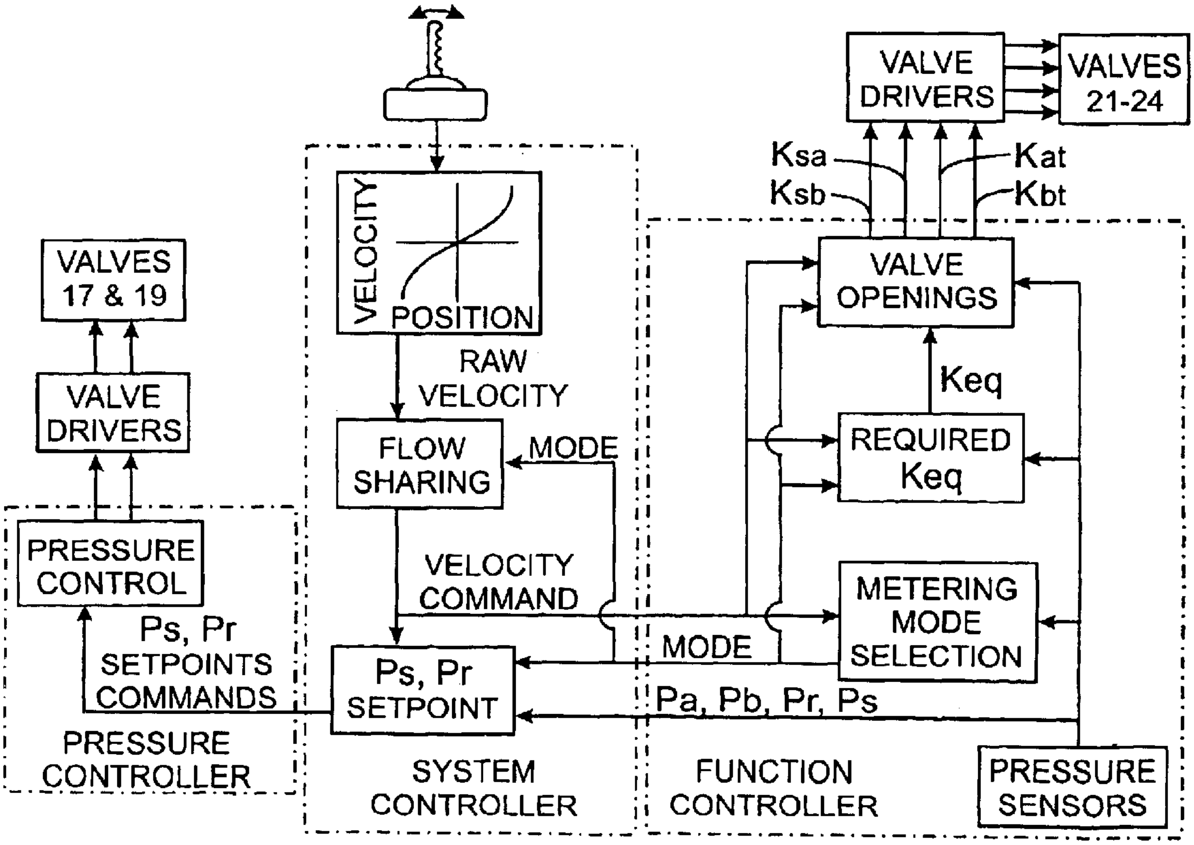

Fig. 2.18 Tabor control scheme for four valves IM Tabor (2005a)

A structure for mobile machines with a common pressure compensator was developed using the minimum number of sensors and simple control algorithms (Lübbert et al., 2016). It was developed to be more acceptable to industry, as illustrated in Figure 2.19. Its main strategy is to control the velocity from the meter-in using an open loop approach. The meter-out is controlled using closed-loop feedback. To overcome the nonlinear relationship between the meter-out signal and the pressure compensator throttling which is inherent in the system due to the closed-loop feedback, the meter-out value should rely on the head chamber pressure which can be determined from the pressure drop value on the pressure compensator.

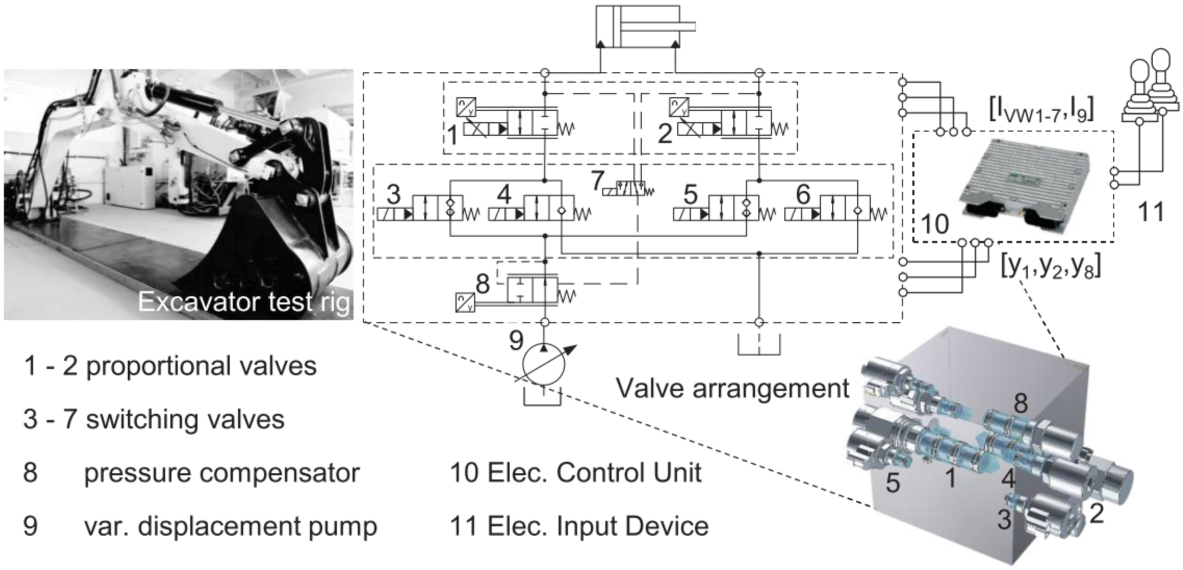

Fig. 2.19 A pressure compensated control scheme (Lübbert et al., 2016)

For a hybrid system, a three-level control system was designed (Lu and Yao, 2014). This control system aims to combine the operations between the main pressure source, the accumulator and the actuators to reduce the power consumption and increase controllability using adaptive control. For STEAM systems, RWTH Aachen university improved a control system using two proportional 2/2 valves and six switch valves for each actuator (Vukovic and Murrenhoff, 2015). This system is shown in Figure 2.20.

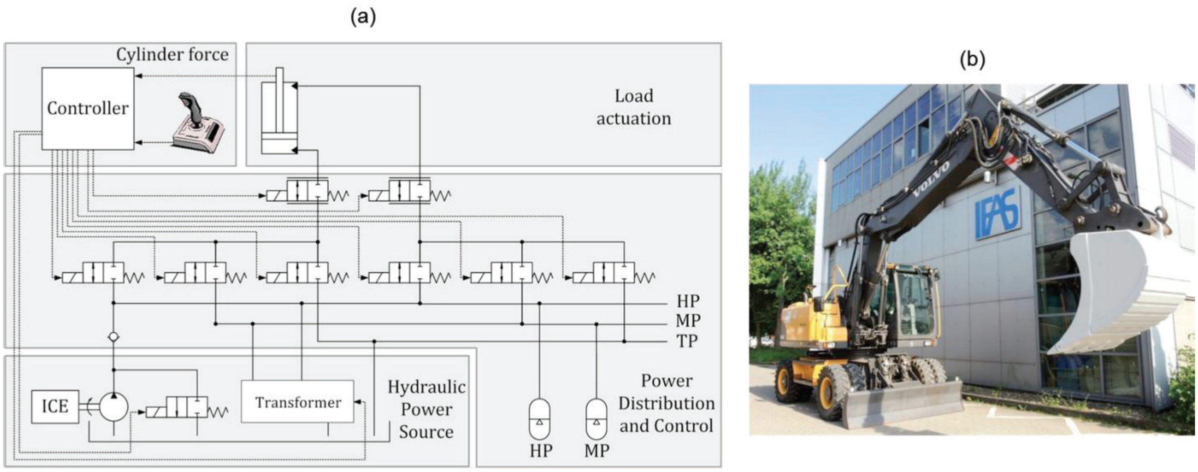

Fig. 2.20 STEAM system configuration for hydraulic excavator (Vukovic and Murrenhoff, 2015)

A system that is able to adapt to load fluctuation was designed (Dengler et al., 2011). Every actuator contains two 3/2 switching valves and one proportional valve. The proportional valve is to control the piston movement while the switch valves are used to connect the proportional valve to the pressure lines as shown in Figure 2.21. The oscillation due to the pressure line switching can be reduced by a step change of the switching valves.

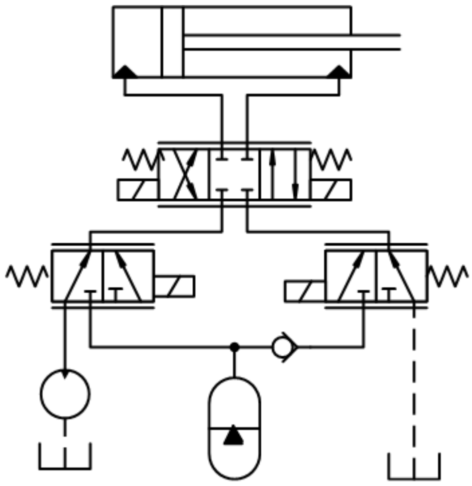

Fig. 2.21 Valve control concept with intermediate pressure line (Dengler et al., 2011)

A meter-out control with a pressure compensator was improved by Vukovic and Murrenhoff (2014). This system, which is illustrated in 2.22, was an improvement because most of the manufacturers do not offer bidirectional poppet valves.

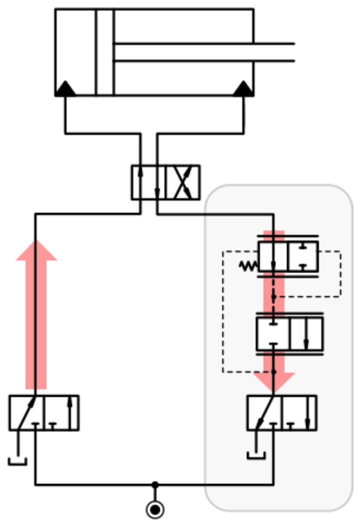

Fig. 2.22 Meter-out control with the pressure compensator (Vukovic and Murrenhoff, 2014)

A flow on demand concept which was developed to reduce the losses in load sensing systems relies on joystick commands or the valve position in contrast to LS that depends on the highest consumer pressure (Scherer et al., 2013) and (Axin, 2015). Combining a flow on demand concept with independent metering leads to better efficiency and controllability (Wydra et al., 2017). As illustrated in Figure 2.23, the controller receives signals from the joystick and the valve positions via Controller Area Network (CAN) communication to control the variable displacement valve. The accumulator is used to allow energy regeneration.

An example of load sensing combined with pressure compensation and independent metering is shown in Figure 2.24. This configuration includes two pressure compensation methods which are the Meter-In Pressure Compensation (MIPC) and the Meter-Out Pressure Compensation (MOPC). The pressure reducing valve is used between the metering valves block and the LS part to reduce the required pressure from the pump to as minimum as possible and this relies on the pressure sensors 1 and 2. The feedback pressure values 3 and 4 are used to form a closed loop control signal for the controller 2.

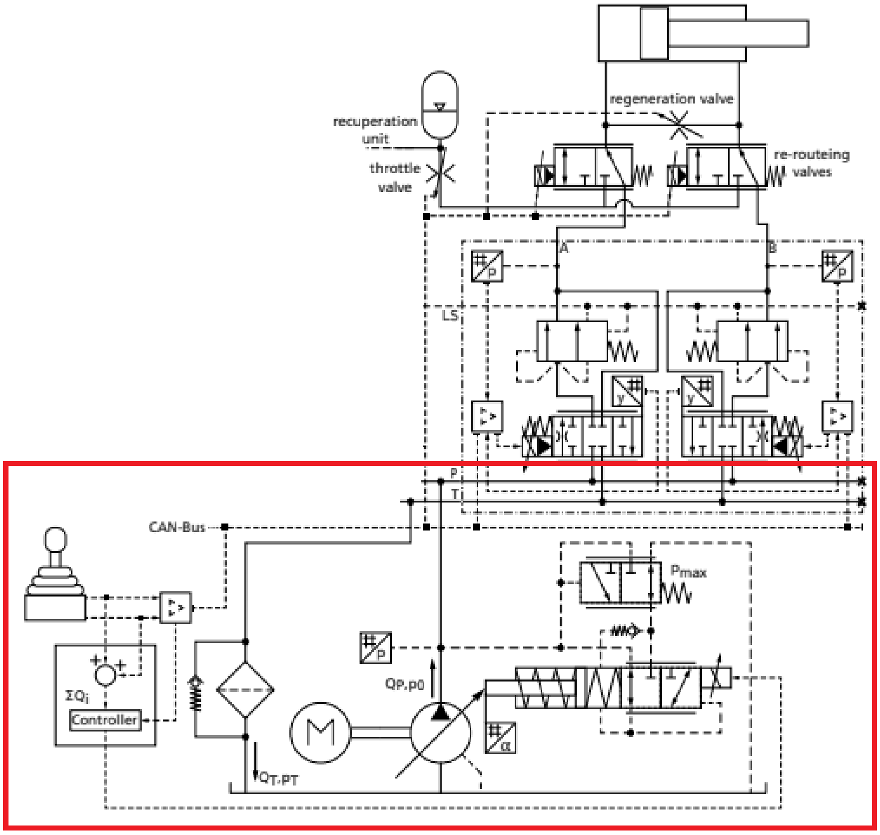

Fig. 2.23 Flow on demand circuit combined with IM system, the highlighted part represents the flow on demand circuit Wydra et al. (2017)

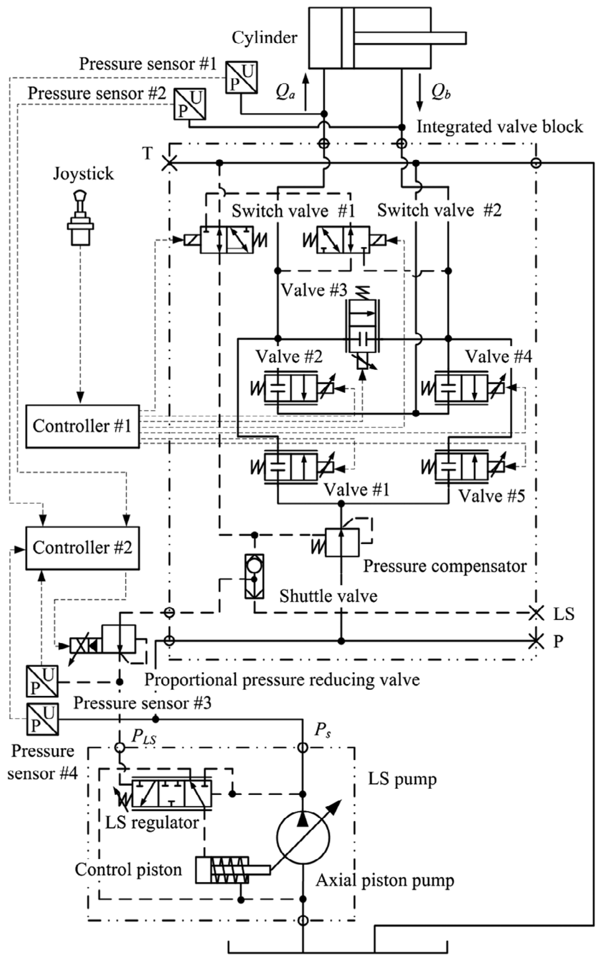

Fig. 2.24 Hydro-mechanical pressure compensated load sensing circuit with independent metering configuration. Liu et al. (2016)

Independent metering has been used to drive motors in hydraulic mobile machines. For example, IM is used to drive the swing part of a hydraulic excavator similar to the driving technique that was developed by Ge et al. (2017, 2015). The study showed that IM improved the dynamic performance of the excavator swing by controlling the throttle orifice size. A control algorithm was developed by Caterpiller to control the swing motor in order to save extra energy (Linerode, 2004). Also, an accumulator was attached to the swing motor to allow energy regeneration as investigated by Thompson et al. (2014). A flow matching technique for hydraulic excavator swing was developed by Huang et al. (2018). This technique reduces the energy losses by producing the required flow by the motor, and improves the system dynamics by a separate control of the throttles for a high inertia component.

2.8 Independent Metering Challenges

There are many drawbacks that prevent IM systems from being used widely in industrial applications. In general, these challenges can be classified as follows:

1. ***Mode Switching.*** The independent metering control algorithm relies on a rule-based transition between many operating modes. This transition contributes to two main types of discontinuity which are the valve control signal and the system dynamics. The effects of the valve control signal disruption are a velocity oscillation and pressure peaks (Shenouda, 2006). A tracking algorithm based on online and offline controllers has been developed to reduce the effect of the control signal interruption. To overcome the dynamics problems, which are the actuator motion instability and velocity oscillation, a continuous mode switching technique was developed by Shenouda (2006), but this solution suffers from extra power losses. However, the possible solutions to this problem can be listed as follows:

    - Slowing the system reaction. This allows the controller to react to the pressure after instability decay, but this technique slows down the system.
    - Slow down the valve using a step-wise or a ramp signal, but this technique slows down the system. (Linjama, 2011).
    - A dwell time technique which detects the signal and executes after sufficient time period that allows decaying the pressure instability to decay. However, the efficiency of this method depends on selecting a suitable time.

2. ***Oscillation.*** Hydraulic actuator oscillation is an important point to investigate. Independent metering reduces energy losses by enlarging the orifices, but this reduces the controllability and produces velocity oscillation due to lack of damping at the enlarged orifices. Also, changing between different operation modes with different dynamic characteristics is another source of oscillation. A high pass filter and Proportional Derivative PD regulator are used to improve the damping and other parameters such as stability margin and vibration reduction for a multi-actuator system (Cheng et al., 2018).

3. ***Coupling.*** The independent metering system transfers the electrohydraulic drives into MIMO systems. For the coupling between the pressure and velocity, in the IM systems, many techniques were developed as discussed in Section 2.4. Each method has some shortcomings, and a new decoupling strategy is an important point to investigate.

4. ***Pump/Valve Coordinate Control.*** IM grants a separation of control of flow and pressure which requires a coordinate control between the pump flow and the IM valves. Many

iterations have been developed and one of them is to fully open the meter-out valve and control the meter-in, but this increases throttle losses by the meter-in. Another solution is to make the meter-in fully open and control the flow using an electronically controlled pump (Liu et al., 2017). This technique prevents implementing the pressure compensation method which is important for IM systems. Another method is to fully open the meter-in and combine the control with the meter-out (Ding et al., 2018a). This method relies on many modes with different dynamic characteristics, so this technique affects the system dynamics overall. This represents an important research point where further study on new systems that combine energy saving and system dynamics can be performed.

5. ***Safety and Reliability.*** Using systems that included software, electronics, and smart valves increases the fault percentage of these systems (Weber, 2018). This is a very important aspect to investigate. Faults in independent metering systems can be classified into:

    - Function fault: it appears if one of the IM valves lost performance or one of them encounters performance deviation. There are three main techniques developed to overcome this fault which are model-based, intelligent control, and neural networks (Bian et al., 2011). The model-based is not suitable for IM applications due to the high non-linearity in fluid applications. A neural network fault detection algorithm was developed by Opdenbosch et al. (2013).
    - Accuracy lost: it appears if one of the sensors lost functionality. A configurable controller is a solution used to deal with sensor faults in IM systems, similar to that used in Siivonen et al. (2009).
    - Stability lost: during mode switching, the system may suffer from a lose of stability. Different iterations have been introduced such as step-wise or dwell time control. These solutions have some drawbacks that affect system dynamics. So, new methods or techniques is an important sector of IM to investigate.

2.9 Summary

This chapter reviews IM technology and its related systems. It represents the background of this research hypothesis which is to develop a new configuration of IM using a stepped rotary flow control valve. This part of the research discussed different hydraulic systems such as Load Sensing, Digital hydraulics, STEAM systems, and Independent Metering. It illustrated the main characteristics of these systems and how they interact with each other. For example, IM can be attached to a variable displacement pump, or a digital valve unit can be used to configure IM. Moreover, the STEAM system is IM with an additional pressure line.

Different control parameters and techniques have been investigated. The control parameters are pressure, velocity, and flow. The effective control parameter is the pressure because the harsh environment burdens the performance of the velocity and flow sensors. Many control techniques can be used with IM such as SISO, MIMO and feedforward or open loop. The open loop is mainly used in hydraulic mobile applications where the driver closes the loop by observing the machine performance.

The IM operation modes and their switching techniques have been researched. There are five operation modes for IM with specific power and speed limitations. These modes are namely, PE, PR, HSRE, LSRR, and LSRE. They were developed to be used during the machine duty cycle to save energy by allowing fluid regeneration. Many techniques were developed to switch between the modes, and selecting the switching technique depends on the IM configuration. Each technique has some advantages and some drawbacks.

The IM system is considered as a programmable hydraulic system which relies on software control. IM has three operation levels which are 1- Mode selecting level, 2- valve activation level, 3- pump pressure and flow control level.

To summarize, the up to date research about Independent Metering can be classified into

1. Independent metering valves.
2. Independent metering configurations which can be four or five valves.
3. Operation modes and switching techniques.
4. Control layouts and their effect on the hydraulic actuator velocity.
5. The control techniques such as adaptive and MIMO control.

Based on a thorough review of these categories, the valves used for developing independent metering are spool, poppet, and digital type. The poppet type is able to make a complete separation between the meter-in and the meter-out of the cylinder. However, the industrial introduction of this valve has been very low due to stability and flow accuracy shortcomings. This research investigates replacing the poppet valve by a rotary control orifice driven by a stepper motor. This substitution can produce a new configuration of independent metering which is expected to increase IM controllability and to grant advanced options for the machine user. The next chapter discusses in more detail the construction, characteristics and, applications of the new proposed system.

Chapter 3

Proposed Novel Independent Metering

3.1 Introduction

Utilizing the rotary flow control orifice developed by Okhotnikov (2018) to form an Independent Metering configuration is a novel concept which led to a universe system in the field. The new system has many characteristics resulted in a wide range of industries and applications that this system can be applied to.

A hydraulic ‘system’ would typically comprise of some prime mover driving a pump, a control valve to direct the flow, a number of either rotary or linear actuators that perform the work, and various other ancillary pieces of equipment that enhance and protect the system and the machine. The proposed system here, Micro-Independent Metering (MIM), has two main parts which are a modern control valve designed for high pressure hydraulics and a significant improvements in the electrical and electronics systems in term of high precision remote control of such control valve.

This control package of the MIM aims to enhance some exiting technology combined with new state of the art algorithm that significantly improves the performance and controllability of the machines that uses it in terms of high precision, stability, damping, and smoothness of the operation even when controlling heavy or high inertia systems. This new control algorithm combined with the new design of the rotary valve made the creation Micro- Independent Metering of large high power hydraulic system a reality.

The perceived advantage of this MIM to large heavy machinery is to improve control-ability of the machine, specifically when a number of services are selected simultaneously. It aims to do this in a more electrically efficient way and provide a level of power, speed and accuracy, which is probably only currently available in high cost, electrically driven high end systems. Also it enables remotely piloted system minimising the need for skilled operator. Another significant improvement can come from the potential improvement is vehicle fuel efficiency using intelligent system that recognises actual and instantaneous operating needs and being able to control and regulate the system accordingly.

This part of the thesis introduces a description of the MIM system in Section 3.2. The main characterstics and key features of the MIM are included in Section 3.3. Section 3.4 is about the possible applications of the MIM system. Then the hydromechatronics circuit studied in this thesis is illustrated in Section 3.5. The summary is in Section 3.6.

3.2 MIM System Architecture

The MIM system comprises two major elements. The first is the control valve, the second is the control system. The control valve has a rotary spool in a housing as opposed to the long used linear spool. The rotary spool is controlled by a stepper motor and as the spool rotates a pair of equal and opposite orifices open or close depending on the rotation of the spool. This variance in orifice size allows flow to pass from the pump to the chosen actuator. At the same time a second rotary valve, again controlled by a stepper motor, allows oil from the other side of the actuator to pass back to tank. The circuit is completed by two further valves which operate the reverse motion to move the actuator in the opposite direction. As each valve is independently controlled then a set of 'standard' valves can be used to operate any function. These rotary spools are designed to minimise losses within the valve, but all valves are identical within a given flow range.

The circuit is completed by two further valves which operate the reverse motion to move the actuator in the opposite direction. As each valve is independently controlled then a set of 'standard' valves can be used to operate any function. These rotary spools are designed to minimise losses within the valve, but all valves are identical within a given flow range. The stepper motor, however, rotates in discrete steps and it can be reasonably assumed that one discrete step may vary the orifice by too great a difference and cause a step change in actuator speed. This is unacceptable and two novel approached are applied here to remedy that. One is the unique profile of the spool opening which no matter how larger steps the opening is gradual and linear. The other is the introduction of micro stepping where a step can be broken down into much smaller steps. This is where the introduction of a new technology that split those 'discrete' steps into much smaller steps hence better controlling the rate of change of the orifice size to suit the application. In a practice the rotation of the control valve spool could be made up of standard steps using standard stepper motor steps but in critical situation where slow opening or stability is important requiring metering, micro steps can be used. This feature of the new system is programmable and can be adapted for use in wide variety of applications. Also, it can be adjusted in real time operation.

The architecture of control system is in such a way that allows flexibility of the modes of operation. It can be configured for or both direct and remote control of the valve and the actuators. In practice, the rotary valve movement is in response to a direct input, primarily by the operator, or the supervisory computer. However it is reasonable to assume that modifications to that rotary spool movement are possible in response to other factors based on for instance sensors in the system, positions and operation of other actuators, load balancing, optimised control per engine speed, safety requirements, etc.

The new proposed control system can be set to maintain the desired actuator speed regardless of changes in system operating conditions. It should be noted here that this ‘flow balancing’ feature is available, but in a different form, in more expensive and complex systems. However, what is proposed here will make the system simple and affordable and with the advantage of having the ability to interface with other sensory or actuator system with the aim of replacing an existing control system.

The control system proposed here is portable and can be transferred across wide range of platforms according to the user requirements. With user friendly interface, the user can easily select the type of application and the required parameters to allow the system to perform the required task.

A typical example of the proposed system is shown in Figure (3.1). As shown, the system has different interfacing techniques and capabilities. It can be used online or via local industrial web. The powerful control system can handle different components/actions simultaneously. The multitasking operation of this system is its key advantage specially multiple components are employed at the same time.

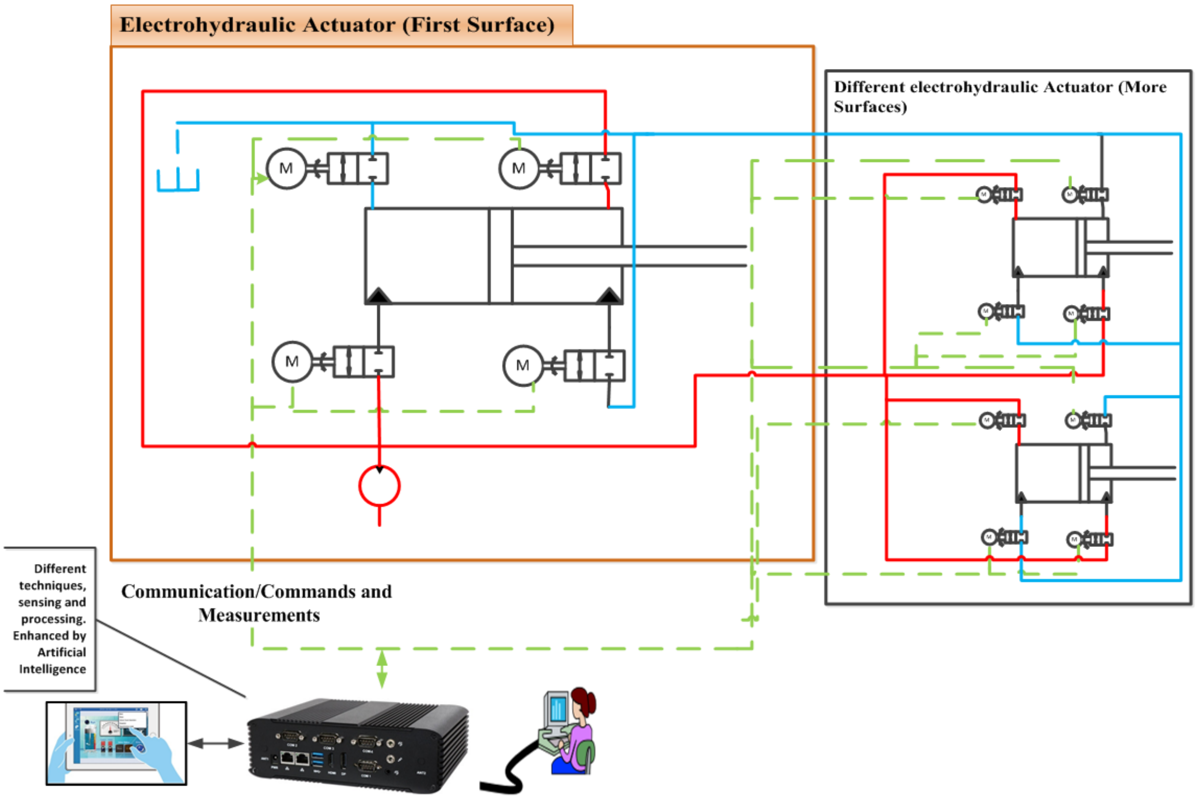

Fig. 3.1 The main configuration of the Micro-Independent Metering System.

3.3 MIM System Characteristics

The system being developed here is an integration of different advance technologies and theories. The key features and benefits of which are :-

- **Interfacing:** The system has a user friendly interface that allows the user to select for a suitable application and associated parameters. Also, the system is able to communicate with other components on that machine to fully advantage control, efficiency, and safety requirements.

- **Parameterization:** This system is able to perform duties precisely. As it uses the micro-stepped rotary valve to control the movement of the actuator either directly or indirectly, the effect of pressure variation on the performance can be sensed and controlled, which is not generally available in the case of the traditional actuators.

- **Miniaturization:** The new valve is more compact in size and that is due to the new design and construction of the rotary valve orifice combined the a stepper motor which requires less space less than the traditional valve, especially the spool or servo type.

- **Expansion:** The system has the ability to be expanded so that one control system can handle all valves within an application and this is one of the main advantages and attractions of the proposal. The actuators can use different advanced communication techniques making it transportable across different applications. The wired/wireless communications allows the actuator to be subsystem of other systems. It can be activated or adjusted via the internet or Laptop using USB or mobile Phone.

- **Portability:** The accompanying software is an important and integral part of this actuator control system. The control parameters can easily be updated or adjusted through a graphical user interface. It can be easily inserted/loaded into any pre-configured system. For example it can be easily inserted into a production line in a factory. The communication with the main control unit can be any form of field bus such as CAN as would be anticipated in this case.

- **Simplicity:** The system relies on a minimum number of sensors hence optimising reliability and efficiency.

- **Safety:** Selecting the stepper motor helps to detect the failure in the system. The stepper motor performs better than servo motor in electronics system failure cases. Any fault is potentially faster to be detected and can directly change the stepper into a locking or other mode. In such situation, the control system can safely redirect the flow into other pipes to reduce the effect of any failure in any other part of the system.

- **Applicability:** Since the actuator valve system is a combination stepper motor and rotary control valve, it has much better power to weight ratio than equivalent 'electrical only' systems. Moreover, the advanced applied techniques in the actuator controller aim to perform the required task with the least possible power consumption.

- **Competitive Pricing:** The rotary control valve has some clear manufacturing cost advantages due its simple construction and use on some off the shelf components.

3.4 MIM System Applications

- **Infrastructure**
  Infrastructure industry is full of examples of electrohydraulic applications used on vehicles such as earth moving and mechanical handling applications. The proposed system is expected to improve the performance and accuracy as it will replace traditional valves with advanced ones. As shown in Figure 3.2, every cylinder in any mobile

machine can have the control valve (IMV Unit) positioned on or close to the Hydraulic Actuator, each IMV Unit being fed by a ring main hydraulic supply, and all the units are connected to the main control unit via some communication, either wired or wireless. This configuration potentially allows easy replacement of any components on the machine just by plug-in. Diagnosis and maintenance is potentially easier than with traditional systems because faults can be detected online from any place just by connecting the machine to the web, and due to the simple construction of the system diagnosis is very trusted. While this feature of online diagnosis is not new, it is an important feature to add to the total possibilities with the new technology.

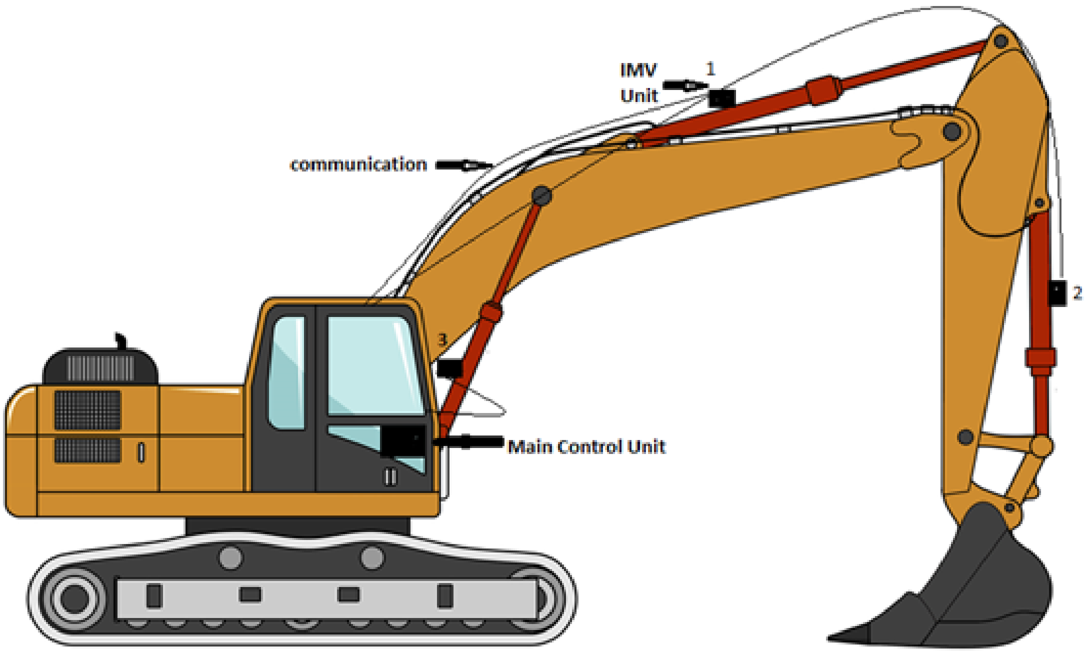

Fig. 3.2 The distribution of valves units on excavator surfaces.

In addition to what is stated above, the MIM allows the integration/interaction of the control system with other technologies in these machines, such as AI, Image Recognition (Figure 3.3 (a)), and Internet of Things (IOT), which are the basic requirements for creating fully automated machines or tractor system of the future (NEWS, 2018). The most significant benefits of this system is the smoothness of operation while maintaining the performance. Using this technique, the user can select the level of smoothness of the piston movement as an option. For example a bucket cylinder, particularly when linked to other sensors The smoothness technique can be used in grading and levelling for piping installations as shown in Figure (Figure 3.3 (b)).

(a) (b)

Fig. 3.3 (a) Image recognition in hydraulic excavator, (b) The grading operating of excavator.

- **Robotics**
  Electrohydraulic is an important actuator that is used in robotic industry Davliakos et al. (2018). The governmental sector, Innovate UK indicates that one of the most important sectors in the UK is the robotics where about £93 million were directed to support it. While many robots are simply 'pick and place' or moving through a predefined set of movements, there are expected applications which would involve extreme environmental applications requiring combining Artificial Intelligent techniques. The proposed system is able to implement AI procedures or works with systems that rely on AI (UK, 2018). Also it accurately moves the manipulator of the robot in applications other than 'pick and place'.

- **Manufacturing**
  Plastic and metal manufacturing are applications where electrohydraulic systems are used. For example, Computerised Numerical Controller (CNC) machine using electrohydraulic actuator. The MIM system could be expected to be installed in 3D printers, particularly larger versions which can be used for buildings of the future, where whole buildings are being created using 3D printing techniques on site in a variety of materials (Figure 3.4).

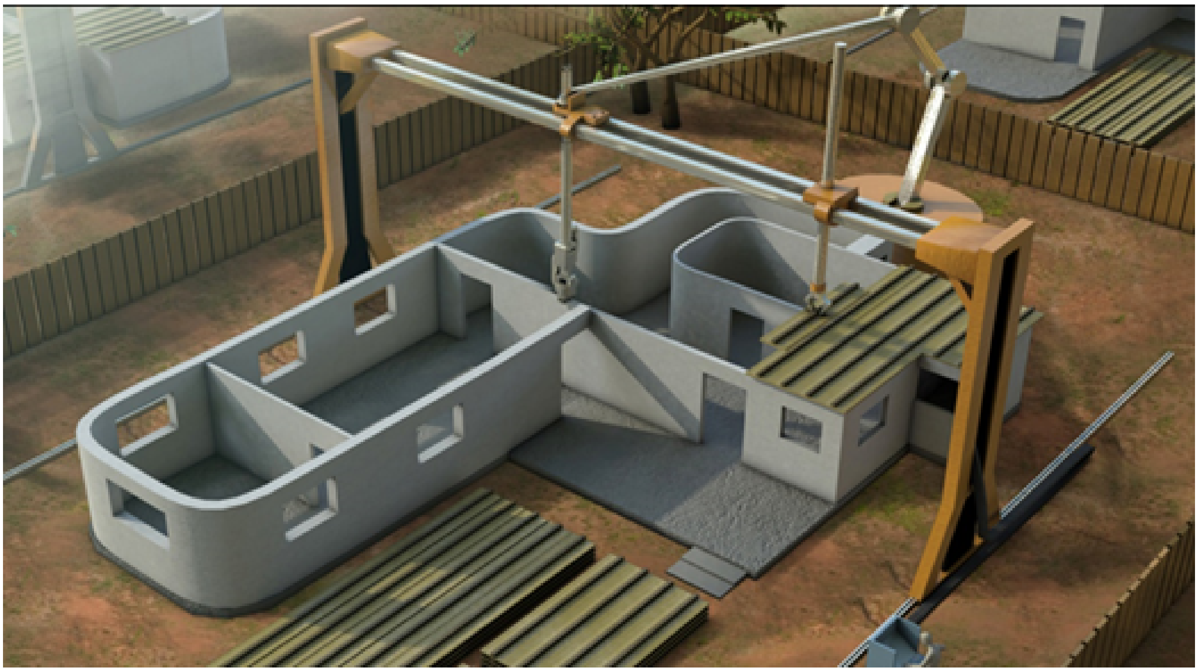

Fig. 3.4 Illustration of large scale 3D printers.

- **Defence and Security Systems**
  Based on the ministry of the defence and security resources, the hydraulic and electrical operation combined with control systems are one of the main priority technologies in this century (Britain, 2006). Different examples of the applications in the defence systems can use this actuator. For example, the hard launchers, radars, jet engines, and autopilots planes require this kind of actuators.

3.5 Main MIM Configuration

In hydraulic mobile machines, many actuators work simultaneously. Each actuator with its own attached control valves is called a surface. For example, (Figure 3.5) has three surfaces and one of them is shown in details. The cylinder (4) is controlled by four valves. Each valve contains driver, motor and rotary orifice which are (1), (2), and (3), respectively. The fluid is pressurized using the fixed displacement pump (9). The return line drains into the tank (12). The unloader valves (13) and (14) are used to control the pressure produced by the pump. A pressure relief valve (8) is used here to protect the hydraulic circuit. The system relies on pressure feed-backs to control the actuator velocity and saves more energy by implementing the fluid flow regeneration techniques. The pressure measurement points are (5), (6), (7), and (15). The diagram shown in Figure 3.5 represents the main system used through this investigation.

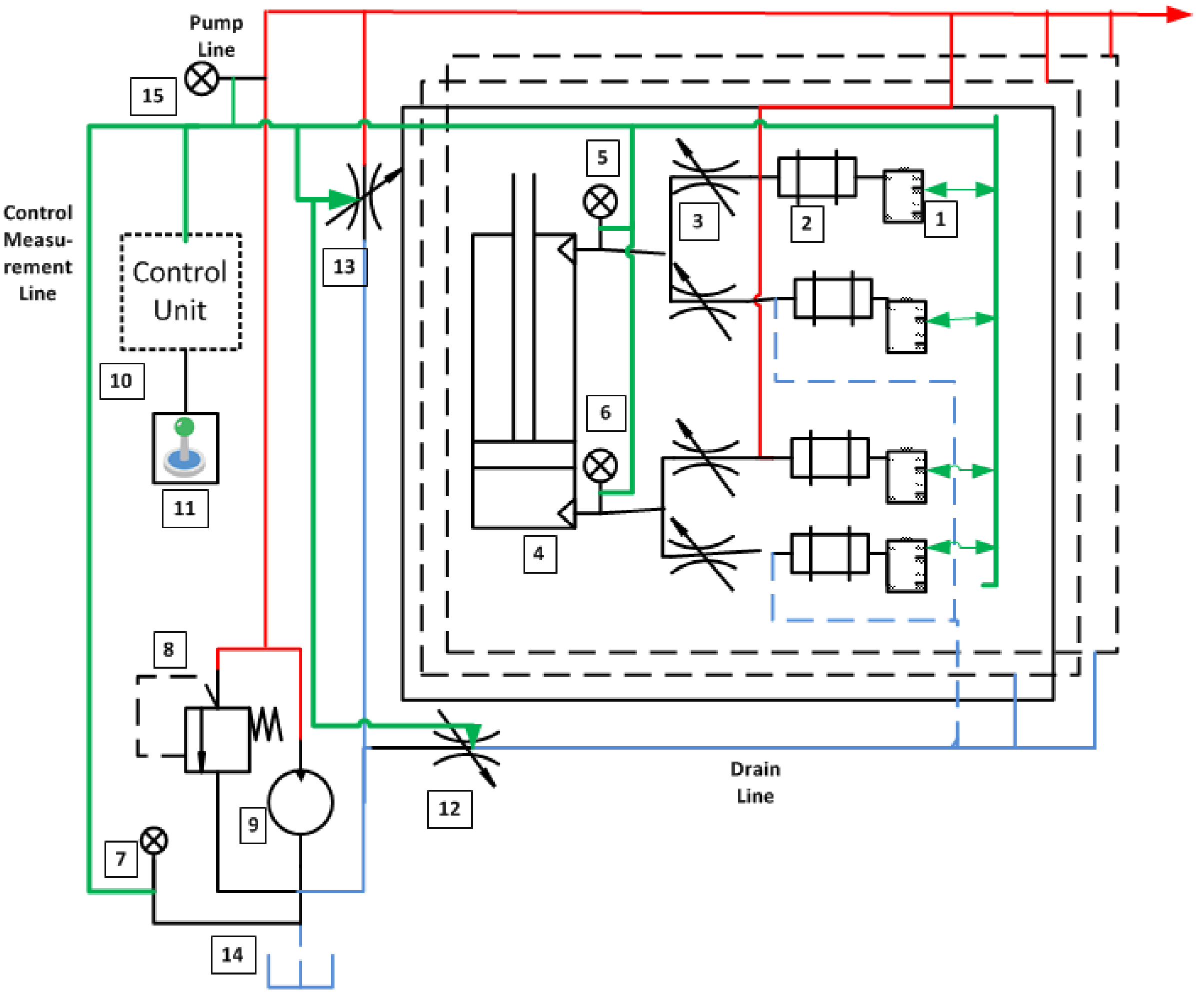

Fig. 3.5 The diagram of the MIM system. 1- motor driver, 2- stepper motor, 3- rotary orifice, 4- cylinder, (5,6,7,15)- pressure sensors, 8- pressure relieve valve, 10- control unit, 11- joystick, (12,13)- unloader valves, 9- fixed displacement pump, and 14- tank

3.6 Summary

This chapter presented the proposed concept of Micro-Independent Metering. MIM is a novel configuration of electrohydraulic systems. It is based on the integration of a new rotary hydraulic control valve with a programmed electronics control system that included a novel algorithm. This new control system contains the motor driving technique micro-stepping, which splits the full step into smaller steps resulted in a smoother operation without pressure ripples. MIM main key features are included here to show the potentials of such a system in industrial applications. The applications of this system including heavy-duty machinery were also discussed in this part. To start the development of such a system, two investigation phases have been followed. The first one is to develop the stepped rotary flow control valve and analyse its performance. The second is to develop a programmable control system that meets the IM requirements. To grasp the IM conditions and requirements, a study of the mathematical description of IM is necessary and it is the topic of the next chapter. Also, a study of the performance of the suggested valve is in Chapter 5.

Chapter 4

Independent Metering Mathematical Analysis

4.1 Introduction

As previously mentioned in Chapter 2, independent metering is a technique to separately control the meter-in and the meter-out of the hydraulic cylinder. It has five operation modes which are Power Extension, Power Retraction, High Side Regeneration Extension, Low Side Regeneration Retraction, and Low Side Regeneration Extension. At least four valves are required to operate one cylinder. Figure 4.1 illustrates the four valve independent metering configuration which will be studied through the thesis. The four valves are termed by K_{sa}, K_{sb}, K_{at}, and K_{bt}. As shown by Figure 4.1, K_{sa} connects the pump line to the cylinder head chamber, K_{sb} connects the pump line to cylinder rod chamber, K_{at} connects the tank line to the cylinder head chamber, and K_{bt} connects the tank line to the cylinder rod chamber. In each mode, two valves are operated to perform independent metering and this allows energy regeneration. The number of degrees of freedom is increased and this improves the actuator controllability. This chapter represents an overview of the mathematical model of the IM operation modes and their valve control developed by Tabor (2004, 2005a,b) and studied by Shenouda and Book (2005b), Alkam (2014). The mathematical model is based on the assumption that the system is quasi static which means that the plant dynamic change is slow and the capacitance of the cylinder chamber and hydraulic lines are neglected. This assumption will be used for the modes mathematical modelling and the valve control analysis. This chapter represents the background of the control system developed in this research. Section 4.2 is the mathematical representation of each operation mode including the overall produced flow rate in the cylinder and the flow rate produced by each valve. Section 4.3 explains the valve control in each mode. The anti-cavitation procedure is explained in Section 4.4 of this chapter and finally, the summary is in Section 4.5.

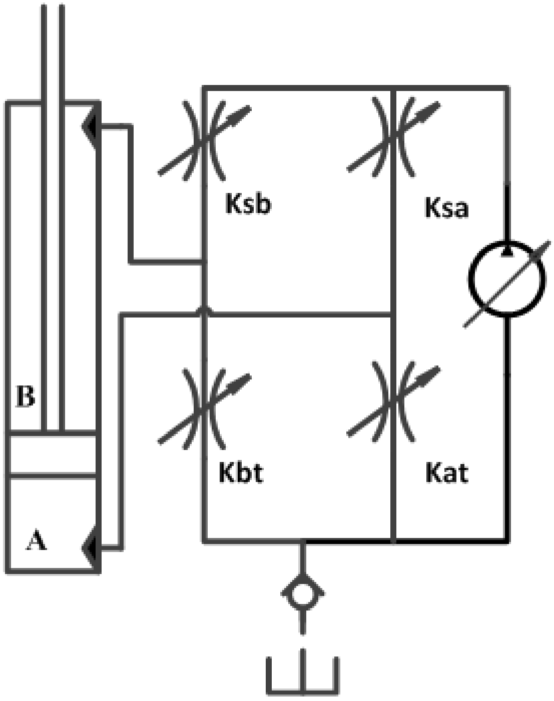

Fig. 4.1 The four valves independent metering configuration

4.2 The Mathematical Model of the Operation Modes

4.2.1 Power Extension Mode

In this mode, the active valves are K_{sa} which directs the fluid from the pump to the head chamber A; and K_{bt} which directs the fluid from chamber B to the tank (Figures 4.1 and 2.10). The equivalent representation of the power extension circuit is shown in Figure 4.2 where the simplified circuit has equivalent pressure P_{eq} and equivalent overall valves conductance or flow rate K_{eq}. These two parameters are used to develop the mathematical representation for every mode.

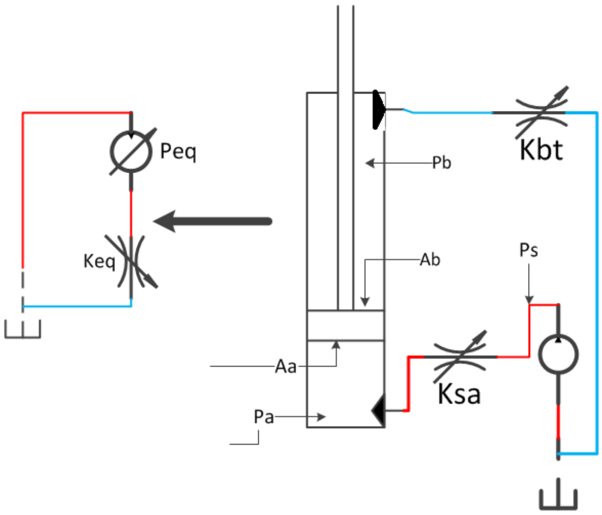

Fig. 4.2 The equivalent circuit for the power extension mode (Liu et al., 2016).

According to Merritt (1967), the pressure difference and flow rate across the valves can be considered as follow,

$$\Delta P_1 = P_s - P_a \tag{4.1}$$

$$\Delta P_2 = P_b - P_r \tag{4.2}$$

$$q_{in} = K_{sa}\sqrt{\Delta P_1} = K_{sa}\sqrt{P_s - P_a} = A_a\dot{x} \tag{4.3}$$

$$q_{out} = K_{bt}\sqrt{\Delta P_2} = K_{bt}\sqrt{P_b - P_r} = A_b\dot{x} \tag{4.4}$$

where P_S is the pump pressure source, P_a is the head chamber pressure, P_b is the rod chamber pressure, A_a is the head chamber area, A_b is the rod chamber area, x is the piston displacement, P_r is the tank pressure, q_{in} is the meter-in flow, and q_{out} is the meter-out flow.

The Newton's second law indicates that the $\sum F = ma$ which can be represented as follows,

$$P_sA_a - P_rA_b = \Delta P_1A_a + (P_aA_a - P_bA_b) + \Delta P_2A_b \tag{4.5}$$

More analysis about the manipulation of this Equation is attached in Appendix (A). By dividing the cylinder chambers areas, $R = A_a/A_b$.

$$RP_s - P_r = R\Delta P_1 + (RP_a - P_b) + \Delta P_2 \tag{4.6}$$

$$(RP_s - P_r) + (-RP_a + P_b) = R\Delta P_1 + \Delta P_2 \tag{4.7}$$

The equivalent pressure P_{eq} of the circuit, based on Equations 4.3, 4.4, and 4.7, is,

$$P_{eq} = (RP_s - P_r) + (-RP_a + P_b) = R\frac{q_{in}^2}{K_{sa}^2} + \frac{q_{out}^2}{K_{bt}^2} \tag{4.8}$$

where q_{in} is the meter-in flow, and q_{out} is the meter-out flow rate.

By dividing Equations 4.3 and 4.4,

$$R = \frac{q_{in}}{q_{out}} \tag{4.9}$$

$$P_{eq} = \frac{R^3 q_{out}^2}{K_{sa}^2} + \frac{q_{out}^2}{K_{bt}^2} = q_{out}^2 \left[\frac{R^3 K_{bt}^2 + K_{sa}^2}{K_{sa}^2 K_{bt}^2}\right] \tag{4.10}$$

By rearranging the Equation 4.10, the parameters q_{out}, K_{eq}, and P_{eq} are as follow:

$$q_{out} = \frac{K_{sa}K_{bt}}{\sqrt{(R^3 K_{bt}^2) + K_{sa}^2}} . \sqrt{P_{eq}} = K_{eq}\sqrt{P_{eq}} \tag{4.11}$$

$$K_{eq} = \frac{K_{sa}K_{bt}}{\sqrt{(R^3 K_{bt}^2) + K_{sa}^2}} \tag{4.12}$$

$$P_{eq} = (RP_s - P_r) + (-RP_a + P_b) \tag{4.13}$$

By combining Equations 4.4 and 4.11 the flow conductance is represented by,

$$K_{eq} = \frac{A_b \dot{x}}{\sqrt{P_{eq}}} = \frac{A_b \dot{x}}{\sqrt{(RP_s - P_r) + (-RP_a + P_b)}} \tag{4.14}$$

where K_{eq} is the equivalent conductance, A_b is the cylinder rod chamber area, $\dot{x}$ is the piston displacement, P_{eq} is the equivalent pressure, R is the ratio between the cylinder's two chambers' areas, P_s is the pump pressure, P_r is the tank pressure, P_a is the head chamber pressure, and P_b is the rod chamber pressure.

Based on the Equations 4.12 and 4.14, the K_{eq} relies on both valves working simultaneously, and it's value represents all the possible combination of the valves conductance, flow rates, to achieve the required piston speed. It also relies on the values of the supply pressure, return pressure, and both chamber pressures. To stop the piston, at least one of the two valves should be closed completely.

4.2.2 Power Retraction Mode

The analysis developed for the PE mode can be applied here for the PR mode. In this mode the two valves used to achieve the required speed are K_{sb} which controls the flow from the pump to the rod chamber B; and K_{at} which controls the flow from the head chamber A to the tank (Figures 4.1 and 2.10). More details about the PR mode mathematical representation can be obtained from Shenouda (2006) and Tabor (2005a). The equivalent conductance of the two valves is,

$$K_{eq} = \frac{K_{sb}K_{at}}{\sqrt{K_{at}^2 + R^3K_{sb}^2}} \tag{4.15}$$

The equivalent pressure is,

$$P_{eq} = (P_s - RP_r) + (-Pb + RP_a) \tag{4.16}$$

By combining the equivalent pressure P_{eq} and the equivalent conductance K_{eq} using the Equation 4.4, the equivalent conductance is,

$$K_{eq} = -\frac{A_b\dot{x}}{\sqrt{(P_s - RP_r) + (-P_b + RP_a)}} \tag{4.17}$$

where K_{eq} is the equivalent conductance, A_b is the cylinder rod chamber area, $\dot{x}$ is the piston displacement, P_{eq} is the equivalent pressure, R is the ratio between the cylinder's two chambers' areas, P_s is the pump pressure, P_r is the tank pressure, P_a is the head chamber pressure, and P_b is the rod chamber pressure.

4.2.3 High Side Regeneration Extension

The HSRE mode is implemented using the two valves K_{sa} and K_{sb} (Figures 4.1 and 2.10). The same analysis can be performed here to obtain the equivalent pressure and conductance, and further details about this mode mathematical analysis can be obtained from Shenouda (2006) and Tabor (2005a). The equivalent conductance of the two valves is,

$$K_{eq} = \frac{K_{sa}K_{sb}}{\sqrt{R^3K_{sb}^2 + K_{sa}^2}} \tag{4.18}$$

The equivalent pressure is,

$$P_{eq} = (R-1)P_s + (-RP_a + P_b) \tag{4.19}$$

By combining the equivalent pressure P_{eq} and the equivalent conductance K_{eq} using the equation 3.4, the equivalent conductance is,

$$K_{eq} = \frac{A_b \dot{x}}{\sqrt{P_{eq}}} = \frac{A_b \dot{x}}{\sqrt{(R-1)P_s + (-RP_a + P_b)}} \tag{4.20}$$

where K_{eq} is the equivalent conductance, A_b is the cylinder rod chamber area, $\dot{x}$ is the piston displacement, P_{eq} is the equivalent pressure, R is the ratio between the cylinder's two chambers' areas, P_s is the pump pressure, P_r is the tank pressure, P_a is the head chamber pressure, and P_b is the rod chamber pressure.

4.2.4 Low Side Regeneration Extension

The same analysis from the power extension section is applied here for the HSRE, but the valves used are K_{at} and K_{bt} to achieve the required speed (Figures 4.1 and 2.10). Further details on this mode mathematical analysis can be obtained from Shenouda (2006),Tabor (2005a), and Alkam (2014). The equivalent conductance of the two valves is,

$$K_{eq} = \frac{K_{at} K_{bt}}{\sqrt{R^3 K_{bt}^2 + K_{at}^2}} \tag{4.21}$$

The equivalent pressure is,

$$P_{eq} = (R-1)P_r + (-RP_a + P_b) \tag{4.22}$$

By combining the equivalent pressure P_{eq} and the equivalent conductance K_{eq} using the Equation 3.4, the equivalent conductance is,

$$K_{eq} = \frac{A_b \dot{x}}{\sqrt{P_{eq}}} = \frac{A_b \dot{x}}{\sqrt{(R-1)P_r + (-RP_a + P_b)}} \tag{4.23}$$

where K_{eq} is the equivalent conductance, A_b is the cylinder rod chamber area, $\dot{x}$ is the piston displacement, P_{eq} is the equivalent pressure, R is the ratio between the cylinder's two chambers' areas, P_s is the pump pressure, P_r is the tank pressure, P_a is the head chamber pressure, and P_b is the rod chamber pressure.

4.2.5 Low Side Regeneration Retraction

The same analysis form the power extension section is applied here for the HSRE, but the used valves are K_{at} and K_{bt} to achieve the required speed (Figures 4.1 and 2.10). Further details on this mode mathematical analysis can be obtained from Shenouda (2006),Tabor (2005a), and Alkam (2014). The equivalent conductance of the two valve is,

$$K_{eq} = \frac{K_{at}K_{bt}}{\sqrt{R^3K_{bt}^2 + K_{at}^2}} \tag{4.24}$$

The equivalent pressure is,

$$P_{eq} = -(R-1)P_r + (+RP_a - P_b) \tag{4.25}$$

By combining the equivalent pressure P_{eq} and the equivalent conductance K_{eq} using the Equation 4.4, the equivalent conductance is,

$$K_{eq} = -\frac{A_b\dot{x}}{\sqrt{P_{eq}}} = \frac{A_b\dot{x}}{\sqrt{-(R-1)P_r + (-P_b + RP_a)}} \tag{4.26}$$

where K_{eq} is the equivalent conductance, A_b is the cylinder rod chamber area, $\dot{x}$ is the piston displacement, P_{eq} is the equivalent pressure, R is the ratio between the cylinder's two chambers' areas, P_s is the pump pressure, P_r is the tank pressure, P_a is the head chamber pressure, and P_b is the rod chamber pressure.

4.3 Valve Control

A general form of the overall conductance through the cylinder that is using both valves in every mode is implemented by the following equation,

$$K_{eq} = \frac{K_aK_b}{\sqrt{K_a^2 + R^3K_b^2}} \tag{4.27}$$

where the K_a can be either K_{sa} or K_{at}, and K_b can be either K_{sb} or K_{bt} based on the selected operation mode. The equivalent conductance of both valves in every mode, is a combination of different openings of these valves. The number of combinations is infinite according to Tabor (2005b), and it depends on the dimensions of the cylinder, mainly R which is the ratio between the two chamber surfaces areas. The plot of the possible combinations between valves with $R = 1.3405$ selected by Shenouda (2006), is shown in Figure 4.3.

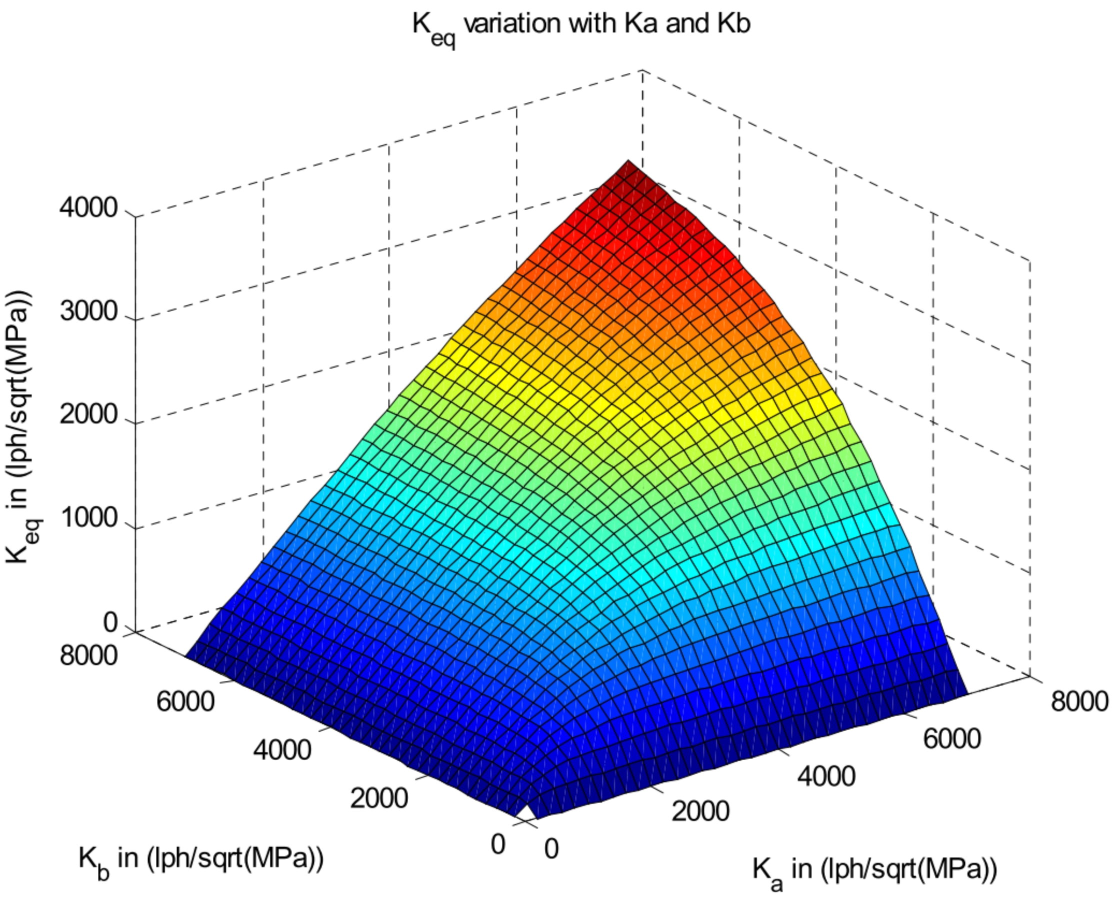

Fig. 4.3 The equivalent conductance from the possible combinations (Shenouda, 2006).

4.3.1 Valve Sensitivity

As there is an infinite number of combinations between the two valves, the question is how to select the most suitable combination? This issue was studied by Tabor (2005a). He built an IM system using solenoid poppet valves. The poppet valve has a controllability problem that the commands may not achieve the desired opening that is selected by the controller. He suggested operating the valves in the region where K_{eq} is least affected by the valve's error or deviation. He used a magnitude of gradient method that is given by the following equation (Tabor, 2005a).

$$|\nabla K_{eq}(Ka, Kb)| = \sqrt{\frac{K_a^6 + R^6 K_b^6}{(K_a^2 + R^3 K_b^2)^3}} \tag{4.28}$$

where $|\nabla|$ is a vector differential calculus.

The graph of the equation is shown in Figure 4.4. As noticed in Figure 4.4, the bottom of the valley in the curve indicates a linear relationship between the values of K_a and K_b where the curve ingredient is minimum (Shenouda, 2006). The relationship is $K_a = \alpha_{opt} K_b$. Where α_{opt} is $R^{(3/4)}$ (Shenouda and Book, 2005b).

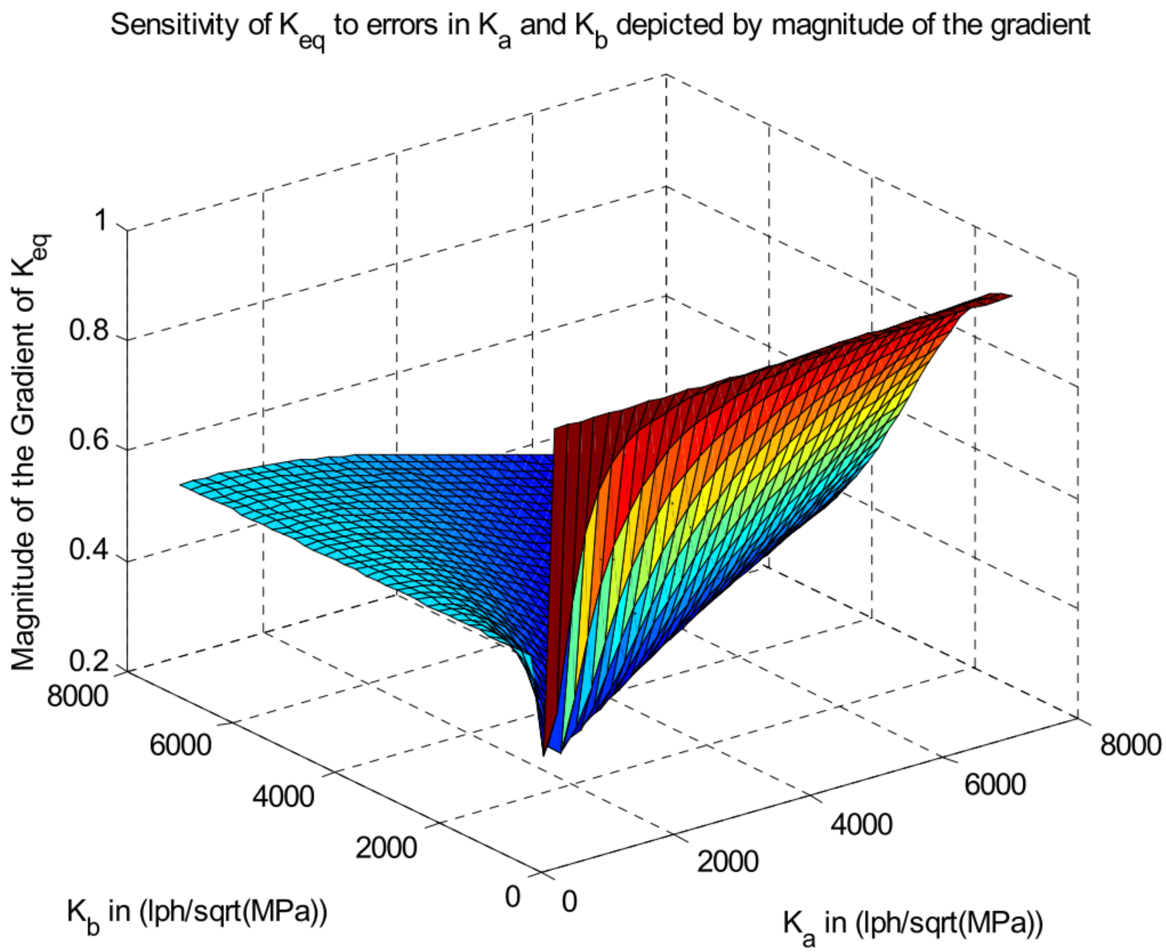

Fig. 4.4 Sensitivity of Keq to errors in Ka and Kb depicted by magnitude of the gradient (Shenouda, 2006).

4.3.2 Work Port Pressure Control

One of the main advantages of the Independent Metering configuration is the ability to control the actuator speed with some control on the work port pressures. These pressures can be selected to avoid cavitation problem which is a phenomena that appears when the rate of fluid filling the actuator chamber is slower than its rate of expansion. The pressure for the head chamber is called P_{ac} and the pressure for the rod is called P_{bc}. The relationship between these pressures and the valve conductance coefficient for each mode are included in Table (3.1).

Table 4.1 Chamber pressures control equation for every mode

Mode	***Inlet Pressure***	***Outlet Pressure***
Power extension	$K_{sa.pc} = \frac{\lvert\dot{x}\rvert A_a}{\sqrt{P_s - P_{ac}}}$	$K_{bt.pc} = \frac{\lvert\dot{x}\rvert A_b}{\sqrt{P_{bc} - P_r}}$
Power retraction	$K_{sb.pc} = \frac{\lvert\dot{x}\rvert A_b}{\sqrt{P_s - P_{bc}}}$	$K_{at.pc} = \frac{\lvert\dot{x}\rvert A_a}{\sqrt{P_{ac} - P_r}}$
High side regeneration extension	$K_{sa.pc} = \frac{\lvert\dot{x}\rvert A_a}{\sqrt{P_s - P_{ac}}}$	$K_{sb.pc} = \frac{\lvert\dot{x}\rvert A_b}{\sqrt{P_{bc} - P_s}}$
Low side regeneration extension	$K_{at.pc} = \frac{\lvert\dot{x}\rvert A_a}{\sqrt{P_r - P_{ac}}}$	$K_{bt.pc} = \frac{\lvert\dot{x}\rvert A_b}{\sqrt{P_{bc} - P_r}}$
Low Side regeneration retraction	$K_{bt.pc} = \frac{\lvert\dot{x}\rvert A_b}{\sqrt{P_r - P_{bc}}}$	$K_{at.pc} = \frac{\lvert\dot{x}\rvert A_a}{\sqrt{P_{ac} - P_r}}$

4.4 Anti-Cavitation Analysis

Cavitation is an obstacle that appears when one of the chambers expands at a rate faster than the fluid filling rate. When cavitation appears, the mathematical equations of the IM cannot be implemented, and the control of the system is lost. To overcome this issue, the pressure drop in the inlet chamber should be reduced to the minimum value. Reducing the pressure drop is performed by increasing the opening degree of the inlet valve. Also, more reducing of the outlet valve opening stops the piston from moving faster. This depends on the ratio between the two used valves in each mode. If cavitation occurs at a particular ratio, then changing this ratio is necessary to avoid it (Tabor, 2005a). The analysis of this procedure for the different modes is in the following subsections (Shenouda, 2006).

4.4.1 Power Extension Mode Cavitation

In the Power Extension mode, caviation occurs when the cylinder movement is in the same direction as the load, as illustrated in Figure 4.5

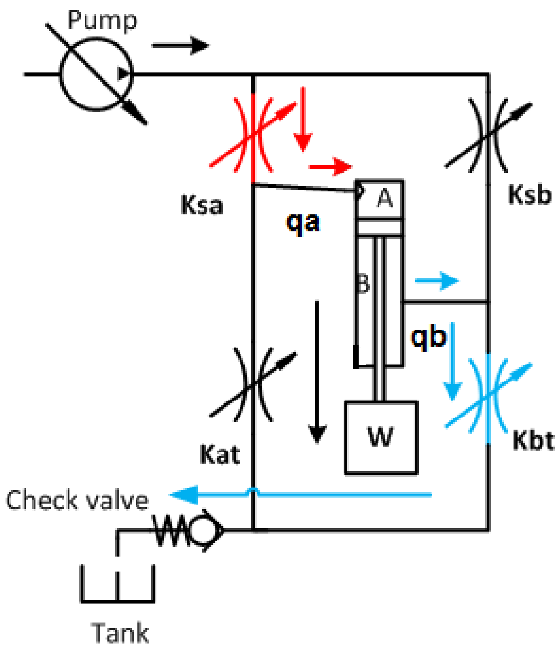

Fig. 4.5 The overrunning load causes cavitation in the power extension mode. For example, it appears on boom cylinder of excavator machine.

The hydraulic force is represented by Equation 4.29. The force acting on the cylinder F_l is produced by the weight of the load.

$$F = P_a A_a - P_b A_b = F_l - F_f \tag{4.29}$$

where P_a is the head chamber pressure, P_b is the rod chamber pressure, A_a is the area of the head chamber, A_b is the rod chamber area, F_l is the load force, and F_f is the cylinder friction force. Rearranging the equation, so that the road chamber pressure is on the left side,

$$P_b = \frac{P_a A_a + F_L - F_f}{A_b} \tag{4.30}$$

The cylinder flow Equations are 4.31 and 4.32, and their division is Equation 4.33,

$$q_a = A_a \dot{x} = K_{sa}\sqrt{(\Delta P1)} = K_{sa}\sqrt{P_s - P_a} \tag{4.31}$$

$$q_b = A_b \dot{x} = K_{bt}\sqrt{(\Delta P2)} = K_{bt}\sqrt{P_b - P_r} \tag{4.32}$$

The division of the two equations is,

$$\frac{q_a}{q_b} = R = \alpha\sqrt{\frac{\Delta p_1}{\Delta p_2}} \tag{4.33}$$

As $\frac{Aa}{Ab} = R$ and $\frac{K_{sa}}{K_{sb}} = \alpha$, the flow ratio, Equation 4.33 can be written as,

$$\Delta p_2 = (\frac{\alpha}{R})^2 \Delta P_1 \tag{4.34}$$

$$P_b - P_r = (\frac{\alpha}{R})^2 (P_s - P_a) \tag{4.35}$$

$$P_b = (\frac{\alpha}{R})^2 (P_s - P_a) + P_r \tag{4.36}$$

Based on Equations 4.30 and 4.36 which are equal, and solving for Pa,

$$P_a A_a + F_L - F_f = P_r A_b + ((\frac{\alpha}{R})^2 P_s - (\frac{\alpha}{R})^2 P_a) A_b \tag{4.37}$$

$$P_a[A_a + (\frac{\alpha}{R})^2 A_b] = (\frac{\alpha}{R})^2 A_b P_s - (F_l - F_f) + P_r A_b \tag{4.38}$$

$$P_a = \frac{(\frac{\alpha}{R})^2 A_b P_s - (F_l - F_f) + P_r A_b}{[A_a + (\frac{\alpha}{R})^2 A_b]} \tag{4.39}$$

$$P_a = \frac{(\frac{\alpha}{R})^2 P_s - \frac{(F_l - F_f)}{A_b} + P_r}{[R + (\frac{\alpha}{R})^2]} \tag{4.40}$$

Caviation appears when the pressure P_a is negative or zero. By substituting the value of P_a as zero and solving the equation for load force F_L,

$$(\frac{\alpha}{R})^2 P_s + P_r = \frac{(F_l - F_f)}{A_b} \tag{4.41}$$

$$F_L = (\frac{\alpha}{R})^2 A_b P_s + P_r A_b + F_f \tag{4.42}$$

Further details on the mathematical analysis can be obtained from Shenouda (2006), Tabor (2005a), and Alkam (2014). An illustration example of cavitaion is an actual tractor laoder backhoe bucket cylinder. The cylinder parameters are $R = 1.658$, $A_b = 4737\ mm^2$, $P_s = 20\ MPa$, P_t=0.7 MPa. As illustrated in Figure 4.6, the red vertical line shows the load force value when cavitation starts to appear, which is 77 KN. By rearranging Equation 3.42,

$$\alpha = R * \sqrt{\frac{F_L - F_f - P_r A_b}{P_s A_b}} \tag{4.43}$$

The friction value is neglected and the load force is obtained. In order to stop cavitation, the valve conductance value K_{sa} shall increase and the valve conductance K_{bt} reduce, which means a new value of α.

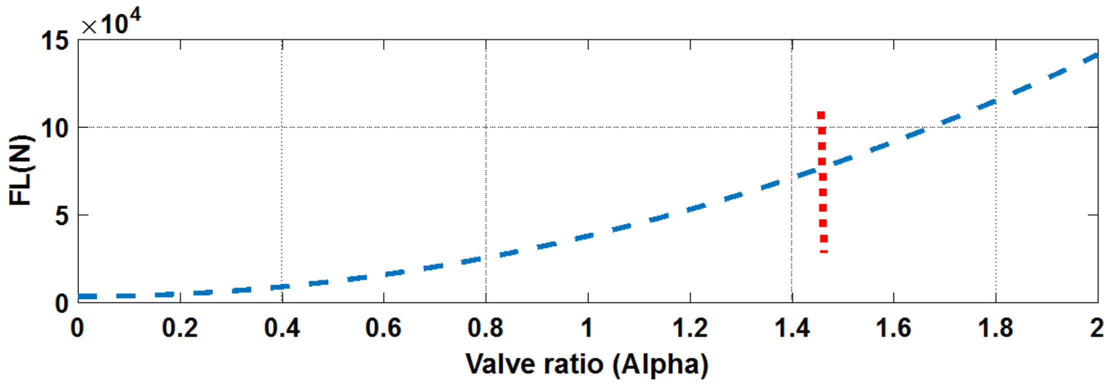

Fig. 4.6 The cavitation load in the Power extension mode.

4.4.2 Power Retraction Cavitation

The cavitation in the power retraction mode is shown in Figure 4.7.

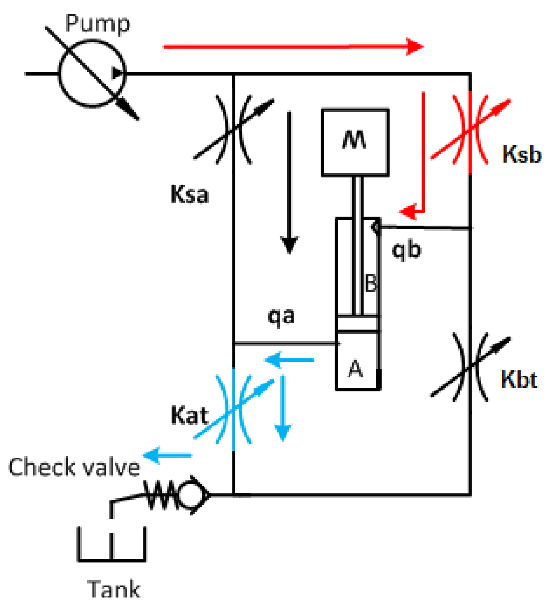

Fig. 4.7 The overrunning load causes cavitation in the power retraction mode.

From Equation 4.29,

$$P_a = \frac{P_b}{R} + \frac{(F_L - F_f)}{A_a} \tag{4.44}$$

By implementing the same analysis of the Equations 4.31 to 4.35 and considering that this mode relies on different valves,

$$P_a = (\frac{R}{\alpha})^2 (P_s - P_b) + P_r \tag{4.45}$$

By rearranging the equations and solving for P_b,

$$P_b = \frac{(\frac{R}{\alpha})^2 P_s - \frac{F_L - F_f}{A_a} + P_r}{\frac{1}{R} + \frac{R}{\alpha}} \tag{4.46}$$

Further details on the mathematical analysis can be obtained from Shenouda (2006),Tabor (2005a), and Alkam (2014). Cavitation in power retraction mode appears when the $P_b <= 0$. As shown in Figure 4.8, the biggest applied load is $F_L = 210\ KN$. Bigger values can be applied by reducing the valve opening K_{at} and increasing the valve conductance K_{sb}.

$$F_L = (\frac{\alpha}{R})^2 A_a P_s + A_a P_r + F_f \tag{4.47}$$

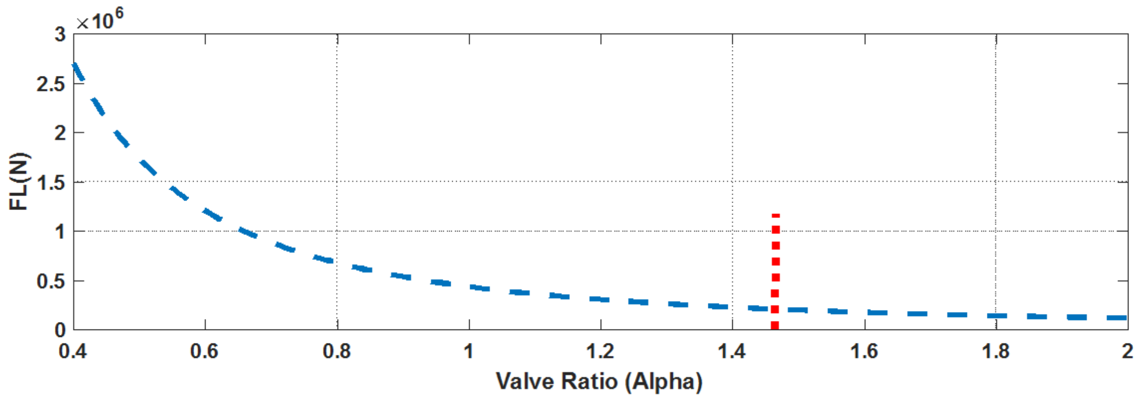

Fig. 4.8 The cavitation load in the power retraction mode

4.4.3 High Side Regeneration Extension Cavitation

The form causes cavition in high side regeneration extension is shown in Figure 4.9. In the case cavitation appears when the high load is lowering and causes the piston to move faster than the fluid filling speed in the head chamber.

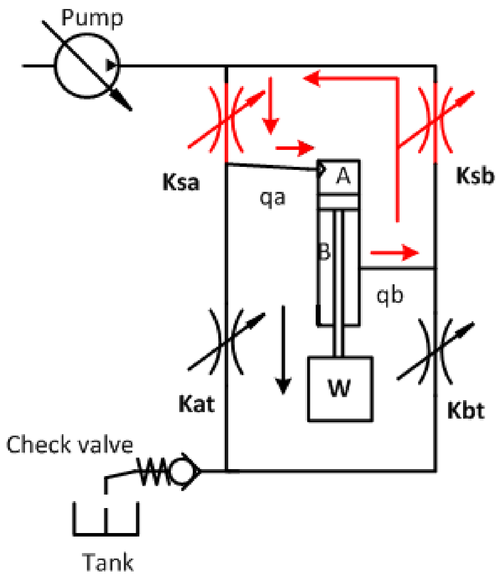

Fig. 4.9 The overrunning load causes caviation in the high side regeneration extension

By solving Equation 4.29 for P_b,

$$p_b = \frac{P_a A_a + F_L - F_f}{A_b} = \frac{RP_a + F_L - F_f}{A_b} \tag{4.48}$$

Following the same analysis of Equations 4.31 to 4.35 and considering that this mode relies on different valves,

$$P_b = (\frac{\alpha}{R})^2 (P_s - P_a) + P_S \tag{4.49}$$

By equating the two previous equations,

$$P_a = \frac{[1 + (\frac{}{R})^2] Ps \frac{F_l - F_f}{A_b}}{[R + (\frac{\alpha}{R})^2]} \tag{4.50}$$

In this mode, cavitation appears when the $P_a <= 0$ then,

$$F_l = [1 + (\frac{\alpha}{R})^2] A_b P_s + F_f \tag{4.51}$$

Further details on the mathematical analysis can be obtained from Shenouda (2006),Tabor (2005a), and Alkam (2014). By using the same parameters from the power extension cavitation section, Figure 4.10 shows that at about 168 KN where the cavaition starts to appear.

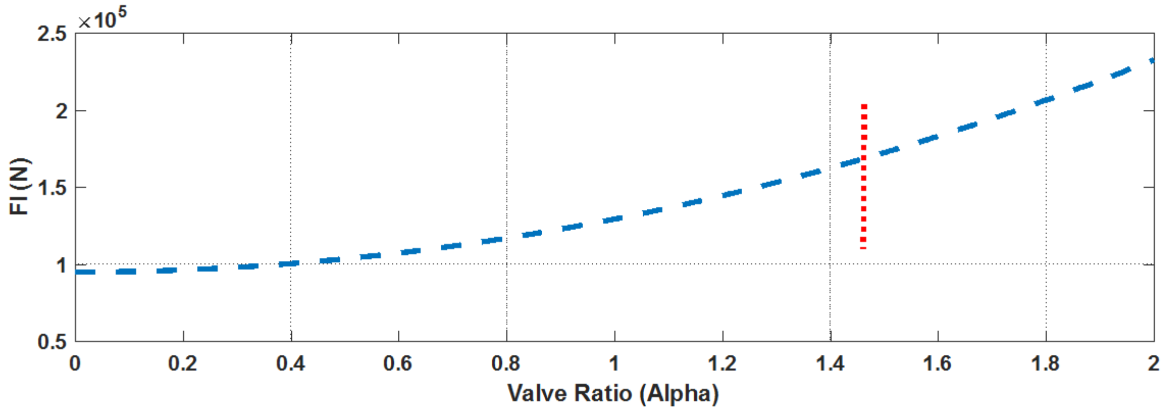

Fig. 4.10 The cavitation load in the high side regeneration extension

4.4.4 Low Side Regeneration Extension Cavitaiton

The low side regeneration extension mode subject to overrunning load is illustrated in Figure 4.11.

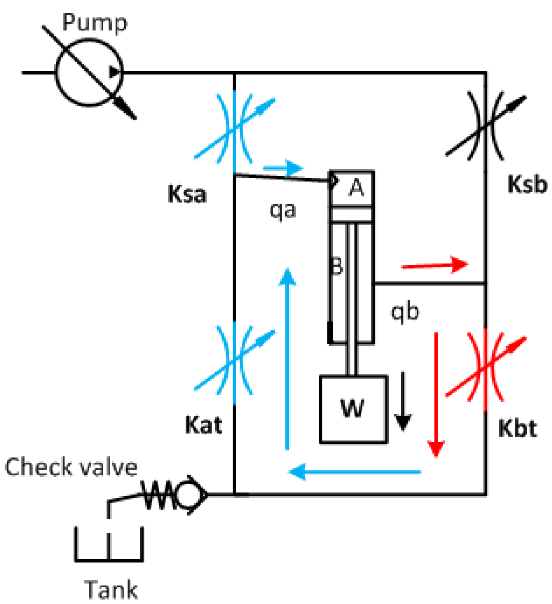

Fig. 4.11 The overrunning load causes cavitation in low side regeneration extension

By rearranging Equation 4.29,

$$P_b = RP_a + \frac{F_l - F_f}{A_b} \tag{4.52}$$

Implementing the same analysis 4.31 to 4.35 and considering that this mode relies on different valves,

$$p_b = (\frac{\alpha}{R})^2 (P_r - P_a) + P_r \tag{4.53}$$

By equating the previous two equations and solving for P_a,

$$P_a = \frac{[1 + (\frac{\alpha}{R})^2] P_r - \frac{(F_l - F_f)}{A_b}}{[R + (\frac{\alpha}{R})^2]} \tag{4.54}$$

Solving for F_l,

$$F_l = [1 + (\frac{\alpha}{R})^2] A_b P_r + F_f \tag{4.55}$$

Further details on the mathematical analysis can be obtained from Shenouda (2006), Tabor (2005a), and Alkam (2014). As shown in Figure 4.12, the load that causes cavitation for the same parameters that are used in the previous section is 5900 N.

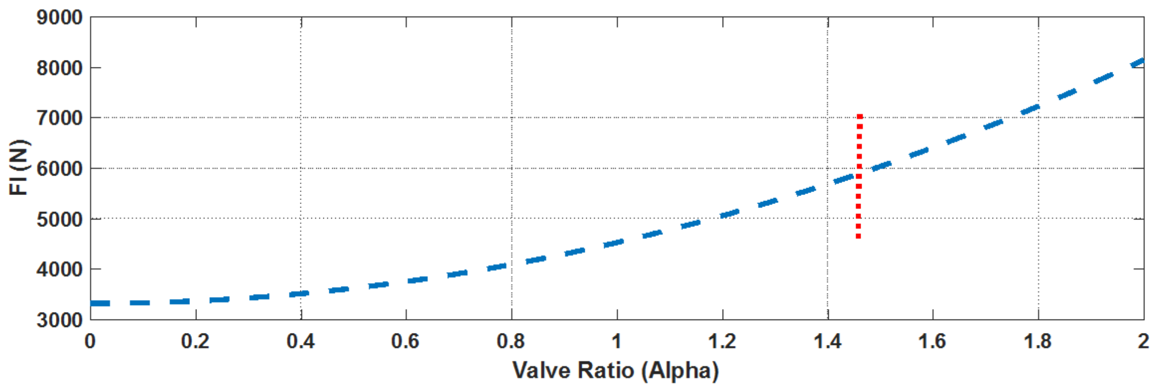

Fig. 4.12 The cavitation load in the low side regeneration extension

4.4.5 Low Side Regeneration Retraction Cavitation

The form of low side regeneration retraction subjected to overrunning load is shown in Figure 4.13.

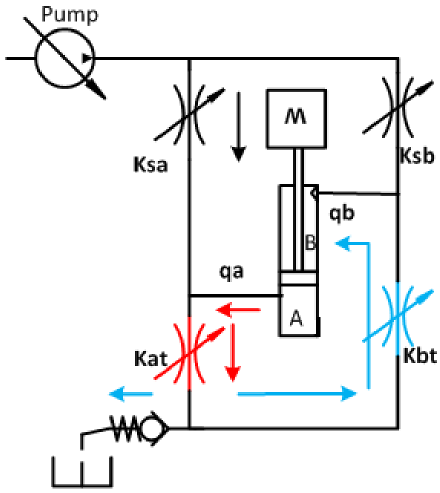

Fig. 4.13 The overrunning load causes cavitation in the low side regeneration retraction

By rearranging the Equation 4.29,

$$P_a = \frac{P_b}{R} + \frac{(F_l - F_f)}{A_A} \tag{4.56}$$

Following the same analysis using Equations 4.31 to 4.35 and considering that this mode relies on different valves,

$$P_a = (\frac{\alpha}{R})^2(P_r - P_b) + P_r \tag{4.57}$$

By equating the two previous equations and solving for P_b,

$$P_a = \frac{[1 + (\frac{\alpha}{R})^2]P_r - \frac{(F_L - F_f)}{A_b} + P_r}{[\frac{1}{R} + \frac{\alpha}{R}^2]} \tag{4.58}$$

Solving for F_L,

$$F_l = [1 + (\frac{\alpha}{R})^2]A_a P_r + F_f \tag{4.59}$$

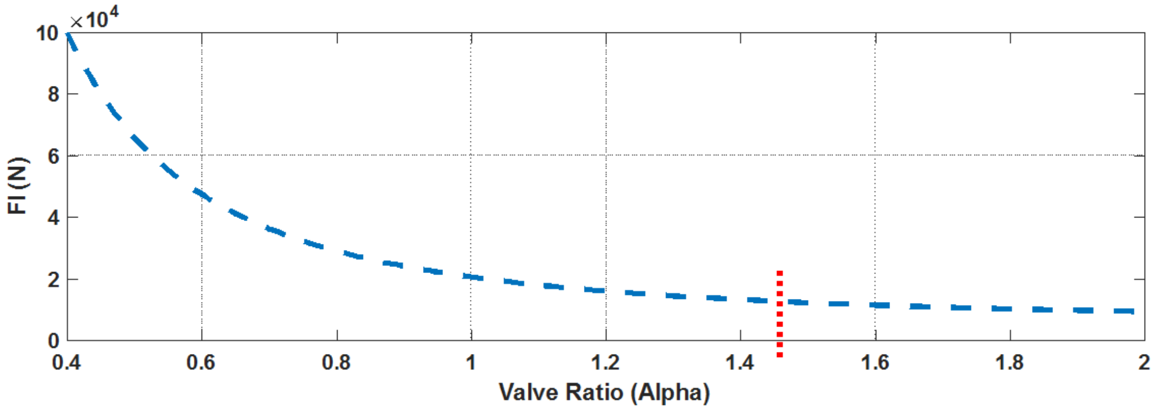

Fig. 4.14 The caviation load in the low side regeneration retraction

Further details on the mathematical analysis can be obtained from Shenouda (2006), Tabor (2005a), and Alkam (2014). By using the same parameters as in the previous example, the load that causes cavitation in this mode is 12.5 KN as shown in Figure (4.14).

4.5 Summary

In this chapter, three main points were studied as follows:

- The mathematical representation of the five Indpendent Metering modes.
- The valve control which includes the sensitivity and port pressure controls.
- The cavitation problem and the method to overcome it.

The equivalent conductance and pressure for every mode were represented mathematically. These mathematical equations are used to build the control algorithm, and they help to select a suitable operating mode during the machine working cycle. According to Tabor (2005a), there are some limitations on the selected valves conductance, and this is because he used the poppet valve to make the IM system. The shortcoming of this valve is the low stability. So to overcome it, he selected an opening ratio between the valves, and by this, he reduced the effect of instability on the system overall. As the mathematical representation can not be applied when cavitation appears, the anti-cavitation procedure was explained and mathematically represented.

Finally, this analysis was studied by previous researchers where the valve used was a poppet type which gave infinite positioning. This raised a research question which is what is the proper procedure to be used for the new proposed valve? This question will be answered by using a novel Close Value Detection procedure which has been developed and inserted into the control algorithm. This procedure is explained in more detail during the control algorithm development in Chapter 5. In order to enhance the algorithm performance, more analysis of the new valve is necessary. The valve work principle, response, and performance limitations are the topics of the next chapter.

Chapter 5

The Stepped Rotary Flow Control Modelling and Performance Analysis

5.1 Introduction

The aim of this research is to investigate independent metering using a new rotary orifice that was developed by Okhotnikov et al. (2017). This research includes developing a control methodology for the proposed system. To develop this control system, the parameters that affect the valve performance need to be identified and analysed. The considerations include the valve construction analysis, mathematical modelling, parameters validation, response analysis, and stability analysis. A previous research project included a mathematical model of a proportional pressure control valve which was developed and represented using Bond graphs (Yang et al., 2012). A servo proportional valve was mathematically analysed and modelled by Anderson and Li (2002) andAcuña-Bravo et al. (2017). A priority flow control valve was modelled by Coskun et al. (2017) and (Tørdal et al., 2015). A linear model of a hydraulic rotary actuator containing coulomb friction was evaluated in (Pollok and Casella, 2017; Heintze et al., 1993). The poppet valve known of the difficulties to model because of its nonlinear characteristics was investigated (Opdenbosch et al., 2009a). A linear and nonlinear models and model validation for a two-stage electrohydraulic valve, Valvistor, were investigated by Zhang et al. (2002a) and Liu et al. (2002). A model of a three way rotary electrohydraulic valve was investigated by Yang et al. (2010). It showed the mathematical model of the valve combined with a DC motor, and illustrated the viscous torque, friction torque and flow torques. The steady flow torque was throughly analyzed for servo-operated rotary directional valve (Wang et al., 2016).

The stepper motor has been widely used for different applications due to its unique characteristics. The main types of stepper motor constructions with dynamical simulation were discussed by Kenjo and Sugawara (1994), and Kępiński et al. (2015). A position control of a Permanent Magnet (PM) stepper motor using an exact linearization technique was evaluated by Zribi and Chiasson (1991). The effect of friction on a stepper motor in robotics applications was modeled and evaluated by Konowrocki et al. (2016). Regarding performance analysis, a study of a two-stage poppet valve was performed using the root locus method for a linear model. This analysis led to developing the valve's mechanical design. The investigations were performed by applying different operating conditions as indicated by Muller and Fales (2008) and Fales (2006).

A descriptive mathematical model of the stepped rotary valve is presented here for the purposes of simulation, analysis, and control algorithm design. In Section 5.2, the construction of this valve is demonstrated. Section 5.3 clarifies the mathematical representation of the valve. Then, Section 5.4 includes practical experiment to quantify some parameters that affect the valve performance. After that, the response analysis is described in the Section 5.5. A linearized state space model is discussed in Section 5.6. The root locus analysis for the valve was performed in Section 5.7. Finally, the summary of this chapter is in Section 5.8.

5.2 The Rotary Flow Valve Structure and Operation Principles

The rotary flow control valve considered in this research is shown in Figure 5.1. The flow is controlled by the position of the rotor in the stepper motor. Figure 5.2 shows the schematic construction of the motor (b) and the orifice (a). When the driving circuit of the motor starts feeding current into the coils, an electromagnetic force is produced in the stators which rotate the rotor. (Kenjo and Sugawara, 1994). The motor rotor is directly coupled with the orifice spool. Consequently, the opening area of the orifice is changed. Figure 5.3 illustrates the relationship between the rotation angle and the flow produced under different pressure drops. The selected motor for this design is a hybrid bipolar stepper motor because of its smaller size and higher torque compared to other kinds such such as variable reluctance. (Kenjo and Sugawara, 1994). The parameters of the selected motor are important to ensure effective valve control.

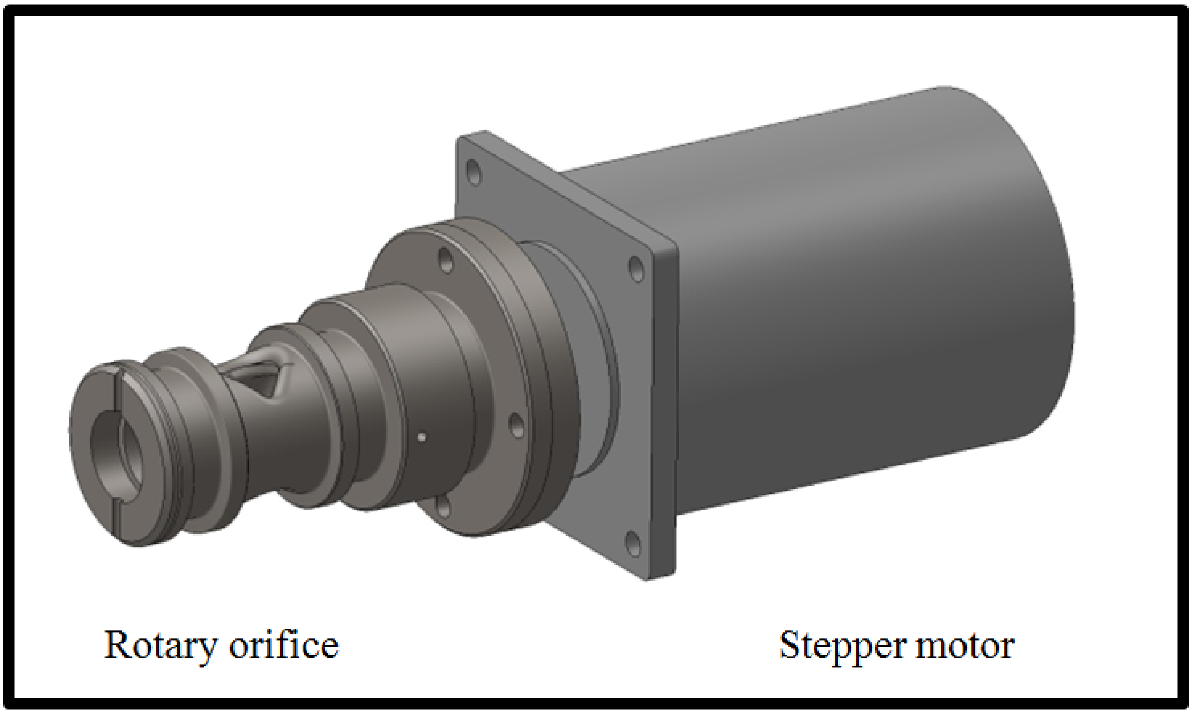

Fig. 5.1 The rotary flow control valve

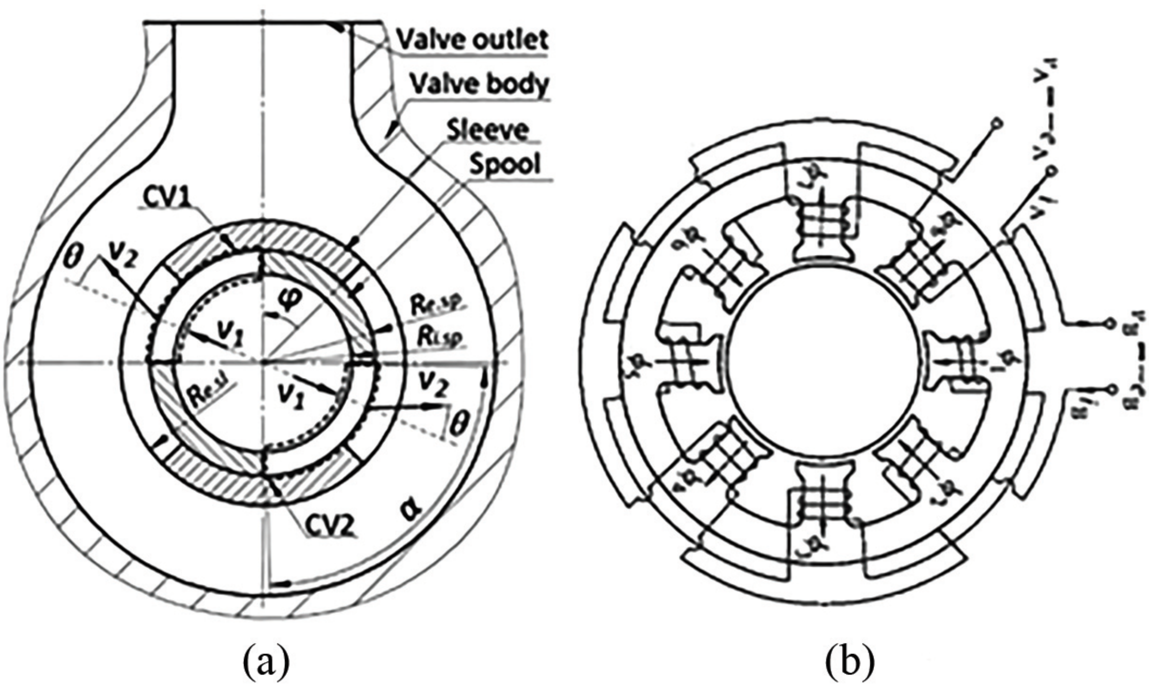

Fig. 5.2 The schematic diagram of the valve construction.

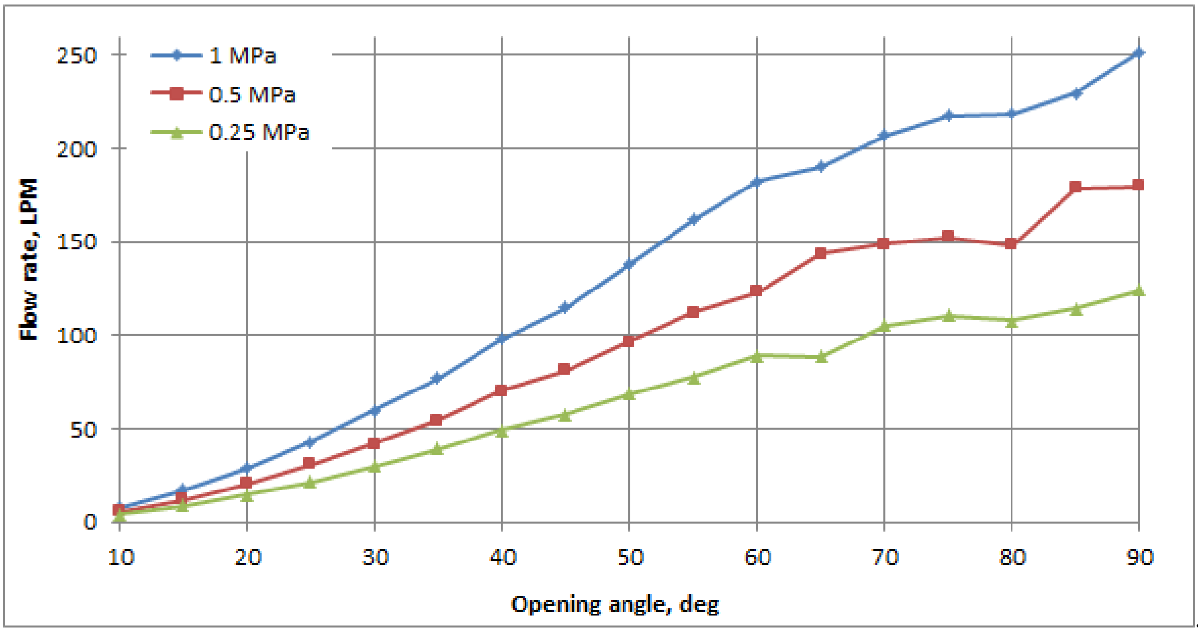

Fig. 5.3 The valve flow regime (Okhotnikov et al., 2017)

5.3 Mathematical Model of the Valve

This stepped rotary flow control valve consists of two main parts which are the stepper motor and the mechanical rotary orifice. The coupling between these two subsystems requires the stepper motor to overcome the torques generated from the mechanical part. The steady state flow torque in Equation 5.6, the transient flow torque in Equation 5.12 and the friction torque in Equation 5.14 have been developed and evaluated by Okhotnikov et al. (2017), Jelali and Kroll (2012), Bisztray-Balku (1995), and Pennestrì et al. (2016). Likewise, the equations representing the stepper motor are included in the state space representation in Equation (5.18).

The steady state flow torque acting on the rotary spool from both orifices (Figure 5.2 a) was investigated by Okhotnikov et al. (2017)

$$T_{st.fl} = C_v Q_t \sqrt{2\Delta p \rho} R_{e.sp} \sin\theta \tag{5.1}$$

where $T_{st.fl}$ is the steady state flow, C_v is the velocity coefficient, Q_t is the flow rate, Δp is the pressure difference, θ is the flow jet angle, ρ is the oil density and $R_{e.sp}$ is the external spool radius. The magnitude of the velocity coefficient depends on the contraction coefficient of the sharp-edged orifice C_c according to a following relation,

$$C_v = 1/\sqrt{1 - C_c^2} \tag{5.2}$$

The contraction coefficient in its turn specifies a ratio of a cross sectional area of a compressed flow in the vena contracta A_{vc} over the orifice area A_o. The coefficient is a function of the geometry of the outlet (Gerhart et al., 2016),

$$C_c = \frac{A_{vc}}{A_o} \tag{5.3}$$

The discharge coefficient is a function of the contraction coefficient as well as the velocity coefficient,

$$C_d = C_v C_c = \frac{C_c}{\sqrt{1 - C_c^2}} \tag{5.4}$$

Thus, the Bernoulli equation expressed through the contraction coefficient takes form,

$$Q_t = \frac{C_c A_o}{\sqrt{1 - C_c^2}} \sqrt{\frac{2\Delta p}{\rho}} \tag{5.5}$$

Substituting Equations 5.2, 5.3, 5.4, and 5.5 into Equation 5.1 , one can obtain

$$T_{st.fl} = \frac{2C_c \Delta p A_o R_{e.sp} \sin\theta}{1 - C_c{}^2} \tag{5.6}$$

where $T_{st.fl}$ is the steady state flow, C_c is the contraction coefficient, Δp is the pressure difference, A_o is the opening area, and $R_{e.sp}$ is the external spool radius,

In sliding spool valves, the transient flow force is proportional the spool velocity and the rate of pressures changes acting on a small fluid element inside the control volume. It is applicable for rotary valves as well with the substitution of linear to angular motion. (Jelali and Kroll, 2012). However, in the hollow rotary spool, the pressure changes in the down and up stream channels do not cause a pressure difference on the edges of the rotary orifice. This does not result in the formation of either a tangential force or torque on the spool. Hence, the only contributor to the transient flow torque is the fluid inertial component, which can be determined from a moment of inertia I_{fl} of a fluid volume and a spool angular acceleration γ,

$$T_{tr.fl} = I_{fl}\gamma = I_{fl}\frac{d\omega}{dt} \tag{5.7}$$

where ω is the angular velocity. The moment of inertia of the fluid body (hollow cylinder or tube) along its longitudinal axis corresponding to the valve main axis is equal to, (Budynas et al., 2008)

$$I_{fl} = m_{fl}\frac{(R_{e.sp}^2 + R_{i.sp}^2)}{2} \tag{5.8}$$

where $R_{e.sp}$ is the external radius of the spool, $R_{i.sp}$ is the internal radius of the spool, m_{fl} is the total fluid mass in both orifices under acceleration. This mass m_{fl} is found from the total volume of tubular control elements V_{fl} in both orifices. Each of these control volumes represents a portion of a hollow cylinder, which is located within an angle α, covered by the spool window,

$$m_{fl} = V_{fl}\rho = \frac{2\Pi\alpha(R_{e.sp}^2 - R_{i.sp}^2)h\rho}{360^\circ} \tag{5.9}$$

The height of the fluid cylinder h is variable along a central arc in the symmetry plane of the opening. Effectively the fluid cylinder height is equal to the width of the window. Thus, it can be expressed through an equivalent area $A_{sp.eq}$, which equates to the spool single window opening area $A_{sp.op}$. Hence, referring to Figure 5.4, the height h is a ratio of the spool opening $A_{sp.op}$ to the central axis arc length l,

$$A_{sp.op} = A_{sp.eq} = hl, \tag{5.10}$$

$$h = A_{sp.eq}/l = \frac{360^\circ A_{sp.op}}{2\Pi\alpha R_{e.sp}} \tag{5.11}$$

Substituting Equations 5.8 to 5.11 into equation (5.7), one can obtain,

$$T_{tr.fl} = \frac{(R_{e.sp}^4 - R_{i.sp}^4)A_{sp.op}\rho}{R_{e.sp}}\frac{d\omega}{dt} \tag{5.12}$$

where $T_{tr.fl}$ is the transient flow torque, $R_{e.sp}$ is the external spool radius, $R_{i.sp}$ is the internal spool radius, ω is the angular velocity, $A_{sp.op}$ is the spool opening area.

The friction torque is represented by Equations 5.13 and 5.14 (Pennestrì et al., 2016),

$$T_f r = \sigma_0 + \sigma_1\frac{dZ}{dt} + \sigma_2\omega \tag{5.13}$$

where σ_0 is the stiffness coefficient, σ_1 is the damping coefficient, σ_2 is the viscous friction coefficient, and ω is the angular velocity.

$$\frac{dZ}{dt} = \omega - \frac{\sigma_0|\omega|}{T_c + (T_s - T_c)\exp - (\frac{\omega}{\omega_s})^2}Z \tag{5.14}$$

where T_c is the columb friction, T_s is the static friction, ω_s is the stribick characterstics velocity, and Z is the deflection average of the asperities on two contacting surfaces. Assuming the spool and the sleeve are concentric parts with a small radial clearance between them; the viscous frictional torque acting on the spool from the annular liquid volume during motion in the clearance can be considered as laminar Couette flow and calculated according to the Newton's law of viscosity,

$$\sigma_2 \omega = \tau A_{sp} R_{e.sp} = \frac{\mu R_{e.sp}^2 A_{sp} \omega}{\delta} \tag{5.15}$$

where τ is shear stress, μ – the dynamic viscosity coefficient of the fluid, A_{sp} – the total area of the spool external cylinder subjected to the shear stress in the annular gap with a clearance

$$\delta = R_{i.sl} - R_{e.sp} \tag{5.16}$$

where $R_{i.sl}$ and $R_{e.sp}$ are the inner sleeve and the external spool radii respectively. The viscous shear stress τ acts on the spool cylindrical surfaces in the annular gap with the clearance δ. The spool external cylinder houses two sets of balancing grooves, which prevent formation of a hydraulic lock and centre the spool concentrically inside the sleeve (Jelali and Kroll, 2012), as well as two throttling orifices. These regions do not contribute to the viscous friction torque on the spool since the radial distance from the spool to the sleeve there is not equal to the clearance δ. Thus, the total area of interest is

$$A_{sp} = 2\Pi R_{e.sp}(L - nw) - 2A_{sp,op} \tag{5.17}$$

where L is the length of the spool located inside the sleeve, n is the number of the balancing grooves, and w is the width of the balancing grooves. The solid-to-solid sliding Coulomb friction in the case of the considered design takes place between the spool and elastomer O-ring seals and back-up rings. Sealing between moving mechanical parts is ensured by squeezed elastomer and plastic back-up rings during assembly. This squeeze produces the drag friction torque from an elastomer ring on the sealant part (Bisztray-Balku, 1995). More details about the drag friction in the rotary orifice are included in Abuowda et al. (2018).

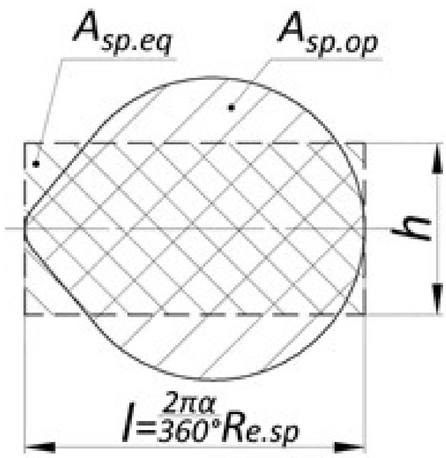

Fig. 5.4 The mean width of the window

The stepper motor model used by Bendjedia et al. (2007) and Kępiński et al. (2015) is shown in Equation (5.18).

$$\begin{bmatrix} \frac{d\theta}{dt} \\ \\ \frac{d\omega}{dt} \\ \\ \frac{di_a}{dt} \\ \\ \frac{di_b}{dt} \end{bmatrix} = \begin{bmatrix} \omega \\ \\ \frac{1}{J}[-K_m i_a \sin(N_r\theta) + K_m i_b \cos(N_r\theta) - B\omega - T_L] \\ \\ \frac{1}{L}[V_a - Ri_a + K_m \sin(N_r\theta)] \\ \\ \frac{1}{L}[V_b - Ri_b - K_m \cos(N_r\theta)] \end{bmatrix} \tag{5.18}$$

where ω is the angular velocity, J is the inertia, K_m is the motor torque constant, N_r is the number of teeth, R is the resistance, T_L is the total load torque, B is the viscous friction constant, i_a is the coil A current, i_b is the coil B current, V_a is the coil A supplied voltage, and V_b is the coil B supplied voltage.

5.4 Experimental Validation of the Torque

The flow performance of the orifice was validated by Okhotnikov (2018). The friction model performance (Figure 5.5) based on Equations 5.6, 5.12, 5.13, and 5.14 has the highest value compared to the steady sate and the transient flow torques that affects the coupling between the valve components.

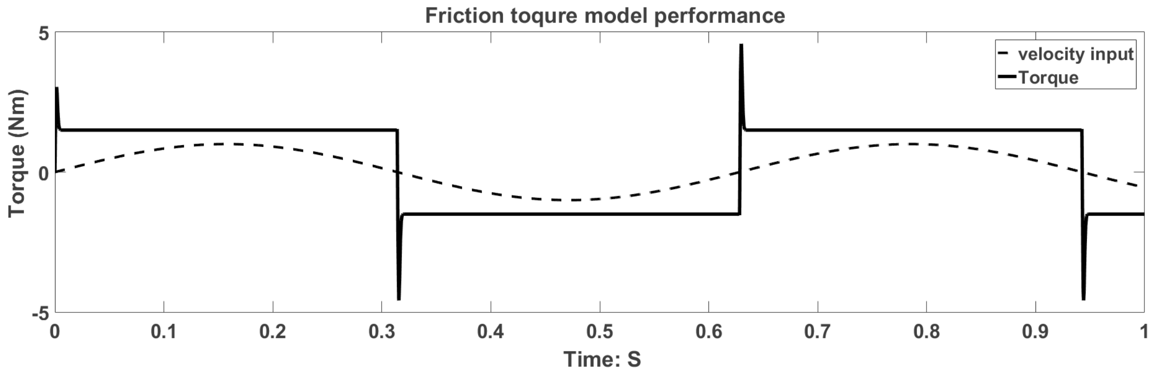

Fig. 5.5 The simulated friction of the orifice part. The input velocity is represented by a sine wave of $1(rad/sec)$ and $1Hz$ frequency.

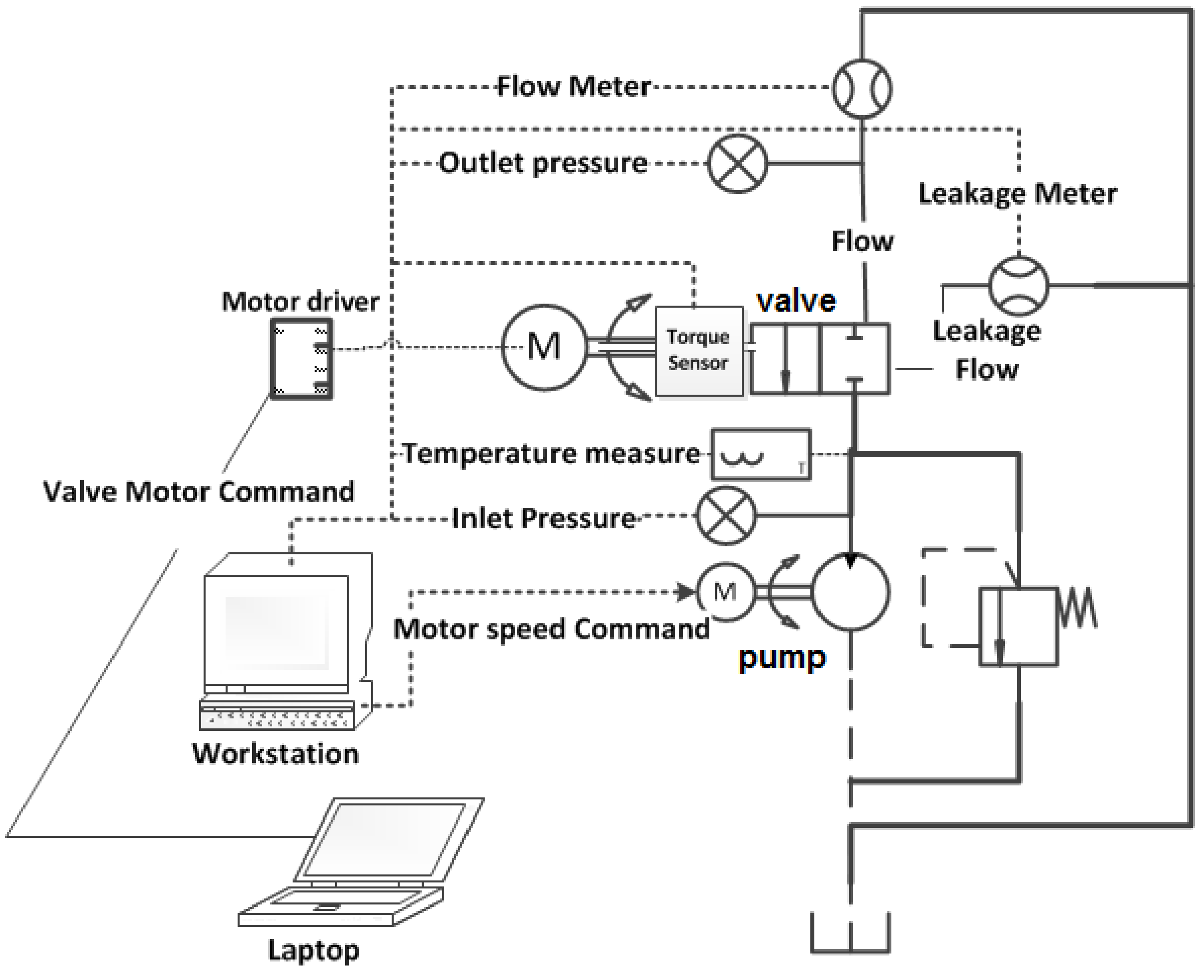

Fig. 5.6 The schematic diagram of the test rig

The torque was measured using a test rig developed for this task. It's schematic diagram is shown in Figure 5.6. The testing procedure starts by fixing the pressure drop around the valve using the pump controlled speed and the pressure relief valve which is used to define the inlet pressure of the valve. Then, the valve opening is adjusted to measure the produced flow, while the torque transducer is used to measure the total applied torque on the stepper motor. The applied torque includes the steady state flow torque, the transient flow torque, and the friction torque. The synthesis of this rig is shown in Figures 5.7 and 5.8. The test was performed with pressure differences 0.25 MPa, 0.5 MPa, and 1 MPa.

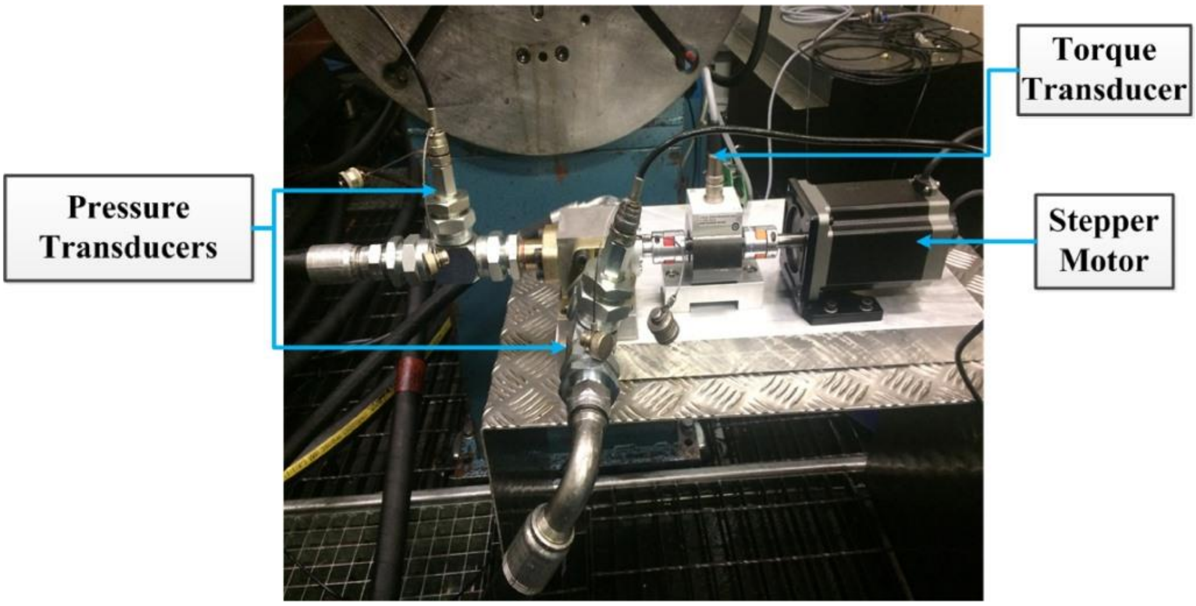

Fig. 5.7 The test rig of the valve which contains the transducers and the stepper motor.

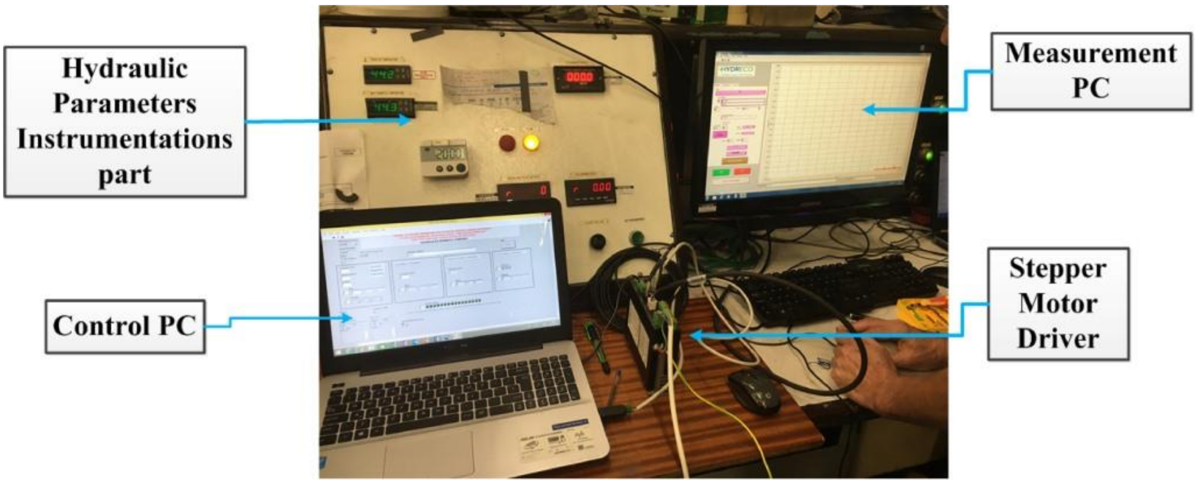

Fig. 5.8 The main control panel which contains a driving system and measurement system

The main tools used in the test are:

- Pressure transducer - this is a Gems 3100B0040G01B000RS pressure transducer (40 *bar*, and 4 to 20 *mA* output).
- Valve Main Flowmeter - this is a 3100 gear motor calibrated against a VC10 Kracht flow meter.
- Leakage flow meter - this is Kracht VC1 calibrated against the VC10 meter.
- Supply pump - this is a hydraulic gear pump 160cc/rev pump (part number 058304) in the R6 Q series from HYDRECO.
- Oil Temperature sensor - this is a K type thermocouple.
- Latptop - this is an Acer machine used to activate the stepper motor driver by sending commands through a Modbus cable using LabView Code. The code developed for this task is in Appendix (A).
- Workstation - this is a computer connected with the measurement components and with the analogue control panel.
- Stepper motor - this is an Orientalmotor RKII series.

Figure 5.9 shows the torque produced at an opening range between 20°to 90° with the flow produced detected using the flow meter. One of the instant dynamic response of produced torque was measured for a valve opening of 45° and 200 kHz stepper motor switching frequency (Figure 5.10). These results are similar to the friction model (Figure 5.5) which represents the highest value of torque that affect the stepper motor performance.

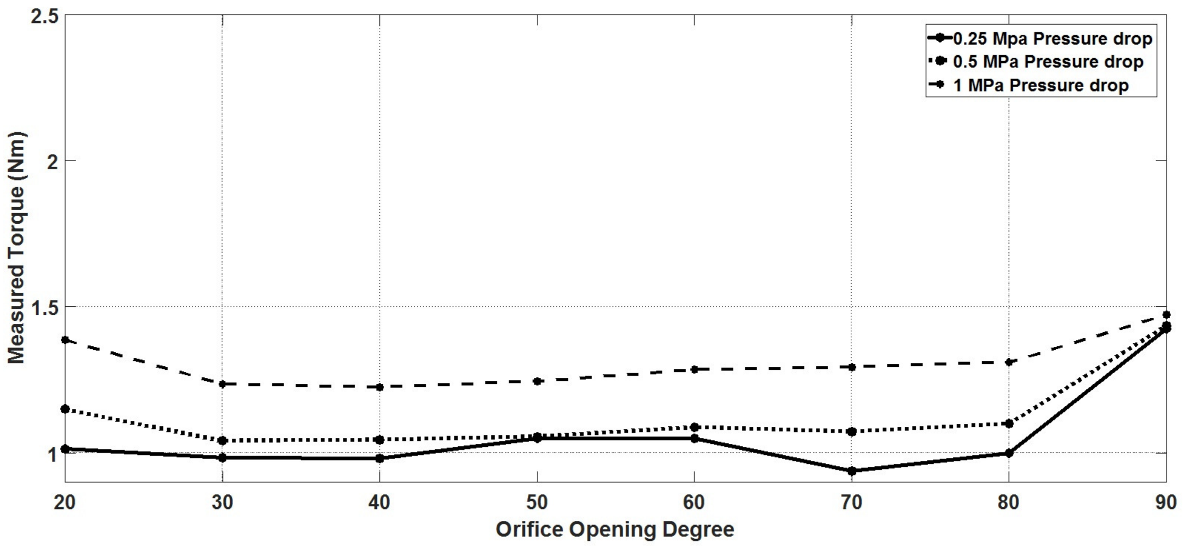

Fig. 5.9 The produced torque from the valve with different pressure drops. This torque is the squeeze force produced by the sealing elastomer O-ring seals and backup rings.

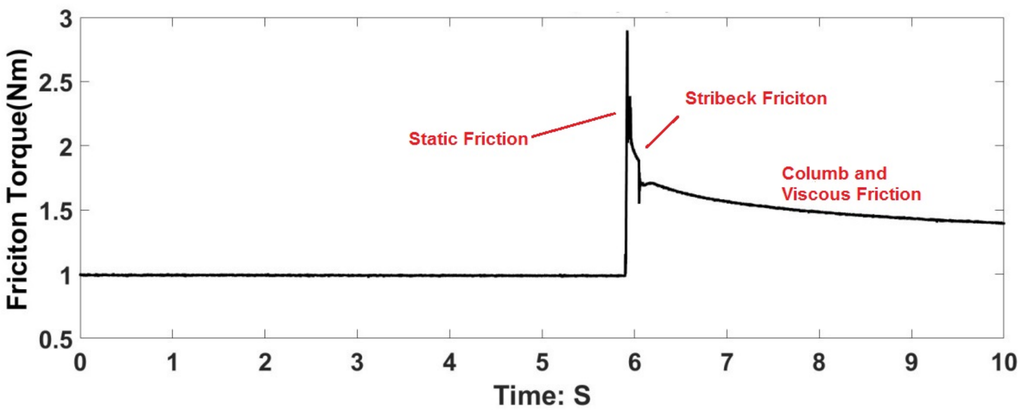

Fig. 5.10 The instant response of the spool friction (45°of 200 KHz
).

Finally, based on this analysis, the selected stepper motor to drive the valve is E/H bipolar stepper motor, Kollmorgen. The motor torque is 4.75 Nm, inductance is 8.9 mH, 0.74 Ω resistance, rated current is 4.1 A, detent torque is 0.30Nm, and the rotor inertia is 0.00120 Kg/m^2.

5.5 Response Analysis

The main electro-mechanical subsystems of this valve are shown in Figure 5.11. When the Pulse Width Modulation (PWM) signals are applied to the H Bridge arms, the resultant voltage changes according to the working principle of a chopper circuit, for more details about this circuit refer to Bellini et al. (2007). This signal arrangement is responsible for the working technique of the motor which can be full step, half step, or micro-step. Each technique has a different effect on the applied voltage to the coils. The applied voltage directly relates to the amount of current in the stepper motor coils according to Ohm's law (Bellini et al., 2007). This amount of current is responsible for the produced electromagnetic torque and the speed of rotation. As the rotation of the rotary orifice produces friction, steady-state flow torque, and transient flow torque, these torques should be held by the resultant torque from the motor electromagnetic field to assure the valve controllability. Modelling and simulation, using the valve mathematical model, was the technique selected to study these relationships. As the stepper motor is directly coupled with the rotary orifice, the dynamic response of the valve can be represented by the response of the stepper motor rotor. There are two types of rotor response analysis, one is a single step response and the other is multi-step response (Acarnley, 2002) and (Robinson, 1969). The multi-step response which relies on a nonlinear model, is able to show a better representation of the performance, hence it was selected for this analysis.

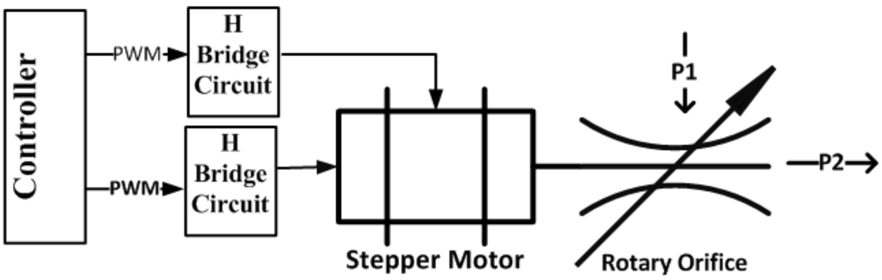

Fig. 5.11 The main subsystems of the valve and the internal interactions

The full step technique is performed when each phase of the stepper motor is supplied separately. The half step method is performed by supplying both phases with equal currents (Bellini et al., 2007). However, these two modes produce a rest position which affects the shaft revolution, torque and rotation velocity. This effect results in poor dynamic torque, torque ripples and mechanical vibration. To overcome these shortcomings, an extra division which is limited by the mechanical tolerance, friction torque in this design, can be introduced (Figure 5.12). The approach used is termed as micro-stepping and leads to reduction in the torque ripples and a smoother shaft operation (Moon and Kim, 2014). Its work principle is conveying current from one coil to another with 90° phase shift.

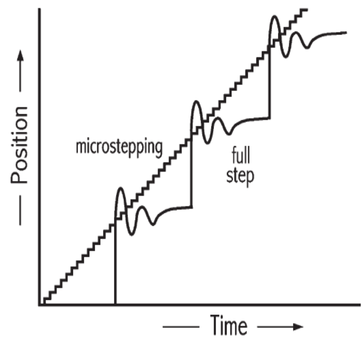

Fig. 5.12 Illustrates the steps responses of the full step and the micro-step techniques.

A H Bridge is used to produce the required current and keeps it at the required level. Its output is based on the applied pulse width modulation (PWM) signal. Different modulation algorithms have been developed to produce the required PWM signal for the H bridge. These algorithms are two level PWM, three-level PWM, mixed mode, a space vector pulse width modulation (SVPWM) technique, and frequency modulation (Gaan et al., 2018). A two-level PWM is used here to simulate the micro-stepping for this valve. Generating the PWM signal for the H bridge using this technique is based on two overlapping signals which are a sine wave with a specific frequency and a triangle wave with a specific frequency. When the triangle wave value is lower than the sine wave value the outcome is zero. When the sine wave is lower than the triangle wave, then the produced value is the maximum. The analysis procedure is shown in Figure (5.13). It starts by selecting the driving technique which can be a full-step or a micro-step, then the current and torque simulation is performed to determine if the produced torque is suitable to overcome the friction torque. The friction torque is a result of the rotary orifice rotation.

In the full step mode, the charging and discharging of coils are performed in series, i,e, the first coil is charged and discharged, then the second coil is charged and discharged. Charging and discharging periods are responsible for the rotation speed. For the analysis of the proposed system, two frequencies which are 150 Hz and 300 Hz have been considered. The PWM signal of the driver was modelled using a logic method based on a voltage to frequency converter (Mihalache et al., 2013). When a 150 Hz pulse train is supplied to the stepper motor, the peak current was 4.25 A, which resulted in a torque of 3.9 Nm, as shown in Figure (5.14(a)). During the rotation of the stepper motor, the speed profile contains high ripples due to the effect of the

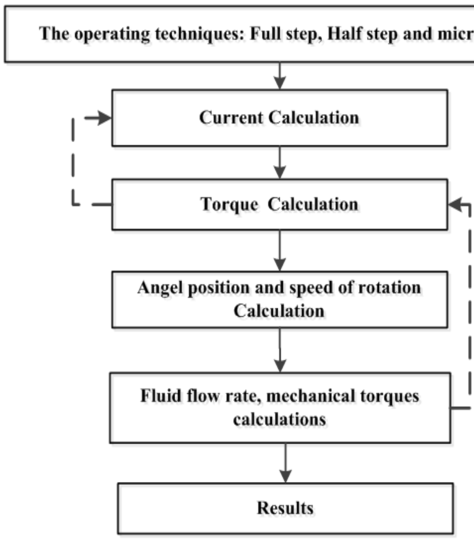

Fig. 5.13 Schematic diagram shows the steps of the illustrative example.

rest points in the full step driving technique, as shown in Figure (5.14(b)). These rest points produce high torque ripples, based on Equation (5.13), as illustrated in Figure (5.14(c)).

Increasing the operation speed by changing the pulses frequency to 300 Hz, reduces the current in the motors coils to 2.4 A and the torque to 1.5 Nm (Figure 5.15(a)). Therefore the stepper motor stopped completely (Figure 5.15(b)). The rest points are responsible about the high instantaneous change of speed which results in high Stribeck value according to Equation 5.13. The friction torque effect is illustrated in Figure (5.15(c)) which is more than the torque produced by the motor. Based on this analysis, this stepper motor can be embedded into the system using the full step technique, but with a limited frequency range. Also, there is still an effect of vibration by friction ripples which effects the hydraulic actuator performance.

The second simulated technique considered in this analysis was micro-stepping. Two different switching frequency of 5 kHz and 20 kHz have been analysed. The resultant electrical current using the micro-stepping technique is a sine-wave 4.5 A peak when 5k Hz switching. The resultant torque is 2.25 Nm as shown in Figure (5.16 (a)). This resulted in a smoother velocity operation compared to the full step during 90° opening as shown in Figure (5.16 (b)). The produced ripple due to the friction is reduced to an acceptable operation limit (Figure 5.16 (c)) where the stepper motor smoothly controls the orifice.

Increasing the switching frequency up to 20kHz produces the current of 4.5 A and torque of 2.25 Nm, (Figure 5.17 (a)). Moreover, the ripples in the velocity profile was reduced which results in smooth performance of the valve (Figure 5.17 (b)). The resultant friction torque is in the range of the stepper motor torque during the operation which is illustrated in Figure (5.17 (c)).

Pulsation Frequency 150Hz

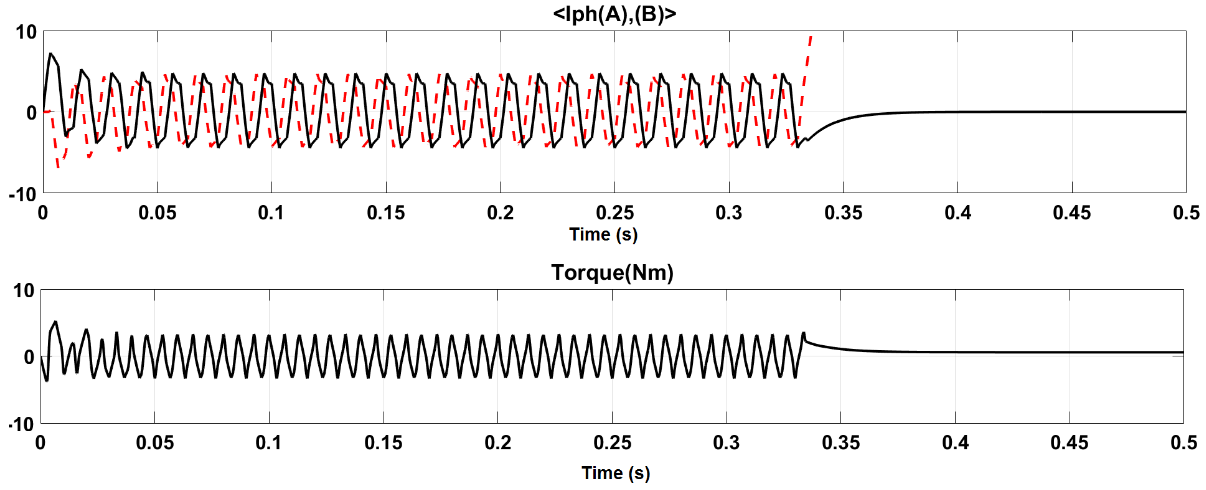

(a): The current in the motor coils is 4.25 A, and the produced torque is 3.9 Nm.

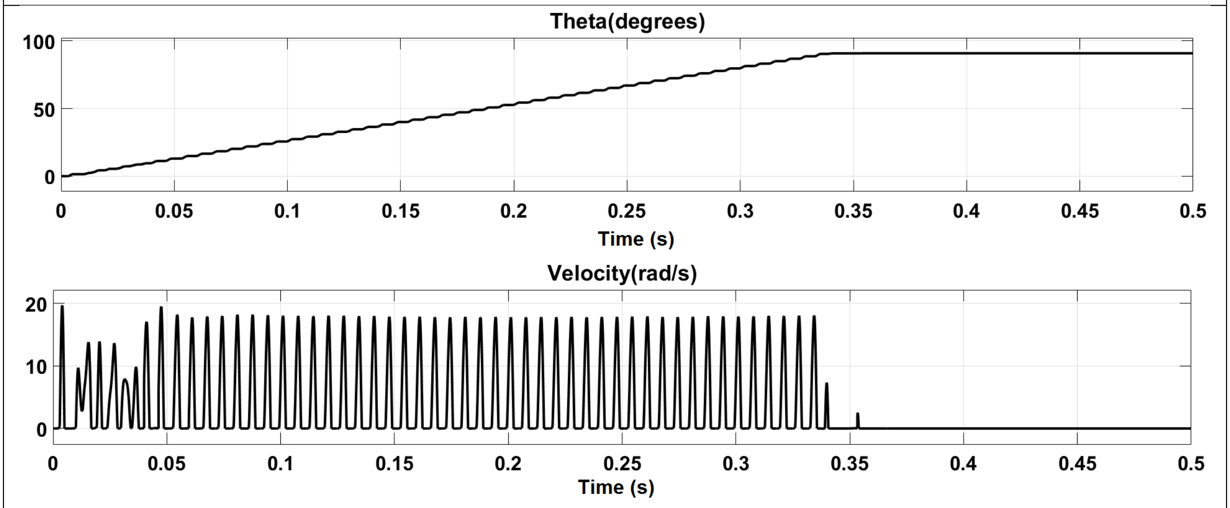

(b): The achieved angle 90° and the rotation velocity $20(rad/s)$

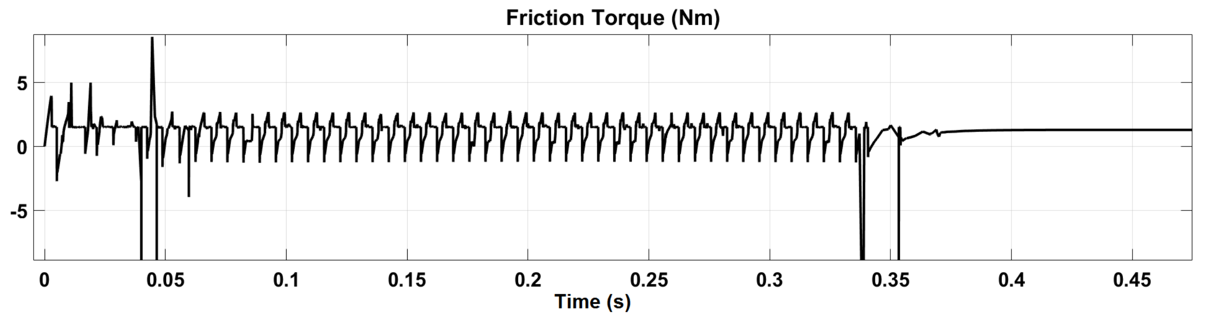

(c) The friction torque produced by the orifice 3 Nm

Fig. 5.14 Response for the full step technique (150 Hz frequency)

Pulsation Frequency 300Hz

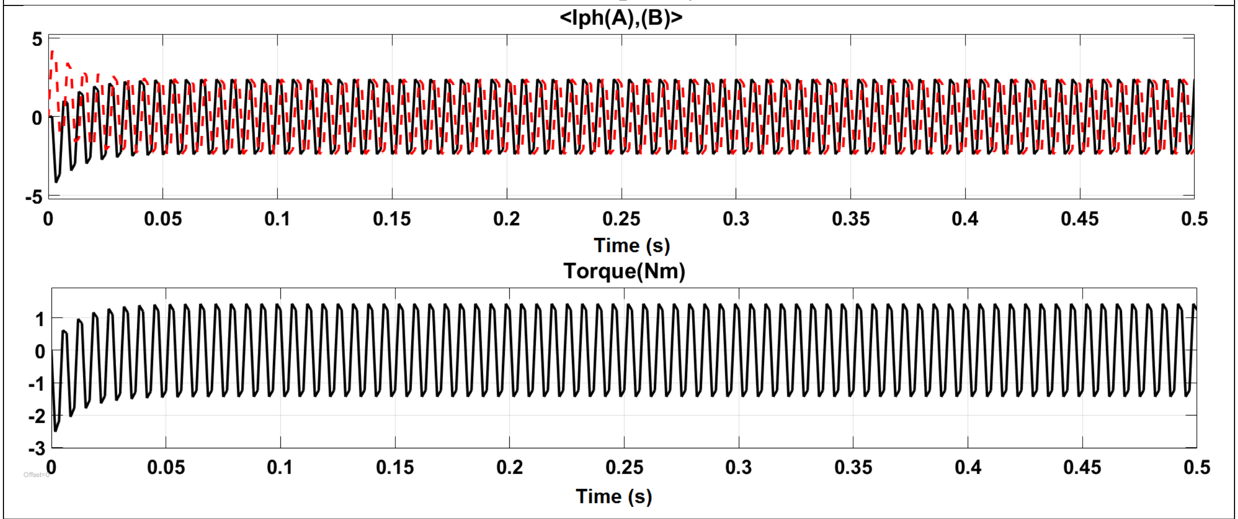

(a): The current in the motor coils is 2.4 A,and the produced torque is 1.5 Nm.

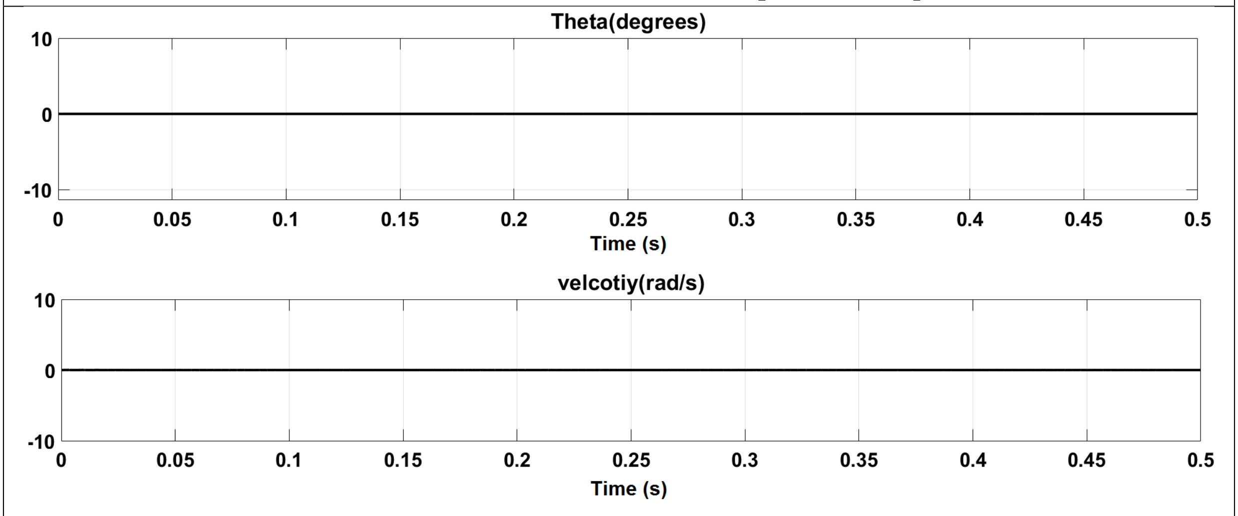

(b) The achieved angle 0° and the rotation velocity $0(rad/s)$

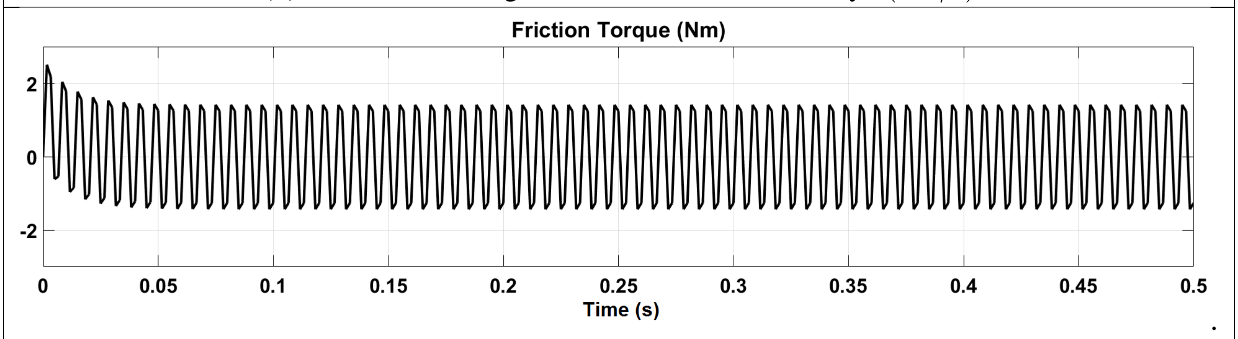

(c) The friction torque produced by the orifice 1.7Nm

Fig. 5.15 Response for the full step technique (300 Hz frequency)

Switching Frequency 5KHz

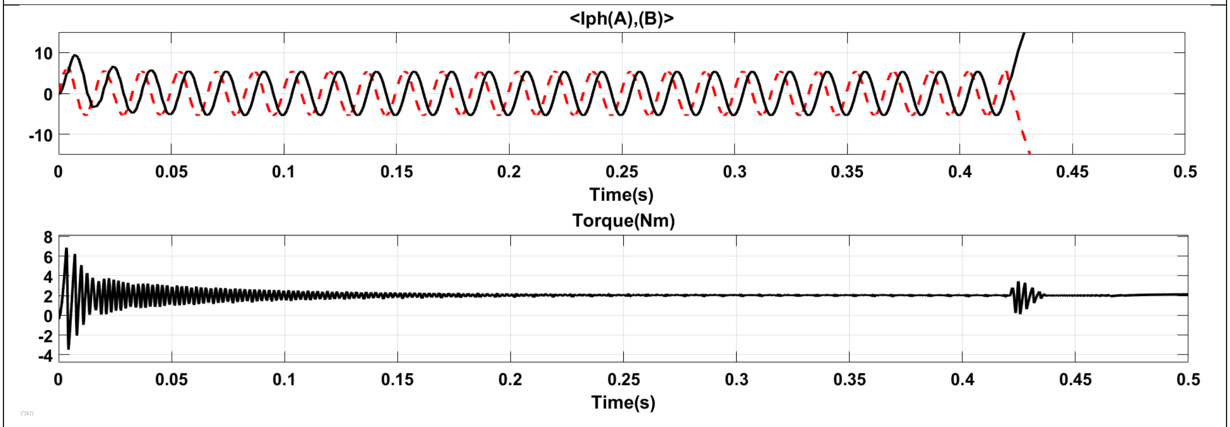

(a): The current in the motor coils is 4.5 A, and the produced torque is 2.25 Nm.

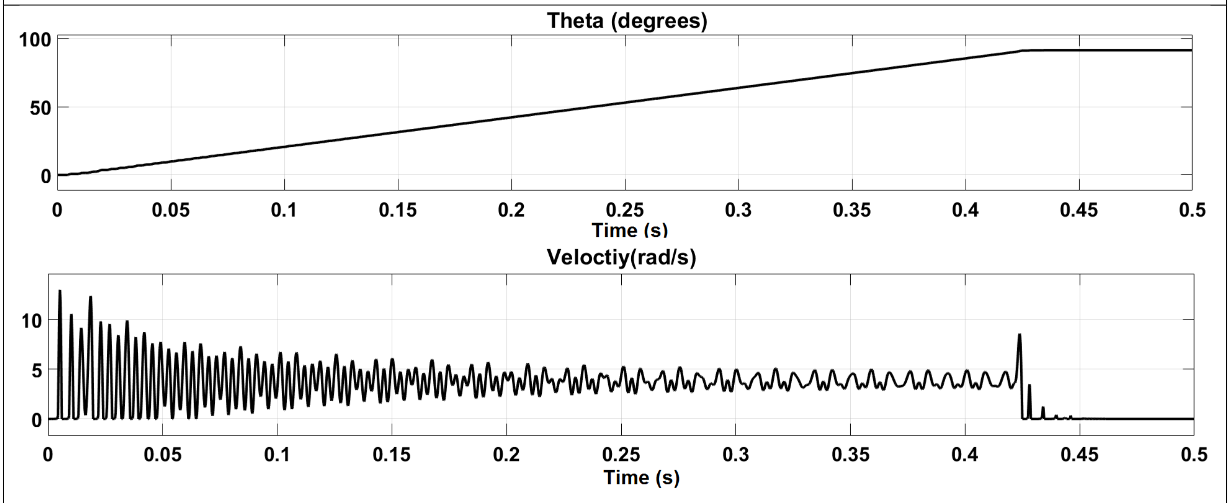

(b): The achieved angle 90° and the rotation velocity $5(rad/s)$

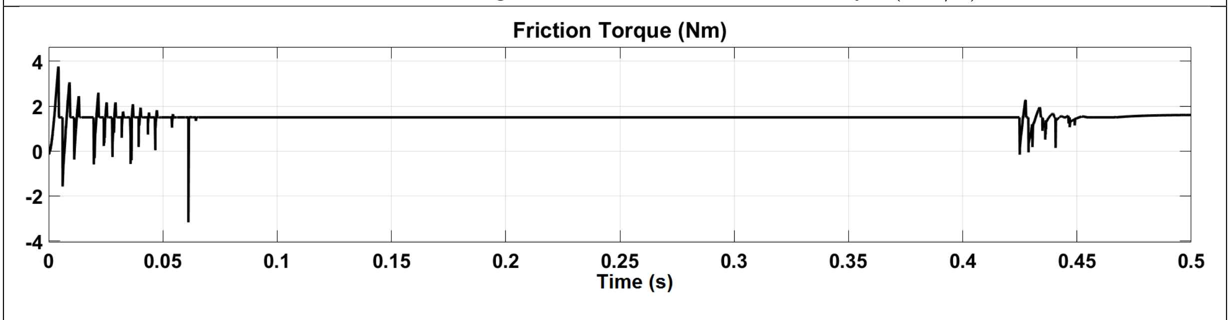

(c) The friction torque produced by the orifice 1.6 Nm

Fig. 5.16 Response for the micro-step technique (5 KHz frequency)

Switching Frequency 20KHz

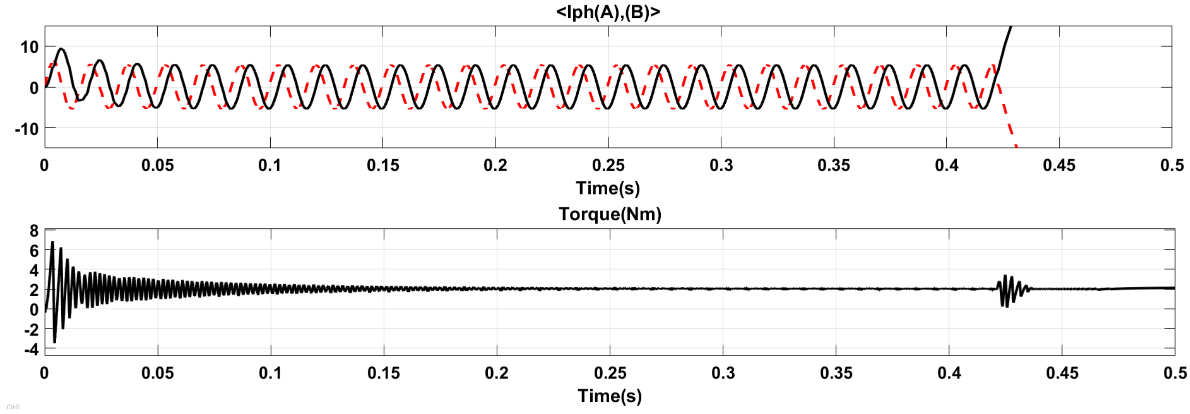

(a): The current in the motor coils is 4.5 A,and the produced torque is 2.25 Nm.

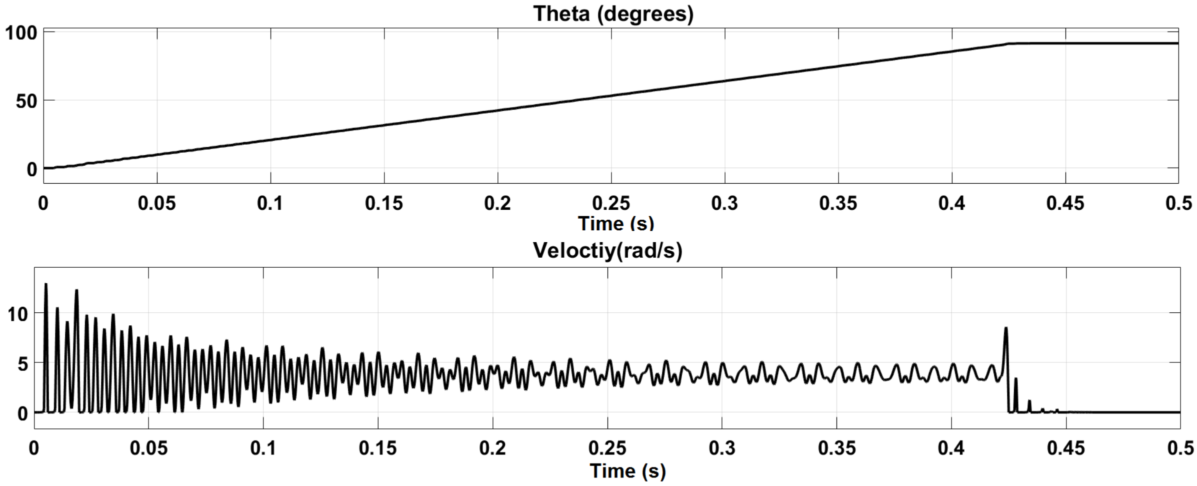

(b) The achieved angle 90° and the rotation velocity $5(rad/s)$

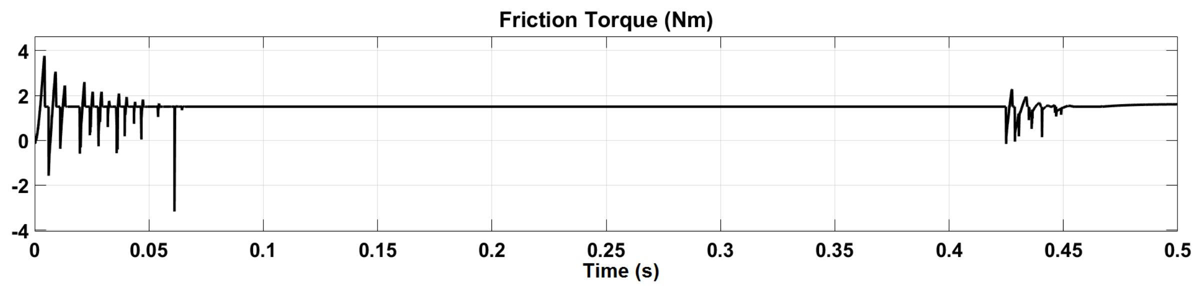

(c) The friction torque produced by the orifice 1.6 Nm

Fig. 5.17 Response for the micro-step technique (20 KHz frequency)

To summarize, implementing this stepper motor as an actuator for the valve using the full step technique is possible, but with limited operating frequency range with the effect of ripples. The micro-step technique reduces the ripple effect and allows a different range of operation. To check this test repeatability, another stepper motor with inductance of 11.8 mH, resistance of 3.07 Ω, torque of 0.068 Nm, and the rotor inertia of 0.022 Kg/m^2 was selected. This motor lost the controllability using full step technique as illustrated in Appendix B.

5.6 The Linearized State Space Model

State space representation is used to display the mathematical description of the valve. It is also used for more analysis such as root locus analysis. The main equations of this representation are,

$$\dot{X}(t) = A(t)X(t) + B(t)U(t) \tag{5.19}$$

$$Y(t) = C(t)X(t) + D(t)U(t) \tag{5.20}$$

where $A(t)$ is the system matrix refer to the valve, $X(t)$ is the state vector, $B(t)$ is the input matrix, $U(t)$ is the input vector, $C(t)$ is the output matrix, and $D(t)$ is the feedforward matrix.

The proposed stepped valve opening area curve is shown in Figure 5.18. A polynomial equation to represent the curve has been obtained using curve regression, that is

$$0.0173x^2 - 0.4883x - 3.5 \tag{5.21}$$

As the discharge coefficient is an important factor in the Bernoulli equation representing the performance of the valve, a linearization point was selected based on the discharge coefficient graph of the valve shown in Figure 5.19. The coefficient effect starts from 10° opening which is selected as the point of linearization. Selecting a 0° detection may eliminate important parameters during analysis.

As previously mentioned, the transient flow torque in Equation 5.12 is very small compared to the rest of the parameters, and this can be eliminated, resulting a model representation based only on Equations 5.6, 5.13, and 5.18. By rearranging these equations,the Equation 5.22 can be obtained.

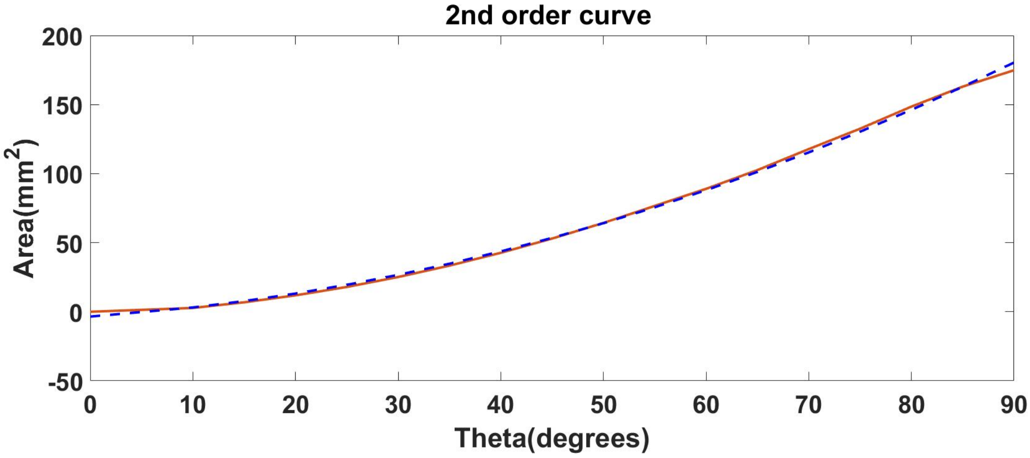

Fig. 5.18 The area and the second polynomial curve regression

$$\begin{bmatrix} \frac{d\theta}{dt} \\ \frac{d\omega}{dt} \\ \frac{di_a}{dt} \\ \frac{di_b}{dt} \\ \frac{dZ}{dt} \\ \frac{dT_c}{dt} \end{bmatrix} = \begin{bmatrix} \omega \\ \frac{1}{J}[-K_m i_a \sin(N_r\theta) + K_m i_b \cos(N_r\theta) - B\omega - T_L] \\ \frac{1}{L}[v_a - Ri_a + K_m \sin N_r\theta] \\ \frac{1}{L}[v_b - Ri_b - K_m \cos N_r\theta] \\ \omega - \frac{\sigma_0|\omega|}{T_c+(T_s-T_c)\exp-(\frac{\omega}{\omega_s})^2} Z \\ 0 \end{bmatrix} \cdot \begin{bmatrix} \theta \\ \omega \\ i_a \\ i_b \\ Z \\ T_c \end{bmatrix} \tag{5.22}$$

By adding Equations 5.6 and 5.13, one can represent the total torque in Equation 5.22 by

$$T_L = T_{fr} + T_{st.fl} = \sigma_0 z + \sigma_1 \dot{z} + \sigma_2 \omega + \frac{2C_c \Delta p A_o R_{e.sp} \sin\theta}{1 - {C_c}^2} \tag{5.23}$$

In a matrix form the Equation 5.22, reads $\dot{X} = A(t)X(t)$, where the state vector is the right hand column X(t) and state matrix is the middle side A(t). The nonlinear parts of the state matrix are $K_m i_a \sin(N_r\theta)$, $K_m i_b \cos(N_r\theta)$, $K_m \sin(N_r\theta)$, $K_m \cos(N_r\theta)$, $\omega - \frac{\sigma_0|\omega|}{T_c + (T_s - T_c)\exp-(\frac{\omega}{\omega_s})^2} z$, and A_o.

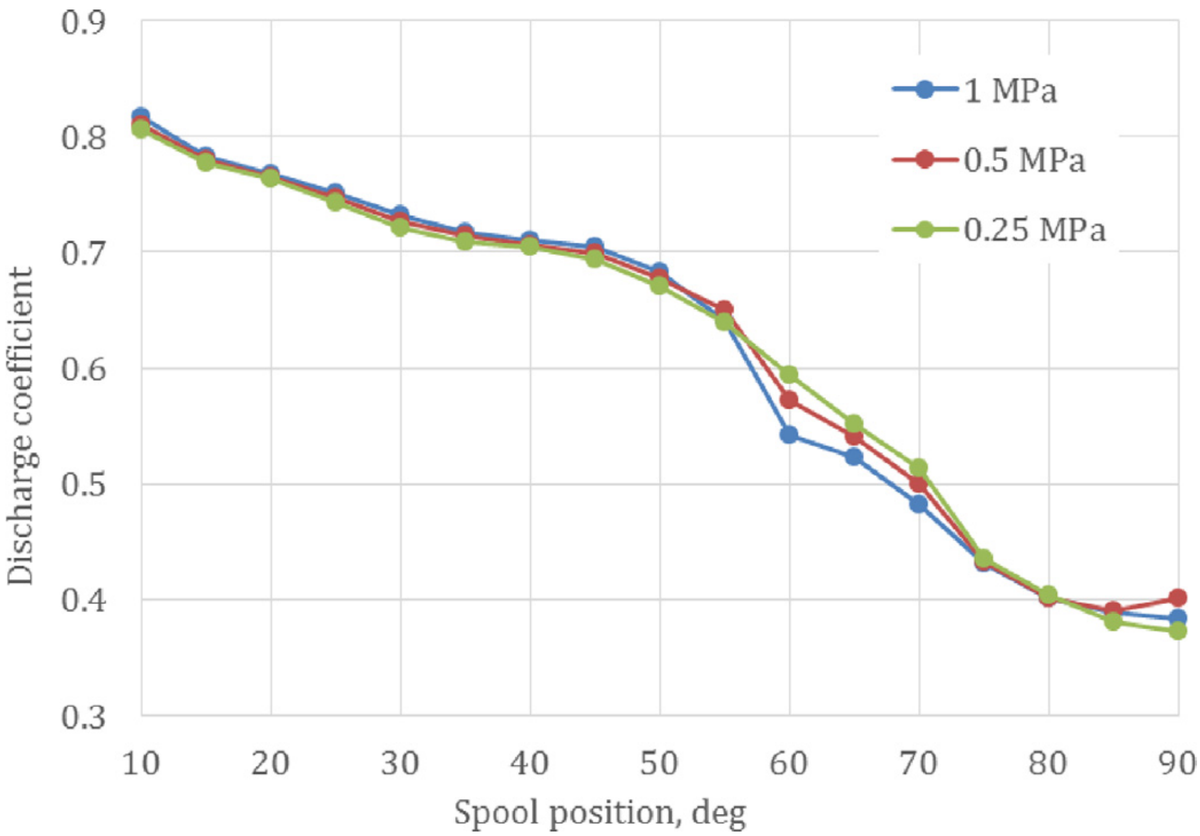

Fig. 5.19 The discharge coefficient perofamnce of the valve (Okhotnikov et al., 2017)

To linearize these parts, a Taylor series was used by Oaks and Cook (1976), that is

$$F(X,U) = A_o + A_1\delta X + B_1\delta U + \varepsilon(X,U) \tag{5.24}$$

where the linearization of the flow curve in Equation 5.21 is given by

$$3\theta - 27 \tag{5.25}$$

Since the operating point is around 10° from Equation 5.23 and 5.25 one can obtain the flow torque as

$$T_L = T_{fr} + T_{st.fl} = \sigma_0 z + \sigma_1 \dot{z} + \sigma_2 \omega + \frac{2C_c \Delta p(3\theta - 27)R_{e.sp}0.2}{1-0.8^2} \tag{5.26}$$

The linearization of expression $\omega - \dfrac{\sigma_0|\omega|}{T_c + (T_s - T_c)\exp -(\frac{\omega}{\omega_s})^2} z$ is represented by Equation 5.27 and can be performed in two forms, that is when the valve is accelerating or when it settles at any point. The first form is with the valve stopped at the opening $\theta = 10°$, $T_c = 0, T_s = 2.5, \omega = 0, Z = 0$, and $\omega_s = 0.001$. The linearization is represented by Equation 5.28. For more details about the mathematical manipulation, please refer to the Analysis (1) in the Appendix (D). The values of the equations parameters are included in Table (D.1) in Appendix (D).

$$
\begin{aligned}
F(\omega, T_c, T_s, z, \omega_s) &= F(\omega_0, T_{c0}, T_{s0}, \omega_{s0}, z_0) + F_\omega(\omega_0, T_{c0}, T_{s0}, \omega_{s0}, z_0)(\omega - \omega_0) \\
&+ F_{Tc}(\omega_0, T_{c0}, T_{s0,s0}, z_0)(T_c - T_{c0}) + F_{Ts}(\omega_0, T_{c0}, T_{s0,s0}, z_0)(T_s - T_{s0}) \\
&+ F_{\omega_s}(\omega_0, T_{c0}, T_{s0}, \omega_{s0}, z_0)(\omega_s - \omega_{s0}) + F_z(\omega_0, T_{c0}, T_{s0}, \omega_{s0}, z_0)(z - z_0)
\end{aligned} \tag{5.27}
$$

$$
F(\omega, T_c, T_s, z, \omega_s) = \omega \tag{5.28}
$$

The stiction friction based on a Coulomb friction model was analyzed by Bisztray-Balku (1995) by considering a linear velocity. Converting the linear velocity into angular velocity using $\omega = v/r$ where r is the external radius of the spool, leads to the initial values of the terms $\omega_0 = 31.25, T_{c0} = 2, T_{s0} = 0, z = 1$, and $\omega_s = 0.001$. For safety reason a margin added to the T_{c0} value to be 2 instead of 1.5. By implementing the manipulations in Analysis (2) in Appendix (D), the linearised equations is,

$$
F(\omega, T_c, T_s, Z, \omega_s) = 26.5 - 21.716\sigma_0 + \omega(\frac{\sigma_0 - 2}{2}) + \frac{125\sigma_0 T_c}{16} - \frac{125\sigma_0 z}{8} \tag{5.29}
$$

The linearization of the term $K_m i_a \sin(N_r\theta)$ in Equation 5.22 can be written as Equation 5.30, while the manipulation of this linearization is included Analysis (3) in Appendix (D).

$$
\begin{aligned}
F(i_a, \theta) &= F(i_{a0}, \theta_0) + F_{ia}(i_{a0}, \theta_0)(i_a - i_{a0}) + F_\theta(i_{a0}, \theta_0)(\theta - \theta_0) \\
&= 0.829 K_m i_a 112.5 K_m \theta - 1125 K_m
\end{aligned} \tag{5.30}
$$

The linearization of the term $K_m i_b \cos(N_r\theta)$ in Equation 5.22 is represented by Equation 5.31. The manipulation of this linearization is included Analysis (4) in Appendix (D),

$$
\begin{aligned}
F(i_b, \theta) &= F(i_{b0}, \theta_0) + F_{ib}(i_{b0}, \theta_0)(i_b - i_{b0}) + F_\theta(i_{b0}, \theta_0)(\theta - \theta_0) \\
&= 0.5624 K_m i_b
\end{aligned} \tag{5.31}
$$

The linearization of the term $K_m \sin(N_r\theta)$ in Equation 5.22 is represented by Equation 5.32. The linearization is included Analysis (5) in Appendix (D).

$$561K_m + 56.24K_m\theta \tag{5.32}$$

The linearization of $K_m \cos(N_r\theta)$ in Equation 5.22 is given by the next equation. The manipulation of the linearization is included Analysis (5) in Appendix (D),

$$821K_m - 82.69K_m\theta \tag{5.33}$$

Then the linearized dynamic system is as follow

$$\begin{bmatrix} \frac{d\theta}{dt} \\ \frac{d\omega}{dt} \\ \frac{di_a}{dt} \\ \frac{di_b}{dt} \\ \frac{dZ}{dt} \\ \frac{dT_c}{dt} \end{bmatrix} = \begin{bmatrix} \omega \\ \frac{1}{J}\Big[-0.829K_m i_a + 0.5624K_m i_b - 112.5K_m\theta + 1126.6K_m \\ -B\omega - \frac{\omega\sigma_0\sigma_1}{2}\omega\sigma_0 - \sigma_2\omega - \\ \frac{125\sigma_0\sigma_1 T_c}{16} + \frac{125\sigma_0\sigma_1 z}{8} - 0.025\Delta p\theta + 0.225\Delta p\Big] \\ \frac{1}{L}[V_a - Ri_a + 561K_m + 56.24K_m\theta] \\ \frac{1}{L}[V_b - Ri_b - 821K_m - 82.369K_m\theta] \\ 62.5 - 21.716\sigma_0 + \omega\frac{\sigma_0 - 2}{2} + \frac{125\sigma_0 T_c}{16} - \frac{125\sigma_0 Z}{8} \\ 0 \end{bmatrix} \cdot \begin{bmatrix} \theta \\ \omega \\ i_a \\ i_b \\ Z \\ T_c \end{bmatrix} \tag{5.34}$$

The main matrices A, B, and U used in this study are presented in in the Appendeix (D).

5.7 Performance Analysis

The Matlab code in Appendix C was developed to find the system poles distribution represented by the eigenvalues of the matrix $A + BU$. Using a loop inside the code, parameter value variations shows the change of the poles distribution. The limit of pressure difference that can be applied to this valve is computed by changing the value of the pressure drop dp in the U vector which represents the input of the state space representation. When the pressure difference is increased up to 10 MPa, as shown in Figure 5.20, the pole distribution shows two straight lines parallel to the X-axis meaning that the system is very stable during the increase in pressure, and the system damping is fixed. The poles around the origin are still to the left of the Y-axis meaning the valve keeps its own stability. Increasing the pressure difference, up to 20 MPa, forces the poles to move toward the Y-axis while the system keeps stability and damping as shown in Figure 5.21. When the pressure difference is located to point between 35 MPa and 37 MPa the valve start losing stability, and is hardly controllable as shown in Figure 5.22.

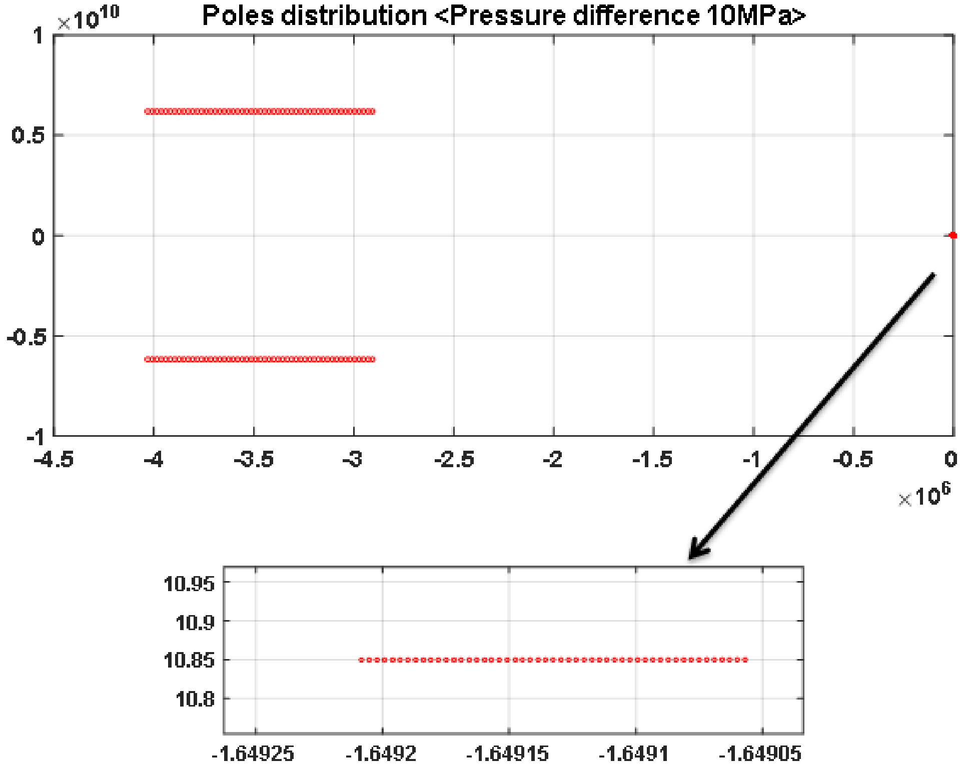

Fig. 5.20 The poles distribution when applying pressure difference upto 10MPa. The zoomed area in the smaller picture is to ensure that the poles around the origin are still to the left side of the origin.

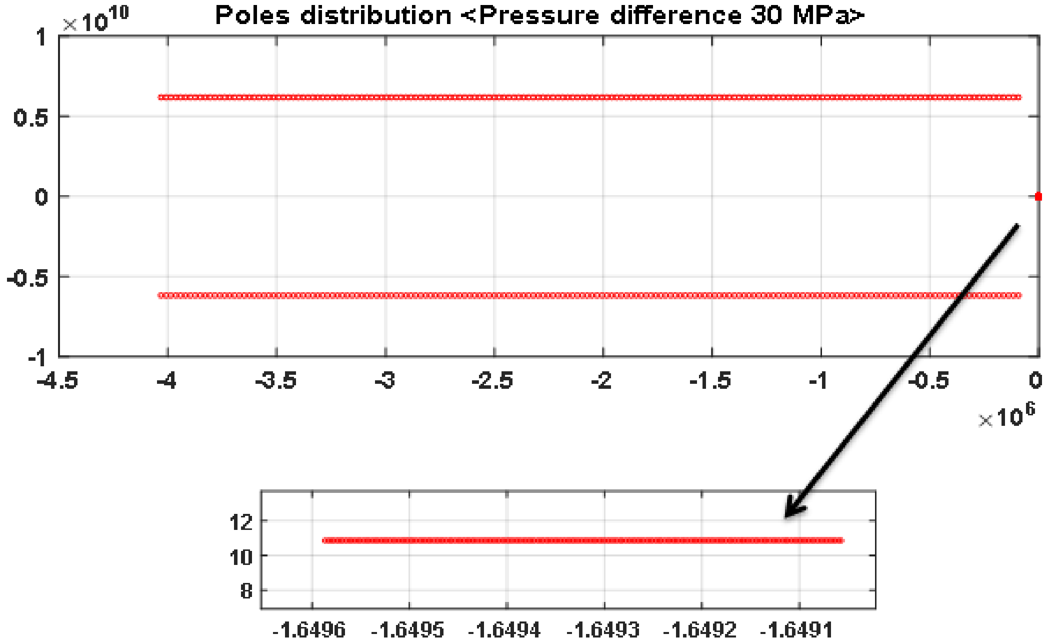

Fig. 5.21 The poles distribution when applying pressure difference upto 20MPa.

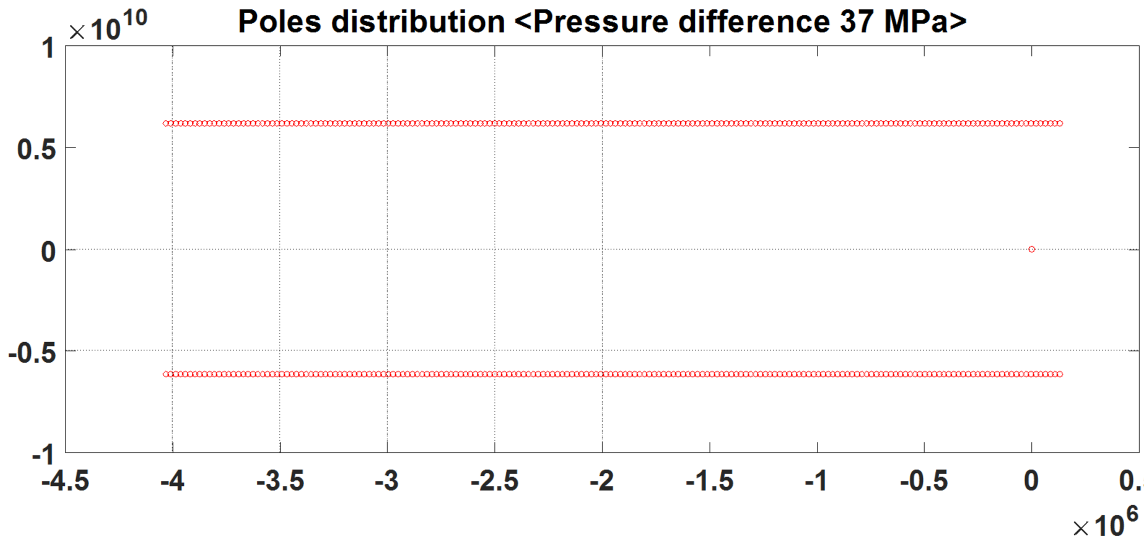

Fig. 5.22 The poles distribution when applying pressure difference upto 37MPa.

The second critical parameter during the design process, especially related to the seal material is the stiffness coefficient. It has been noticed that an increase in stiffness is improving the valve stability. Initially, the stiffness coefficient was selected to be $1e^5$ N/m as shown in Figure 5.23. By increasing the coefficient upto $1e^7$ N/m the poles start to leave the area around the origin, which is critical, and move back to left side to be distributed along the X-axis, Figure 5.24. As shown in Figure 5.25, it can be seen that the system has the best stability when the stiffness value increased to $1e^8\ N/m$.

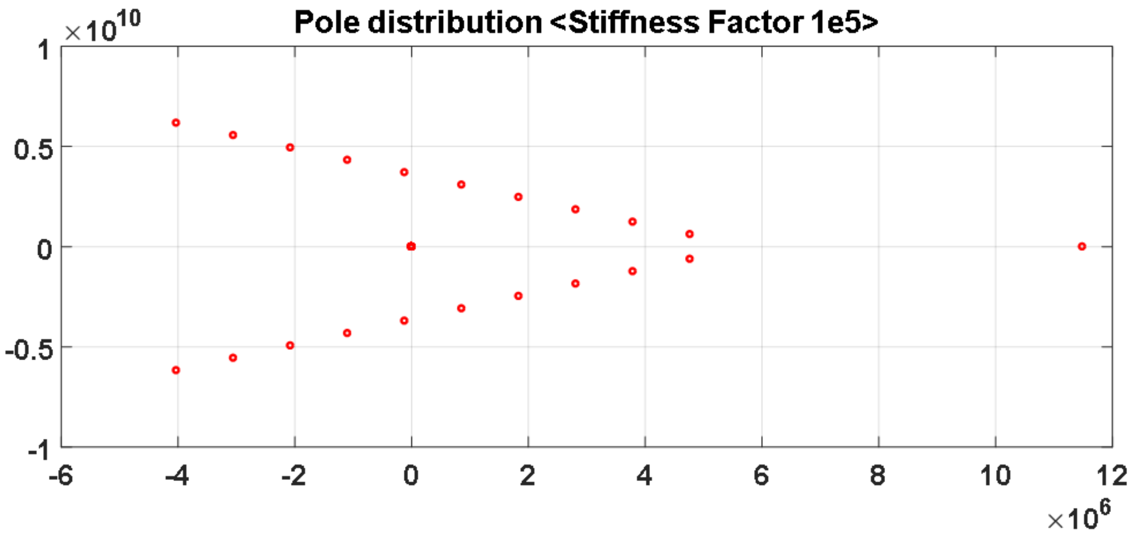

Fig. 5.23 The poles distribution by changing the stiffness coefficient to $1e5$.

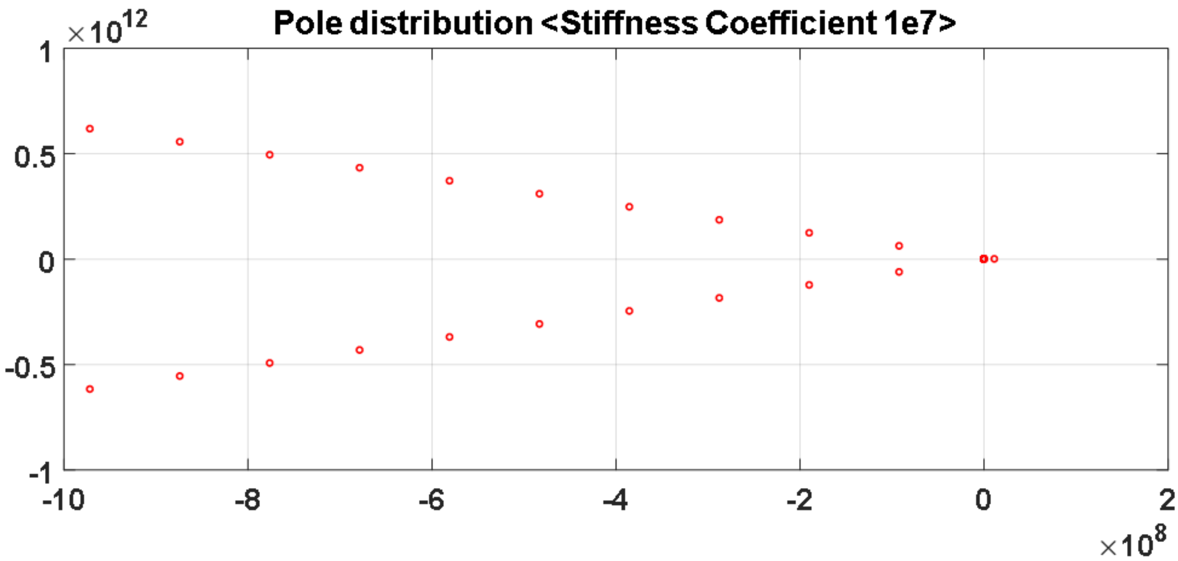

Fig. 5.24 The poles distribution by changing the stiffness coefficient to $1e7$.

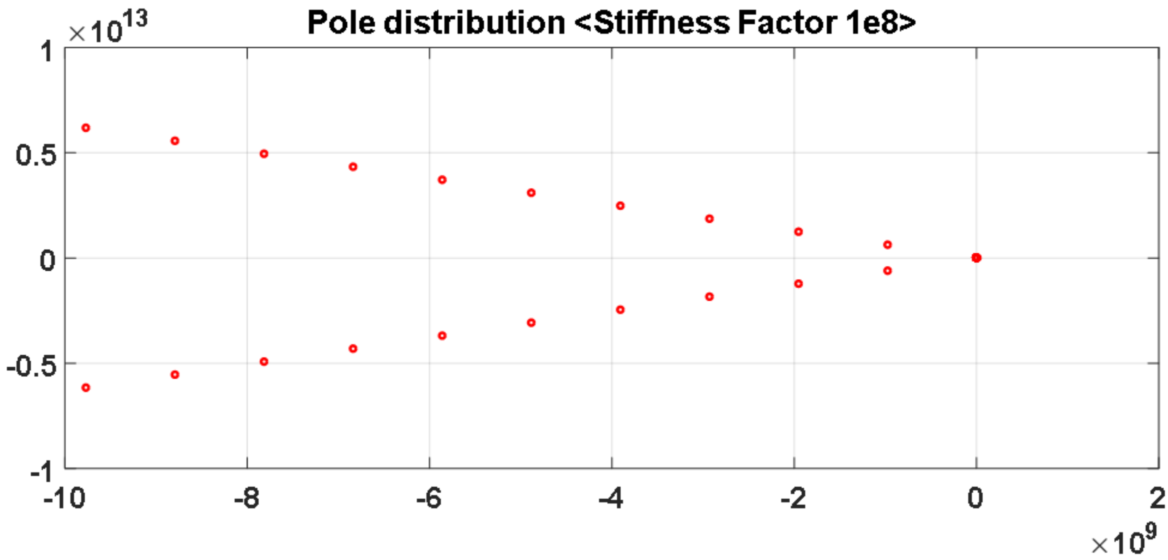

Fig. 5.25 The poles distribution by changing the stiffness coefficient to $1e8$.

The model damping coefficient effect is illustrated for the poles moving away from the X-axis toward the right side as shown in Figure 5.26. The increase in the friction coefficient is shown in Figure 5.27. As indicated in the figure, there is a great similarity in performance between the dp and the friction coefficient, Figures 5.20, 5.21, and 5.22. The correlation between these two factors agrees with the results obtained during testing. As illustrated by Figure 5.9, increasing the pressure drop increased the sealing squeezing on the spool which resulted in higher values of friction torque.

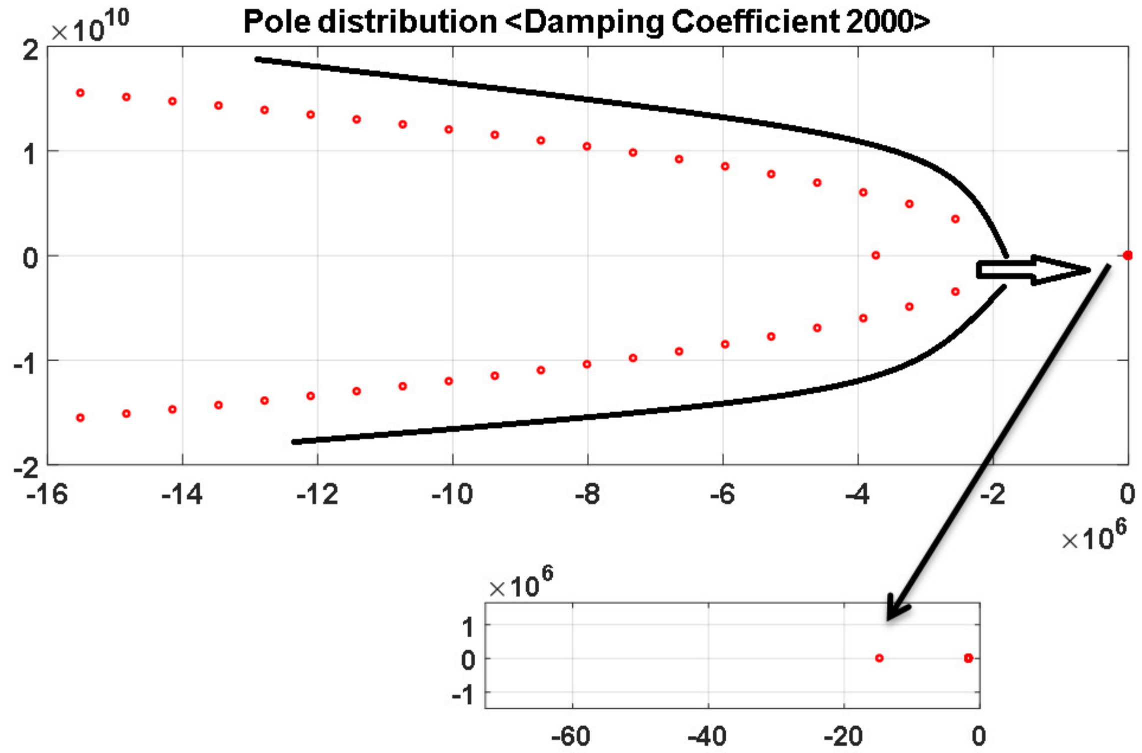

Fig. 5.26 The pole distribution due to damping coefficient change upto 2000.

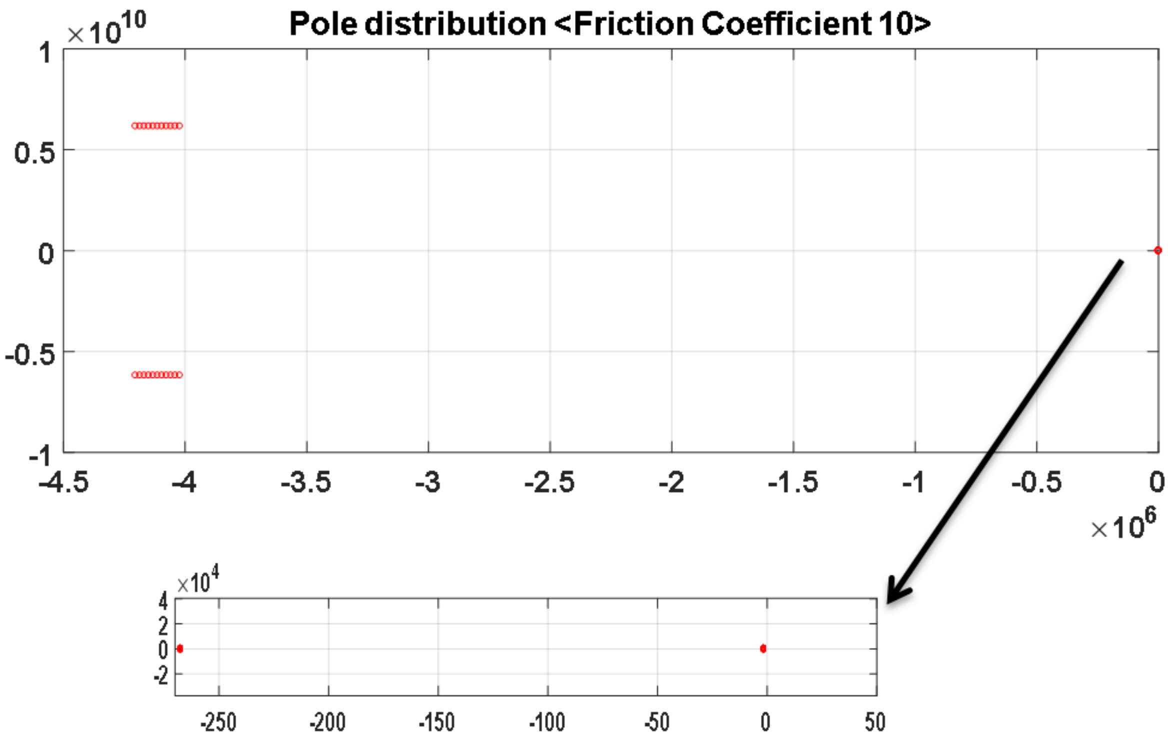

Fig. 5.27 The pole distribution due to friction coefficient change upto 10.

5.8 Summary

In this chapter, a descriptive mathematical model of the new rotary valve was developed. The model contains mechanical, fluid, electrical and electromagnetic parts of the valve. Moreover, the valve simulation indicates that there is an internal relationship between it's subsystems which affects the valve performance. This is shown by the direct relationship between the step angle and the friction produced in the rotary orifice which affects the stability of the stepper motor. Furthermore, the micro-stepping technique produces a better and more controllable performance compared with the full step technique. Root locus analysis has been used to determine this design stability and performance limitations due to its parameters variations. In this analysis, different coefficients namely the pressure difference, viscous friction coefficient, damping coefficient, and bristle or stiffness coefficient have been considered for the design and control process. The effect of variation of these parameters illustrates that the applied pressure difference could be up to 35 MPa while the valve maintains the stability. On the other hand, increasing the bristle coefficient improves the valve performance. This relationship was also concluded in a friction model design by Canudas (1995). The other parameter, which is the damping coefficient, should be increased to stop the poles moving towards the right side of the origin which reduces the system stability. The friction coefficient follows the same performance as the pressure difference which indicates the expected relationship between the pressure difference effect and the friction coefficient during design. After this analysis, building the system model including the developed programmable control algorithm is the next stage of the MBD process, which is the topic of the next chapter.

Chapter 6

Software-in-the-Loop Simulation of the MIM System

6.1 Introduction

In the previous chapters, the proposed stepped rotary flow control valve has been studied from many aspects which are modelling and simulation, dynamical performance, and stability analysis. Also, the mathematical representation of the IM system has been analysed for the five different operation modes, which are PE, PR, HSRE, LSRE, and LSRR. The analysis included the anti-cavitation procedure because if cavitation appears, the IM rules cannot be implemented. The Software-in-the-Loop simulation is an important step for the control algorithm development in the Model-Based Design method. (Chen et al., 2008). In this chapter a model and simulation for the MIM system including a hydraulic boom cylinder and the four valves is established. The simulation aims to analyse the control algorithm and determined the advantages obtained before being implemented on the controller. Also, it helps to compare the performance between the traditional IM and the novel MIM system. This simulation starts with the Model-in-the-Loop. At this stage, a model of the algorithm has been formed to evaluate the algorithm and prepare the control code for the next stage of the research. Software-in-the-Loop (SIL) can be described as the stage of the process where the model of the system and the code are connected together on the same platform (Soltani and Assadian, 2016). The SIL is used in many applications such as Mechatronics, Robotics, Aerospace and Automotive. For example, this approach is used to develop a control unit software in the automotive industry (Lamberg, 2006). To summarize, the algorithm Stateflow model was built as explained in Section 6.2. In Section 6.3, the simulation platform is explained in detail. Tests for the five operation modes have been performed in

Section 6.4. Section 6.5 is an analysis for the velocity performance compared to the traditional IM on the same model. Finally, the summary is in Section 6.6.

6.2 The Control Algorithm

The control algorithm for the MIM system has been produced based on the mathematical analysis of the IM technique which was introduced in Chapter 3. The main aim of this algorithm is to control the velocity of the actuator, which could be a cylinder or a motor. Besides, it saves the system's energy by implementing the regeneration modes, which are HSRE, LSRE, and LSRR. The flowchart of the Micro-Independent Metering algorithm is shown in Figure 6.1. The technique is developed for a separate metering approach that uses stepper motors to operate the metering valves, especially the rotary type. As shown in Figure 6.1, it starts by defining the resolution degree vector which contains the possible steps of the motor. As different stepper motor degrees can be adjusted based on the motor type and the motor driver used, setting up the degree of the stepper motor is important at the start to generate the valve conductance vector. This vector includes the possible flow conductance based on the valve opening degree. The vector is expandable and depends on the possible step division. A limit check is used in the case when the selected step division is not achievable by the motor driver and is used in the case when the selected step division produces torque that leads to loss of valve controllability.

The measurements for this approach, which are the actuator chamber pressures, the pump pressure, the tank pressure, and the required velocity, are collected to select the suitable operation mode. Selecting the operation mode is based on the applied load and the capability of the force and speed of every mode as indicated in Section 2.5. The mode selection technique is included in the next Section 6.2.1. After that, the conductance values of the two valves, a pair for each mode, are calculated using the mathematical equations in Section 4.2. These values should be matched to the conductance of the valve at every step of the stepper motor. A Close Value Detection (CVD) technique is developed to determine the closest degree at which the valve can produce the required conductance as will be explained in the Section 6.2.2 of this chapter. The activation of the valves produces the required flow and thus the actuator velocity.

As this control algorithm is not applicable if cavitation appears, the anti-cavitation check, which is performed before activating the valves, is important. If cavitation is detected, different values of the valve steps have to be selected using the analysis in Section 4.4. The user or the driver of the machine has the ability to change the step resolution which could be achieved by using a scroll wheel in the joystick which is termed as a smoothness technique.

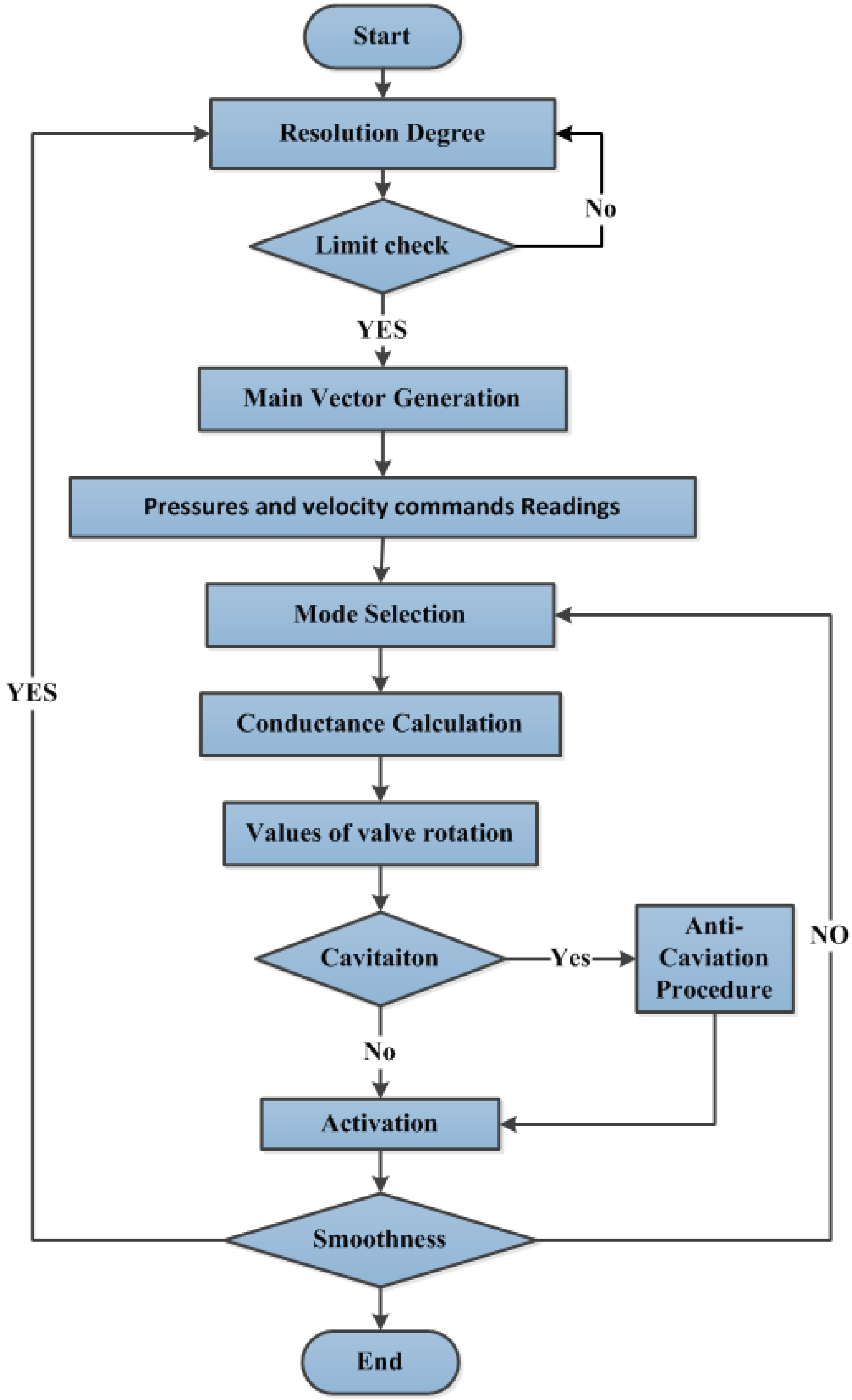

Fig. 6.1 The MIM control algorithm flowchart

Because of its elegant modelling (Prabhu and Mosterman, 2004), and giving the designer abilities to follow signals through simulation, StateFlow which is algorithms simulation tool was used in this research. It was chosen to present the MIM control algorithm in the Model-in-the-Loop stage. The StateFlow representation of the algorithm is shown in Figure 6.2. The inputs for this model are the head chamber pressure, rod chamber pressure, pump pressure, tank pressure, speed command, division status, and division value. The outputs of this model are the selected mode, valve conductance, and the surface pressure valve commands. This model starts by the mode selection. Then the state of the selected modes is activated. The selected mode can be Power Extension, High Side Regeneration Extension, Low Side Regeneration Extension, and Power Retraction as shown in Figure 6.2. Next, the close value detection is performed for all valves which are k_{bt}, k_{sb}, k_{sa}, and K_{at}. Then, the anti-cavitation is triggered for checking before sending the final commands to the stepper drivers.

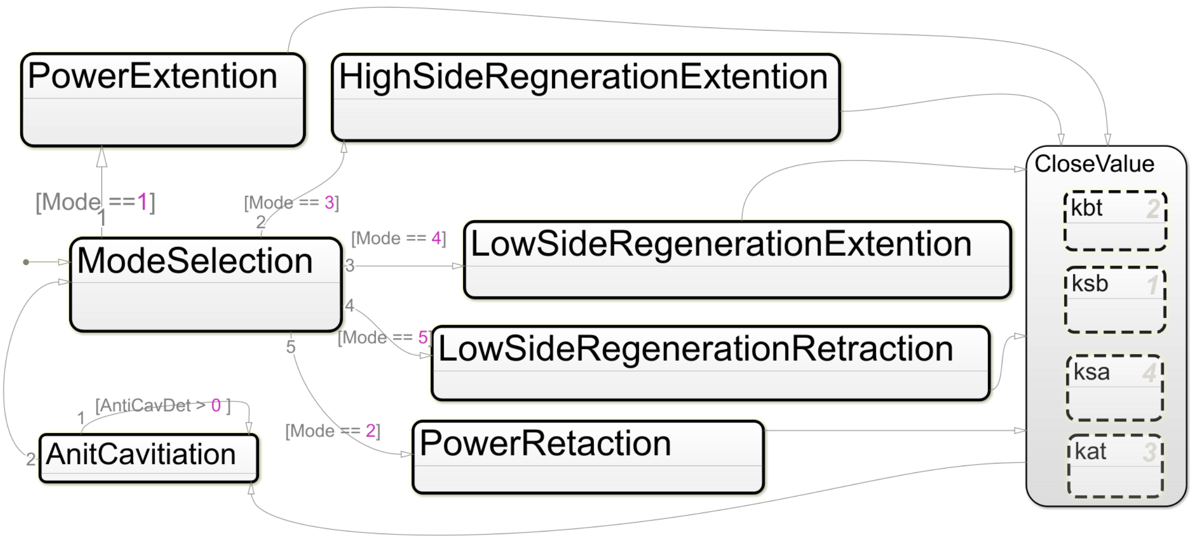

Fig. 6.2 The StateFlow diagram for the control algorithm

6.2.1 Mode Selection

The main inputs for the mode selection procedure (Figure 6.3) are the cylinder load, which is represented by the following equations obtained from Tabor (2004), and the speed which is input from the joystick.

$$F = (P_a * A_a - P_b * A_b) \tag{6.1}$$

$$L = \frac{Fx}{Ab} = (R * Pa - Pb) \tag{6.2}$$

where F is force, P_a is the head chamber pressure, A_a is the head chamber area, P_b is the road chamber pressure, L is the load, F_x is the applied force, and R is the ratio between the two chambers' areas. The mode is selected based on the applied load and the required speed. As illustrated in Figure (6.3) and presented by the Mode Selection Algorithm (1), if the speed is in the positive direction, then the mode can be Power extension, High side regeneration extension, or Low side regeneration extension. If the speed is in the negative direction, the selected mode can be Low side regeneration retraction or Power retraction (Figure 6.3). A StateFlow model of this procedure is included in Appendix (C).

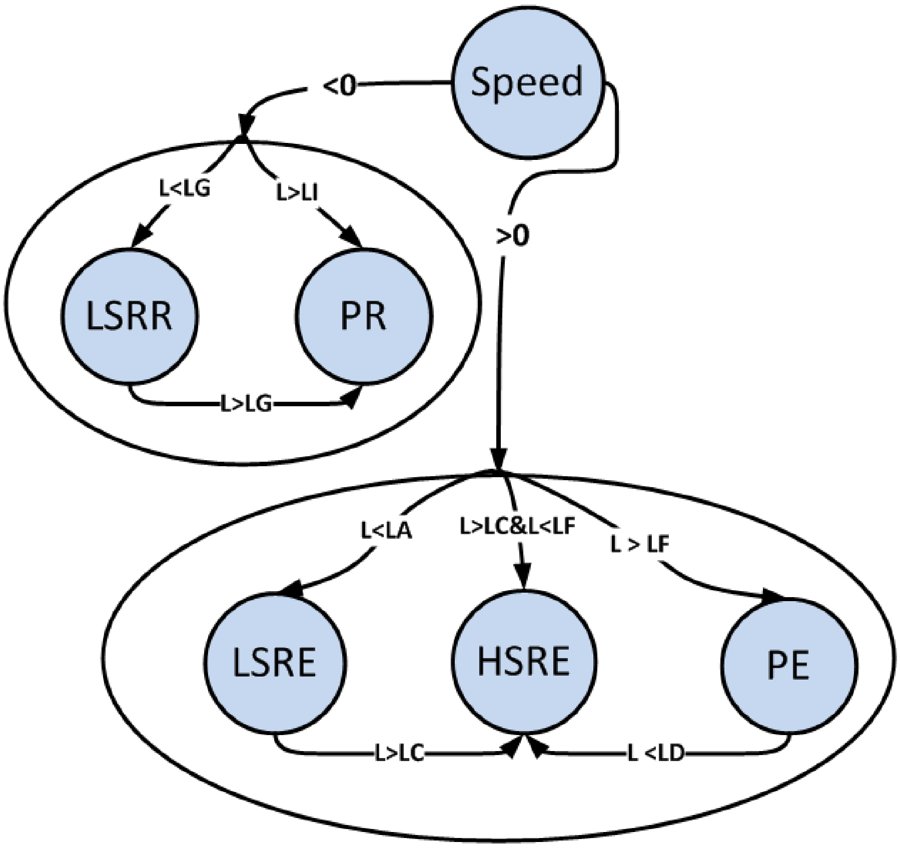

Fig. 6.3 The operation mode selection procedure for the MIM system.

The thresholds between the operation modes are determined using the driving pressures for the operation modes which are represented by Equations 4.13, 4.16, 4.19, 4.22, and 4.25. When the pressure driving is zero, no movement is produced by the actuator. As indicated by Pfaff and Tabor (2005), substituting Equation 6.2 into the pressure driving equations resulted into the following equations,

$$LA = R * Pr - Pr - N \tag{6.3}$$

$$LB = R * Pr - Pr - M \tag{6.4}$$

$$LC = R * Pr - Pr - K \tag{6.5}$$

$$LD = R * Ps - Ps - N \tag{6.6}$$

$$LE = R * Ps - Ps - M \tag{6.7}$$

$$LF = R * Ps - Ps - K \tag{6.8}$$

$$LG = R * Pr - Pr + K \tag{6.9}$$

$$LH = R * Pr - Pr + M \tag{6.10}$$

$$LI = R * Pr - Pr + N \tag{6.11}$$

where LA is the upper limit of the LSRE mode load, LB is the upper limit of the LSR pressure for the return pressure, LC is the lower limit of the Minimum Pressure for the return pressure and it is the lower limit of the HSRE from the LSRE side, LD is the upper limit of the HSRE from the PE side, LE is the upper limit of the HSRE pressure from the PE pressure for the supply pressure, LF is the lower limit for the PE pressure for the supply pressure, LG is the upper limit of the Minimum Pressure for the return pressure, LH is the lower limit of the LSR pressure for the return pressure, and LI is the upper limit of the PR pressure for the supply pressure. (Pfaff and Tabor, 2005) includes more details about the manipulation of these equations. To overcome the cylinder friction and valves' loses, the minimum value of the pressure driving in each mode must exceed a pressure margin K which is in Equations 6.5, 6.8, and 6.9. M in Equation 6.10, 6.4, and (6.7 is selected to ensure that the pressure change appears before the metering mode transition happens. The pressure selecting procedure for the five modes is shown in Figure (6.4). N in Equations 6.6, 6.3, and 6.11 is used to provide the desired degree of hysteresis between the modes transition. The values of theses parameters (K,M, and N) have to be $K \leq M \leq N$. Moreover, the values of the parameters N and M are variant and depend on how fast the pump and the load pressure change. For this simulation, the value of K is 0.5 MPa. The values of N and M were selected to be 1 and 0.75 $M\ Pa$ because the supply and return pressures are fixed in this simulation process.

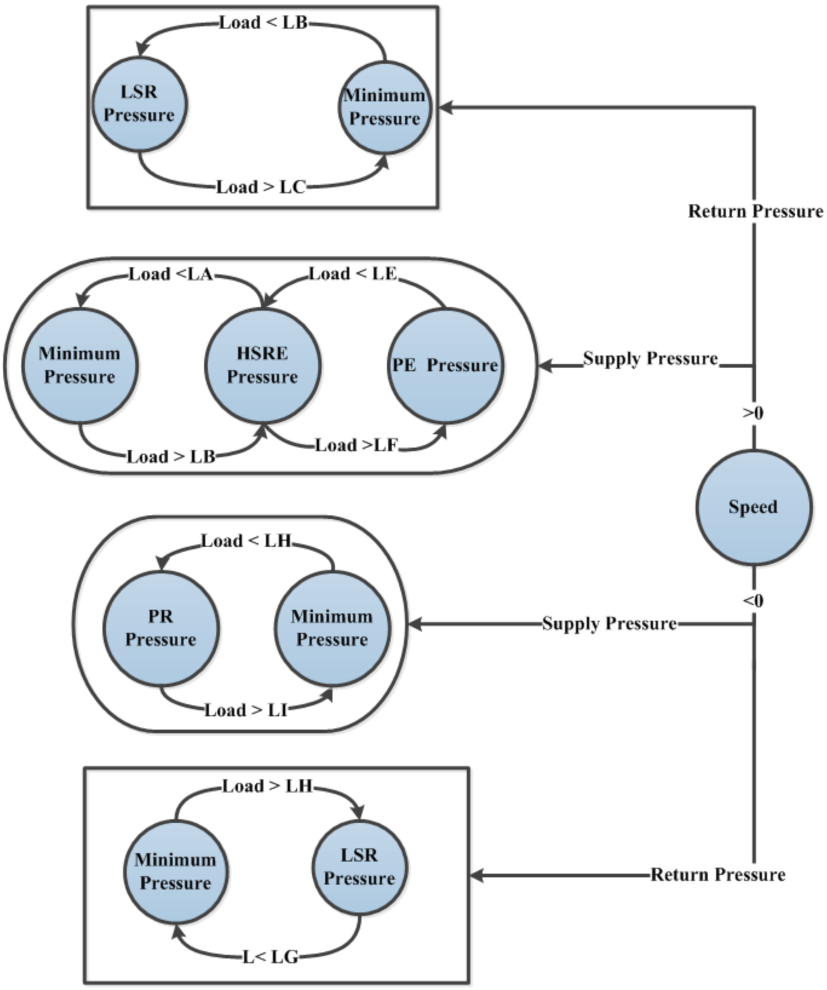

Fig. 6.4 The operation pressure for the selected modes.

When the state of the selected mode is activated, the conductance value of each valve is calculated according to the mathematical expressions 4.14, 4.17, 4.20, 4.23, and 4.26 in Section 4.2. The StateFlow representation of the five modes are included in Appendix (E). Algorithm (2) is the procedure for the power extension mode, where the values of valves K_{sb} and K_{sa} are evaluated.

6.2.2 Close Value Detection

Once the conductance value of each valve is obtained, the Close Value Detection Procedure in Figure 6.5 and Algorithm (3) is used to send the stepping degrees to the stepper motor driver. The StateFlow model of this procedure is shown in Appendix (C). When the procedure receives the activation signal from the selected mode state, three possible scenarios can be activated which are as follows:

Algorithm 1 : The Mode Selection Algorithm

procedure MODESELECTION($Pa, Pb, Aa, Ab, Speed$)
    $Load = (Aa/Ab) * Pa - Pb$
    $LF = R * Ps - Ps - K$
    $LD = R * Ps - Ps - N$
    $LC = R * Pr - Pr - K$
    $LA = R * Pr - Pr - N$
    $LG = R * Pr - Pr + K$
    $LI = R * Pr - Pr + N$
    if $Speed > 0$ **then**
        if $Load > Lf$ **then**
            $Mode \leftarrow PE$
        else if $Load < LD || Load > LCL < LF$ **then**
            $Mode \leftarrow HSRE$
        else
            $Mode \leftarrow LSRE$
        end if
    else if $Speed < 0$ **then**
        if $Load < LG$ **then**
            $Mode \leftarrow LSRR$
        else
            $Mode \leftarrow PR$
        end if
    else
        $NoAction$
    end if
return $Mode$
end procedure

Terms: *LA* is the upper limit of the LSRE mode load, *LC* is the lower limit of the Minimum Pressure for the return pressure, *Lc* is the lower limit of the HSRE from the LSRE side, *LD* is the upper limit of the HSRE from the PE side, *LF* is the lower limit for the PE pressure for the supply pressure, *LG* is the upper limit of the Minimum Pressure for the return pressure, and *LI* is the upper limit of the PR pressure for the supply pressure.

Algorithm 2 : The Activation Procedure for the PE Mode

procedure ACTIVATION(R, Ps, Pt, Ps, Pb, Ab)
  $Dp = (R*(P_s - P_t) + (P_s - Pb))$ ▷ The driving pressure for the piston
  if Dp > 0 **then** ▷ The driving pressure is enough
    $PSV \leftarrow 0$
    $Keq \leftarrow \frac{(Speed*Ab)}{(\sqrt{R*(P_s-P_a)+(P_b-P_t)})}$
    $K_{bt} \leftarrow \frac{\sqrt{(Opt^2+R^3)*K_{eq}}}{Opt}$
    $K_{sa} \leftarrow Opt * K_{bt}$
  end if
  if Dp <= 0 **then** ▷ The driving pressure is not enough, for safety no action
    $K_{bt} \leftarrow 0$
    $K_{sa} \leftarrow 0$
    Increase the Ps
  end if
end procedure

Terms: R is the ratio between the cylinder chambers' areas, Ps is the supply pressure, Pt is the tank pressure, Pb is the rod chamber pressure, Ab is the head chamber area, K_{eq} is the conductance equivalent, K_{sa} is the inlet valve conductance, K_{bt} is the outlet valve conductance, Dp is the driving pressure, Opt is the relationship between the two valves conductance.

(a) The No Action procedure, it keeps the stepper motor in its position. This path is followed when no action is required from this valve.

(b) The Normal Action procedure which is activated when the smoothness command is deactivated. The smoothness command is an input from the driver using the joystick. In this scenario, it gives the stepper motor a command to move based on the full step value which is 1.8° for the selected stepper motor in this design. The vector of differences between the required conductance and the stored vector, based on the valve design, is calculated. The aim of this process is to find the suitable angle to adjust the command for the motor driver. A For-Loop is used to find smallest difference value, which reflects the selected degree to be sent for the driver.

(c) The Smoothness Action procedure, is used when the step division is activated by the driver. Two scenarios can be followed in this event. In the first scenario, the difference vector is generated, then the smallest difference in selected. The chosen value could be more or less than the conductance value. If the difference is positive which means that the required conductance value is bigger than the selected value, the difference between the required conductance and the selected point is divided by the step division, then the closest value of the divisions is to be added the selected value. On the other hand, if the difference is negative, the selected point shifted back by one step. Then, the difference between the required conductance and the selected point is divided by the step division. After that, the closest value of the divisions is added to the selected value.

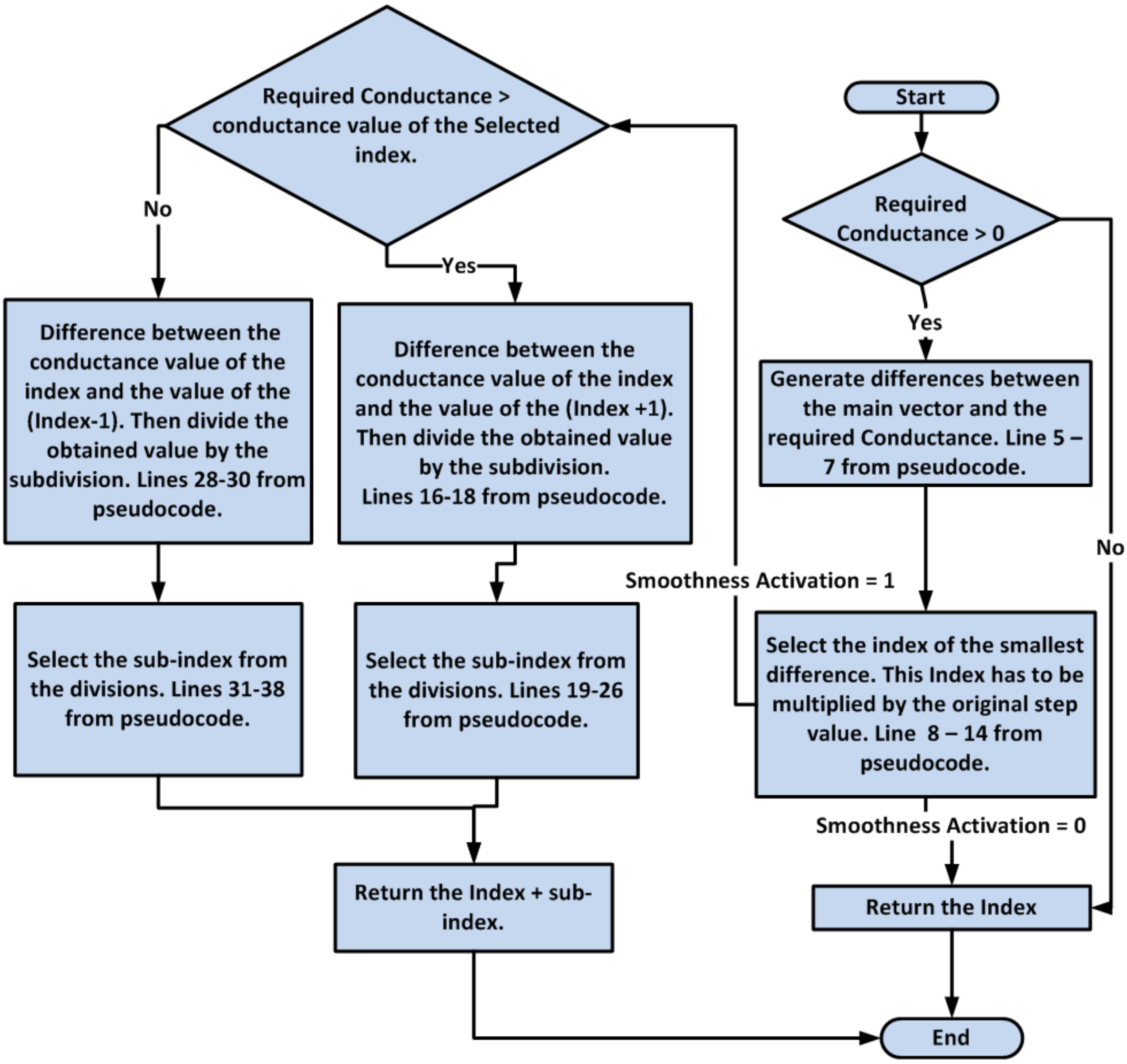

Fig. 6.5 The flowchart of the close value detection technique.

Algorithm 3 : The Close Value Detection Algorithm

```
procedure CLOSE VALUE DETECTION(StCon, Ind1, Sdiv, K)
    if K == 0 then                                   ▷ The required conductance
        NoNewAction                                  ▷ This to keep the motor on it's position
    else
        for i = 0 to 50 do                           ▷ Difference between the steps conductance and K
            Diff(i) = abs(StCon(i) − K)
        end for
        SValue ← Diff(1)                             ▷ Set the first value as smallest difference
        for i = 0 to 50 do                           ▷ To find the smallest difference
            if Diff(i) < SValue then
                SValue ← Diff(i)                     ▷ Change the value of the smallest
                Ind1 ← i                             ▷ Set the step to be the index
            end if
        end for
        if SmAct == 1 then                           ▷ if the micro-step is activated
            if Ind1 < 50 & K > StCon(Ind1) then
                DifM1 ← abs(StCon(Ind1 + 1) − StCon(Ind1))/Sdiv
                F1 = 1
                while F1 < (Sdiv + 1) do             ▷ To select from the subdivsions
                    if K > StCon(Ind1)&K < (StCon(Ind1) + DifM1) then
                        DifM12 ← F1                  ▷ Keep the number of this subdivision
                    else
                        StCon(Ind1) ← StCon(Ind1) + DifM1
                    end if
                    F1 ← F1 + 1                      ▷ Move for the next stepdivision
                end while
            end if
            if Ind1 < 50 & K < StCon(Ind1) then
                DifM1 ← abs(StCon(Ind1) − StCon(Ind1 − 1))/Sdiv
                F1 = 1
                while F1 < (Sdiv + 1) do             ▷ To select from the subdivsions
                    if K > StCon(Ind1)&K < (StCon(Ind1) + DifM1) then
                        DifM12 ← F1                  ▷ Keep the number of this subdivision
                    else
                        StCon(Ind1) ← StCon(Ind1) + DifM1
                    end if
                    F1 ← F1 + 1                      ▷ Move for the next stepdivision
                end while
            end if
        end if
    end if
    return Steps = Ind1 + DifM12
end procedure
```

Terms: *StCon* is the vector of conductance value at each step of the motor, $Ind1$ is aparameter to contain the suitable step from the vector, *Sdiv* is the required micro-step, K is the required conductance for the valve.

Algorithm 4 : The Anti-Cavitation Detection Algorithm

procedure ANTICAVITATION($Opt, R, Ab, Ps, Pt, Ab, Index1, Index4$)
  $AntiCav = (Opt/R)^2 * A_b * P_s + P_t * A_b$ ▷ Calculate the force causes cavitation
  if $AntiCav == Fx$ **then**
    $AntiCavDet = 1$
    $Index1 = Index1 - 1$ ▷ Decrease the meter-out angle
    $DiffMode12 = 0$ ▷ Deactivate the mico-stepping
    $Index4 = Index4 + 1$ ▷ Increase the meter-in angle
    $DiffMode42 = 0$ ▷ Deactivate the mico-stepping
  else
    $AntiCavDet = 0$
    $No\ Action$
  end if
  if $Index1 < 0 || Index4 > 50$ **then** ▷ If the commands are maximum
    $Index1 = 0$
    $Index4 = 50$
  else
    $No\ Action$
  end if
end procedure

Terms: R is the ratio between the cylinder chambers' areas, Ps is the supply pressure, Pt is the tank pressure, Pb is the rod chamber pressure, Ab is the head chamber area, K_{eq} is the conductance equivalent, K_{sa} is the inlet valve conductance, K_{bt} is the outlet valve conductance, Dp is the driving pressure, Opt is the relationship between the two valves conductance, $Index1$ is the inlet valve opening degrees, and $Index2$ is the outlet valve opening degrees.

As the cavitaition is prevented in this algorithm, if it appears, the stepping degrees should be changed. An anti-cavitation procedure, which is represented by Procedure (4), is developed to check and act to prevent pressure in side cylinder chambers from decreasing to zero or negative. As shown in Figure C.8 in Appendix (C), anti-cavitation is checked for each mode, and if cavitaion is detected, consequently, the opening degree of the valves are changed. Deciding on the angle of change is based on the anti-cavatition calculation in Section (4.4). For example, if the mode is Power Extension, the force which causes cavitation is calculated. If it appears, then the outlet valve which is Kbt (Figure 4.2) is reduced by one step and the input is increased by one step. After that, cavitation checking is repeated until it disappears and mode selection starts again.

6.3 Software-in-the-Loop Platform

The simulation platform which is shown in Figure 6.6 was developed in the MathWorks Simulink platform. It contains the controller model, the valves models and the hydraulic cylinder model connected with variable and fixed loads. At this stage of research and to reduce the complexity of the system, the stepper motor is represented by a simple second order transfer function and the friction and flow torques are neglected. The controller has many inputs which are the cylinder pressures, the pump pressure, and the tank pressure. Also, it contains the input commands which are the speed, the smoothness activation, and the subdivision value.

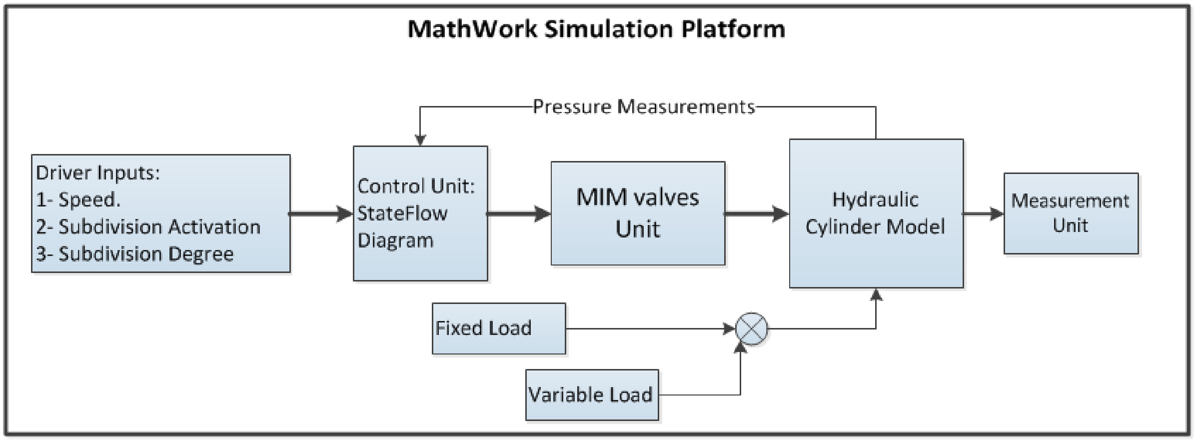

Fig. 6.6 The simulation platform of the system that was used to test the control algorithm

The mathematical model of a hydraulic actuator, obtained from Shenouda (2006) and Hansen et al. (2016), is as follow,

- As the IM configuration is four valves connected to one cylinder, then the four orifices flows rates obtained from Shenouda (2006) are,

$$Q_{sa} = K_{sa}\sqrt{|p_s - P_a|}sgn(p_s - p_a) \tag{6.12}$$
$$Q_{sb} = K_{sb}\sqrt{|P_s - P_b|}sgn(p_S - p_b) \tag{6.13}$$
$$Q_{at} = K_{at}\sqrt{|p_a - P_r|}sgn(p_a - P_r) \tag{6.14}$$
$$Q_{bt} = K_{bt}\sqrt{|p_b - p_r|}sgn(p_b - p_r) \tag{6.15}$$

where Q_{sa} is the flow rate from the pump to the head chamber, Q_{sb} is the flow rate from the pump to the rod chamber, Q_{at} is the flow are from the head chamber to the tank, and Q_{bt} is the flow rate from the rod chamber to the tank. The K factor represents the discharge coefficients for these orifices sa,sb,at, and bt, respectively. The pressures are

p_s for the pressure source, p_a for the head chamber, p_r for the tank pressure, and p_b for the road chamber.

- The compressability of the actuator obtained from Shenouda (2006) is,

$$Q_{ca} = \frac{V_{a0} + A_a x}{B_e} \dot{P}_a \tag{6.16}$$

$$Q_{cb} = \frac{V_{b0} - A_b x}{B_e} \dot{P}_b \tag{6.17}$$

where Q_{ca} is the volume flow in the head chamber, Q_{cb} is the volume flow in the rod chamber. V_{a0} is the initial volume of the head chamber and $V_{a0}$is the initial volume of the rod chamber. A_a and A_b are the areas of the head chamber and rod chamber respectively. $\dot{P}_a$ and $\dot{P}_b$ are the respective changes of pressure. B_e is the bulk modulus.

- The conversion of mass is,

$$Q_{sa} - Q_{at} - Q_L = Q_{ca} + A_a \dot{x} \tag{6.18}$$

$$Q_{sb} - Q_{bt} + Q_L = Q_{cb} - A_b \dot{x} \tag{6.19}$$

- The equations can be written as,

$$Q_{sa} - Q_{at} = \frac{V_{a0} + A_a x}{B_e} \dot{P}_a \tag{6.20}$$

$$Q_{sb} - Q_{bt} = \frac{V_{b0} - A_b x}{B_e} \dot{P}_a \tag{6.21}$$

$$\tag{6.22}$$

- The conversion of momentum is,

$$P_a A_a - P_b A_b = M\ddot{x} + F_l + f_f \tag{6.23}$$

The cylinder leakage is neglected and the parameters of the selected cylinder are included in the next table.

6.4 Operation Modes Simulation

To check the performance of the system and the control algorithm, different scenarios with initial assumptions have been selected and performed. For the hydraulic cylinder model (Figure

Table 6.1 The main parameters of the selected hydraulic cylinder

Symbol	Parameter	Value	Unit
Ps	supply pressure	20	MPa
Be	Bulk Modulus	689.476	MPa
Aa	Head chamber area	12272	mm^2
Ab	Rod chamber area	9444	mm^2
x	Cylinder Stroke	845	mm
Ff	Viscous Friction	90000	$N.s/m$
M	mass	478.4	Kg

6.6), the assumed initial head chamber pressure is 3.1228 MPa, and the assumed initial rod chamber pressure is 1 MPa. The fixed load on the cylinder is 28.773 KN to keep the cylinder velocity at 0 m/s when the four valves are fully closed, and the added variable load is between $+70$ KN and -70 KN. The operation modes numbers are 1, 2, 3, 4 , and 5 where 1 is the power extension, 2 is the power retraction, 3 is the high side regeneration extension, 4 is the low side regeneration extension, and 5 is the low side regeneration retraction, respectively. The pressure source for this surface is 20 MPa and the drain pressure is 0.2 MPa. It is important to again mention that the speed command is a joystick input for an open loop system. The relationship between it's handle movement and the signal that is provided into the algorithm can be changed according to the design requirement. For example, the joystick movement can be set to four quarters. In this five operation modes simulation, the smoothness mode is deactivated. The simulation aims to reach a fixed speed of 0.2 m/s for the five modes, and show the rotation angles of the opened valves.

Firstly, for the power extension mode, the selected variable load is 50 KN. As shown in Figure 6.7, the selected mode started at 3 and changed into 1, and this is because the initial pressures in the chambers are 3.1228 MPa and 1 MPa for the head and the rod chambers, respectively. The flow for the head chamber is $2.43e^{-3}$ m^3/s and the rod chamber flow is $1.87e^{-3}$ m^3/s. The speed obtained is 0.2 m/s, and in one second of simulation the piston moved 0.2 m. The head chamber pressure is 13.5 MPa, while the rod chamber pressure is 6.59 MPa. The activated valves are K_{sa} and K_{bt} and their values are 27° and 23.4°, respectively.

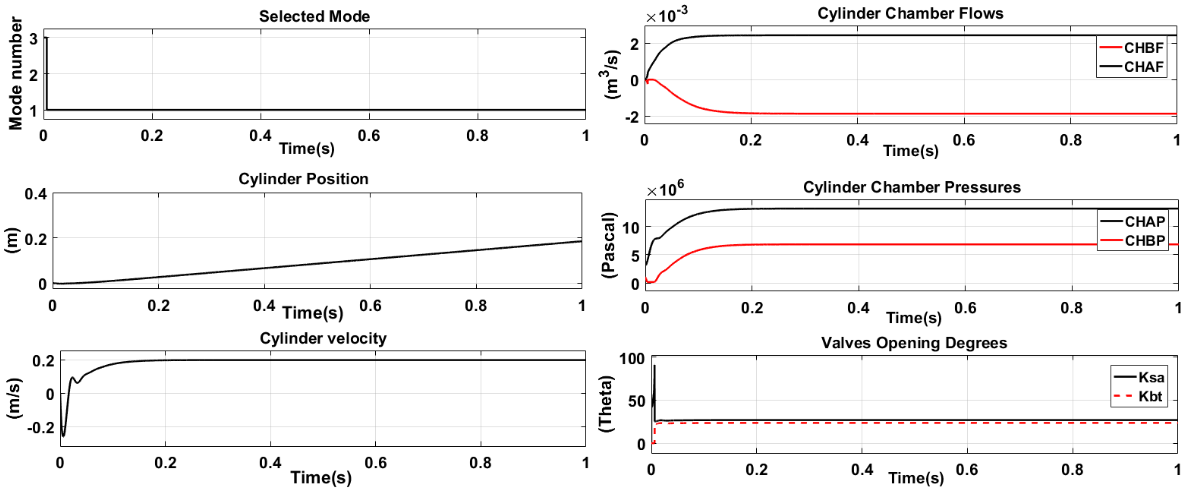

Fig. 6.7 The power extension mode simulation: selected mode, chambers flows, position, pressures, velocity, and valve opening degrees

Secondly, in the power retraction mode (Figure 6.8), the selected variable load is $-50\ KN$, and as the joystick is in the negative direction, the selected mode is 5 and then changes into 2 because of the initial assumed pressures in the cylinder chambers. The fluid flow rates in the rod chamber and the head chamber are $1.87e^{-3}\ m^3/s$ and $-2.43e^{-3}\ m^3/s$, respectively. The achieved position after 1 s of simulation is $-0.2\ m$. The rod chamber pressure is 13.2 MPa, and the head chamber is 7 MPa. The activated valves K_{at} and K_{sb} opening degrees are 27° and 23.4°, respectively.

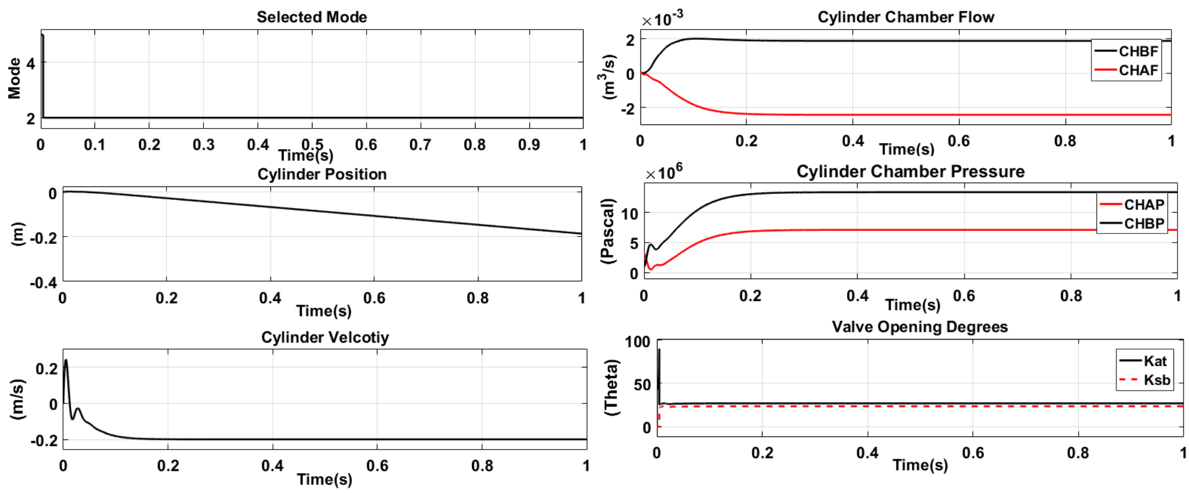

Fig. 6.8 The power retraction mode simulation: selected mode, chambers flows, position, pressures, velocity, and valve opening degrees

Thirdly, the simulation of the low side regeneration extension mode. This is shown in Figure 6.9. It is performed by applying the same initial assumption, but the variable load is changed to be -50 KN, and the joystick is in the positive direction. The selected mode started at 3 because of the initial assumptions, and was then converted directly to 4 when the algorithm detected the applied load and the speed direction. As this mode is regenerative, the inlet flow from the pump to the head chamber is almost zero. The fluid is recirculated from the rod chamber to the head chamber by passing in the low pressure side of the hydraulic circuit (Figure 2.10). The recirculated flow is not included in this simulation because the simulation is a mathematical representation and it presents the direct flow from the pump to the cylinder chamber. After one second of simulation, the position of the piston is 0.2 m. The rod chamber pressure is $5e^5$ Pa, and the head chamber pressure is $2e^5$ Pa. The head chamber valve K_{at} opened 72° degrees and the rod chamber valve K_{bt} opened 57.6° degrees.

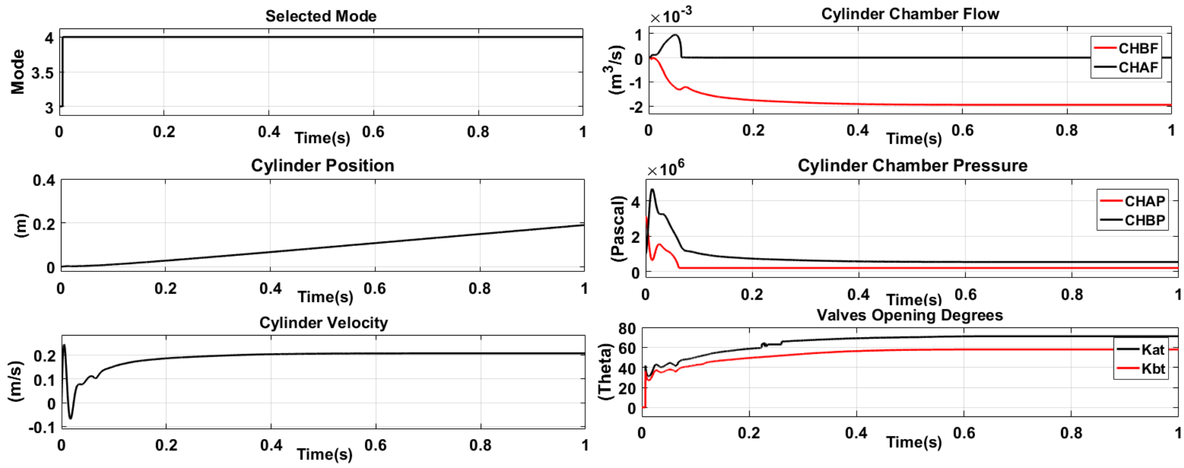

Fig. 6.9 The low side regeneration extension mode simulation: selected mode, chambers flows, position, pressures, velocity, and valve opening degrees

Fourthly, in the low side regeneration retraction mode simulation which is shown in Figure 6.10, the variable load was adjusted to be 50 KN and the joystick was in the negative direction. In this mode, which is a regenerative one by lowering the load, the fluid flows from the head chamber and is recirculated to the rod one using the low side of the surface circuit, which is the hydraulic cylinder connected to four valves (Figure 2.10). The recirculated flow is not included in this simulation which is a mathematical representation that presents the direct flow from the pump to the cylinder chamber. The position of the cylinder is -0.2 m after after 1 s. The head chamber pressure is 5.17 MPa and the rod one 0.2 MPa. The inlet valve for the head chamber opened 28.8° and the rod chamber is 25.2° .

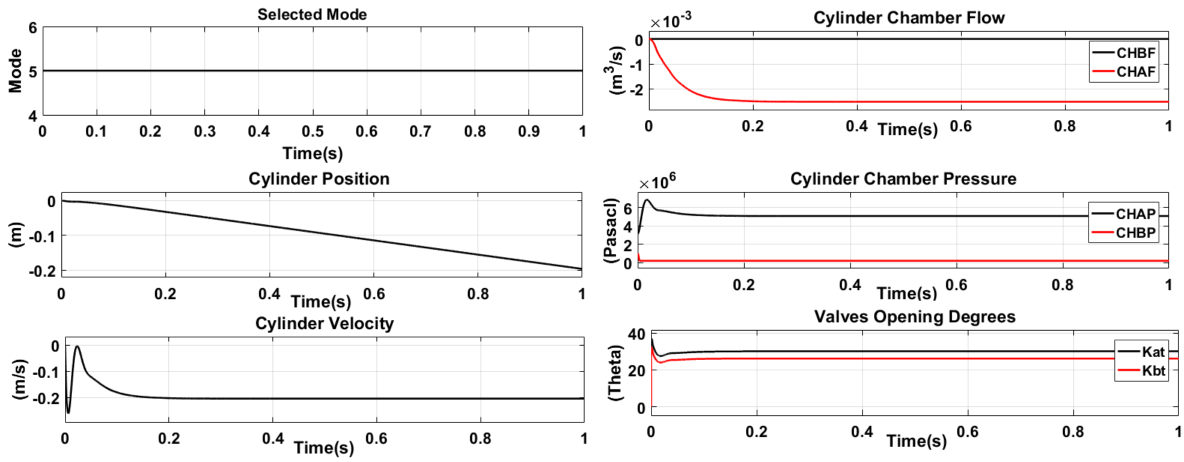

Fig. 6.10 The low side regeneration retraction mode simulation: selected mode, chambers flows, position, pressures, velocity, and valve opening degrees

Fifthly, the high side regeneration extension mode simulation is illustrated in Figure 6.11. It was performed by deactivating the variable load and keeping the fixed load which is 28.77 KN. When the joystick was moved in to the positive direction, the selected mode was 3 without changes. The fluid recirculated from the rod chamber to the head chamber through the high side of the circuit (Figure 2.10). The fluid flow into the head chamber is $2.5e^{-3}$ m^3/s and the drained flow from the rod chamber is $2.35e^{-3}$ m^3/s. The achieved position after 1 s of simulation is 0.2 m. The pressures of the head and rod chambers are 4 MPa and 0.2 MPa, respectively. The recirculated flow is not included in this simulation because it is a mathematical representation and it presents the direct flow from the pump the cylinder chamber. The inlet valve k_{sa} opening degree is 21.6°, and the drain valve k_{sb} is 18.8°.

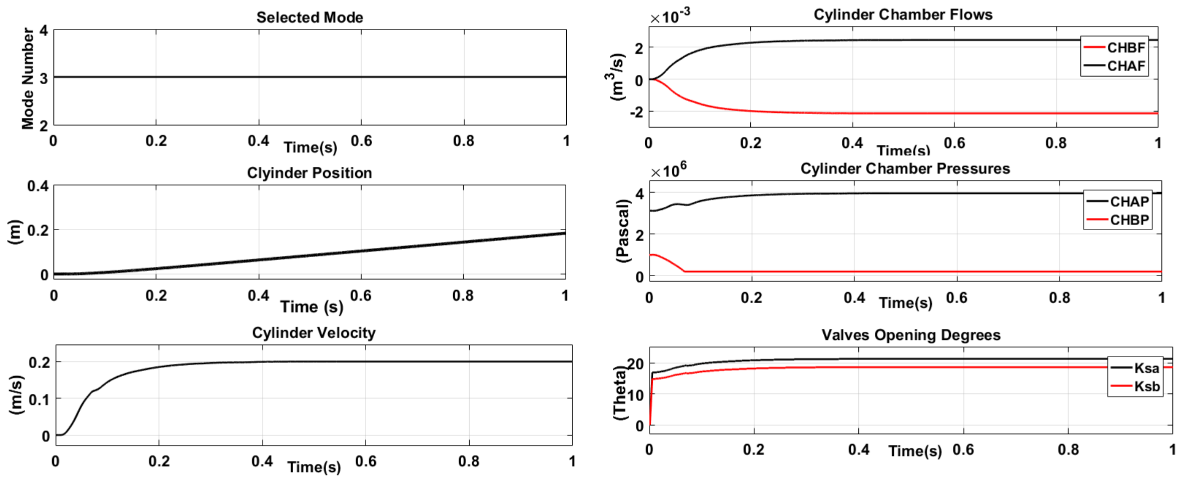

Fig. 6.11 The high side regeneration extension mode simulation: selected mode, chambers flows, position, pressures, velocity, and valve opening degrees

Finally the mode switching is an important action in the independent metering operation. It is necessary to keep selecting the mode which consumes the least energy. In this example, the mode switching is simulated between the Low side regeneration retraction and power retraction modes. The variable load started at 50 KN, and at 0.5 s it was changed to -50 KN. As shown in the Figure 6.12, the modes changed at 0.5 s. Also, the pressures and flows changed between the two modes at the same time. The activated valves changed from k_{at} and K_{bt} into k_{at} and K_{sb}.

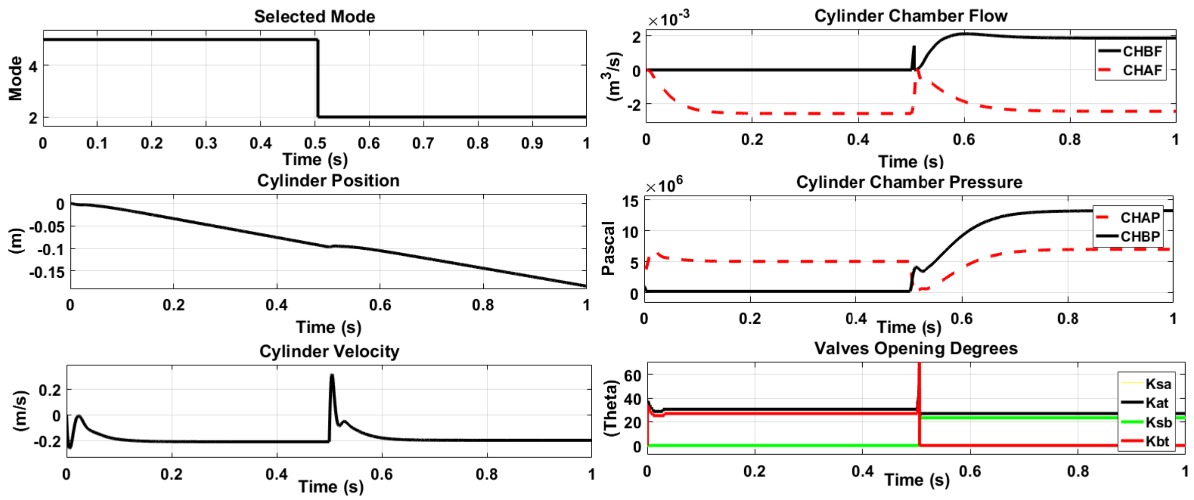

Fig. 6.12 The capability of the algorithm to switch between two modes. *HSRR* to *PR*

The step division is an important advantage of Micro-Independent Metering, and the effect of this technique is shown in Figure 6.13. For the power extension mode, the smoothness technique was activated to the value of $1/16$ which led to the selection of a precise opening of the valves and thus a deviation in the cylinder velocity. The interfacing for this technique can be included in the driver joystick and it is useful for some applications such as trenching for pipes where a precise movement and less vibration are required.

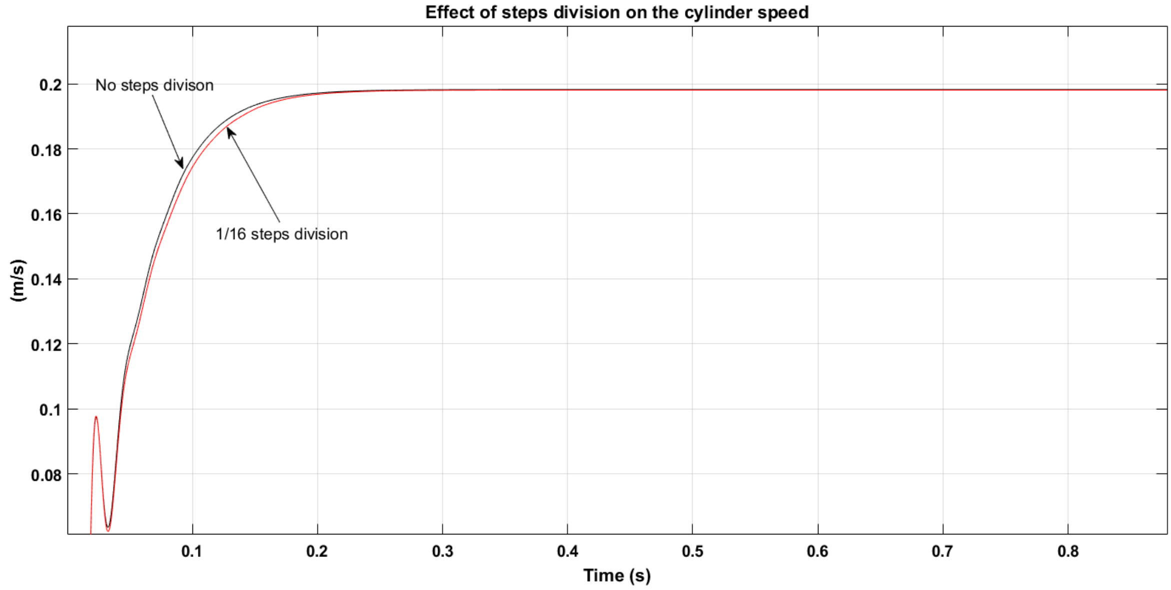

Fig. 6.13 The effect of step division on the velocity of the hydraulic cylinder

6.5 The Controlability Comparison

This part of the research determines the effect of the MIM technique on the actuator velocity performance. It also illustrates the achieved improvements in the hydraulic actuator performance. The effect has been detected by comparing the performance of conventional Independent Metering system, which uses the Valvistor valve, with Micro-Independent Metering, which uses the stepped rotary valve. This study was performed using a model of each system including the same actuator and the same conditions. The Valvistor valve has been deeply studied and modelled by many researchers. For example, Luo (2006) and Opdenbosch et al. (2009a) studied the valve construction and validated a linear and nonlinear model for it.

6.5.1 Valvistor Valve Model

To understand the effect of using different valves on the IM, it is first necessary to analyse the construction and the working principle of the Poppet valve "Valvistor". It contains two main parts which are the Pilot valve and the Main valve. As shown in Figure (6.14), the valve actuator, which is a PWM solenoid, controls the flow in the pilot circuit. The produced flow Q_p leads to a pressure difference between $(P_a - P_p)$ across the main poppet valve m_m and causes it to move. The movement of the main poppet changes the orifice area and therefore Q_1 is changed. Also, the main poppet movement changes the area of the pressure feedback slot x_m. Based on the valve working principle, the hydraulic fluid is one of the control elements, and it is an output at the same time. This is a shortcoming in this valve's controllability, and the fluid nonlinearity or disturbances can affect the actuator performance.

The valve, Valvistor, model used in this study was studied by Zhang et al. (2002a) and Fales (2006). It can be modelled as two sets of mass-spring-damper systems and a compressible fluid volume between them. The model can be split into the pilot pressure control, the main valve dynamics, and the orifice flow. Regarding the pilot pressure, it is controlled by the pilot dynamics, the pilot orifice, slot orifice flow, and inter-stage fluid compressability.

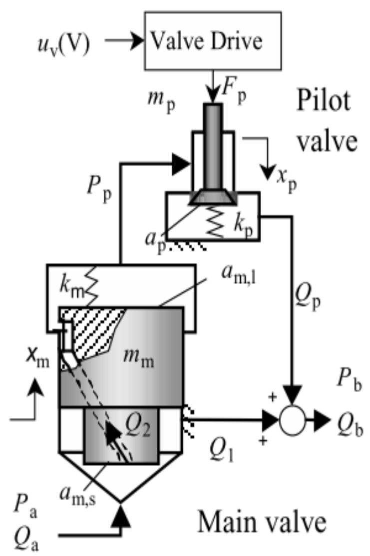

Fig. 6.14 The schematic diagram of the Valvisor valve

The movement of the pilot valve according to Zhang et al. (2002a) is,

$$m_p\ddot{x_p} + b_p\dot{x_p} + k_p x_p = F_p + (P_p - P_b)a_p \tag{6.24}$$

where m_p is the mass of the pilot poppet, and K_p is the pilot poppet spring rate, a_p is the cross sectional area of the pilot poppet, b_p is the pilot poppet damping rate, and F_P is electromagnetic force which is represented by the following equation.

$$F_p = K_e * U_v \tag{6.25}$$

The pilot valve movement produces a flow Q_p which is,

$$Q_p = K_p x_p\sqrt{P_p - P_b} + a_p\dot{x_p} = K_p x_P\sqrt{P_p - P_b} \tag{6.26}$$

The flow of the pressure feedback slot can be is represented by the orifice flow,

$$Q_2 = K_s x_m \sqrt{P_a - P_p} \tag{6.27}$$

where x_m is the main movement, P_p is the pilot pressure, P_a is the inlet pressure.

The pressure P_p changes at a rate described by the net flow into the volume:

$$\dot{P}_p = \frac{\beta}{v_p}(Q_2 + a_{m,1} - Q_p) = \frac{\beta}{v_p}(Q_2 - Q_p). \tag{6.28}$$

where β is the fluid bulck modulus, $a_{m,1}$ is the area of main poppet exposed to control pressure, v_p is volume of the pilot circuit line. The main valve poppet dynamics is represented by,

$$m_m \ddot{x_m} + b_m \dot{x}_m + K_m x_m = a_{m,s} P_a - a_{m,1} P_p + (a_{m,1}) P_b + d_F \tag{6.29}$$

where d_F is the flow disturbance force and $a_{m,s}$ is area of main poppet exposed to supply pressure.

Finally, the flow through the main orifice is determined by x_m:

$$Q_1 = K_m x_m \sqrt{P_a - P_b} \tag{6.30}$$

The values of the valve model parameters are collected from Luo (2006) and Fales (2006) and included in Table D.2 in Appendix (D). For the same valve as shown in Figure 6.15, the disturbances df can effect the produced flow due to the main construction of the valve where the fluid is a contributor to the control system. This performance of this model is very enclose to the real measurement obtained from Opdenbosch et al. (2009a) and shown in Figure 6.16.

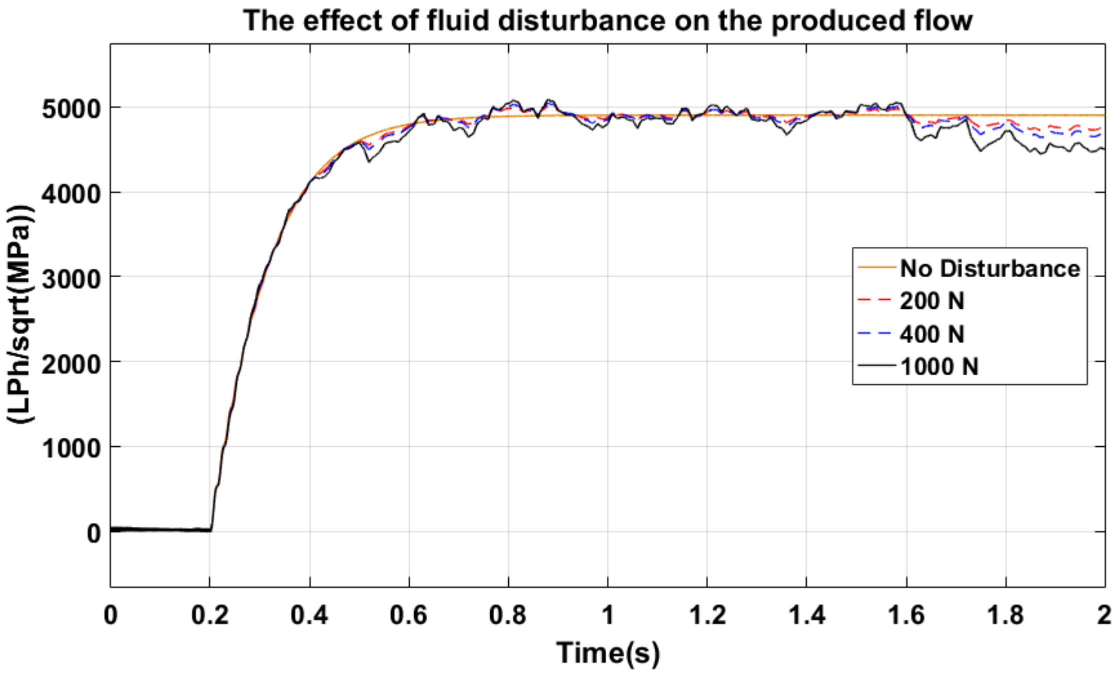

Fig. 6.15 The performance of the valvisotr valve with different values of disturbances

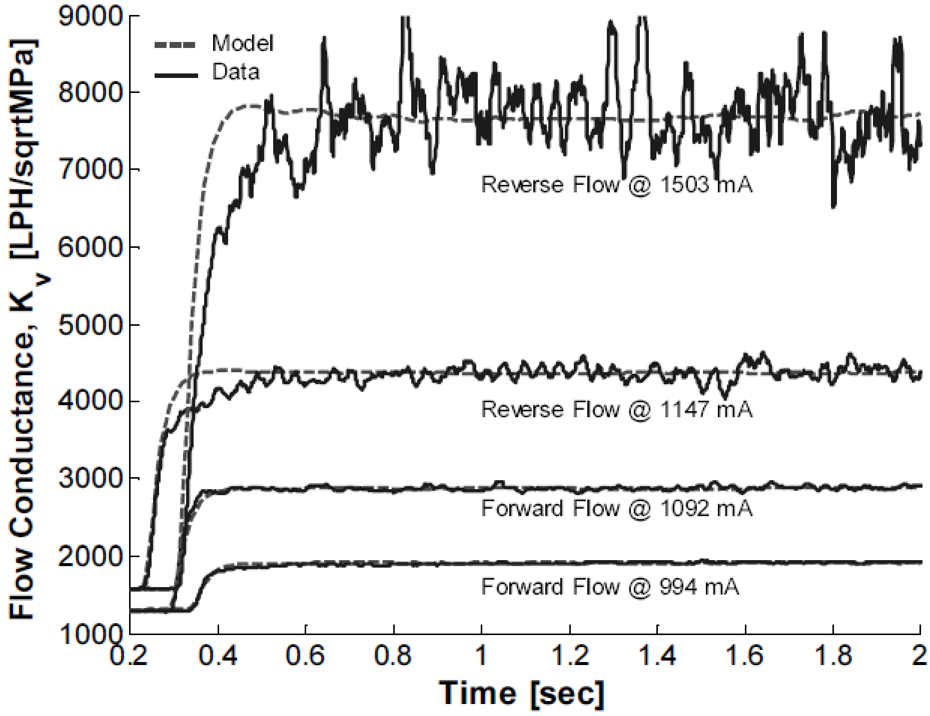

Fig. 6.16 The real performance of the poppet valvistor valve. (Opdenbosch et al., 2009a).

This analysis started by designing two IM models for the same cylinder that was used in the previous sections in the Software-in-the-loop simulation. The selected mode to be performed was the power extension mode, so the activated valves were the one between the pump and the head chamber, which is the inlet, and the one between the rod chamber and the tank, which is the outlet. Then disturbances were inserted into the two models to recognize the difference in performance. These disturbances can be due to fluid non-linearity caused by heat, air, or machine vibration. One of the models is based on the poppet valve, Valvistor, while the other is based on the rotary valve developed during this research. The stepped rotary valve model that is used here is nonlinear to study the disturbance effects on the valve construction that effects the actuator performance. This model is using Equations 5.6, 5.12, and 5.13.The disturbances were added to the new valve in the Equation 5.6 to be,

$$T_{st.fl} = \frac{2C_c(\Delta pA_o + df)R_{e.sp}\sin\theta}{1 - C_c{}^2} \tag{6.31}$$

where $T_{st.fl}$ is the steady state flow, C_c is the contraction coefficient, Δp is the pressure difference, A_o is the opening area, $R_{e.sp}$ is the external spool radius, and df is the disturbances force.

The schematic diagram of the models is shown in Figure 6.17. Assumed 200 N force disturbances were inserted to the the model of both systems. Figure 6.18 indicates that the MIM configuration is able to reject the fluid disturbances which is the obstacle in the traditional IM that relies on the Valvistor type. As noticed in the results the traditional system is affected by the fluid disturbances, and this is due to the design of the valvistor valve. It relies on the fluid as a control element for the pilot stage (Figure 6.14). Therefore, the fluid's nonlinearities produce deviations in the piston position and thus the amount of flow produced. In contrasts, the new valve design is based on one stage, and the flow effect is just only on the edges of the rotary orifice which is a very small area that does not change the torque of the hollow that attached to the stepper motor, Figure (5.2).

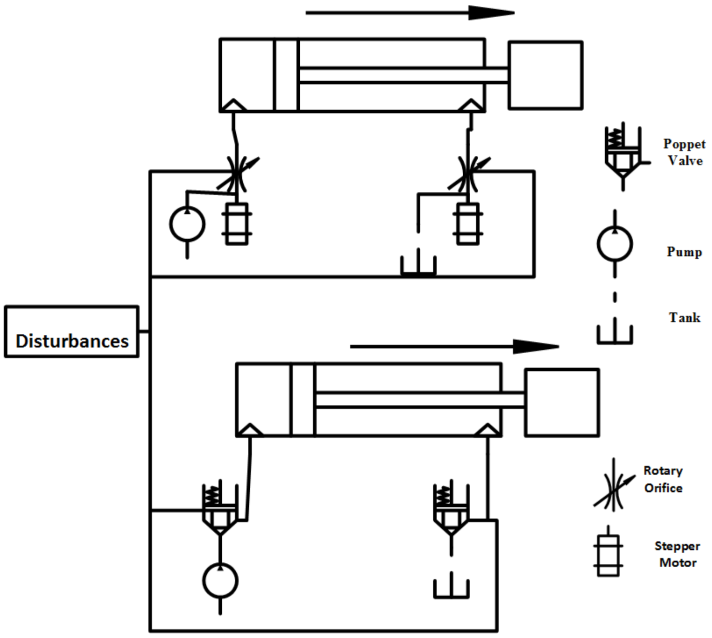

Fig. 6.17 The comparison model between the MIM and the traditional IM configurations. The used disturbances is 200N with 0.01 average.

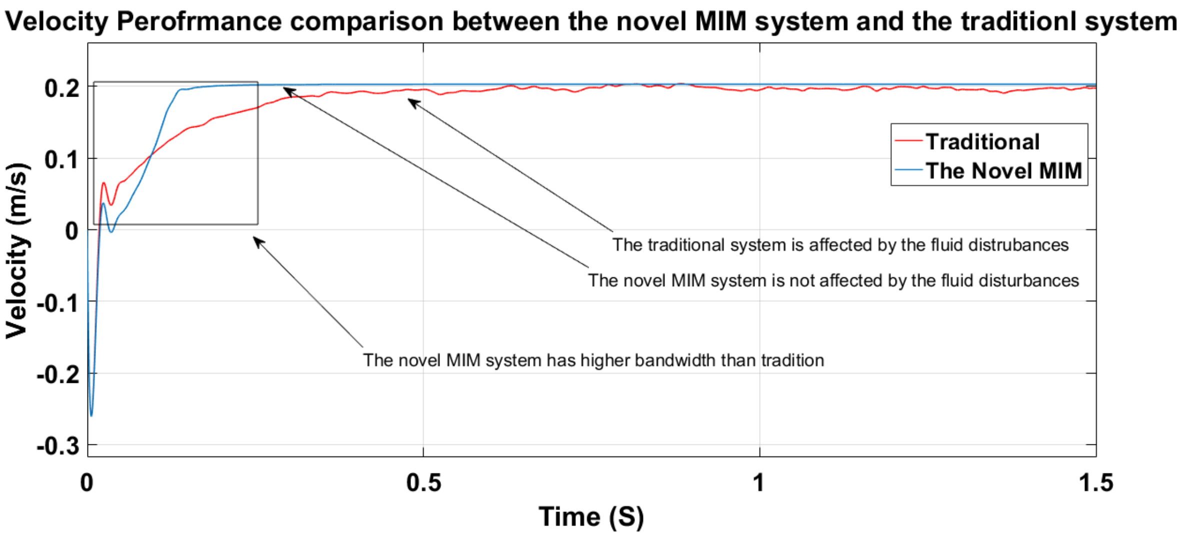

Fig. 6.18 The comparison of the velocity performance between the MIM configuration and traditional IM under fluid disturbances effect.

6.6 Summary

This chapter represents an important stage of the Model Based Design method which has been selected to be the development method in this research. It is about the Model-in-the-loop and the Simulation-in-the loop of the MIM system. It aims to analyse the performance of the system under different conditions, and it is also necessary to prepare for the hardware testing.

The MIM control algorithm has been established using the StateFlow tool in Mathwork. This model helped to analyse each stage of the algorithm and showed its reaction under different conditions. The algorithm model was connected to the model of the valves and the cylinder to form a simulation platform. The input parameters for this platform were the speed, pressures, and loads. The outputs were the cylinder velocity and position. The parameters of the hydraulic actuator were obtained from Shenouda (2006). Simulation tests were performed on the five operation modes. It showed the selected operation mode by the algorithm, cylinder position, cylinder velocity, chambers flows, and chambers pressures.

The mode switching and step division have been analysed for the system. It showed the ability to change between modes to save more energy. Regarding smoothness using step division, it indicated that there is a light change in the cylinder velocity performance.

Moreover, a comparison of velocity performance between the traditional independent metering system using the valvistor type valve and the new MIM system using the stepped rotary valve has been studied. The MIM system showed the ability to reject fluid disturbances, while the traditional system was affected by disturbances because of the Valvistor valve construction which relies on the fluid as a part of the control system.

Chapter 7

System Integration and Hardware-in-the-Loop Testing of the MIM System

7.1 Introduction

In this chapter, a Hardware-in-the-loop test was performed on the MIM system. The Hardware-in-the-loop testing or Model-in-the-loop testing is an important part of the Model Based Design method and it requires a real time simulation to be performed (Plummer, 2006). The real time simulation is accurate when the simulation produces a variable over a time length similar to that is used by the hardware (Bacic, 2005). To ensure the accuracy of the Hardware-in-the-loop test, a target computer is used for the simulation. The target computer operates on a specific operation frequency not like the normal operation system such as Windows. They produce repeatable and guaranteed latencies (Martin and Emami, 2006). The HIL test functionality can be quantitative or qualitative. The quantitative method depends on the software to hardware ratio, HIL transparency and robustness, and accuracy of integration. The qualitative method depends on the fidelity and level of modeling (Grepl, 2011). As the target PC is not included in the research, this part of the research studies the qualitative performance of the system in order to show the ability of the controller to follow the operator commands and change between the operation modes.

In this system, a model of the the actuator connected with the valves package is modelled on the PC using a normal operating system, and serial communication has been created between the hardware and the simulation. The aim of this connection is to transfer the pressures from the hydraulic actuators to the hardware; to study the rotations of the stepper motors. In Section

7.2, the hardware platform is explained in detail. Then, the five mode tests are included in Section 7.3. Section 7.4 is the analysis of the stepper rotations produced. The summary is in Section 7.5.

7.2 The Hardware Platform Design

The platform developed for the test (Figure 7.1) contains four stepper motors, a power supply, four stepper motor drivers, a joystick, and three Arduino Uno controllers. The first controller is used to import data from the simulation part via serial communication. This controller is connected to the LCD screen to show the pressure values that are received based on changing the flows or the load on the actuator, simulated cylinder. The second controller is used to implement the control algorithm and transfer the valves rotation degrees to the activation controller which is the third Arduino controller. It also sends the rotation degrees to the simulation part via serial communication. Moreover, it reads the operator commands which are from the joystick. These commands are used to implement the algorithm calculations. The activation controller contains the software that translates the commanded degrees into pulses for every stepper motor driver.

The stepper motors are used to represent the actuators that should be attached to the real rotary orifices. The four rotary orifice models are included in the simulation part on the PC. These orifices are directly connected to the actuator which is a cylinder model. The commands which are the opening degrees sent from the main controller to the activation controller are simultaneously sent to the orifices on the simulated part. For example, if the main controller sends commands for the first and the third valve to open 45 degrees, these commands are sent directly to the orifices at the PC. The flow produced from the orifices to the actuator lead to changes in the chamber pressures and thus the actuator velocity.

The real hardware-in-the-loop testing platform is shown in the Figure 7.2. As indicated in Figure 7.3, the system contains four stepper motors called K_{sa}, K_{sb}, K_{at}, and K_{bt}, respectively. These motor drivers are supplied from a 24 V DC and 3 A power supply. These drivers have been adjusted to $1/16$ step division and 2 A current consumption. A simple joystick is connected to represent the driver command.

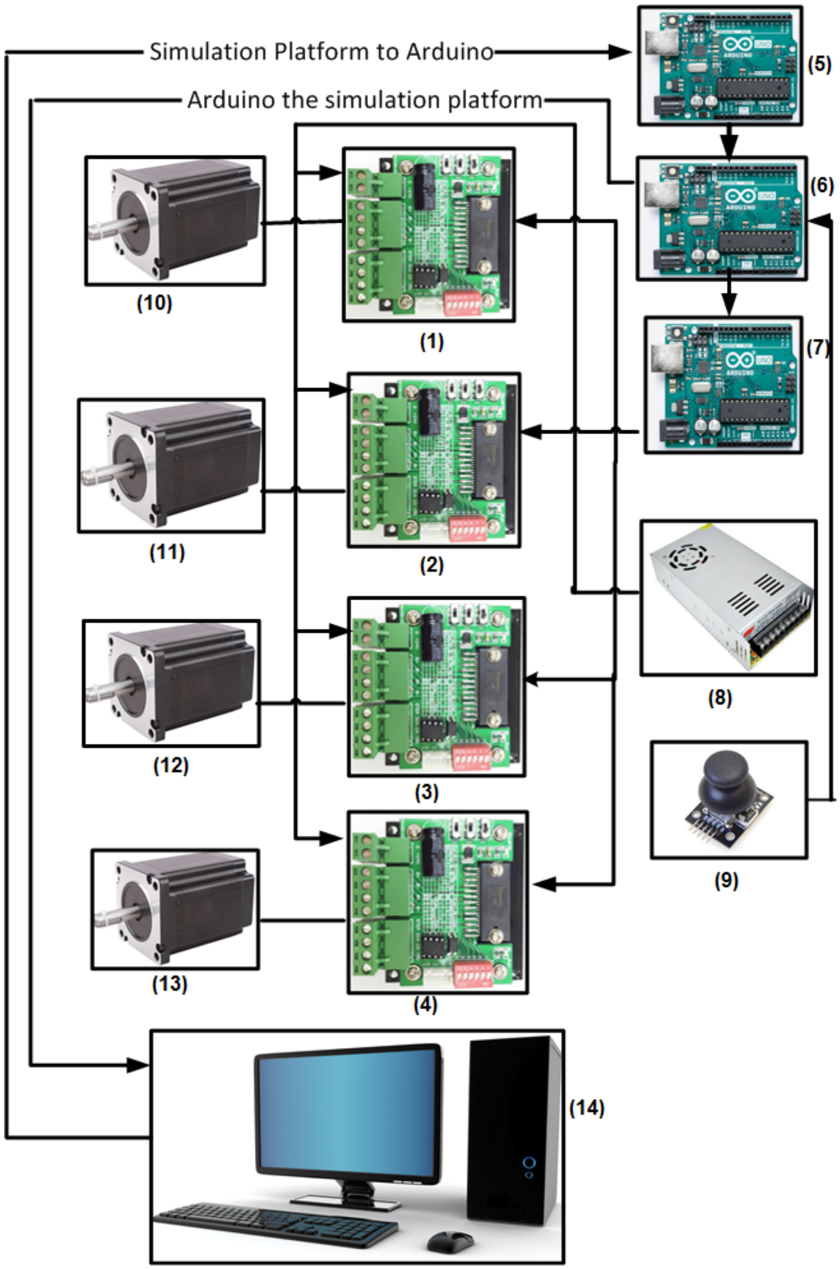

Fig. 7.1 The schematic diagram of the Hardware-in-the-Loop platform. (1,2,3,4)- the stepper motor drivers, (10,11,12,13)- motors for the valves k_{sa}, k_{sb}, K_{at} and K_{bt} respectively, (s)- receiver from the PC, (6)- algorithm controller, and (7)- drivers controller.

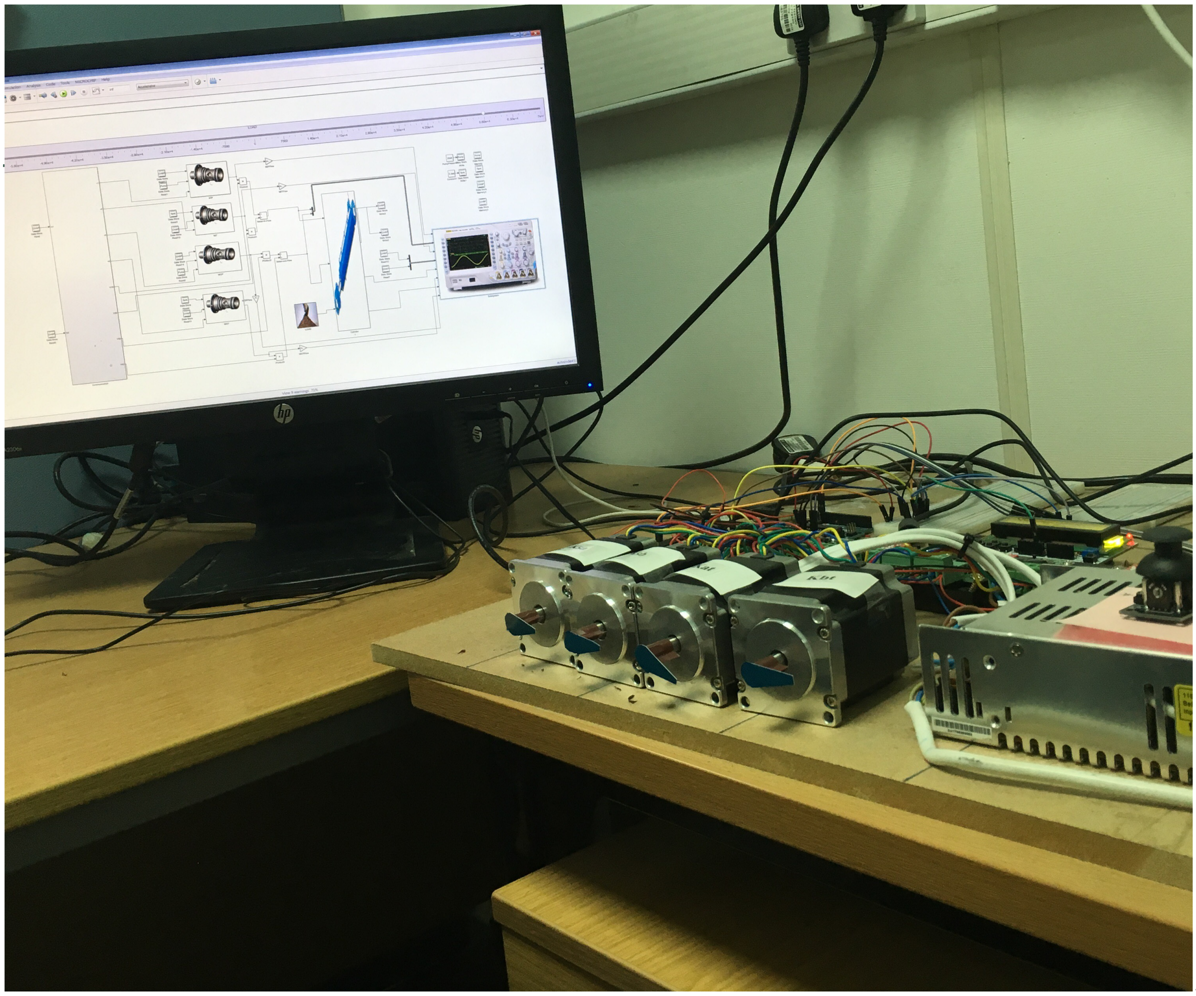

Fig. 7.2 The simulation part of the Hardware-in-the-loop platform

7.3 Testing

This testing procedure is to change the applied variable load in the simulation part, thus the pressures inside the cylinder chambers are changed. The pressure values are transmitted via serial communication into the first controller and displayed on the LCD screen. They are also used by the second Arduino controller to rotate the stepper motors. The stepper motors rotation are the result of the test. These rotation values are sent to the simulated system at the same time to take action on the flow.

This simple data transmission represents a closed circle of communication between the hardware and the simulation. The test is repeated for the five modes, and they are explained in the following subsections.

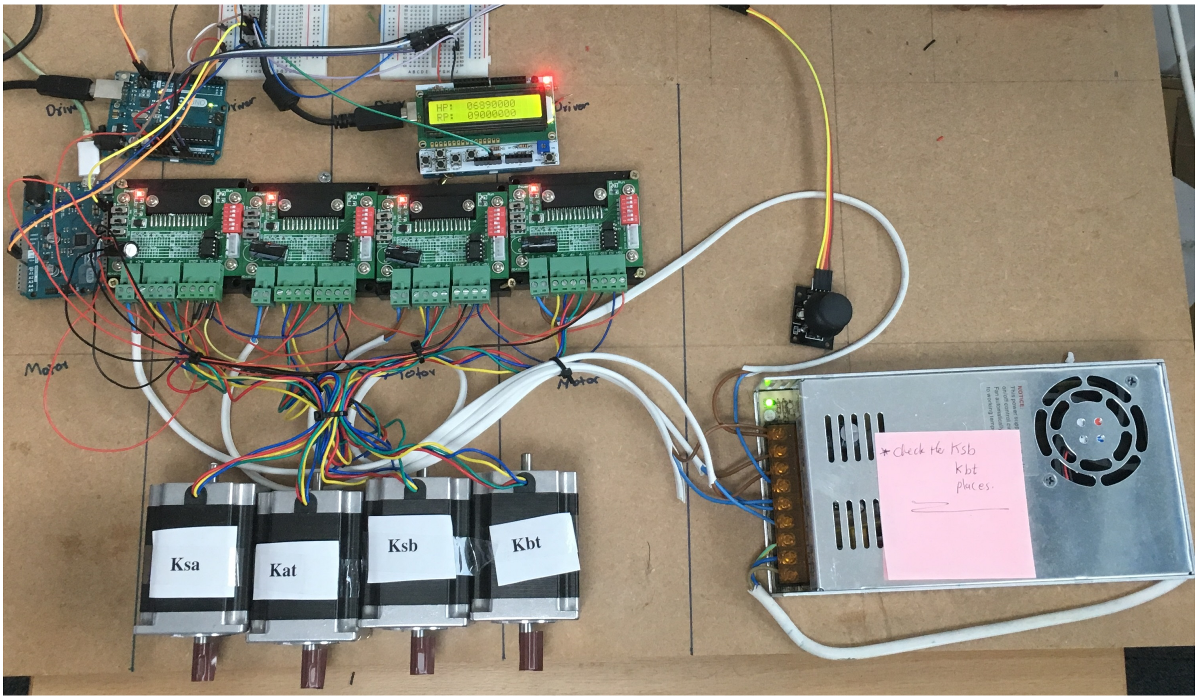

Fig. 7.3 The hardware parts of the Hardware-in-the-Loop platform

7.3.1 Power Extension and Low Side Regeneration Retraction Modes

For the power extension mode, the variable applied force was 50 KN and the transmitted pressures at the start of the test were about 10 MPa in the head chamber and 1.7 MPa in the rod chamber, as illustrated in Figure 7.4. Then, the joystick is moved into the positive direction to produce a power extension mode as shown in Figure 7.5. In this mode, the K_{sa} and K_{bt} have to move as shown in Figure 7.5. The test results are shown in Figure 7.6.

At the same pressure levels, the joystick is moved backwards, and directly the system detected the signal to activate the low side regeneration retraction mode (Figure 7.7). In this test, two valves K_{at} and K_{bt} are activated as illustrated in Figure 7.7. The test results are shown in Figure 7.8.

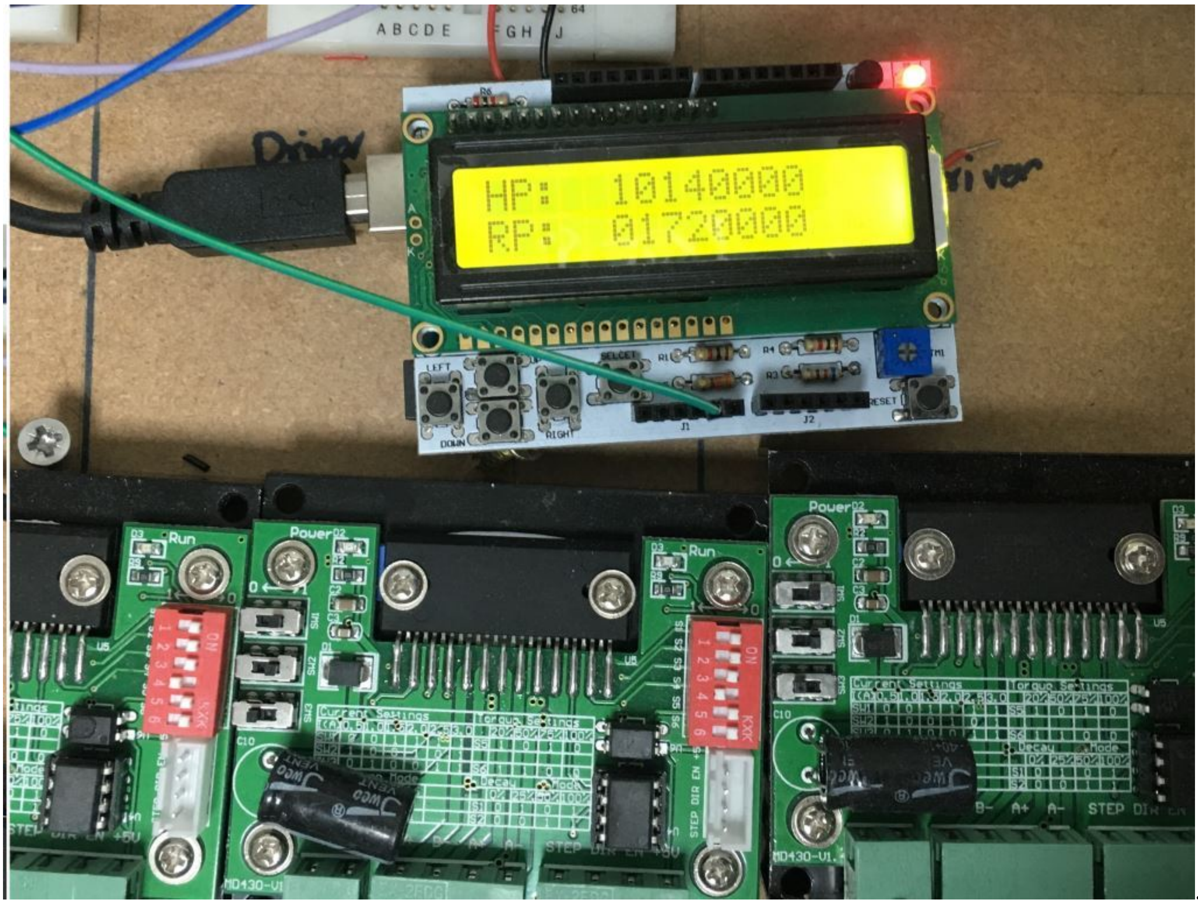

Fig. 7.4 The pressure for the power extension and the low side regeneration retraction modes.

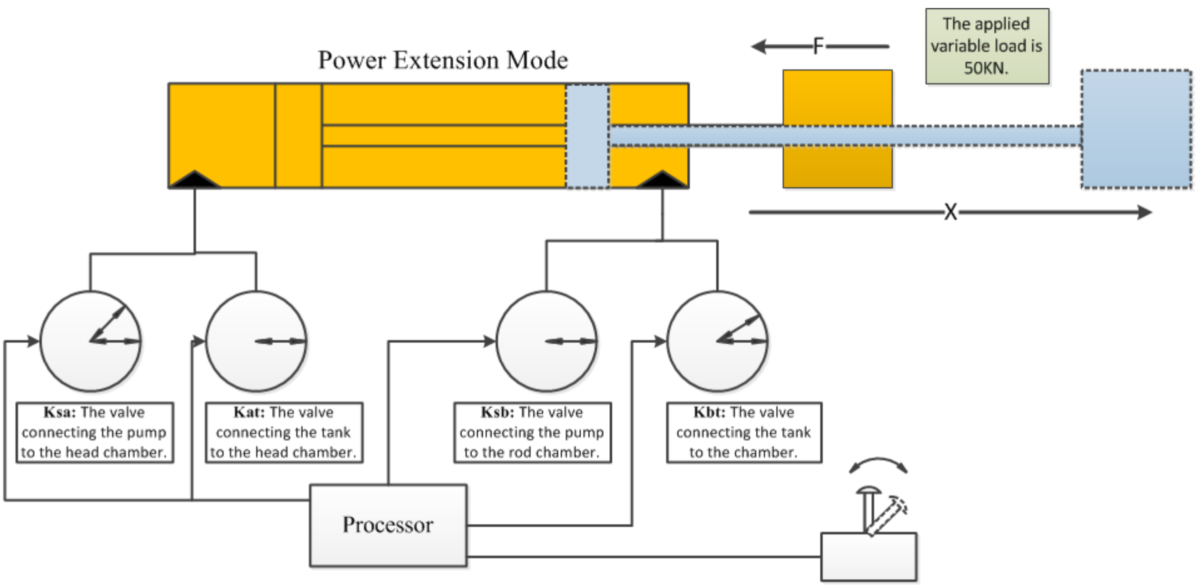

Fig. 7.5 The testing procedure for the power extension mode.

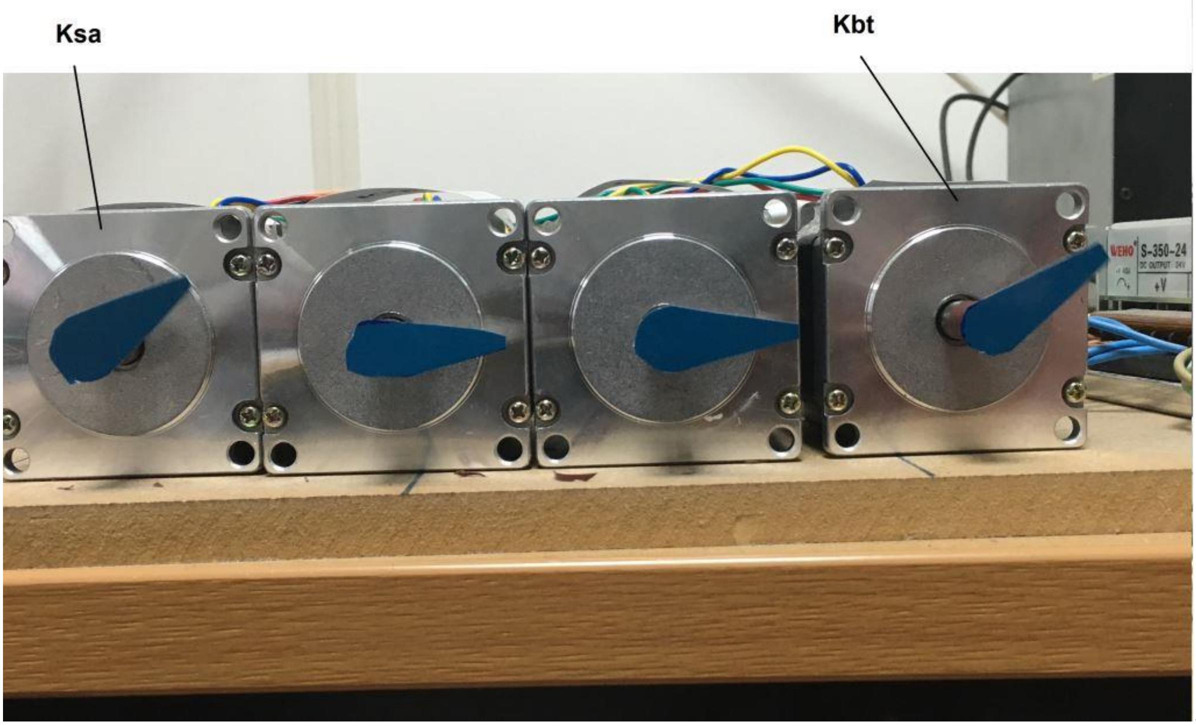

Fig. 7.6 The K_{sa} and K_{at} valves rotation in the power extension mode.

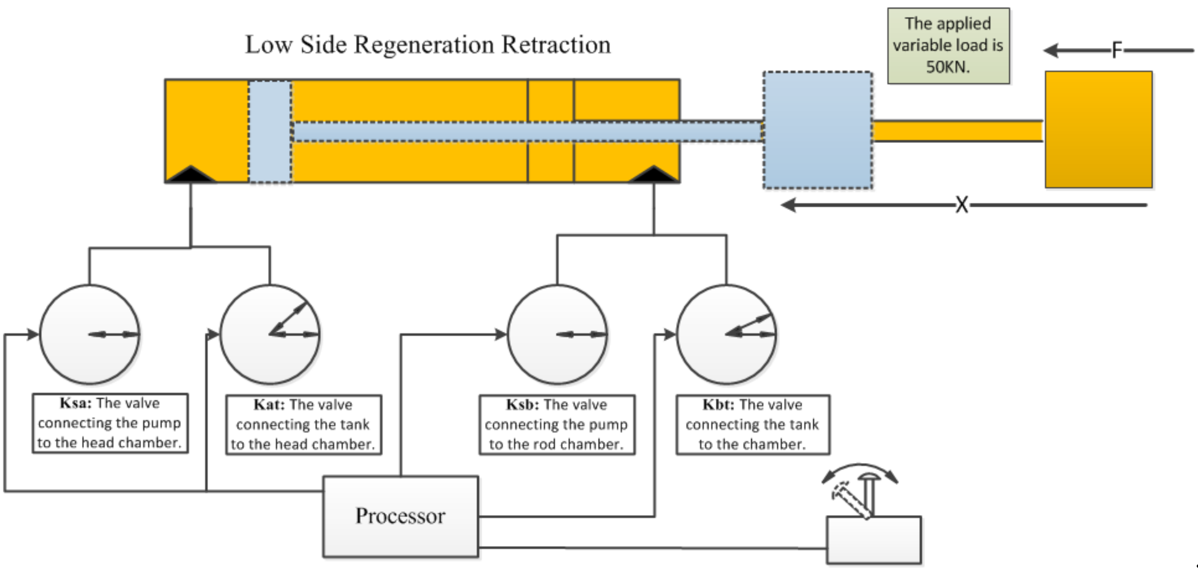

Fig. 7.7 The testing procedure for the low side regeneration retraction mode.

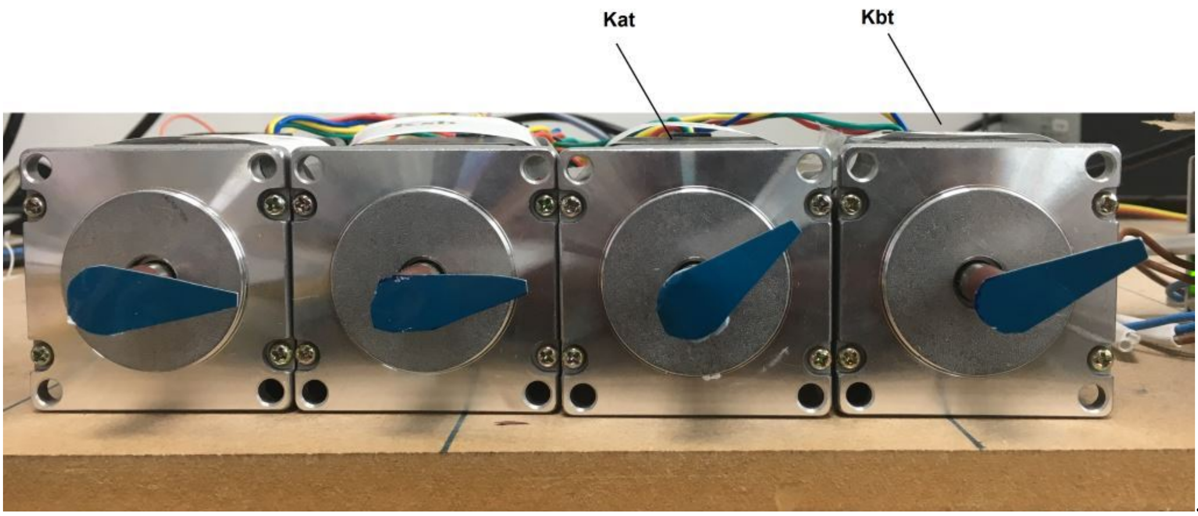

Fig. 7.8 The K_{at} and K_{bt} valves rotation in the low side regeneration retraction.

7.3.2 Power Retraction and Low Side Regeneration Extension Modes

For the power retraction mode, the variable applied force was -50 KN and the transmitted pressures at the start of the test were about 8.2 MPa in the rod chamber and 5.5 MPa in the head chamber, as illustrated in Figure 7.9. Then, the joystick was moved into the negative direction to produce a power retraction mode (Figure 7.10). In this mode, K_{sb} and K_{at} have to move as shown in Figure 7.10. The test result is shown in Figure 7.11.

At the same pressure levels, the joystick is moved forewords, and directly the system detected the signal to activate the low side regeneration extension mode (Figure 7.12). The two valves K_{at} and K_{bt} are activated as illustrated in Figure 7.12. The test results are indicated in Figure 7.13.

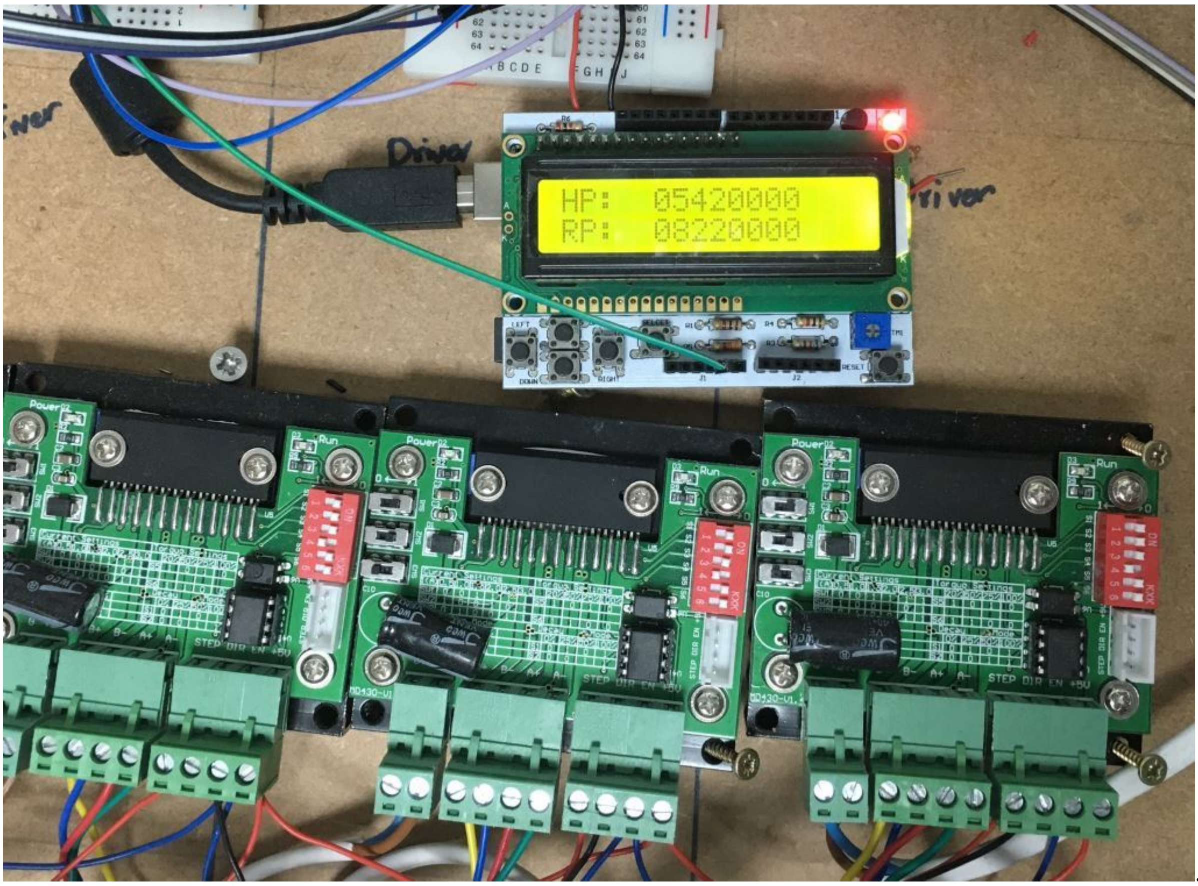

Fig. 7.9 The cylinder pressures for the power retraction and the low side regeneration extension modes

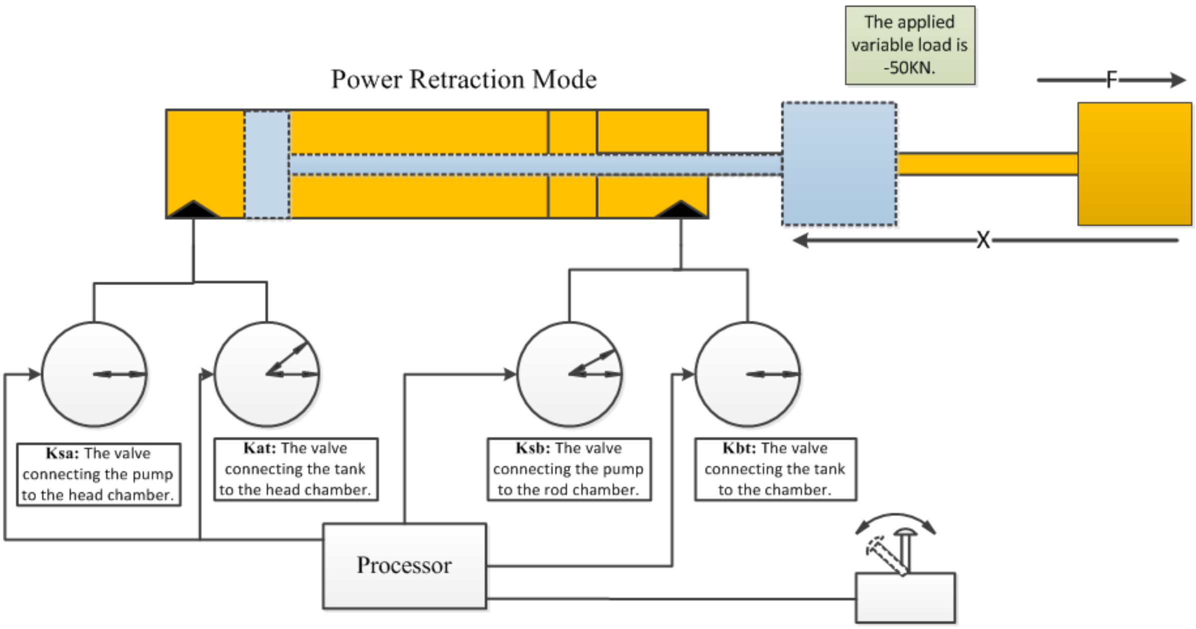

Fig. 7.10 The testing procedure for the power retraction mode.

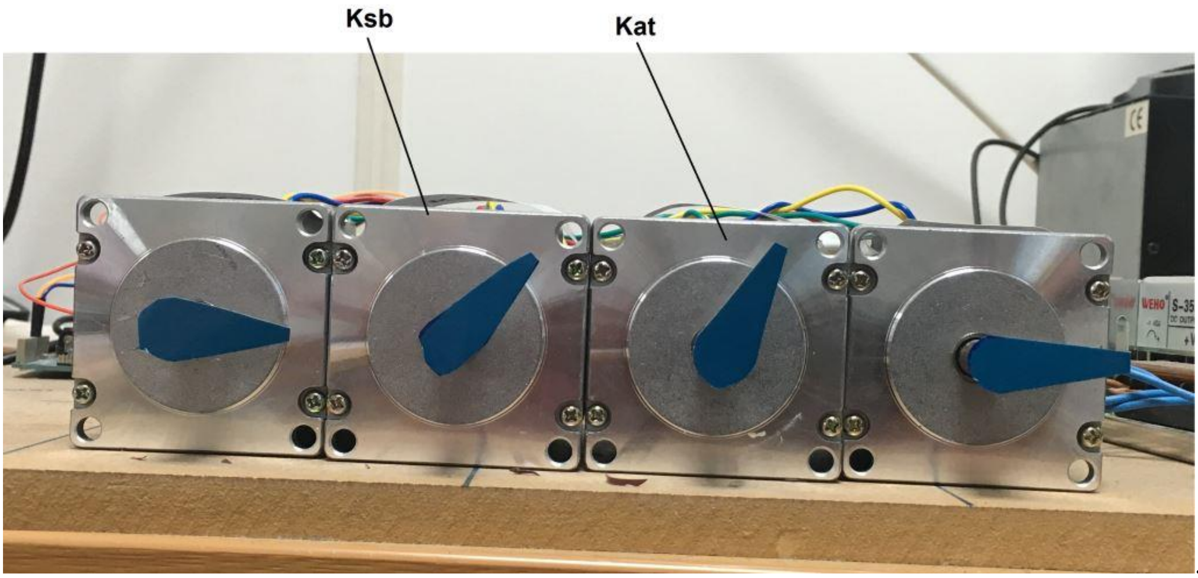

Fig. 7.11 The K_{sb} and K_{at} valves rotation in the power retraction mode.

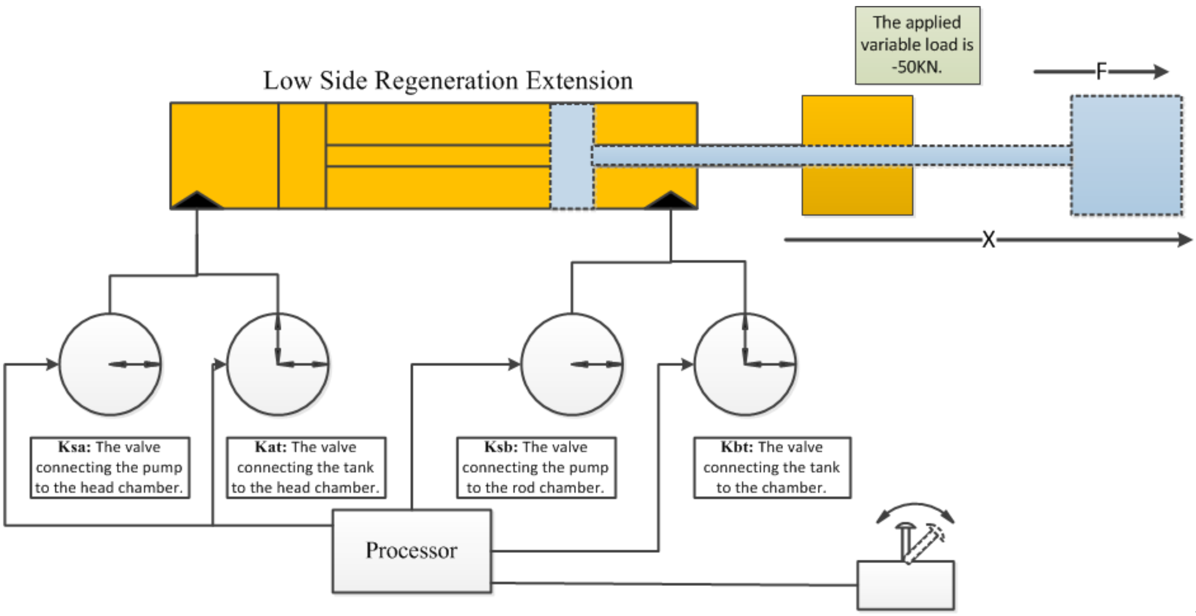

Fig. 7.12 The testing procedure for the low side regeneration extension mode.

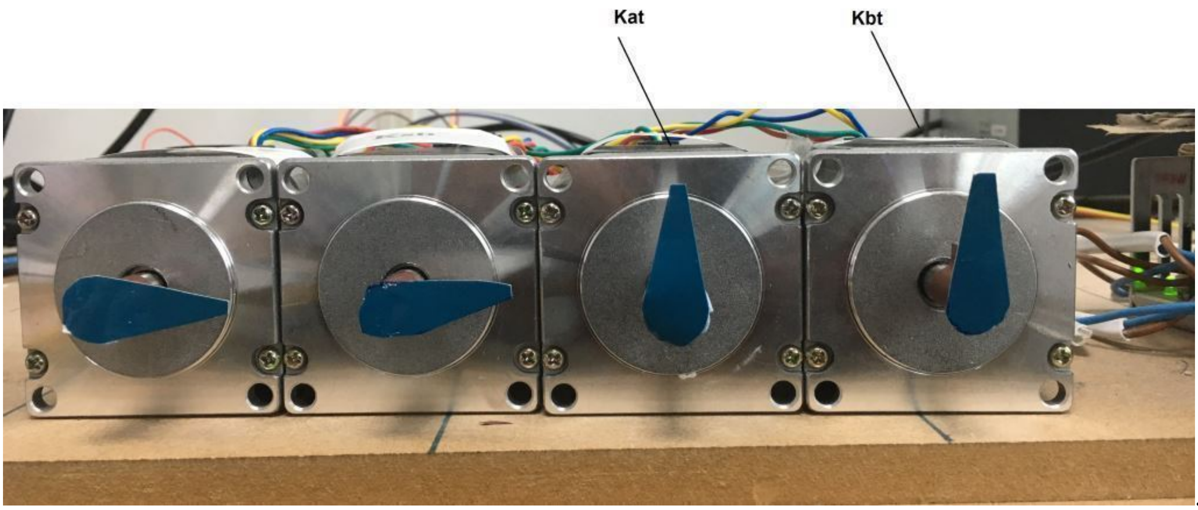

Fig. 7.13 The K_{bt} and K_{at} valves rotation in the low side regeneration extension.

7.3.3 High Side Regeneration Extension

For the high side regeneration extension mode, the variable applied force was 0 KN and the transmitted pressures at the start of the test were about 7.7 MPa in the head chamber and 5 MPa in the rod chamber, as illustrated in Figure 7.14. Then, the joystick is moved into the positive direction to produce a power retraction mode (Figure 7.15). In this mode, K_{sb} and K_{sa} have to move as shown in Figure 7.15. The test result is shown in Figure 7.16.

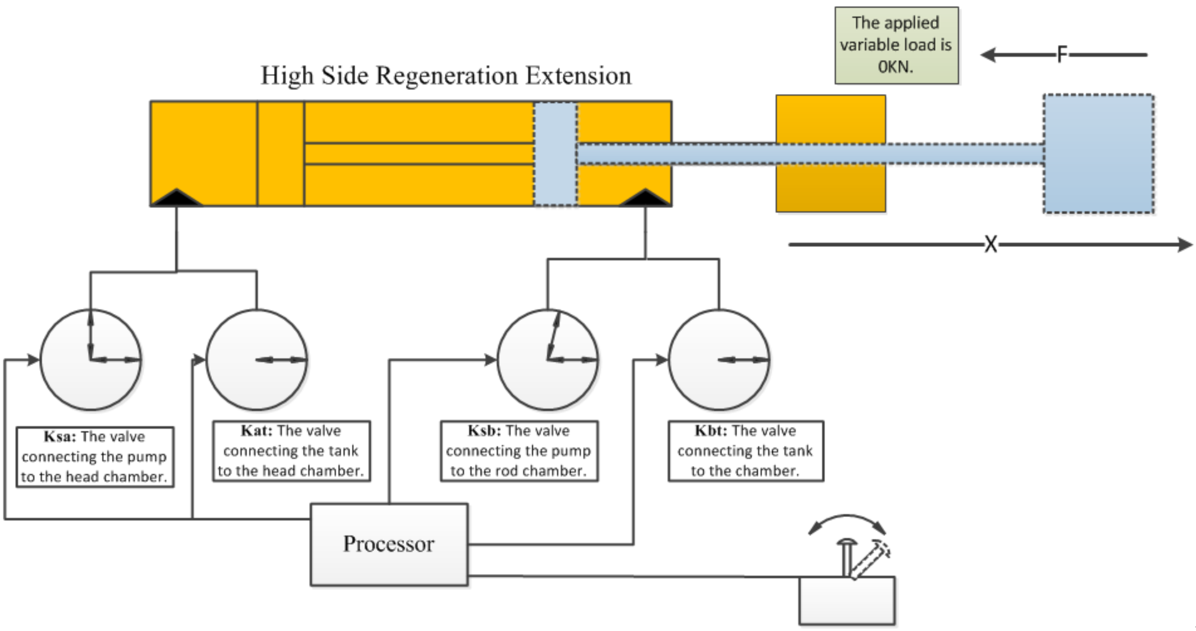

Fig. 7.15 The testing procedure for the high side regeneration extension mode.

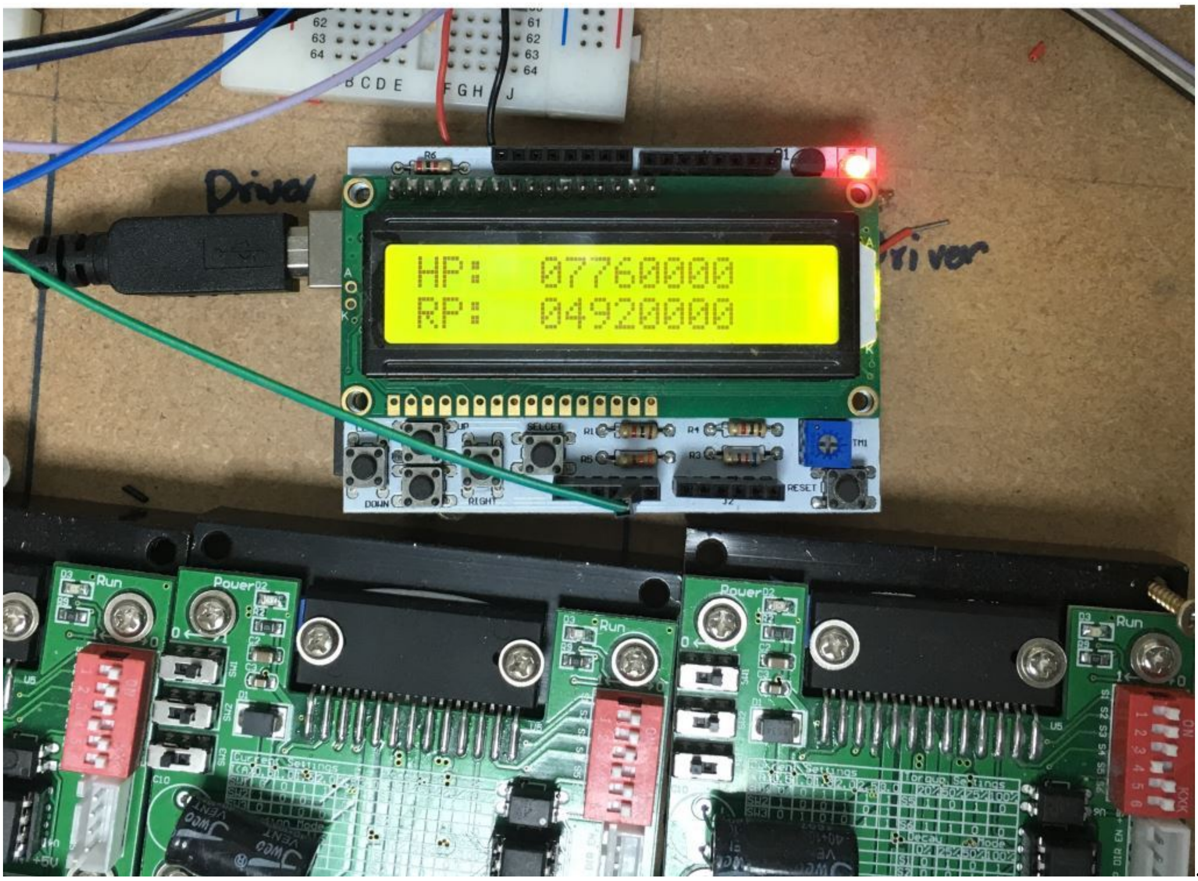

Fig. 7.14 The cylinder pressures for the high side regeneration extension mode

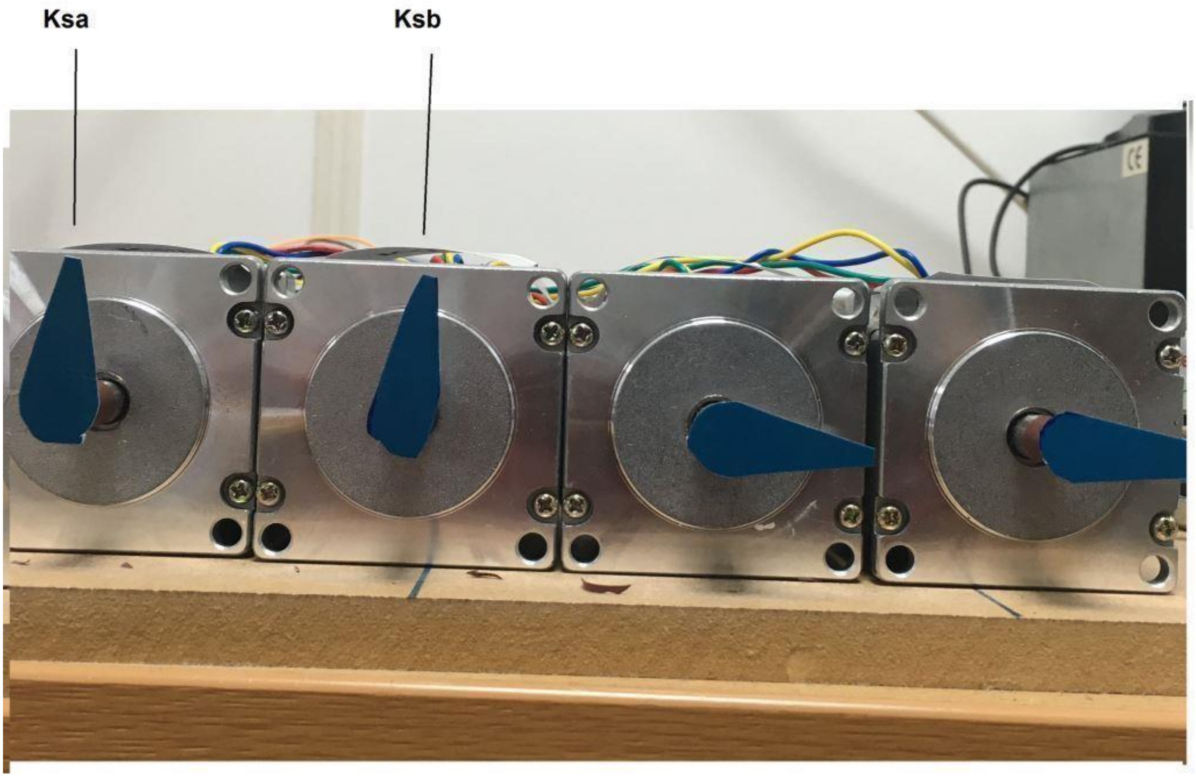

Fig. 7.16 The K_{sa} and K_{sb} valves rotation in the high side regeneration extension mode.

7.4 Results Analysis

This section contains an analysis of the hardware in the loop results, especially the control algorithm implementation. The analysis is performed by measuring the stepper motor angles using the angle finder and comparing them with the calculated values using the mathematical model equations in Chapter 4. By implementing the pressure values from each mode in (7.1) into the conductance Equations 4.14, 4.17, 4.20, 4.23, and 4.26 in Chapter 4, the measured angles were shown to be enclose agreement with their calculated values.

Table 7.1 The results of the HIL test for the IM five operation modes

Operation Mode	Head Pressure	Rod Pressure	Meter-in Angle	Meter-out angle
PE	10 MPa	1.7 MPa	$Ksa = 39.6°$	$Kbt = 34.2°$
LSRR	10 MPa	1.7 MPa	$Kat = 43.2°$	$Kbt = 37.8°$
PR	5.5 MPa	8.2 MPa	$Ksb = 32.4°$	$Kat = 37.8°$
LSRE	5.5 MPa	8.2 MPa	$Kat = 90°$	$Kbt = 90°$
HSRE	7.7 MPa	5 MPa	$Ksa = 90°$	$Ksb = 86.4°$

7.5 Summary

In this chapter, a simple qualitative Hardware-in-the-Test has been performed. The hardware platform was developed by synthesizing stepper motors, controllers and a simulation PC. In the test, the hardware platform receives a command from the driver using the joystick connected to the main controller. It also obtains pressures values from the simulated platform for the main controller which contains the control algorithm. The analysis was preformed for the five operation modes of the IM system, and showed stepper motor rotations based on the selected operation mode.

Chapter 8

Conclusions and Discussions

8.1 Introduction

The research is an investigation for a new hydromechatronics system that aims to improve the performance of hydraulic mobile machines. The proposed system obeys the rules of the well-known hydraulic driving technique Independent Metering. The system in question is termed Micro-Independent Metering (MIM), and this is due to the actuating technique used for the main control component of the system, which is a stepped rotary valve. The valve has been developed using a rotary orifice, that was developed for high flow rate applications in another project at Bournemouth University.

8.2 Discussion

Mobile hydraulic machines are very useful and contribute to the quality of life through their use such as infrastructure, agriculture, and industrial applications. However, these machines still have high energy losses and poor controllability. For example, non-linearity which is one of the main disadvantages of a hydraulic fluid affects the hydraulic actuator performance. For more energy saving and controllability, a separate meter-in and meter-out structure can be used. It allows energy to be regenerated and advanced control techniques to be implemented. The separation of cylinder inlet (meter-in) and outlet (meter-out) is called Independent Metering. A poppet, or valvistor valve was developed to be inserted in the IM structure, but it has not been used widely in industry due to its low stability and fluid accuracy. Therefore, the research conducted here is to investigate replacing the poppet valve by a new stepped rotary type valve.

Similar to any hydraulic system, mobile machines use valves to control the fluid flow rate and direction. According to the literature, different hydraulic valves were developed for use in hydraulic applications. The common types are the spool and poppet valves. The spool valve is widely used in place of one valve for every cylinder. This type increases energy losses due to the connection between the two-meter sides of the cylinder, which are the meter-in and the meter-out. Also, only a single cylinder chamber pressure can be controlled at the same time. Using spool valves for IM applications are more expensive and can still suffer from energy losses.

A poppet valve has been used to implement independent metering. It successfully led to saving energy, but the valve performance was highly affected by the fluid which decreased it's use in mobile hydraulic applications. This valve construction relies on the fluid as a part of the control system, which limits the valve controllability due to the fluid disturbances. However, Bournemouth University developed a rotary orifice to control hydraulic flow rate. The development of a valve using an orifice instead of the poppet led to a new IM configuration. Using the stepper motor in this IM configuration increases the system controllability.

8.3 Conclusions

In this study, a stepped rotary valve which had been developed developed at Bournemouth University was used instead of poppet or spool types, to create a new independent metering configuration. Due to the different construction of this valve, a novel control system has been implemented to meet the IM rules. The control system is considered as hydromechatronics because it is an integration of different aspects ranging from hydraulic, mechanical, electrical, software, and signal processing. Due to the system complexity, the development method pursued was Model-Based Design. The main steps of the selected procedure are determining the system requirements, modelling and simulation, model-in-the-loop simulation, software-in-the-loop simulation, and hardware-in-the-loop test. For this method of implementation, nonlinear and linear models of the valve have been developed. Also, the dynamic performance of the valve, including the multi-step response and root locus analysis have been studied. A model of a hydraulic cylinder was attached to four stepped rotary valve models to form a micro-independent metering simulation platform. This platform includes the model of the control algorithm which has been developed for the system. Moreover, a hardware synthesis containing four stepper motors with their drivers, three Arduino controllers, power supply, and interfacing components were developed.

Modelling and simulation of the valve have been achieved during this research. This includes a stepper motor model and the rotary orifice model. Different activation techniques for the stepper motor was performed and the most suitable for the system was formed to be micro-stepping. This technique reduces the orifice friction torques, which leads to the use of different rotation frequencies, and reduces the fluid pulsation effect. Parts of the model were validated and based on the results, some parameters in the model were modified, especially the Coulomb and static frictions. Then a performance analysis of the valve using the root locus technique was investigated to show the liability and limitations of the valve controllability. The root locus method required model linearization which was developed using a Taylor series expansion. According to the analysis, the stability criteria of the valve were defined for different parameters such as pressure drop, friction, stiffness, and damping coefficient.

A control algorithm was developed based on independent metering mathematical analysis which included a novel procedure called Close Value Detection. The algorithm starts by reading measurements and defining suitable operation modes, which have to be one of the five operating modes that are used to implement the IM technique. The modes are power extension, power retraction, low side regeneration extension, low side regeneration retraction, and high side regeneration extension. The mode selected by the algorithm produces the required conductance for the valves. The Close Value Detection technique was used to determine the valve opening degree which would produce the required flow conductance. Before sending commands to the drivers, anti-cavitation technique was activated because the algorithm cannot be implemented if hydraulic cavitation appears.

A Stateflow model was designed for the algorithm, and it was used to build the software-in-the-loop platform. The five operation modes were simulated and the algorithm produced different valve opening degrees according to the user requirements. Part of the research is to compare performance between the traditional IM system and the new configuration. Using models of the traditional IM system based on the Valvistor type valve, and the new MIM system, the MIM system showed the ability to reject the effect of hydraulic fluid disturbances on the control valves. Rejecting these disturbances improves hydraulic actuator velocity performance. In the valvistor valve, the fluid is considered as a part of the control system which transfers the fluid non-linearity into the cylinder performance.

Finally, to evaluate the system performance, a hardware platform containing four stepper motors, drivers, interfacing, controllers, and power supply were synthesized and connected to the simulated parts to form a simple hardware-in-the-loop test. The test aimed to perform a qualitative study of system performance. The platform showed the ability to work in the five operating modes and the change between them was possible. Also, it showed the ability to interact with the driver inputs and select suitable valve opening degrees.

8.4 Novelty

The novelty of this research includes the following:

- The friction torque of the rotary orifice in the valve is affected by the full step driving technique. The full step produces high change of speed after each rest point, and this leads to high ripples of the friction torque. However, the Micro-step technique reduces this effect and produces a smoother operation. Hence, it was selected to be the driving technique for the valve.

- Root locus analysis of the new stepped rotary flow control valve investigated the effect of many parameters on the valve performance. It also demonstrated that the current valve design remains stable throughout the entire range of pressure drop up to 35 MPa.

- Anew algorithm including the proposed Close Value Detection technique was developed, investigated, and tested for the MIM system. This algorithm depends on finite number of possible positions using a stepper motor.

- The MIM system is able to manage the effect of fluid disturbances on the hydraulic cylinder velocity compared to traditional IM systems. This results in decreasing the errors in the produced velocity.

8.5 Recommendations for Further Work

Based on this investigation, a new independent metering configuration can be used in mobile hydraulic machinery. The configuration is also able to control the hydraulic actuator velocity and is not highly affected by fluid disturbances. It is more efficient due to implementing energy regeneration or recovery techniques. Further research is required in many aspects of the system. Suggestions for future work are:

- Valve Performance Analysis.

  Performance of the valve has to be considered in more detail in order to develop an accurate control system. In this research, a mathematical model was developed based on analysis and this relied on previous studies. More analysis can be performed on the transient flow torque model, the friction torque model, and the steady-state torque model. It was noticed during experimentation that there is a correlation between the pressure drop and the friction torque. This correlation was only tested up to 1 MPa, so testing for higher pressure drops is important. Moreover, the performance of the parameters that were evaluated using root locus, which are damping coefficient, stiffness coefficient, and friction coefficients, can be practically evaluated.

A step response analysis is necessary to study performance. Based on the valve model, an initial multi-step response analysis was performed. The outcome of this analysis was that micro stepping performance which was more suitable compared to the full step technique. So, practical testing and a comparative study have to be performed in order to determine the valve rotating velocity and supply power limitations.

Other parameters which have to be considered in the future researches are the valve bandwidth and the dead-band. The bandwidth was initially assumed to be the same as the stepper motor bandwidth and this requires further testing and analysis. The valve flow dead-band is considered to be an important parameter in flow control and it should be evaluated and considered during the system improvement process.

- Software-in-Loop-Simulation. The SIL is an important stage of mechatronics systems design. For this research, further developments on the simulation have to be considered. The model for the valve used in the simulation platform was a second-order transfer function for the stepper motor, connected to a look-up table, representing the flow. This model needs to be practically evaluated. The model used for the hydraulic cylinder was obtained from previous research, so a more precise model is required. The applied used variable value with in the assumed range, this can be improved by applying a model of a real operation load cycle.

  The energy regeneration used in IM requires a direct connection between the two valves operating in the regeneration modes. For example, in the high side regeneration extension, the rod chamber meter-in valve and the head chamber meter-in valve have to be connected on the same fluid line in order to perform fluid recirculation. However, in the model, it cannot be accomplished, so the simulated fluid was just from the pump to the cylinder.

  The algorithm was developed based on mathematical analysis by other researchers, and one of the points to be considered for further research is the relationship between the two valve used in every mode. It was selected to be $R^{3/4}$ which is the same value used in the previous researches. This relationship was selected because of the poppet valve controllability problems such as fluid flow force disturbances, but in this design, the valve controllability is not affected by fluid disturbances so a study should be performed to find the possible relationship between the two valves in the operation modes.

- Hardware-in-the-Loop-Test.

  It was developed in this research using hardware containing simple drivers and stepper motors, controllers, power supplies and interfacing components. This platform was directly connected to the simulation on the PC via serial communication. It aimed to qualitatively study the performance of the system. This test lacks a target real-time simulation PC due to research resource limitations. The target PC has many interfacing techniques, and it's able to work in fixed time step solver. It is important to study the system quantitatively and precisely define the required developments.

- Sensor-less motor activation technique. This is a very advanced driving technique that can be used instead of a position sensor. The sensor-less technique is based on measuring the current inside the motor coils during operation.

- Field Testing.

  The last suggested future work is test in the field where different applications can be used ranging from back-loader, excavator or even industrial robotics. Moreover, to study new possible applications is important future work. As some of the traditional independent metering system shortcomings has been tackled in this research such as fluid disturbances, new applications for this design can be studied.

Finally, as this research is a study of a novel system, the developments can be investigated from different points, hydraulic, electronic, mechanical, electrical, and control.

References

Aardema, J. A. and Koehler, D. W. (1999). System and method for controlling an independent metering valve. US Patent 5,947,140.

Abuowda, K., Okhotnikov, I., Noroozi, S., and Godfrey, P. (2018). Friction analysis and modelling of a novel stepped rotary flow control valve. In *15th International Conference on Condition Monitoring and Machinery Failure Prevention Technologies, CM 2018/MFPT 2018*, pages 117 – 128.

Acarnley, P. P. (2002). *Stepping motors: a guide to theory and practice*. Number 63. Stevenage: Institute of Electrical Engineers.

Acuña-Bravo, W., Canuto, E., Agostani, M., and Bonadei, M. (2017). Proportional electro-hydraulic valves: An embedded model control solution. *Control Engineering Practice*, 62:22–35.

Ahn, K. K., Nam, D. N. C., and Jin, M. (2014). Adaptive backstepping control of an electrohydraulic actuator. *IEEE/ASME transactions on mechatronics*, 19(3):987–995.

Alkam, S. N. (2014). *New Methods in Modeling and Control of Modern Electrohydraulic Systems*. PhD thesis.

Anderson, R. T. and Li, P. Y. (2002). Mathematical modeling of a two spool flow control servovalve using a pressure control pilot. *Journal of dynamic systems, measurement, and control*, 124(3):420–427.

Axin, M. (2013). *Fluid power systems for mobile applications: With a focus on energy efficiency and dynamic characteristics*. PhD thesis, Linköping University Electronic Press.

Axin, M. (2015). *Mobile working hydraulic system dynamics*, volume 1697. Linköping University Electronic Press.

Bacic, M. (2005). On hardware-in-the-loop simulation. In *Decision and Control, 2005 and 2005 European Control Conference. CDC-ECC'05. 44th IEEE Conference on*, pages 3194–3198. IEEE.

Bellini, A., Concari, C., Franceschini, G., and Toscani, A. (2007). Mixed-mode pwm for high-performance stepping motors. *IEEE transactions on industrial electronics*, 54(6):3167–3177.

Bendjedia, M., Ait-Amirat, Y., Walther, B., and Berthon, A. (2007). Sensorless control of hybrid stepper motor. In *Power Electronics and Applications, 2007 European Conference on*, pages 1–10. IEEE.

Bian, M., Shi, J., and Wang, S. (2011). Fta-based fault diagnose expert system for hydraulic equipments. In *Proceedings of 2011 International Conference on Fluid Power and Mechatronics*, pages 959–963. IEEE.

Bisztray-Balku, S. (1995). Tribology of hydraulic seals for alternating motion. *Periodica Polytechnica. Engineering. Mechanical Engineering*, 39(3-4):225.

Borghi, M., Zardin, B., Pintore, F., and Belluzzi, F. (2014). Energy savings in the hydraulic circuit of agricultural tractors. *Energy Procedia*, 45:352–361.

Britain, G. (2006). *Defence Technology Strategy for the demands of the 21st century*. Ministry of Defence.

BUCHER (2016). 2/2 cartridge seat valve, size 5. https://www.bucherhydraulics.com/30971/start/start.aspx, access date (02/12/2019).

Budynas, R. G., Nisbett, J. K., et al. (2008). *Shigley's mechanical engineering design*, volume 8. New York: McGraw-Hill.

Campanini, F., Bianchi, R., Vacca, A., and Casoli, P. (2017). Optimized control for an independent metering valve with integrated diagnostic features. In *ASME/BATH 2017 Symposium on Fluid Power and Motion Control*, pages V001T01A051–V001T01A051. American Society of Mechanical Engineers.

Canudas, C. (1995). A new model for control of systems with friction. *IEEE Trans. Automatic Control*, 40(3):419–425.

Chen, G., Wang, J., Wang, S., Zhao, J., and Shen, W. (2017). Indirect adaptive robust dynamic surface control in separate meter-in and separate meter-out control system. *Nonlinear Dynamics*, 90(2):951–970.

Chen, G., Wang, J., Wang, S., Zhao, J., and Shen, W. (2018). Energy saving control in separate meter in and separate meter out control system. *Control Engineering Practice*, 72:138–150.

Chen, X., Salem, M., Das, T., and Chen, X. (2008). Real time software-in-the-loop simulation for control performance validation. *Simulation*, 84(8-9):457–471.

Cheng, M., Zhang, J., Xu, B., Ding, R., and Wei, J. (2018). Decoupling compensation for damping improvement of the electrohydraulic control system with multiple actuators. *IEEE/ASME Transactions on Mechatronics*, 23(3):1383–1392.

Choi, K., Seo, J., Nam, Y., and Kim, K. U. (2015). Energy-saving in excavators with application of independent metering valve. *Journal of Mechanical Science and Technology*, 29(1):387–395.

Corey, Q. (2019). Incova designs intelligent valve-control system for a 20-ton excavator. https://uk.mathworks.com/company/user_stories/incova-designs-intelligent-valve-control-system-for-a-20-ton-excavator.html access date (02/12/2019).

Coskun, G., Kolcuoglu, T., Dogramacı, T., Turkmen, A. C., Celik, C., and Soyhan, H. S. (2017). Analysis of a priority flow control valve with hydraulic system simulation model. *Journal of the Brazilian Society of Mechanical Sciences and Engineering*, 39(5):1597–1605.

Crosser, J. A. (1992). Hydraulic circuit and control system therefor. US Patent 5,138,838.

Davliakos, I., Roditis, I., Lika, K., Breki, C.-M., and Papadopoulos, E. (2018). Design, development, and control of a tough electrohydraulic hexapod robot for subsea operations. *Advanced Robotics*, 32(9):477–499.

de Brun Mangs, J. and Tillquist, M. (2018). Evaluation of a programmable hydraulic valve for drill rig applications.

DeBoer, C. C. and Yao, B. (2001). Velocity control of hydraulic cylinders with only pressure feedback. In *ASME International Mechanical Engineering Congress and Exposition*, pages 1–9. ASME New York, USA.

Dell, T. W., editor (2017). *Hydraulic systems for mobile equipment*, chapter Load sensing pressure compensating (LSPC) hydraulic system.

Dell'Amico, A., Carlsson, M., Norlin, E., and Sethson, M. (2013). Investigation of a digital hydraulic actuation system on an excavator arm. In *13th Scandinavian International Conference on Fluid Power; June 3-5; 2013; Linköping; Sweden*, number 092, pages 505–511. Linköping University Electronic Press.

Dengler, P., Geimer, M., Baum, H., Schuster, G., Wessing, C., et al. (2012). Efficiency improvement of a constant pressure system using an intermediate pressure line. In *Proceedings 8th International Fluid Power Conference, Dresden*, volume 1, pages 577–578.

Dengler, P., Groh, J., and Geimer, M. (2011). Valve control concepts in a constant pressure system with an intermediate pressure line. In *21st International Conference on Hydraulics and Pneumatics*.

Ding, R., Xu, B., Zhang, J., and Cheng, M. (2016). Bumpless mode switch of independent metering fluid power system for mobile machinery. *Automation in Construction*, 68:52–64.

Ding, R., Xu, B., Zhang, J., and Cheng, M. (2017). Self-tuning pressure-feedback control by pole placement for vibration reduction of excavator with independent metering fluid power system. *Mechanical Systems and Signal Processing*, 92:86–106.

Ding, R., Zhang, J., and Xu, B. (2018a). Advanced energy management of a novel independent metering meter-out control system: A case study of an excavator. *IEEE Access*, 6:45782–45795.

Ding, R., Zhang, J., Xu, B., and Cheng, M. (2018b). Programmable hydraulic control technique in construction machinery: Status, challenges and countermeasures. *Automation in Construction*, 95:172–192.

Ding, R., Zhang, J., Xu, B., Cheng, M., and Pan, M. (2019). Energy efficiency improvement of heavy-load mobile hydraulic manipulator with electronically tunable operating modes. *Energy Conversion and Management*, 188:447 – 461.

EATON (2010). Ultorincs ZTS16 Twin Spool Valve. https://www.eaton.com/us/en-us.html, access date (02/12/2019).

EATON (2016a). Cma200 advanced independent-metering mobile valve. https://www.eaton.com/us/en-us.html, access date (02/12/2019).

EATON (2016b). Cma90 advanced independent-metering mobile valve. https://www.eaton.com/us/en-us.html, access date (02/12/2019).

EATON (2019). Epv10 - proportional valve. https://www.eaton.com/us/en-us.html, access date (02/12/2019).

Edge, K. (1997). The control of fluid power systems-responding to the challenges. *Proceedings of the Institution of Mechanical Engineers, Part I: Journal of Systems and Control Engineering*, 211(2):91–110.

Eriksson, B. (2007). *Control strategy for energy efficient fluid power actuators: Utilizing individual metering*. PhD thesis, Linköping University Electronic Press.

Eriksson, B. (2010). *Mobile fluid power systems design: with a focus on energy efficiency*. PhD thesis, Linköping University Electronic Press.

Eriksson, B. and Palmberg, J.-O. (2011). Individual metering fluid power systems: challenges and opportunities. *Proceedings of the institution of mechanical engineers, part I: journal of systems and control engineering*, 225(2):196–211.

Fales, R. (2006). Stability and performance analysis of a metering poppet valve. *International Journal of Fluid Power*, 7(2):11–17.

Gaan, D. R., Kumar, M., and Sudhakar, S. (2018). Real-time precise position tracking with stepper motor using frequency modulation based microstepping. *IEEE Transactions on Industry Applications*, 54(1):693–701.

Ge, L., Dong, Z., Huang, W., Quan, L., Yang, J., and Li, W. (2015). Research on the performance of hydraulic excavator with pump and valve combined separate meter in and meter out circuits. In *2015 International Conference on Fluid Power and Mechatronics (FPM)*, pages 37–41. IEEE.

Ge, L., Quan, L., Zhang, X., Zhao, B., and Yang, J. (2017). Efficiency improvement and evaluation of electric hydraulic excavator with speed and displacement variable pump. *Energy conversion and management*, 150:62–71.

Gerhart, P., Gerhart, A., and Hochstein, J. (2016). *Munson, Young and Okiishi's Fundamentals of Fluid Mechanics, 8th Edition*. USA, Wiley.

Gong, J., Zhang, D., Liu, C., Zhao, Y., Hu, P., and Quan, W. (2019). Optimization of electro-hydraulic energy-savings in mobile machinery. *Automation in Construction*, 98:132–145.

Grepl, R. (2011). Real-time control prototyping in matlab/simulink: Review of tools for research and education in mechatronics. In *Mechatronics (ICM), 2011 IEEE International Conference on*, pages 881–886. IEEE.

Habibi, S. and Goldenberg, A. (1999). Design of a new high performance electrohydraulic actuator. In *Advanced Intelligent Mechatronics, 1999. Proceedings. 1999 IEEE/ASME International Conference on*, pages 227–232. IEEE.

Hajek Jr, T. J. and Tolappa, S. T. (2004). Independent and regenerative mode fluid control system. US Patent 6,715,403.

Hansen, A. H., Pedersen, H. C., Andersen, T. O., and Wachmann, L. (2011). Design of energy efficient smismo-els control strategies. In *Fluid Power and Mechatronics (FPM), 2011 International Conference on*, pages 522–527. IEEE.

Hansen, A. H., Schmidt, L., Pedersen, H. C., and Andersen, T. O. (2016). A generic model based tracking controller for hydraulic valve-cylinder drives. In *9th FPNI Ph. D. Symposium on Fluid Power*, pages V001T01A016–V001T01A016. American Society of Mechanical Engineers.

Hansen, R. H. (2009). Advanced power management of a telehandler using electronic load sensing. In *10th international workshop on research and education in mechatronics*. University of Strathclyde Glasgow, UK.

Heikkilä, M. and Linjama, M. (2013). Displacement control of a mobile crane using a digital hydraulic power management system. *Mechatronics*, 23(4):452–461.

Heintze, J., Van Schothorst, G., Van der Weiden, A., and Teerhuis, P. (1993). Modeling and control of an industrial hydraulic rotary vane actuator. In *Decision and Control, 1993., Proceedings of the 32nd IEEE Conference on*, pages 1913–1918. IEEE.

Heybroek, K. (2008). *Saving energy in construction machinery using displacement control hydraulics: Concept realization and validation*. PhD thesis, Linköping University Electronic Press.

Hippalgaonkar, R. and Ivantysynova, M. (2013). A series-parallel hydraulic hybrid mini-excavator with displacement controlled actuators. In *13th Scandinavian International Conference on Fluid Power; June 3-5; 2013; Linköping; Sweden*, number 092, pages 31–42. Linköping University Electronic Press.

Hu, H. and Zhang, Q. (2003). Multi–function realization using an integrated programmable e/h control valve. *Applied engineering in agriculture*, 19(3):283.

Huang, W., Quan, L., Huang, J., and Yang, J. (2018). Flow matching with combined control of the pump and the valves for the independent metering swing system of a hydraulic excavator. *Proceedings of the Institution of Mechanical Engineers, Part D: Journal of Automobile Engineering*, 232(10):1310–1322.

Huang, X. and Lunzman, S. V. (2003). Electro-hydraulic valve control system and method. US Patent 6,662,705.

Huova, M. (2015). Energy efficient digital hydraulic valve control. *Tampereen teknillinen yliopisto. Julkaisu-Tampere University of Technology. Publication; 1298.*

International, H. (2019). Ehpv. http://pdf.directindustry.com/pdf/husco-international/ehpv/117113-608498.html.

Ivantysyn, R. and Weber, J. (2014). Novel open circuit displacement control architecture in heavy machinery. In *8th FPNI Ph. D Symposium on Fluid Power*, pages V001T02A002–V001T02A002. American Society of Mechanical Engineers.

Jackson, R. S., Clanton, R. R., and Pfaff, J. L. (2006). Hydraulic control valve system with electronic load sense control. US Patent 7,089,733.

Jansson, A., Krus, P., and Palmberg, J.-O. (1991). Decoupling of response and pressure level in a hydraulic actuator. In *The 4th Bath International Fluid Power Workshop*.

Jansson, A. and Palmberg, J.-O. (1990). Separate controls of meter-in and meter-out orifices in mobile hyraulic systems. *SAE transactions*, pages 377–383.

Jelali, M. and Kroll, A. (2012). *Hydraulic servo-systems: modelling, identification and control*. Springer Science & Business Media.

Karpenko, M. and Sepehri, N. (2009). Hardware-in-the-loop simulator for research on fault tolerant control of electrohydraulic actuators in a flight control application. *Mechatronics*, 19(7):1067–1077.

Karvonen, M. (2016). Energy efficient digital hydraulic power management of a multi actuator system. *English. PhD thesis. Tampere University of Technology*, pages 16–29.

Karvonen, M., Heikkilä, M., Huova, M., and Linjama, M. (2014). Analysis by simulation of different control algorithms of a digital hydraulic two-actuator system. *International journal of fluid power*, 15(1):33–44.

Kenjo, T. and Sugawara, A. (1994). *Stepping motors and their microprocessor controls*. Clarendon Press Oxford.

Kępiński, R., Awrejcewicz, J., and Lewandowski, D. (2015). Dynamical simulation of a nonlinear stepper motor system. *International Journal of Dynamics and Control*, 3(1):31–35.

Ketonen, M. and Linjama, M. (2017a). High flowrate digital hydraulic valve system. In *Proc. of The Ninth Workshop on Digital Fluid Power, Aalborg, Denmark*.

Ketonen, M. and Linjama, M. (2017b). Simulation study of a digital hydraulic independent metering valve system on an excavator. In *Proceedings of 15: th Scandinavian International Conference on Fluid Power, June 7-9, 2017, Linköping, Sweden*, number 144, pages 136–146. Linköping University Electronic Press.

Kleitsch, A. J. (2017). Independent metering valve with flow sharing. US Patent 2017/0108015.

Koivumäki, J., Zhu, W.-H., and Mattila, J. (2019). Energy-efficient and high-precision control of hydraulic robots. *Control Engineering Practice*, 85:176 – 193.

Kolks, G. and Weber, J. (2016a). Controller design for precise and efficient industrial cylinder drives using independent metering valves. In *9th FPNI Ph. D. Symposium on Fluid Power*, pages V001T01A009–V001T01A009. American Society of Mechanical Engineers.

Kolks, G. and Weber, J. (2016b). Modiciency-efficient industrial hydraulic drives through independent metering using optimal operating modes. In *Proceedings of the 10th International Conference on Fluid Power*.

Kong, X., Shan, D., Yao, J., and Gao, Y. (2004). Study on experiment and modeling for the multifunctional integrated valve control system. In *Intelligent Mechatronics and Automation, 2004. Proceedings. 2004 International Conference on*, pages 455–459. IEEE.

Konowrocki, R., Szolc, T., Pochanke, A., and Pręgowska, A. (2016). An influence of the stepping motor control and friction models on precise positioning of the complex mechanical system. *Mechanical Systems and Signal Processing*, 70:397–413.

Krus, P. (1988). On load sensing fluid power systems. *Division of Fluid Power Control Department of Mechanical Engineering, Linkoping University, Sweden*.

Laamanen, M. S. A. and Vilenius, M. (2003). Is it time for digital hydraulics. In *The Eighth Scandinavian International Conference on Fluid Power*.

Lamberg, K. (2006). Model-based testing of automotive electronics. In *Design, Automation and Test in Europe, 2006. DATE'06. Proceedings*, volume 1, pages 1–1. IEEE.

Lee, J.-C., Jin, K.-C., Kwon, Y.-M., Choi, L.-G., Choi, J.-Y., and Lee, B.-K. (2016). Development of the independent metering valve control system and analysis of its performance for an excavator. In *BATH/ASME 2016 Symposium on Fluid Power and Motion Control*, pages V001T01A021–V001T01A021. American Society of Mechanical Engineers.

Lennon, T. and Mass, N. (2008). Model-based design for mechatronic systems. *ELECTRONICS WORLD-SUTTON THEN CHEAM-*, 1865:23.

Lettini, A., Havermann, M., Guidetti, M., and Fornaciari, A. (2010). Electro-hydraulic load sensing: A contribution to increased efficiency through fluid power on mobile machines. In *Proceedings of the 7. IFK: International Fluid Power Conference, Aachen, Germany*, pages 22–24.

Lim, T.-H., Cho, H.-C., Lee, H.-S., and Yang, S.-Y. (2005). Development of hardware in the loop system (hils) for hydraulic excavator. In *22nd International Symposium on Automation and Robotics in Construction ISARC 2005*, pages 11–14.

Linerode, J. D. (2004). Swing control algorithm for hydraulic circuit. US Patent 6,761,029.

Linjama, M. (2011). Digital fluid power: State of the art. In *12th Scandinavian International Conference on Fluid Power, Tampere, Finland, May*, pages 18–20.

Linjama, M., Huova, M., Karhu, O., and Huhtala, K. (2016). High-performance digital hydraulic tracking control of a mobile boom mockup. In *10th International Fluid Power Conference (10. IFK)*, page 12.

Linjama, M., Huova, M., and Vilenius, M. (2008). Online minimization of power losses in distributed digital hydraulic valve system. In *Proceedings of the 6th International Fluid Power Conference Dresden, Fluid Power in Motion, 6iFK, April 1.-2.2008, Dresden*.

Linjama, M., Paloniitty, M., Tiainen, L., and Huhtala, K. (2015). Mechatronic design of digital hydraulic micro valve package. *Procedia engineering*, 106:97–107.

Liu, B., Quan, L., and Ge, L. (2017). Research on the performance of hydraulic excavator boom based pressure and flow accordance control with independent metering circuit. *Proceedings of the Institution of Mechanical Engineers, Part E: Journal of Process Mechanical Engineering*, 231(5):901–913.

Liu, K., Gao, Y., and Tu, Z. (2016). Energy saving potential of load sensing system with hydro-mechanical pressure compensation and independent metering. *International Journal of Fluid Power*, 17(3):173–186.

Liu, S., Krutz, G., and Yao, B. (2002). Easy5 model of two position solenoid operated cartridge valve. In *ASME 2002 International Mechanical Engineering Congress and Exposition*, pages 63–67. American Society of Mechanical Engineers.

Liu, S. and Yao, B. (2002). Energy-saving control of single-rod hydraulic cylinders with programmable valves and improved working mode selection. Technical report, SAE Technical Paper.

Liu, S. and Yao, B. (2004). Programmable valves: a solution to bypass deadband problem of electro-hydraulic systems. In *American Control Conference, 2004. Proceedings of the 2004*, volume 5, pages 4438–4443. IEEE.

Liu, S. and Yao, B. (2006). Automated onboard modeling of cartridge valve flow mapping. *IEEE/ASME transactions on mechatronics*, 11(4):381–388.

Liu, S. and Yao, B. (2008). Coordinate control of energy saving programmable valves. *IEEE Transactions on Control Systems Technology*, 16(1):34–45.

Lodewyks, J. and Zurbrügg, P. (2016). Decentralized energy-saving hydraulic concepts for mobile working machines. In *Proc. IFK*, pages 79–90.

Lovrec, D., Kastrevc, M., and Ulaga, S. (2009). Electro-hydraulic load sensing with a speed-controlled hydraulic supply system on forming-machines. *The International Journal of Advanced Manufacturing Technology*, 41(11-12):1066–1075.

Lu, L. and Yao, B. (2014). Energy-saving adaptive robust control of a hydraulic manipulator using five cartridge valves with an accumulator. *IEEE Transactions on Industrial Electronics*, 61(12):7046–7054.

Lübbert, D.-I. J., Sitte, D.-I. A., and Weber, I. J. (2016). Pressure compensator control–a novel independent metering architecture. In *10th International Fluid Power Conference*, volume 1, pages 231–245.

Luo, Y. (2006). *System modeling and control design of a two-stage metering poppet-valve system*. PhD thesis, University of Missouri–Columbia.

Martin, A. and Emami, M. R. (2006). An architecture for robotic hardware-in-the-loop simulation. In *Mechatronics and Automation, Proceedings of the 2006 IEEE International Conference on*, pages 2162–2167. IEEE.

Mattila, J., Koivumäki, J., Caldwell, D. G., and Semini, C. (2017). A survey on control of hydraulic robotic manipulators with projection to future trends. *IEEE/ASME Transactions on Mechatronics*, 22(2):669–680.

Mattila, J. and Virvalo, T. (2000). Energy-efficient motion control of a hydraulic manipulator. In *Robotics and Automation, 2000. Proceedings. ICRA'00. IEEE International Conference on*, volume 3, pages 3000–3006. IEEE.

Merritt, H. E. (1967). Hydraulic control systems, john wiley & sons. *New York*.

Mihalache, G., Zbant, A., and Livint, G. (2013). Open-loop control of hybrid stepper motor with two phases using voltage to frequency converter. In *Advanced Topics in Electrical Engineering (ATEE), 2013 8th International Symposium on*, pages 1–4. IEEE.

Moon, S. and Kim, D. H. (2014). Step-out detection and error compensation for a micro-stepper motor using current feedback. *Mechatronics*, 24(3):265–273.

Muller, M. T. and Fales, R. C. (2008). Design and analysis of a two-stage poppet valve for flow control. *International Journal of Fluid Power*, 9(1):17–26.

Murrenhoff, H., Sgro, S., and Vukovic, M. (2014). An overview of energy saving architectures for mobile applications. In *Proceedings of the 9th International Fluid Power Conference, Aachen, Germany*, pages 24–26.

Nahian, S., Truong, D., and Ahn, K. (2015). Introduction of independent metering valve for energy saving excavator system. · , 12(1):45–52.

NEWS, B. (2018). Why robots will build the cities of the future. https://www.bbc.co.uk/news/business-46034469, access date (02/12/2019).

Nielsen, B. K. (2005). *Controller development for a separate meter-in separate meter-out fluid power valve for mobile applications*. PhD thesis, Citeseer.

Oaks, O. J. and Cook, G. (1976). Piecewise linear control of nonlinear systems. *IEEE Transactions on Industrial Electronics and Control Instrumentation*, (1):56–63.

Okhotnikov, I. (2018). *Design and performance evaluation of a rotary flow control valve for independent metering hydraulics*. PhD thesis, Bournemouth University.

Okhotnikov, I., Noroozi, S., Sewell, P., and Godfrey, P. (2017). Evaluation of steady flow torques and pressure losses in a rotary flow control valve by means of computational fluid dynamics. *International Journal of Heat and Fluid Flow*, 64:89–102.

Opdenbosch, P., Sadegh, N., and Book, W. (2008). Learning control applied to electro-hydraulic poppet valves. In *2008 American Control Conference*, pages 1525–1532.

Opdenbosch, P., Sadegh, N., and Book, W. (2013). Intelligent controls for electro-hydraulic poppet valves. *Control Engineering Practice*, 21(6):789–796.

Opdenbosch, P., Sadegh, N., Book, W., and Enes, A. (2011). Auto-calibration based control for independent metering of hydraulic actuators. In *Robotics and Automation (ICRA), 2011 IEEE International Conference on*, pages 153–158. IEEE.

Opdenbosch, P., Sadegh, N., Book, W., Murray, T., and Yang, R. (2009a). Modelling an electro-hydraulic poppet valve. *International Journal of Fluid Power*, 10(1):7–15.

Opdenbosch, P., Sadegh, N., Book, W., Murray, T., and Yang, R. (2009b). Modelling an electro-hydraulic poppet valve. *International Journal of Fluid Power*, 10(1):7–15.

Park, H. G., Nahian, S. A., and Anh, K. K. (2016). A study on energy saving of imv circuit using pressure feedback. · , 13(4):31–44.

Parr, A. (2011). *Hydraulics and pneumatics: a technician's and engineer's guide*, chapter 1, page 8. Elsevier.

Pedersen, H. C., Andersen, T. O., Skouboe, T., and Jacobsen, M. S. (2013). Investigation and comparison of separate meter-in separate meter-out control strategies. In *ASME/BATH 2013 Symposium on Fluid Power and Motion Control*, pages V001T01A047–V001T01A047. American Society of Mechanical Engineers.

Pennestrì, E., Rossi, V., Salvini, P., and Valentini, P. P. (2016). Review and comparison of dry friction force models. *Nonlinear dynamics*, 83(4):1785–1801.

Pfaff, J. L. and Tabor, K. A. (2005). Method of selecting a hydraulic metering mode for a function of a velocity based control system. US Patent 6,880,332.

Plummer, A. R. (2006). Model-in-the-loop testing. *Proceedings of the Institution of Mechanical Engineers, Part I: Journal of Systems and Control Engineering*, 220(3):183–199.

Pollok, A. and Casella, F. (2017). Modelling and simulation of self-regulating pneumatic valves. *Mathematical and Computer Modelling of Dynamical Systems*, 23(3):243–261.

Prabhu, S. M. (2007). Model-based design for off-highway machine systems development. Technical report, SAE Technical Paper.

Prabhu, S. M. and Mosterman, P. J. (2004). Model-based design of a power window system: Modeling, simulation and validation. In *Proceedings of IMAC-XXII: A Conference on Structural Dynamics, Society for Experimental Mechanics, Inc., Dearborn, MI*. sn.

Rannow, M. (2016). Fail operational controls for an independent metering valve. In *Proceedings of the 10. International Fluid Power Conference*.

Rath, G. and Zaev, E. (2017). Optimal control for hydraulic system with separate meter-in and separate meter-out. In *Proceedings of the 15th Scandinavian International Conference on Fluid Power, SICFP'17*.

Robinson, D. J. (1969). Dynamic analysis of permanent magnet stepping motors.

Sakurai, Y., Nakada, T., and Tanaka, K. (2002). Design method of an intelligent oil-hydraulic system (load sensing oil-hydraulic system). In *Intelligent Control, 2002. Proceedings of the 2002 IEEE International Symposium on*, pages 626–630. IEEE.

Scherer, M., Geimer, M., and Weiss, B. (2013). Contribution on control strategies of flow-on-demand hydraulic circuits. In *13th Scandinavian International Conference on Fluid Power; June 3-5; 2013; Linköping; Sweden*, number 092, pages 531–540. Linköping University Electronic Press.

Schneider, M., Koch, O., and Weber, J. (2016). Green wheel loader–improving fuel economy through energy efficient drive and control concepts. In *Proceedings of the 10th International Fluid Power Conference (10. IFK), Dresden, Germany*, pages 8–10.

Shenouda, A. (2006). *Quasi-static hydraulic control systems and energy savings potential using independent metering four-valve assembly configuration*. PhD thesis, Georgia Institute of Technology.

Shenouda, A. and Book, W. (2005a). Energy saving analysis using a four-valve independent metering configuration controlling a hydraulic cylinder. In *SAE Technical Paper*. SAE International.

Shenouda, A. and Book, W. (2008). Optimal mode switching for a hydraulic actuator controlled with four-valve independent metering configuration. *International Journal of Fluid Power*, 9(1):35–43.

Shenouda, A. and Book, W. J. (2005b). Selection of operating modes of a multi-functional hydraulic device. In *ASME 2005 International Mechanical Engineering Congress and Exposition*, pages 99–109. American Society of Mechanical Engineers.

Shi, J., Quan, L., Zhang, X., and Xiong, X. (2018). Electro-hydraulic velocity and position control based on independent metering valve control in mobile construction equipment. *Automation in Construction*, 94:73–84.

Siivonen, L., Linjama, M., Huova, M., and Vilenius, M. (2009). Jammed on/off valve fault compensation with distributed digital valve system. *International Journal of Fluid Power*, 10(2):73–82.

Sitte, A. and Weber, J. (2013). Structural design of independent metering control systems. In *13th Scandinavian International Conference on Fluid Power; June 3-5; 2013; Linköping; Sweden*, number 092, pages 261–270. Linköping University Electronic Press.

Smith, D. P. (1999). Electrohydraulic valve arrangement. US Patent 5,868,059.

Smith, D. P. and Mather, D. T. (2007). Electro-hydraulic metering valve with integral flow control. US Patent 7,240,604.

Smith, D. P. and Mather, D. T. (2008). Hydraulic regeneration system. US Patent 7,444,809.

Soltani, A. and Assadian, F. (2016). A hardware-in-the-loop facility for integrated vehicle dynamics control system design and validation. *IFAC-PapersOnLine*, 49(21):32–38.

Tabor, K. A. (2004). Velocity based method of controlling an electrohydraulic proportional control valve. US Patent 6,775,974.

Tabor, K. A. (2005a). A novel method of controlling a hydraulic actuator with four valve independent metering using load feedback. Technical report, SAE Technical Paper.

Tabor, K. A. (2005b). Optimal velocity control and cavitation prevention of a hydraulic actuator using four valve independent metering. Technical report, SAE Technical Paper.

Thompson, B., Yoon, H.-S., Kim, J., and Lee, J. (2014). Swing energy recuperation scheme for hydraulic excavators. Technical report, SAE Technical Paper.

Toman, J., Kerlín, T., and Singule, V. (2011). Application of the v-cycle development in the aerospace industry. *Engineering Mechanics*, 18(5-6):297–306.

Tørdal, S. S., Klausen, A., and Bak, M. K. (2015). Experimental system identification and black box modeling of hydraulic directional control valve. *Modeling, Identification and Control*, 35:225–235.

UK, I. (2018). Predictions - the future of robotics. https://innovateuk.blog.gov.uk/2018/05/30/the-future-of-robotics/, access date (02/12/2019).

Vukovic, M., Leifeld, R., and Murrenhoff, H. (2016). Steam–a hydraulic hybrid architecture for excavators. In *10th International Fluid Power Conference (10. IFK)*, pages 8–10.

Vukovic, M. and Murrenhoff, H. (2014). Single edge meter out control for mobile machinery. In *ASME/BATH 2014 Symposium on Fluid Power and Motion Control*, pages V001T01A009–V001T01A009. American Society of Mechanical Engineers.

Vukovic, M. and Murrenhoff, H. (2015). The next generation of fluid power systems. *Procedia engineering*, 106:2–7.

Vukovic, M., Sgro, S., and Murrenhoff, H. (2013). Steam: A mobile hydraulic system with engine integration. In *ASME/BATH 2013 Symposium on Fluid Power and Motion Control*, pages V001T01A005–V001T01A005. American Society of Mechanical Engineers.

Vukovic, M., Sgro, S., and Murrenhoff, H. (2014). Steam–a holistic approach to designing excavator systems. In *Proceedings of the 9th International Fluid Power Conference, Aachen, Germany*, pages 24–26.

Wang, H., Gong, G., Zhou, H., and Wang, W. (2016). Steady flow torques in a servo motor operated rotary directional control valve. *Energy Conversion and Management*, 112:1–10.

Watton, J. (2009). *Fundamentals of fluid power control*, volume 10, page 494. Cambridge University Press.

Weber, J. (2018). Independent metering systems. *International Journal of Hydromechatronics*, 1(1):91–106.

Weber, J., Beck, B., Fischer, E., Ivantysyn, R., Kolks, G., Kunkis, M., Lohse, H., Lübbert, J., Michel, S., Schneider, M., et al. (2016). Novel system architectures by individual drives. In *10th International Fluid Power Conference, IFK Conference proceedings*, volume 2.

Wydra, M., Geimer, M., and Weiss, B. (2017). An approach to combine an independent metering system with an electro-hydraulic flow-on-demand hybrid-system. In *Proceedings of 15: th Scandinavian International Conference on Fluid Power, June 7-9, 2017, Linköping, Sweden*, number 144, pages 161–170. Linköping University Electronic Press.

Xu, B., Ding, R., Zhang, J., Cheng, M., and Sun, T. (2015). Pump/valves coordinate control of the independent metering system for mobile machinery. *Automation in Construction*, 57:98–111.

Yan, G. (2011). The design of control system for sz-40 injection molding machine base on plc. In *Mechanic Automation and Control Engineering (MACE), 2011 Second International Conference on*, pages 7815–7818. IEEE.

Yang, K. U., Hur, J. G., Kim, G. J., and Kim, D. H. (2012). Non-linear modeling and dynamic analysis of hydraulic control valve; effect of a decision factor between experiment and numerical simulation. *Nonlinear Dynamics*, 69(4):2135–2146.

Yang, Y., Guglielmino, E., Dai, J. S., Boaventura, T., and Caldwell, D. G. (2010). Modeling of a novel 3-way rotary type electro-hydraulic valve. In *Information and Automation (ICIA), 2010 IEEE International Conference on*, pages 1463–1468. IEEE.

Yao, B. and DeBoer, C. (2002). Energy-saving adaptive robust motion control of single-rod hydraulic cylinders with programmable valves. In *American Control Conference, 2002. Proceedings of the 2002*, volume 6, pages 4819–4824. IEEE.

Yoo, B., Hughes, E. C., and Vance, R. D. (2009). Method for calibrating independent metering valves. US Patent 7,562,554.

YUAN, H., SHANG, Y., VUKOVIC, M., WU, S., MURRENHOFF, H., and JIAO, Z. (2014). Characteristics of energy efficient switched hydraulic systems. *JFPS International Journal of Fluid Power System*, 8(2):90–98.

Zhang, J., Jiao, S., Liao, X., Yin, P., Wang, Y., Si, K., Zhang, Y., and Gu, H. (2009). Design of intelligent hydraulic excavator control system based on pid method. In *International Conference on Computer and Computing Technologies in Agriculture*, pages 207–215. Springer.

Zhang, R., Alleyne, A. G., and Prasetiawan, E. A. (2002a). Performance limitations of a class of two-stage electro-hydraulic flow valves. *International Journal of Fluid Power*, 3(1):47–53.

Zhang, R., Alleyne, A. G., and Prasetiawan, E. A. (2002b). Performance limitations of a class of two-stage electro-hydraulic flow valves. *International Journal of Fluid Power*, 3(1):47–53.

Zhong, Q., Zhang, B., Niu, M., Hong, H., and Yang, H. (2017). Research on dynamic performance of independent metering control system. In *ASME/BATH 2017 Symposium on Fluid Power and Motion Control*, pages V001T01A006–V001T01A006. American Society of Mechanical Engineers.

Zribi, M. and Chiasson, J. (1991). Position control of a pm stepper motor by exact linearization. *IEEE Transactions on automatic control*, 36(5):620–625.

Appendix A

Based on the quasi static assumption and the newton's second low, The summation of forces acting on a cylinder $F = Ma = 0$.

$$Fx + PaAa - PbAb = 0 \tag{A.1}$$

$$Pa = Ps - \Delta P1 \tag{A.2}$$

$$Pb = \Delta P2 - Pr \tag{A.3}$$

$$Fx + (Ps - \Delta Pr)Aa - (\Delta P2 - Pr)Ab = 0 \tag{A.4}$$

$$Fx + PsAa - \Delta PrAa - \Delta P2Ab - PrAb = 0 \tag{A.5}$$

$$PsAa - PrAb = \Delta PrAa + \Delta P2Ab - Fx \tag{A.6}$$

$$PsAa - PrAb = \Delta P1Aa + (PaAa - PbAb) + \Delta P2Ab \tag{A.7}$$

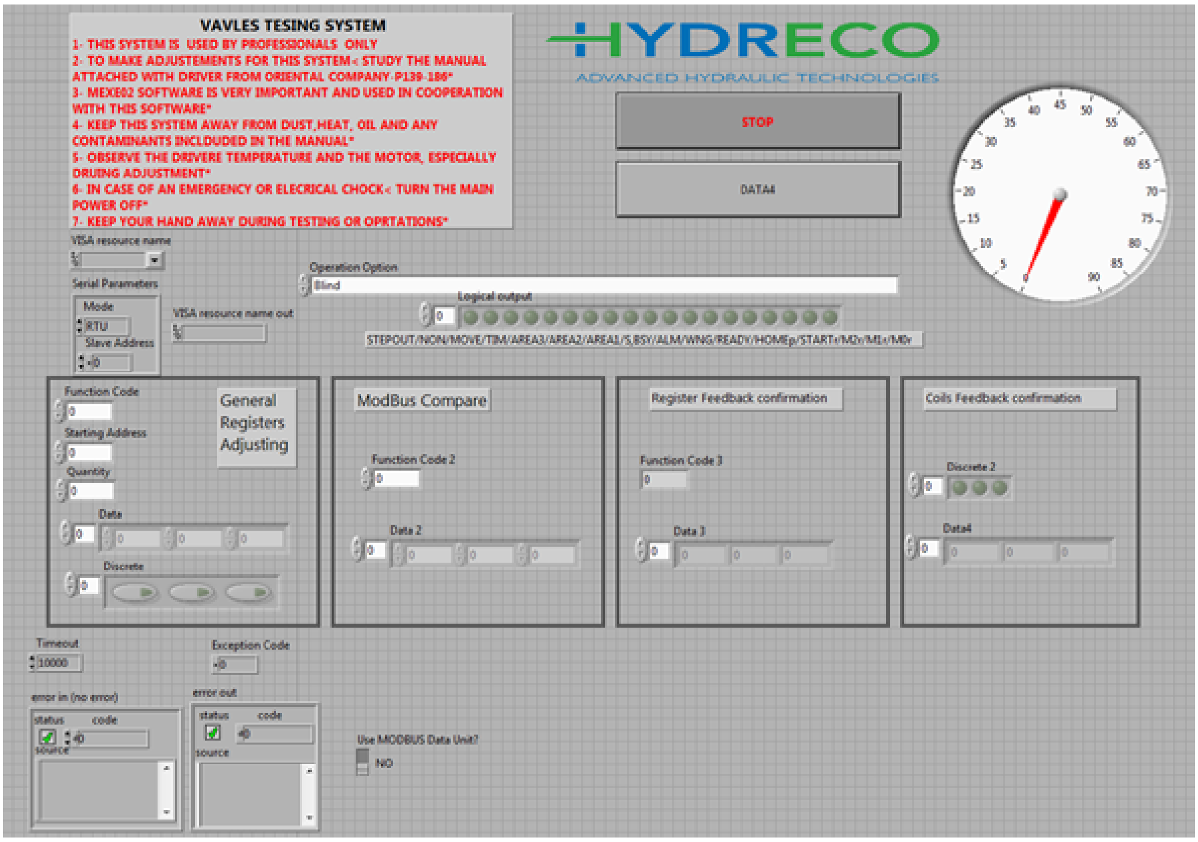

Fig. A.1 The LABview interfacing system that was developed to drive the advanced stepper motor during the valve testing

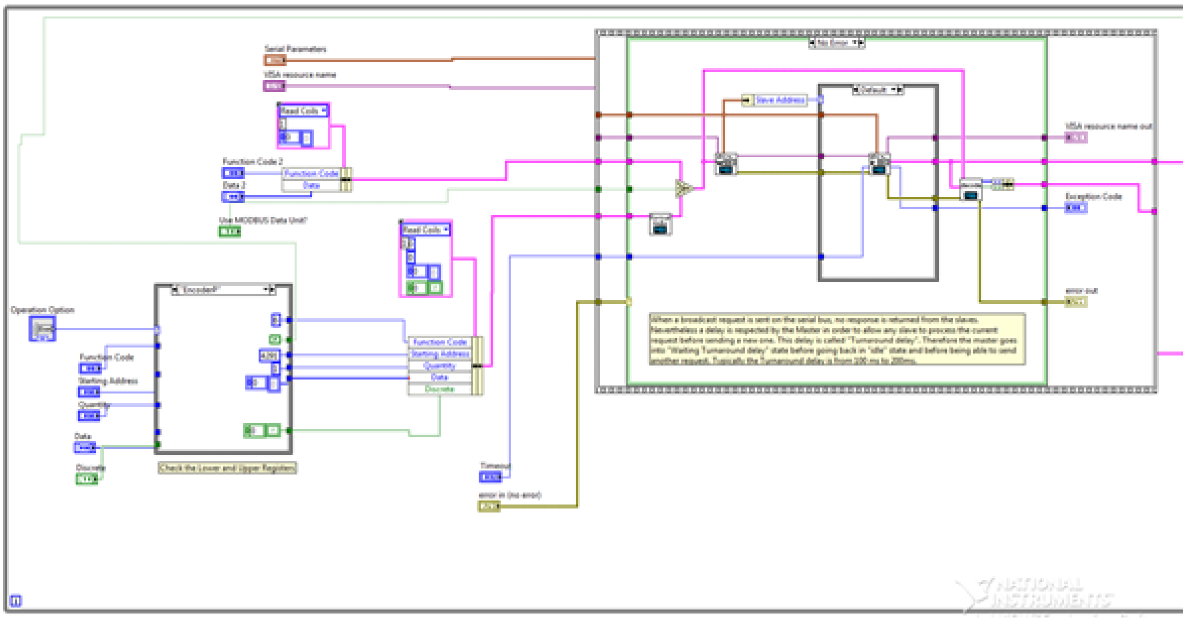

Fig. A.2 The LABview diagram for the interfacing system that was developed to drive the advanced stepper motor during the valve testing

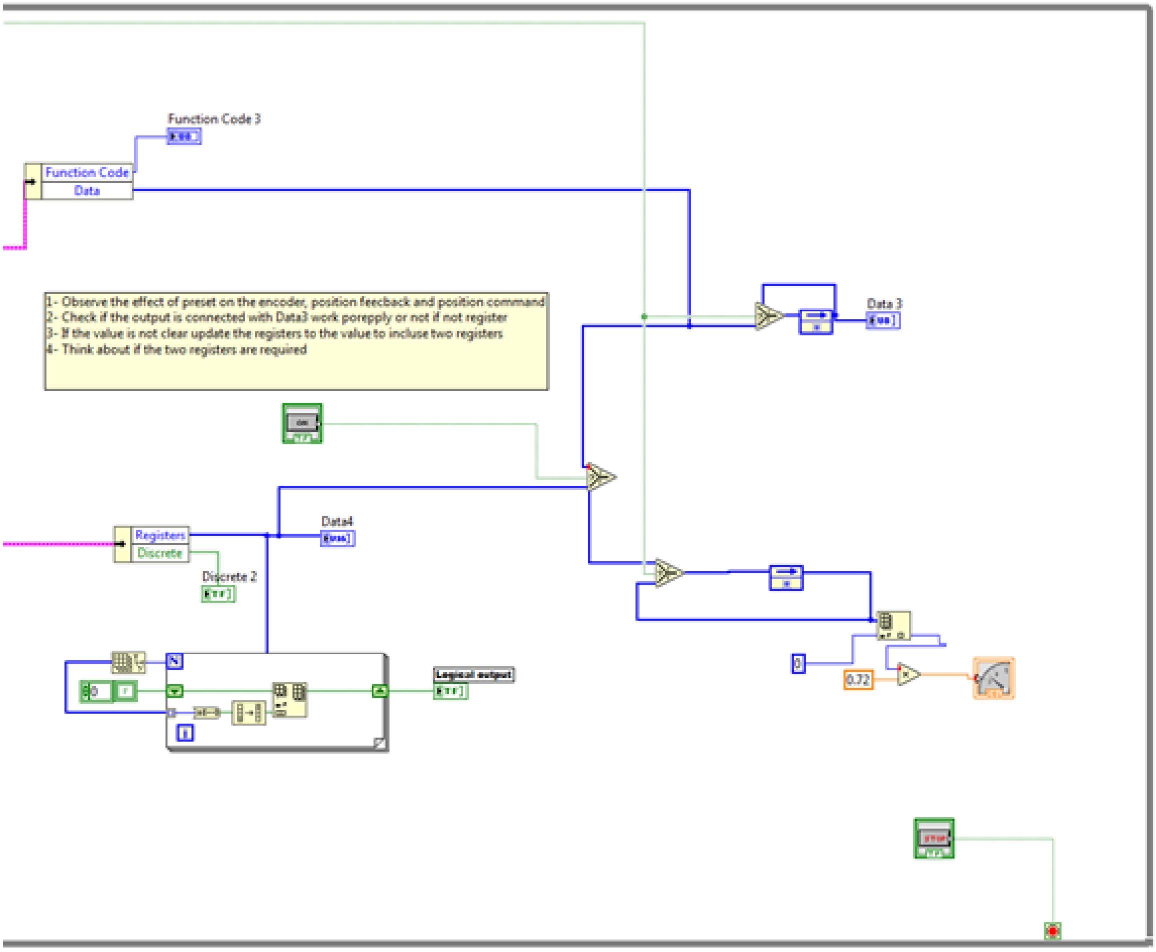

Fig. A.3 The LABview diagram for the interfacing system that was developed to drive the advanced stepper motor during the valve testing

Appendix B

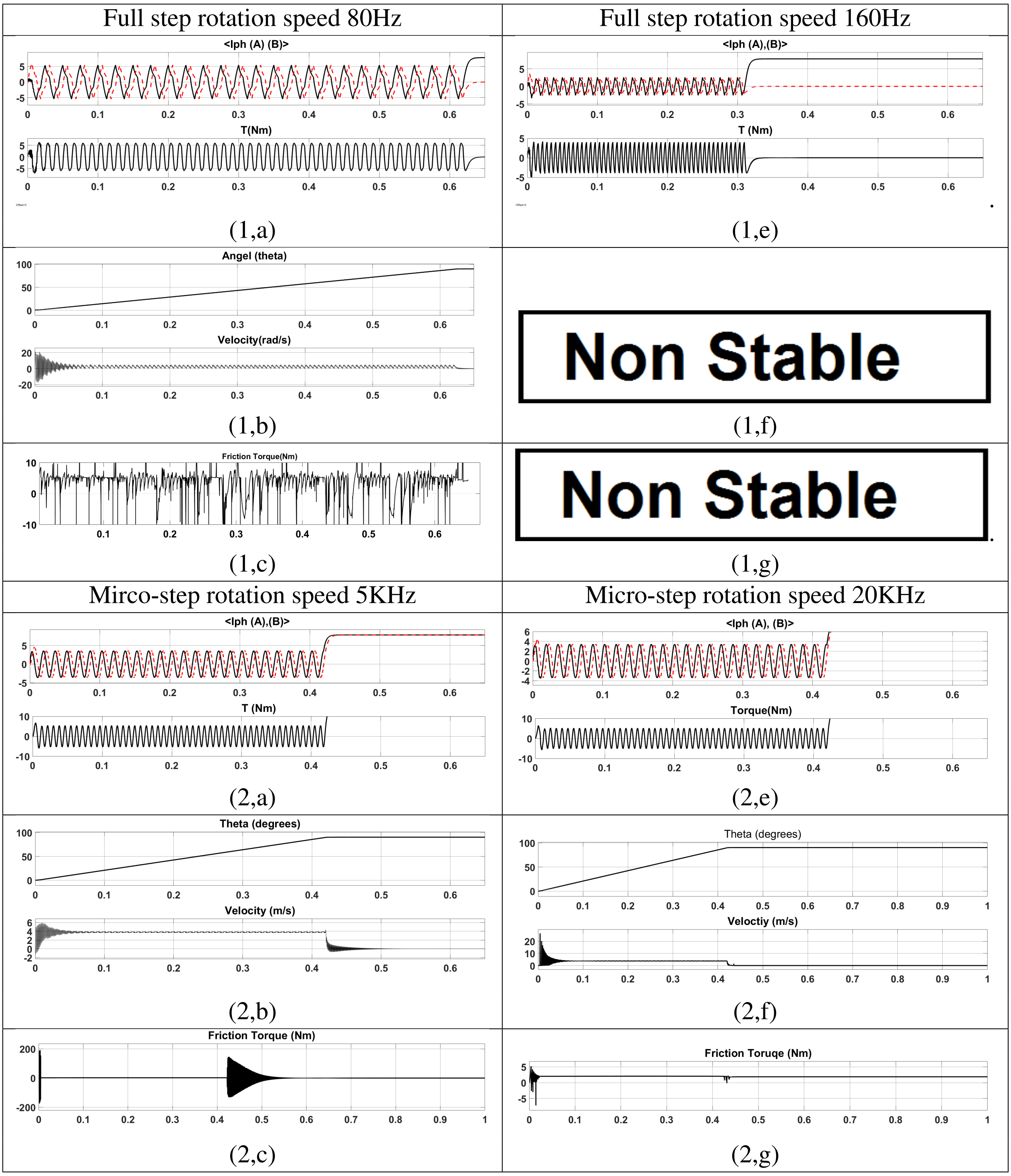

Fig. B.1 Responses for the full step and the micro-step techniques using the first stepper motor model

Appendix C

.

Fig. C.1 The mode selection procedure of the MIM algorithm

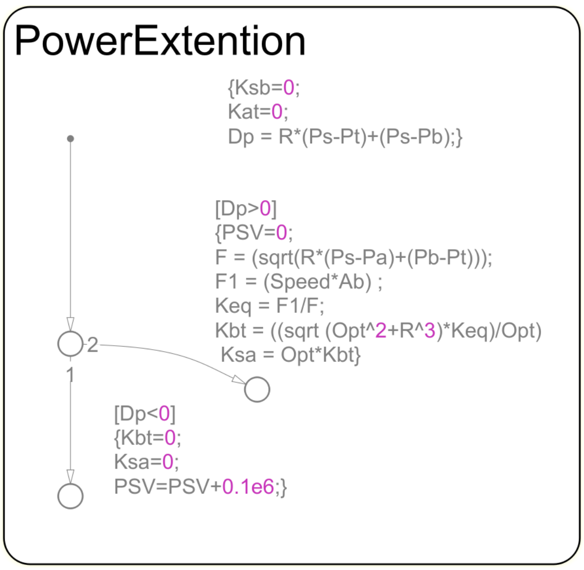

.

Fig. C.2 StateFlow diagram of the Power Extension Mode

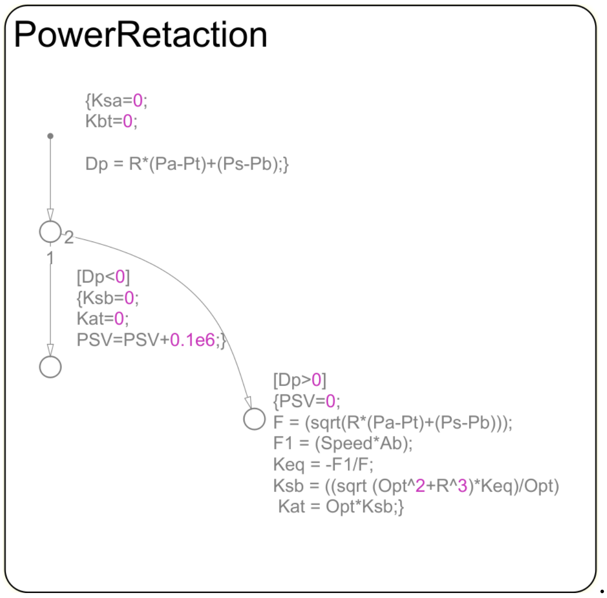

Fig. C.3 StateFlow diagram of the Power Retraction Mode

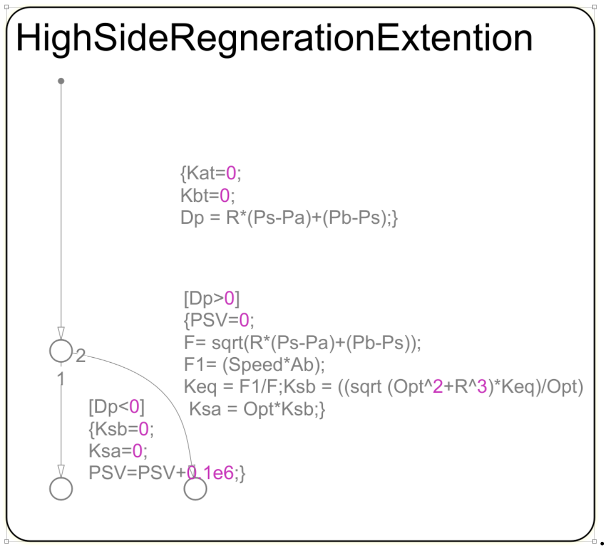

Fig. C.4 StateFlow diagram of the High Side Regeneration Extension Mode

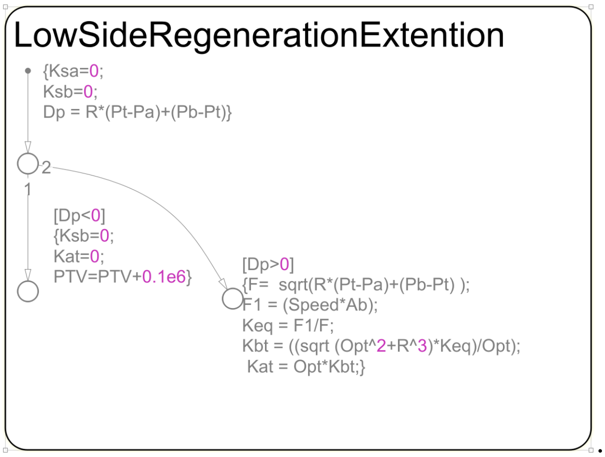

Fig. C.5 StateFlow diagram of the Low Side Regeneration Extension Mode

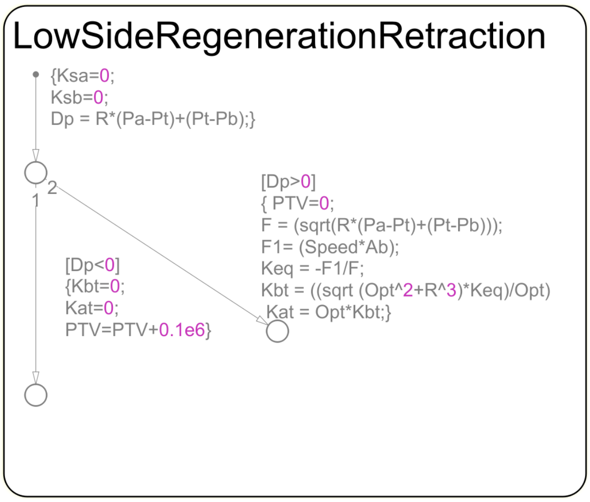

Fig. C.6 StateFlow diagram of the Low Side Regeneration Retraction Mode

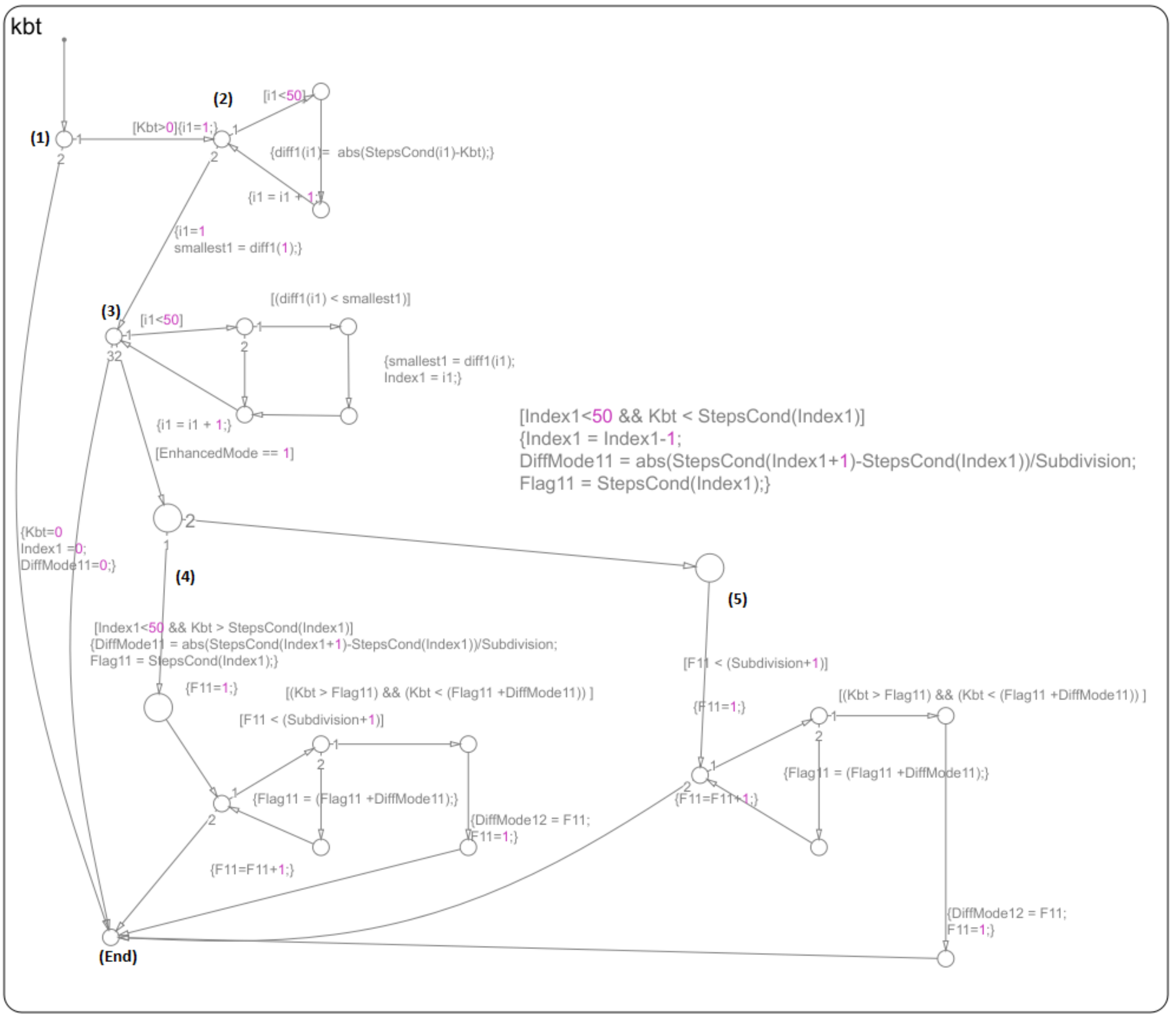

Fig. C.7 The Close Value Detection procedure for the MIM

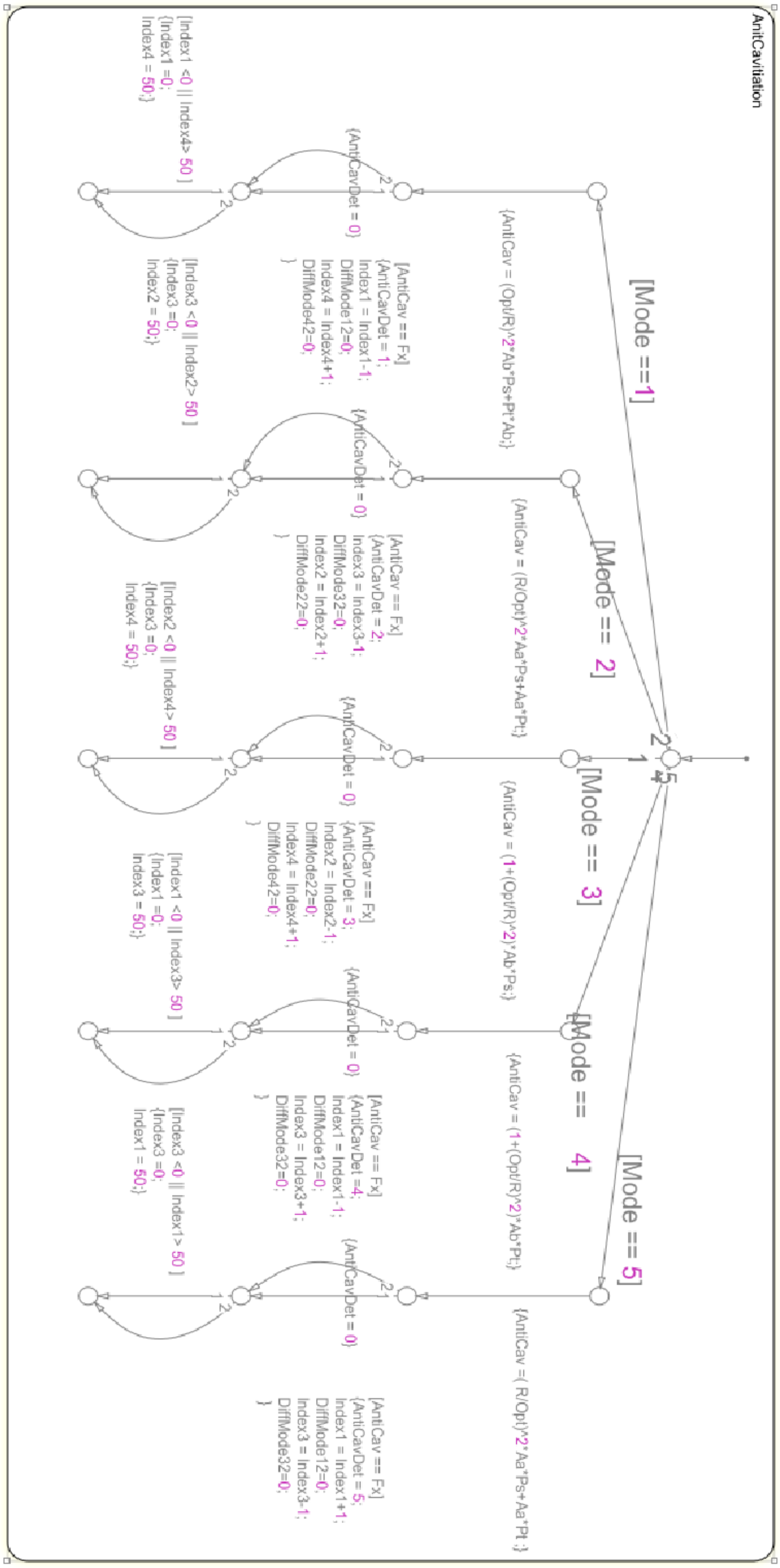

Fig. C.8 The anti-cavitation procedure for the MIM control algorithm

Appendix D

Analysis (1)

$$F(\omega_0, T_{c0}, T_{s0}, \omega_{s0}, z_0) = \omega - \frac{(\sigma_0 \omega z)}{T_C + (T_S - T_C) e^{-\left(\frac{\omega}{\omega_S}\right)^2}} = 0$$

$$F_\omega(\omega_0, T_{c0}, T_{s0}, \omega_{s0}, z_0) = \frac{2\sigma_0 \omega^2 z e^{-\left(\frac{\omega}{\omega_s}\right)^2} (T_c - T_s)}{\left(\omega_s^2 \left(T_c - e^{-\left(\frac{\omega}{\omega_s}\right)^2} * (T_c - T_s)\right)^2\right)} - \frac{\sigma_0 z}{\left(T_c - e^{-\left(\frac{\omega}{\omega_s}\right)^2} * (T_c - T_s)\right)} + 1 = 1$$

$$F_\omega(\omega_0, T_{c0}, T_{s0}, \omega_{s0}, z_0).(\omega - \omega_0) = \omega$$

$$F_{Tc}(\omega_0, T_{c0}, T_{s0}, \omega_{s0}, z_0) = \frac{-(\sigma_0\, \omega\, z\, e^{-\left(\frac{\omega}{\omega_s}\right)^2} - 1)}{\left(T_c - e^{-\left(\frac{\omega}{\omega_s}\right)^2} * (T_c - T_s)\right)^2} = 0$$

$$F_{Ts}(\omega_0, T_{c0}, T_{s0}, \omega_{s0}, z_0) = \frac{(\sigma_0\, \omega\, z\, e^{-\left(\frac{\omega}{\omega_s}\right)^2})}{\left(T_c - e^{-\left(\frac{\omega}{\omega_s}\right)^2} * (T_c - T_s)\right)^2} = 0$$

$$F_z(\omega_0, T_{c0}, T_{s0}, \omega_{s0}, z_0) = \frac{-\sigma_0\, \omega}{\left(T_c - e^{-\left(\frac{\omega}{\omega_s}\right)^2} * (T_c - T_s)\right)} = 0$$

$F_{\omega s}(\omega_0, T_{c0}, T_{s0}, \omega_{s0}, z_0)(\omega_s - \omega_{s0}) = 0$, this is because ω_s is constant value

$$F(\omega, T_c, T_s, z, \omega_s) = \omega$$

Analysis (2)

$$F(\omega_0, T_{c0}, T_{s0}, \omega_{s0}, z_0) = \quad \omega - \frac{(\sigma_0 \omega z)}{T_C + (T_S - T_C) e^{-\left(\frac{\omega}{\omega_S}\right)^2}} = \frac{125}{4} - \frac{3125\,\sigma_0}{513}$$

$$F_\omega(\omega_0, T_{c0}, T_{s0}, \omega_{s0}, z_0) = \frac{2\sigma_0 \omega^2 z e^{-\left(\frac{\omega}{\omega_s}\right)^2}(T_c - T_s)}{\left(\omega_s^2\left(T_c - e^{-\left(\frac{\omega}{\omega_s}\right)^2} * (T_c - T_s)\right)^2\right)} - \frac{\sigma_0 z}{\left(T_c - e^{-\left(\frac{\omega}{\omega_s}\right)^2} * (T_c - T_s)\right)} + 1 = (1 - \frac{\sigma_0}{2})$$

$$F_\omega(\omega_0, T_{c0}, T_{s0}, \omega_{s0}, z_0).(\omega - \omega_0) = -\left(\frac{\sigma_0}{2} - 1\right) * (\omega - 31.25)$$

$$F_{Tc}(\omega_0, T_{c0}, T_{s0}, \omega_{s0}, z_0) = \frac{-(\sigma_0\, \omega\, z\, e^{-\left(\frac{\omega}{\omega_s}\right)^2} - 1)}{\left(T_c - e^{-\left(\frac{\omega}{\omega_s}\right)^2} * (T_c - T_s)\right)^2} = (\frac{125\sigma_0}{16} * (T_c - 2))$$

$$F_{Ts}(\omega_0, T_{c0}, T_{s0}, \omega_{s0}, z_0) = \frac{(\sigma_0\, \omega\, z\, e^{-\left(\frac{\omega}{\omega_s}\right)^2})}{\left(T_c - e^{-\left(\frac{\omega}{\omega_s}\right)^2} * (T_c - T_s)\right)^2} = 0$$

$$F_z(\omega_0, T_{c0}, T_{s0}, \omega_{s0}, z_0) = \frac{-\sigma_0\, \omega}{\left(T_c - e^{-\left(\frac{\omega}{\omega_s}\right)^2} * (T_c - T_s)\right)} = -\frac{125\sigma_0}{8} * (z - 1)$$

$F_{\omega s}(\omega_0, T_{c0}, T_{s0}, \omega_{s0}, z_0)(\omega_s - \omega_{s0}) = 0$, this is because ω_s is constant value

$$F(\omega, T_c, T_s, z, \omega_s) = -\left(\frac{\sigma_0}{2} - 1\right) * (\omega - 31.25) + (\frac{125\sigma_0}{16} * (T_c - 2)) - \frac{125\sigma_0}{8} * (z - 1)$$

$$F(\omega, T_c, T_s, z, \omega_s) = 62.5 - 21.716\sigma_0 + \omega\left(\frac{\sigma_0 - 2}{2}\right) + \frac{125\sigma_0 T_c}{16} - \frac{125\sigma_0 z}{8}$$

Analysis (3)

$$F(i_a, \theta) = F(i_{a0}, \theta_0) + F_{i_a}(i_{a0}, \theta_0)(i_a - i_{a0}) + F_\theta(i_{a0}, \theta_0)(\theta - \theta_0)$$

$F(i_{a0}, \theta_0) = 1.6538\, K_m$

$F_{i_a}(i_{a0}, \theta_0)(i_a - i_{a0}) =$

$K_m \sin(N_r\theta)\,(i_a - i_{a0}) = K_m \sin(N_r 10)\,(i_a - 2) = K_m * 0.8269(i_a - 2) = 0.829\, K_m i_a - 1.6583\, K_m$

$F_\theta(i_{a0}, \theta_0)(\theta - \theta_0) = K_m N_r i_a 0.5624\,(\theta - \theta_0) = K_m\ 112.5\,(\theta - 10) = 112.5\, K_m \theta - 1125\, K_m$

$F(i_a, \theta) = 0.829\, K_m i_a + 112.5\, K_m \theta - 1126.6 K_m$

Analysis (4)

$F(i_b, \theta) = F(i_{b0}, \theta_0) + F_{i_b}(i_{b0}, \theta_0)(i_b - i_{b0}) + F_\theta(i_{b0}, \theta_0)(\theta - \theta_0)$

$F(i_{b0}, \theta_0) = 0$

$F_{i_a}(i_{b0}, \theta_0)(i_b - i_{b0}) = K_m \cos(N_r \theta)(i_b - i_{b0}) = K_m\, 0.5624\, (i_b) = 0.5624\, K_m\, i_b$

$F_\theta(i_{a0}, \theta_0)(\theta - \theta_0) = -K_m N_r i_{b0} \sin(N_r \theta)(\theta - \theta_0) = 0 =$

$F(i_b, \theta) = 0.5624\, K_m\, i_b$

.

The matrices of the state space main equations $A, U and B$ are:

$$A = \begin{bmatrix} 0 & 1 & 0 & 0 & 0 & 0 \\ \frac{-11.25K_m - 0.025\Delta p}{J} & \frac{-B - \frac{\sigma_0 \sigma_1}{2} + \sigma_1 - \sigma_2}{J} & \frac{-0.829K - m}{J} & \frac{0.5624K_m}{J} & \frac{\frac{125\sigma_0\sigma_1}{8}}{J} & \frac{\frac{-125\sigma_0\sigma_1}{16}}{J} \\ \frac{56.24K_m}{L} & 0 & \frac{-R}{L} & 0 & 0 & 0 \\ \frac{98K_m}{L} & 0 & \frac{-R}{L} & 0 & 0 & 0 \\ 0 & \frac{\sigma_0 - 2}{2} & 0 & 0 & \frac{-125\sigma_0}{8} & \frac{+125\sigma_0}{16} \\ 0 & 0 & 0 & 0 & 0 & 0 \end{bmatrix}$$

$$B = \begin{bmatrix} 0 & 1 & 0 & 0 & 0 & 0 \\ 0 & 1125.6 & 0 & 0 & 0.225 & 0 \\ 0 & 561 & \frac{1}{L} & 0 & 0 & 0 \\ 0 & 821 & 0 & \frac{1}{L} & 0 & 0 \\ 0 & 0 & 0 & 0 & 0 & 1 \\ 0 & 0 & 0 & 0 & 0 & 0 \end{bmatrix}$$

$$U = \begin{bmatrix} 0 \\ K_m \\ V_a \\ V_b \\ d_p \\ 62.5 - 21.16\sigma_0 \end{bmatrix}$$

The sate space representation of the system $\dot{x} = Ax + BU$ is,

$$
\begin{bmatrix} \frac{d\theta}{dt} \\ \frac{d\omega}{dt} \\ \frac{di_a}{dt} \\ \frac{di_b}{dt} \\ \frac{dZ}{dt} \\ \frac{dT_c}{dt} \end{bmatrix} =
$$

$$
\begin{bmatrix}
0 & 1 & 0 & 0 & 0 & 0 \\
\frac{-11.25K_m - 0.025\Delta p}{J} & \frac{-B - \frac{\sigma_0\sigma_1}{2} + \sigma_1 - \sigma_2}{J} & \frac{-0.829K - m}{J} & \frac{0.5624K_m}{J} & \frac{\frac{125\sigma_0\sigma_1}{8}}{J} & \frac{\frac{-125\sigma_0\sigma_1}{16}}{J} \\
\frac{56.24K_m}{L} & 0 & \frac{-R}{L} & 0 & 0 & 0 \\
\frac{98K_m}{L} & 0 & \frac{-R}{L} & 0 & 0 & 0 \\
0 & \frac{\sigma_0 - 2}{2} & 0 & 0 & \frac{-125\sigma_0}{8} & \frac{+125\sigma_0}{16} \\
0 & 0 & 0 & 0 & 0 & 0
\end{bmatrix} * \begin{bmatrix} \theta \\ \omega \\ i_a \\ i_b \\ Z \\ T_c \end{bmatrix} +
$$

$$
\begin{bmatrix}
0 & 1 & 0 & 0 & 0 & 0 \\
0 & 1125.6 & 0 & 0 & 0.225 & 0 \\
0 & 561 & \frac{1}{L} & 0 & 0 & 0 \\
0 & 821 & 0 & \frac{1}{L} & 0 & 0 \\
0 & 0 & 0 & 0 & 0 & 1 \\
0 & 0 & 0 & 0 & 0 & 0
\end{bmatrix} * \begin{bmatrix} 0 \\ K_m \\ V_a \\ V_b \\ d_p \\ 62.5 - 21.16\sigma_0 \end{bmatrix} \quad \text{(D.1)}
$$

Table D.1 The parameters of the rotary orifice

Symbol	Parameter	Value	Unit
L	Spool length	0.04	m
n	number of balancing groove	10	
w	width of balancing groove	0.0006	m
$A_{sp,op}$	The spool opening area	170	mm^2
R_{isl}	Internal sleeve radius	0.0097	mm
R_{esl}	External sleeve radius	0.0125	mm
R_{isp}	Internal spool radius	0.0075	mm
R_{esp}	External spool radius	0.0096	mm
μ	Dynamic viscosity coefficient	$3e^-5$	$\frac{N*S}{m^2}$
τ	Shear stress	1	N/m^2
Tc	Coulomb friction	1.5	N
Ts	Static friction	3	N
Wc	Stribick characteristic velocity	0.001	rad/s
σ_0	Stiffness coefficient	100000	N/m
σ_1	Damping coefficient	317	Ns/m
ρ	Density unit	853	$\frac{Kg}{m^3}$

Table D.2 The parameters of the Valvistor model Fales (2006)

Symbol	Parameter	Value	Unit
m_m	Mass of the main poppet	0.0605	Kg
m_p	Mass of the pilot poppet	0.003	Kg
a_{ms}	Area of main poppet exposed to supply pressure	$1.53e^-4$	m^2
a_{ml}	Area of main poppet exposed to control pressure	$3.14e-4$	m^2
km	Main poppet spring rate	700	N/m
bm	Main poppet damping rate	$1e-3$	$N/(m/s)$
ap	Cross sectional area of the pilot poppet	$5e-5$	m^2
Vp	volume of the pilot circuit line	$1.62e-5$	m^3
β	Fluid bulk modulus	$1.334e^9$	Pa
bp	Pilot poppet damping rate	3.50	$N/(m/s)$
kp	Pilot poppet spring rate	35025	N/m

Appendix E

```
clear all;
clc;
close all
L1=8.9e-3;
R=0.74;
PSIM=0.015;
Tdm=0.30;
J=0.120e-3;
B1=1e-3;
Km= 0.054;
Resp=9.5*10^-3;
Va = 24;
Vb = 24;
D1 = 1;
D2 = 1;
dp = 1;
Segma0 = 100000;
Segma1 = 316.227777;
Segma2 = 0.4;
fori = 0 : 100 : 2000;
Segma1 = i

    A = [ 0 1 0 0 0 0 ;
    (-112.5*Km-0.025*dp)/J (-B1-(Segma0*Segma1-2*Segma1)/2)+(Segma1-Segma2)/J -0.829*Km/J
0.5624*Km/J (125*Segma0*Segma1)/8/J -(125*Segma0*Segma1)/16/J ;
    56.24*Km/L1 0 -R/L1 0 0 0 ;
    82.69*Km/L1 0 -R/L1 0 0 0 ;
```

```
0 (Segma0-2)/2 0 0 (-125*Segma0/8) 125*Segma0/16 ;
0 0 0 0 0 0 ];

B = [ 0 0 0 0 0 0 ; 0 1126.6 0 0 0.225 0 ; 0 561 1/L1 0 0 0 ; 0 821 0 1/L1 0 0 ; 0 0 0 0 0 1 ; 0 0 0 0 0 0 ];

U = [ 0 ; Km ; Va ; Vb ; dp ; (62.5-21.716*Segma0) ];

H= A+B*U;

lambda = eig(H)
for u=0:3
T1(D1)=real(lambda (D2));
T2(D1)=imag(lambda (D2));
D1=D1+1;
D2=D2+1;
end

if D2>4
D2=1;
end

end
z = complex (T1,T2);
plot(z,'>')
grid on
```

Appendix F

```
// MIM technology main controller algorithm.
// Author: Karem Abuowda.
// Last update date: 28/09/2018.
// Company: Bournemouth University and Hydraeco Hydraulic.
// Comments: No comments.

///////////////////////////////////////////////////////////////////////////////////////
#include <Wire.h>
const byte SlaveAddress = 10; // Motor Activation Borad
const byte SlaveAddress1 = 11; // Read from Simulink Borad
const byte MasterAddress = 9; // Main Algorithm borad
const byte numChars = 18;     // Number of data from communication board
const byte SendChars = 8;     // Number to be send into Motor Activation Board
char sendChars[SendChars];     // Array of Data to be send for the motor
    Activation Borad: This represents the opening degrees.
int recievedNumber [18];
///////////////////////////////////////////////////////////////////////////////////////
int yAxis =0;                  // Analog joystick reading
const int Y_pin = 0;
const int range = 48;
int center = range / 2;
int threshold = range /8;
///////////////////////////////////////////////////////////////////////////////////////
float Ps =20*pow(10,6);          //Pressure source sensor.
float Pr= 0.2*pow(10,6);         //Tank pressure.
//float Pa;                      //Head chamber pressure.
//float Pb;                      //Rod chamber pressure.
float Ab = 0.009485;             //The cylinder rod chamer Area.
```

```
float  Aa = 0.0126;                //The cylinder head chanber Area.
float R = Aa/Ab;                   //Ratio between the head and the chamber.
float Opt= pow (R,0.75);           //Ration R^(3/4).
float Dp;                          // Pressure detection point
int FinalLength =0;                // This shows the length of the Degrees array
float FinalArray [86];             // This is the final aaray of conductances.
//float Data [4] = {0,0,0,0};      // {Ksa,Ksb,Kat,Kbt}
char Cases;                        // For serial communcation
char incomingBytes [numChars];     // For communiction
float Vcommand =0;
float Pa=0;
float Pb=0;

////////////////////////////////////////////////////////////////////////////////////

void setup() {
Serial.begin(9600);
Wire.begin (MasterAddress);
Cases=0;
/*************************************************************************************
int Divdegree = 5;
float SectionArea []= {0, 2.76e-6, 6.84e-6, 11.88e-6, 17.96e-6, 25.16e-6,
    33.4e-6,
42.68e-6, 53e-6, 64.32e-6, 76.64e-6, 89e-6, 102.56e-6, 117.76e-6, 132.52e-6,
    148.52e-6, 163e-6, 174.84e-6};
float DischargeCoffecient [] = {0, 0.971319638, 0.858418876, 0.827443256,
    0.823940386,
0.809327165, 0.803555571, 0.796149633, 0.746981081, 0.732892461, 0.693851216,
    0.687533179,
0.592043911, 0.615549626, 0.574716354, 0.500120599, 0.481329477, 0.489362736 };
float ValveCondutance [18] = {0,0,0,0,0,0,0,0,0,0,0,0,0,0,0,0,0,0};
float ConcutanceSubs [18] = {0,0,0,0,0,0,0,0,0,0,0,0,0,0,0,0,0,0};
FinalLength = 17*Divdegree+1;
float FinalArray1[FinalLength];
int x=0;
int F=0;
for(int i =0; i <18; i++)
  {
   ValveCondutance[i] = SectionArea [i]*DischargeCoffecient [i];
```

```
  }

for (int i =0; i <17; i++)
  {
   ConcutanceSubs [i] = ((ValveCondutance[i+1] - ValveCondutance [i])/
       Divdegree);
  }
  ConcutanceSubs [18] =0;
for (int i = 0; i <FinalLength; i++)
  {
   for( x =0; x < Divdegree; x++)
  {
   FinalArray1[i+x] = ValveCondutance[F]+ (ConcutanceSubs[F]*x);
  }
   i=i+(Divdegree-1);
   F=F+1;
   if (F==18) F=0;
  }

  for (int i=0; i < FinalLength; i++)
  {
    FinalArray [i] = FinalArray1 [i];
  }
}
/***********************************************************************************************


void loop() {
float Ksa = 0;   //Conducatance coeffecient for the valve betweeb piston head
    and the pressure source.
float Ksb = 0;   //Conducatance coeffecient for the valve betweeb piston head
    and the tank.
float Kat = 0;   //Conductance Coefficient for the valve between the piston
    rod and the pressure source.
float Kbt = 0;

float Pa1=0;
float Pb1=0;
float Keq=0;
```

```
int Z=0;
float Data [4] = {0,0,0,0};

Vcommand = -1*( readAxis(Y_pin )); // Reading the Joystick
//Serial.println (Vcommand);
 /*********** REQUESTING DATA FROM THE COMUNICATION CONTROLLER: Copied from
     UNO file */
Wire.requestFrom(SlaveAddress1, 18);
for (int i =0; i <18;i++)
    {
    char c = Wire.read();
    recievedNumber [i] = c-'0';
    Cases=1;
    }
    for (int i =0; i <18;i++)
    {
    }
        if ((recievedNumber [0]==0||recievedNumber [0]==1) || ((recievedNumber
            [9]==0||recievedNumber [9]==1) ))
        {
        Pa1 = Pa1 +recievedNumber [8]*1;
        Pa1 = Pa1 +recievedNumber [7]*10;
        Pa1 = Pa1 +recievedNumber [6]*100;
        Pa1 = Pa1 +recievedNumber [5]*1000;
        Pa1 = Pa1 +recievedNumber [4]*10000;
        Pa1 = Pa1 +recievedNumber [3]*100000;
        Pa1 = Pa1 +recievedNumber [2]*1000000;
        Pa1 = Pa1 +recievedNumber [1]*10000000;
           float G = 10;
          Pa=Pa1;
        Pb1 = Pb1 +recievedNumber [17]*1;
        Pb1 = Pb1 +recievedNumber [16]*10;
        Pb1 = Pb1 +recievedNumber [15]*100;
        Pb1 = Pb1 +recievedNumber [14]*1000;
        Pb1 = Pb1 +recievedNumber [13]*10000;
        Pb1 = Pb1 +recievedNumber [12]*100000;
        Pb1 = Pb1 +recievedNumber [11]*1000000;
        Pb1 = Pb1 +recievedNumber [10]*10000000;
          Pb=Pb1;
```

```
        }
        else
        {

        }
int x = ModeSelection(Ps,Pa,Pb,Aa,Ab,Vcommand);

switch (x)
{
   case 0:
   {
   Ksa =0;
   Ksb=0;
   Kat=0;
   Kbt=0;
   DataCommunication(0, Data);
   }
                                 break;
   /************************************POWER EXTENTION
       MODE************************************/
   case 1:
   {
   Ksb=0;
   Kat=0;
   Keq = (Vcommand*Ab)/(sqrt(R*(Ps-Pa)+(Pb-Pr)));
   Dp = R*(Ps-Pa)+(Pb-Pr);
   if (Dp>0)
   {

    Kbt= (sqrt(pow(Opt,2)+pow(R,3))*Keq)/Opt;
    Kbt= CloseValueDetection(FinalArray,Kbt,0,FinalLength);
    Ksa=Opt* Kbt;
    Ksa= CloseValueDetection(FinalArray,Ksa,0,FinalLength);
   }
   else
   {
    Kbt=0;
    Ksa=0;
   }
```

```
Z = AnitCavitation ( Ksa, Ksb, Kat, Kbt, 1);
if (Z == 1)
{
 Ksa= CloseValueDetection(FinalArray,Ksa,1,FinalLength);
 Kbt= CloseValueDetection(FinalArray,Kbt,2,FinalLength);
}
Data[0] = Ksa;
Data[3] = Kbt;
DataCommunication(1, Data);
}
                                break;


/**************************************POWER RETRACTION
    MODE*****************************************/
case 2:
{
  Ksa=0;
  Kbt=0;
  Keq = -(Vcommand*Ab)/(sqrt(R*(Pa-Pr)+(Ps-Pb)));
  Dp = R*(Pa-Pr)+(Ps-Pb);
  if (Dp>0)
  {
  Ksb=sqrt(pow(Opt,2)+pow(R,3))*Keq/Opt;
  Ksb=CloseValueDetection(FinalArray,Ksb,0,FinalLength);
  Kat=Opt*Ksb;
  Kat=CloseValueDetection(FinalArray,Kat,0,FinalLength);
  }
  else
  {
   Ksb=0;
   Kat=0;
  }

 Z = AnitCavitation ( Ksa, Ksb, Kat, Kbt, 2);
 if (Z==1)
 {
 Ksb=CloseValueDetection(FinalArray,Ksb,1,FinalLength);
 Kat=CloseValueDetection(FinalArray,Kat,2,FinalLength);
```

```
 }
 Data[1] = Ksb;
 Data[2] = Kat;
 DataCommunication(2, Data);
}
                              break;


/************************HIGH SIDE REGENERATION EXTENTION
   MODE*************************/
case 3:
{
 Kat=0;
 Kbt=0;
 Keq=(Vcommand*Ab)/sqrt((R*(Ps-Pa))+(Pb-Ps));
 Dp=R*(Ps-Pa)+(Pb-Ps);

 if (Dp>0)
 {
    Ksb = sqrt(pow(Opt,2)+pow(R,3))*Keq/Opt;
    Ksb=CloseValueDetection(FinalArray,Ksb,0,FinalLength);
    Ksa=Opt* Ksb;
    Ksa= CloseValueDetection(FinalArray,Ksa,0,FinalLength);
 }
 else
 {
 Ksb=0;
 Ksa=0;
 }
 Z = AnitCavitation ( Ksa, Ksb, Kat, Kbt, 3);
 if (Z==1)
 {
 Ksb=CloseValueDetection(FinalArray,Ksb,1,FinalLength);
 Ksa=CloseValueDetection(FinalArray,Kat,2,FinalLength);
 }
 Data[0] = Ksa;
 Data[1] = Ksb;
 DataCommunication(3, Data);
}
```

```
                                        break;
 /********************LOW SIDE REGENERATION
    Extention*******************************************/
  case 4:
  {
   Ksa=0;
   Ksb=0;
   Keq = (Vcommand*Ab)/sqrt((R*(Pr-Pa))+(Pb-Pr));
   Dp= R*(Pr-Pa)+(Pb-Pr);
   if (Dp>0)
   {
     Kbt= (sqrt(pow(Opt,2)+pow(R,3))*Keq)/Opt;
     Kbt = CloseValueDetection(FinalArray,Kbt,0,FinalLength);
     Kat= Opt*Kbt;
     Kat = CloseValueDetection(FinalArray,Kat,0,FinalLength);
   }
   else
   {
    Kbt=0;
    Kat=0;
   }
   Z = AnitCavitation ( Ksa, Ksb, Kat, Kbt, 4);
    if (Z==1)
   {
   Kbt=CloseValueDetection(FinalArray,Ksb,1,FinalLength);
   Kat=CloseValueDetection(FinalArray,Kat,2,FinalLength);
   }
   Data[3] = Kbt;
   Data[2] = Kat;
   DataCommunication(4, Data);
  }
                                        break;
/**********************LOW SIDE REGENERATION
   RETRACTION************************************/
  case 5:
  {
   Ksa=0;
   Ksb=0;
   Keq = (-Vcommand*Ab)/sqrt(R*(Pa-Pr)+(Pr-Pb));
```

```
    Dp= R*(Pa-Pr)+(Pr-Pb);
    if (Dp>0)
    {
     Kbt= (sqrt(pow(Opt,2)+pow(R,3))*Keq)/Opt;
     Kbt = CloseValueDetection(FinalArray,Kbt,0,FinalLength);
     Kat=Opt*Kbt;
     Kat = CloseValueDetection(FinalArray,Kat,0,FinalLength);

    }
    else
    {
      Kbt=0;
      Kat=0;
    }
    Z = AnitCavitation ( Ksa, Ksb, Kat, Kbt, 4);
      if (Z==1)
    {

    Kbt=CloseValueDetection(FinalArray,Ksb,1,FinalLength);
    Kat=CloseValueDetection(FinalArray,Kat,2,FinalLength);

    }
    Data[3] = Kbt;
    Data[2] = Kat;
    DataCommunication(5, Data);
   }  break;

}
}

/*********************************************************************************/



int ModeSelection(float Ps,float Pa,float Pb,float Aa,float Ab,int Vcommand)
{
  int X=0;
  float Fx = -(Pa*Aa)+(Pb*Ab);
  float HPRE = Ps*(Aa-Ab) ;
```

```
  if (Vcommand >0)
  {
    if (Fx<0)
    { float H= -1*Fx;
       if(H > HPRE)
       {
        X=1; // Power extention mode;
       }

        if (H < HPRE)
       {
        X=3; // High side regeneration extention;
       }
    }
    if (Fx>=0)
    {
      X = 4; //LOW side regeneration extention;
    }

  }

  if (Vcommand < 0)
  {
    if (Fx>0)
    {
      X=2; // Power retraction mode
    }
    if (Fx<0)
    {
       X=5;// Low side regeneration retraction.
    }

  }
  return X;

}

float CloseValueDetection(float FinalArray [], float value, int P,int
    FinalArrayLenght)
```

```
{
  float Largest = FinalArray [FinalArrayLenght-1];
  float H;
  int x =0;
  int f=0;
  float TheValue;

  if (value > Largest)
     {
       value = Largest;
     }
  // To find the closest value
   if (P==0)
   {

    //Serial.println ("We are here");
    for (int i=0 ; i<FinalArrayLenght;i++)
    {
      H=abs(FinalArray[i]- value);
      if (H <= Largest)
      {
        Largest = H;
        x = i;
      }
    }
    TheValue = FinalArray [x];
   }



  //To move it foreward by one step
   if (P==1)
   {
    for (int i=0 ; i<FinalArrayLenght;i++)
    {

      H=abs(FinalArray[i]- value);
      if (H <= Largest)
      {
```

```
        Largest = H;
        x = i;
      }
    }
    f= x+1;
    if (f > FinalArrayLenght)
    {
      TheValue = FinalArray[x];
    }
    else
    {
      TheValue = FinalArray[f];
    }
   }

 //To move it backword by one step
   if (P==2)
   {
    for (int i=0 ; i<FinalArrayLenght;i++)
    {
      H=abs(FinalArray[i]- value);
      if (H <= Largest)
      {
        Largest = H;
        x = i;
      }
    }
    f= x-1;
    if (f<=0)
    {
      TheValue = FinalArray[0];
    }
    else
    {
    TheValue = FinalArray[f];
    }
   }
 return TheValue;
}
```

```
int AnitCavitation ( float Ksa, float Ksb, float Kat, float Kbt, int
    OperationMode)

{
  double Fl;
  double Fx;
  int x =0;
 if (OperationMode == 1)
 {
   Fx=Pb*Ab-Aa*Pa;
   Fl=pow((Opt/R),2)*Ab*Ps+Pr*Ab;
    if ( Fx==Fl)
    {
       x=1;
    }
 }

 if (OperationMode == 2)
 {
    Fx= Pa*Aa-Pb*Ab;
    Fl =pow((R/Opt),2)*Aa*Ps+Aa*Pr;
     if ( Fx==Fl)
    {
       x=1;
    }
 }

if (OperationMode == 3)
 {
   Fx=Pb*Ab-Aa*Pa;
   Fl=(1+pow((Opt/R),2))*Ab*Ps;
   if ( Fx==Fl)
    {
       x=1;
    }

 }
```

```
if (OperationMode == 4)
 {
   Fx= Pb*Ab-Aa*Pa;
   Fl=(1+pow((Opt/R),2))*Ab*Pr;
    if ( Fx==Fl)
    {
       x=1;
    }
 }

if (OperationMode == 5)
 {
   Fx=Pa*Aa-Pb*Ab;
   Fl=pow((R/Opt),2)*Aa*Ps+Aa*Pr;
   if ( Fx==Fl)
    {
       x=1;
    }
 }

return x;
}

void DataCommunication(int F, float Data [])
{
//Serial.println("THE DATA IS BEING CALLED");
int ExpData [16]= {0,0,0,0,0,0,0,0,0,0,0,0,0,0,0,0};
char SendData [18];
int sendData2 [4]= {0,0,0,0};
int sendData22[8] = {0,0,0,0,0,0,0,0};
String str;
char x [1];
int  A=0;
int A_0=0;
int A_1=0;
int A_2=0;
int A_3=0;
int B=0;
int B_0=0;
```

```
int B_1=0;
int B_2=0;
int B_3=0;
int C=0;
int C_0=0;
int C_1=0;
int C_2=0;
int C_3=0;
int D=0;
int D_0=0;
int D_1=0;
int D_2=0;
int D_3=0;

 for (int i =0; i <= FinalLength; i++)
 {
   if (Data[0] == FinalArray [i])
   {
   A = (i)/0.1125;
   A_0= A%10;
   ExpData[3]= A_0;
   A_1=(A/10)%10;
   ExpData[2]= A_1;
   A_2=(A/100)%10;
   ExpData[1]= A_2;
   A_3=(A/1000)%10;
   ExpData[0]= A_3;
   sendData2 [0]= i;
   }
    if (Data[1] == FinalArray [i])
   {
    B = (i)/0.1125;
    B_0= B%10;
    ExpData[7]= B_0;
    B_1=(B/10)%10;
    ExpData[7]= B_1;
    B_2=(B/100)%10;
    ExpData[5]= B_2;
    B_3=(B/1000)%10;
```

```
    ExpData[4]= B_3;
    sendData2 [1]= i;
   }

    if (Data[2] == FinalArray [i])
   {
    C = (i)/0.1125;
    C_0= C%10;
    ExpData[11]= C_0;
    C_1=(C/10)%10;
    ExpData[10]= C_1;
    C_2=(C/100)%10;
    ExpData[9]= C_2;
    C_3=(C/1000)%10;
    ExpData[8]= C_3;
    sendData2 [2]= i;
   }

    if (Data[3] == FinalArray [i])
   {
    D = (i)/0.1125;
    D_0= D%10;
    ExpData[15]= D_0;
    D_1=(D/10)%10;
    ExpData[14]= D_1;
    D_2=(D/100)%10;
    ExpData[13]= D_2;
    D_3=(D/1000)%10;
    ExpData[12]= D_3;
    sendData2 [3]= i;
   }
 }
////////////////DATA ARRANGEMT///////////////////////////

sendData22 [1] = sendData2[0]%10;
sendData22 [0] =(sendData2[0]/10)%10;
sendData22 [3] = sendData2[1]%10;
sendData22 [2] =(sendData2[1]/10)%10;
sendData22 [5] = sendData2[2]%10;
```

```
sendData22 [4] =(sendData2[2]/10)%10;
sendData22 [7] = sendData2[3]%10;
sendData22 [6] =(sendData2[3]/10)%10;

Serial.print('x');
Serial.print (F);
 for (int i=0; i<8;i++)
  {
   Serial.print(sendData22 [i]);
  }
  Serial.println();
SendData [0]= '<';
for (int i=1; i < 17; i++)
{
 str = String((ExpData[i-1]));
 str.toCharArray(x,16);
 SendData[i] = x[0];
}
SendData [17]= '>';
 Wire.beginTransmission(SlaveAddress);
 Wire.write((char*)SendData);
 Wire.endTransmission(SlaveAddress);
  delay (500);
}


////////////////////////////////////////////////////////////
// READ AXIS FUNCTION
int readAxis(int thisAxis) {
  // read the analog input:
  int reading = analogRead(thisAxis);
  // map the reading from the analog input range to the output range:
  reading = map(reading, 0, 1023, 0, range);
  // if the output reading is outside from the rest position threshold, use it:
  int distance = reading - center;
  if (abs(distance) < threshold) {
    distance = 0;
  }
  return distance;
```

```
}

/*****************ReadFromSimulink********************/
#include <LiquidCrystal.h>
#include <Wire.h>
char incomingByte1 [10];
char incomingByte2 [10];
char incomingByte11[10];
char incomingByte22[10];
char incomingByte3 [1];
int i =0; // for incoming serial data
int Count=0;
int empty=0;
int flag= 0;
int flag1=0;
const int rs = 8, en = 9, d4 = 4, d5 = 5, d6 = 6, d7 = 7;
LiquidCrystal lcd(rs, en, d4, d5, d6, d7);
const byte SlaveAddress1 = 11;
const byte MasterAddress = 9;
void setup()
   {
        lcd.begin(16, 2);
         Serial.begin(9600);   // opens serial port, sets data rate to 9600 bps
        Wire.begin(SlaveAddress1);
        Wire.onRequest(requestEvent);

   }


void loop()
{
       if (Serial.available() >0)
       {
         if (Serial.read ()-'0' == 9)
           {
             for (int i=0; i<10; i++)
             {
             incomingByte1 [i] = Serial.read();
             }
```

```
            //flag=1;

            //incomingByte3 [0] = Serial.read();
        /* for(i=0;i<19;i++)
         {
         incomingByte [i] = Serial.read();
         }*/
            }

         else
         {
           while (Serial.available ()>0)
           {
             flag=0;
             char empty= Serial.read ();
           }
         flag=1;

         }

       }


if (incomingByte1 [0]=='0' || incomingByte1 [0]=='1')
{
  for (int i =0; i <10; i++)
  {
    incomingByte11 [i] = incomingByte1 [i];

  }
}



         lcd.setCursor(0, 0);
         lcd.print("HP:");
         lcd.setCursor(0, 1);
         lcd.print("RP: ");
         for (int i=1; i<5;i++)
         {
```

```
        lcd.setCursor(i+4, 0);
        lcd.print(incomingByte1 [i]);
        }
        for (int i=5; i<9;i++)
        {
        lcd.setCursor(i+4, 0);
        lcd.print(0);
        }

        for (int i=6; i<10;i++)
        {
        lcd.setCursor(i-1, 1);
        lcd.print(incomingByte1 [i]);
        }
        for (int i=5; i<9;i++)
        {
        lcd.setCursor(i+4, 1);
        lcd.print(0);
        }
        //lcd.setCursor(9, 1);
        //lcd.print(incomingByte3 [0]);
        delay (500);
        flag =0;
        flag1=0;

}

void requestEvent()
  {
      if (flag ==1)
      {

       for (int i=0; i<5; i++)
       {
       Wire.write(char (incomingByte1 [i]));
       }
        for (int i=0; i<4; i++)
       {
       Wire.write ('0');
```

```
      }
       for (int i=5; i<10; i++)
      {
      Wire.write(char (incomingByte1 [i]));
      }
       for (int i=0; i<4; i++)
      {
      Wire.write('0');
      }
     }

     else
     {
      for (int i=0; i<5; i++)
      {
      Wire.write(char (incomingByte11 [i]));
      }
       for (int i=0; i<4; i++)
      {
      Wire.write ('0');
      }
       for (int i=5; i<10; i++)
      {
      Wire.write(char (incomingByte11 [i]));
      }
       for (int i=0; i<4; i++)
      {
      Wire.write('0');
      }
     }
 }

/************************************SendToSimulink*******************************/

#include <LiquidCrystal.h>
int outcoming1 [4] = {90,0,50,0};
int outcoming2 [4] = {20,0,10,0};
int outcoming3 [4] = {0,0,0,0};
int outcoming4 [4] = {0,50,0,60};
```

```
int incomingByte [16];
int flag= 0;
int flag1=0;
const int rs = 8, en = 9, d4 = 4, d5 = 5, d6 = 6, d7 = 7;
LiquidCrystal lcd(rs, en, d4, d5, d6, d7);
void setup()
    {
        lcd.begin(16, 2);
        Serial.begin(9600);   // opens serial port, sets data rate to 9600 bps

    }
void loop ()
{


  for (int i=0; i<4;i++)
  {
  Serial.println(outcoming1 [i]);
  }
  delay (1000);
   for (int i=0; i<4;i++)
  {
  Serial.println(outcoming2 [i]);
  }
 delay (1000);
    for (int i=0; i<4;i++)
  {
  Serial.println(outcoming3 [i]);
  }
 delay (1000);
  for (int i=0; i<4;i++)
  {
  Serial.println(outcoming4 [i]);
  }
   delay (1000);
}
```